25 January 2013 | $10

Science

AAAS

PRIX COUPS D'ÉLAN POUR LA RECHERCHE FRANÇAISE

2012 PRIZE WINNERS

FRANÇOIS-XAVIER BARRE
Contribution of Xer recombination of the maintenance and the evolution of bacterial genomes
CENTER OF MOLECULAR GENETICS
CNRS • GIF-SUR-YVETTE • FRANCE

VINCENT GALY
Mechanisms of maternal uniparental mitochondrial genome transmission
DEVELOPMENTAL BIOLOGY LABORATORY
CNRS • PARIS • FRANCE

RAPHAEL SCHARFMANN
Dissecting pancreatic endocrine cell development: a basis for new therapies for diabetes
RESEARCH CENTER GROWTH AND SIGNALING
INSERM • PARIS • FRANCE

CHRISTOPHE TZOURIO
i-Share cohort study (Internet-based Health Research Students Enterprise)
UNIVERSITY OF BORDEAUX SEGALEN
INSERM • BORDEAUX • FRANCE

THERA Conseil

Now in its 12th year, The Bettencourt Schueller Foundation "Coups d'Elan Prize for French Research" has been awarded to four top-performing French laboratories.

The prize rewards teams specifically chosen for the promising nature of their research programs. It enables them to optimize their infrastructure (construction / renovation of their premises, the purchasing of new equipment) and to receive practical assistance when required.

From the year 2000 onwards, 42 research laboratories, from both the Inserm (French National Institute of Health and Medical Research) and the CNRS (National Center for Scientific Research), have received € 250,000 each. As a direct result, over 500 researchers have been able to benefit from optimal physical working conditions.

Recognised in 1987 as a public interest foundation, the Bettencourt Schueller Foundation was set up by Liliane Bettencourt, in memory of her father Eugène Schueller, a renowned researcher and chemist. Its goal is to constantly expand the boundaries of knowledge in the life sciences in order to improve public health; to reveal talent and pass on expertise within the field of artistic creativity; and to relieve suffering, combat exclusion and respond to social welfare emergencies.

FONDATION BETTENCOURT SCHUELLER

Fondation Bettencourt Schueller
27-29 rue des Poissonniers
92200 Neuilly-sur-Seine • France
www.fondationbs.org
Contact : sciences@fondationbs.org

R&D Systems Cytokines & Growth Factors

Setting the Standard for the Life Science Industry for over 25 Years

✓ R&D Systems currently offers more than 3,000 bioactive recombinant proteins

✓ We are the most referenced manufacturer of recombinant & natural proteins

✓ Our scientists are dedicated to developing the highest quality products & new processes that meet the needs of researchers

High purity proteins, traditional & cell culture grade • Animal-free proteins • GMP proteins

A.

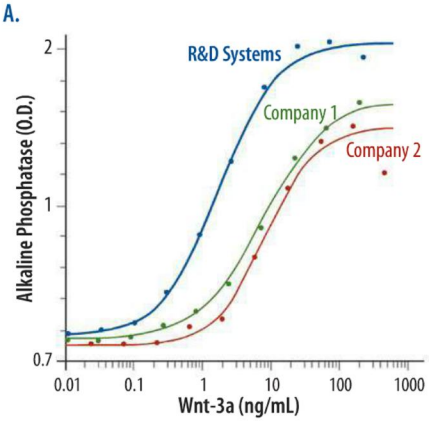

B.

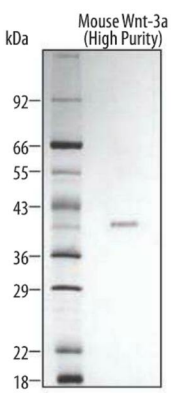

A. Activity Comparison Data for Recombinant Mouse Wnt-3a. The MC3T3-E1 mouse preosteoblast cell line was treated with increasing concentrations of R&D Systems Recombinant Mouse Wnt-3a (Catalog # 1324-WN) or with mouse Wnt-3a from two other companies. The R&D Systems protein shows greater than a four-fold increase in activity compared to the other commercially available proteins.

B. SDS-PAGE Analysis of High Purity Recombinant Mouse Wnt-3a. High Purity Recombinant Mouse Wnt-3a (Catalog # 1324-WNP; 1 µg/lane) was loaded on a 12% SDS-PAGE gel under reducing conditions and visualized by silver staining.

www.RnDSystems.com/CytokinesGrowthFactors

R&D Systems Tools for Cell Biology Research™

For research use only. Not for use in diagnostic procedures.

R&D SYSTEMS®

NEW ENGLAND BioLabs® Inc.
enabling technologies in the life sciences

Make ends meet.

Gibson Assembly™ Cloning Kit

New England Biolabs has revolutionized your laboratory's standard cloning methodology. The Gibson Assembly Cloning Kit combines the power of the Gibson Assembly Master Mix with NEB 5-alpha Competent *E. coli*, enabling fragment assembly and transformation in just under two hours. Save time, without sacrificing efficiency.

Making ends meet is now quicker and easier than ever before, with the Gibson Assembly Cloning Kit from NEB.

Gibson Assembly Cloning Kit provides robust transformation efficiencies

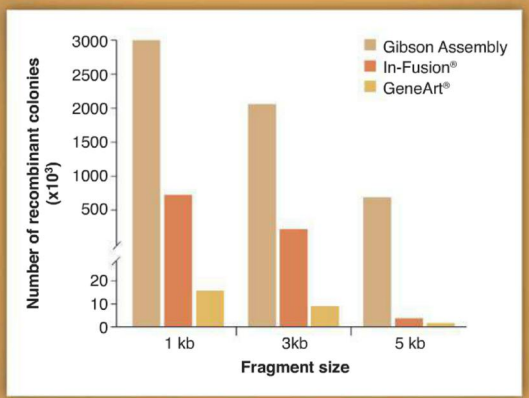

Assembly reactions containing 25 ng of linear pUC19 vector and 0.04 pmol of each fragment were performed following individual suppliers' recommended protocols and using the competent cells provided with the kit. The total number of recombinant colonies was calculated per 25 ng of linear pUC19 vector added to the assembly reaction.

NEBuilder™ for Gibson Assembly

Visit **NEBGibson.com** to view the latest tutorials and to try our primer design tool.

IN-FUSION® is a registered trademark of Clontech Laboratories, Inc.
GENEART® is a registered trademark of Life Technologies, Inc.
GIBSON ASSEMBLY™ is a trademark of Synthetic Genomics, Inc.

SYNTHETIC GENOMICS®

Some components of this product are manufactured by New England Biolabs, Inc. under license from Synthetic Genomics, Inc.

EDITORIAL

373 They Never Saw It Coming
Norman R. Augustine

NEWS OF THE WEEK

378 A roundup of the week's top stories

NEWS & ANALYSIS

381 Gun Control Agenda Is a Call to Duty for Scientists

382 Soot Is Warming the World Even More Than Thought

383 'Brussels Ranking' of Universities Off to a Rocky Start

384 Foreigners Run Afoul of China's Tightening Secrecy Rules

NEWS FOCUS

386 Shaking Up Science
>> Science *Podcast*

390 2013 Society for Integrative and Comparative Biology Annual Meeting
Eating Was Tough for Early Tetrapods
Nervous System May Have Evolved Twice
Snapshots From the Meeting

LETTERS

392 Accidental Island Voyagers
G. D. Ruxton and D. M. Wilkinson

Response
A. Simmons

Extend Data Exclusivity to Save Drug Development
J. R. Colca

392 The BUZZ: Skin-Deep Learning

393 TECHNICAL COMMENT ABSTRACTS

BOOKS *ET AL.*

394 Are We Getting Smarter?
J. R. Flynn, reviewed by A. Schleicher

395 The Afterlives of Animals
S. J. M. M. Alberti, Ed., reviewed by K. A. Rader

EDUCATION FORUM

396 Science Learning Progressions
R. G. Duncan and A. E. Rivet

PERSPECTIVES

398 Membrane Protein Twists and Turns
J. U. Bowie

399 (Pseudo-)Symmetrical Transport
L. R. Forrest

401 Ferroelectric Organic Materials Catch Up with Oxides
D. A. Bonnell
>> *Report p. 425*

402 Deconstructing Dimensionality
M. A. Schwartz and C. S. Chen

404 Corralling Positively Charged Molecular Radicals
A. Benniston
>> *Report p. 429*

405 How Big Is the Proton?
H. S. Margolis
>> *Research Article p. 417*

406 Chaperones That SNARE Neurotransmitter Release
F. M. Hughson
>> *Research Article p. 421*

SCIENCE PRIZE ESSAY

408 Keeping an Eye on Biology
S. R. Singer et al.

CONTENTS continued >>

page 381

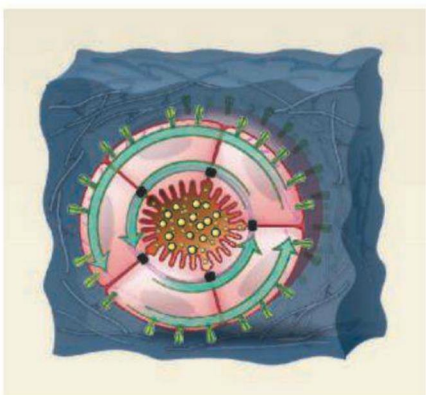

page 402

Explore our rich online offerings, including multimedia, news, *Science* Careers, and our two research journals—*Science Signaling* and *Science Translational Medicine*—at www.sciencemag.org

COVER

A juvenile male *Pteropus alecto* (black flying fox) spreading its wings (for adults, average wing span: ~1 meter; average weight range: 500 to 1000 grams). Bats, the only mammals capable of sustained flight, are among the world's most diverse mammals and are host to numerous deadly viruses. Comparative genome analyses have shed new light on the evolution of bat-specific traits, including flight and immunity. See page 456.

Photo: Martin Asser Hansen/www.maasha.dk

DEPARTMENTS

371 This Week in *Science*
374 Editors' Choice
376 *Science* Staff
410 AAAS News & Notes
468 New Products
469 *Science* Careers

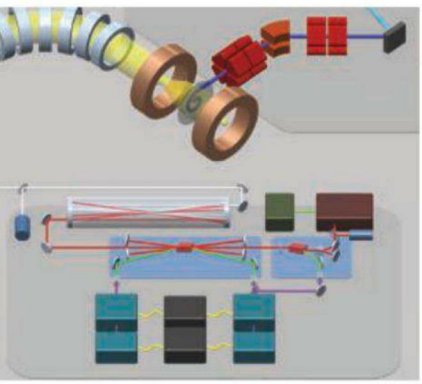

pages 405 & 417

page 413

REVIEW

413 Can We Name Earth's Species Before They Go Extinct?
M. J. Costello et al.
>> Science *Podcast*

RESEARCH ARTICLES

417 Proton Structure from the Measurement of 2S-2P Transition Frequencies of Muonic Hydrogen
A. Antognini et al.
A precision spectroscopic measurement of the proton radius indicates a growing discrepancy with respect to scattering results.
>> *Perspective p. 405*; Science *Podcast*

421 Reconstitution of the Vital Functions of Munc18 and Munc13 in Neurotransmitter Release
C. Ma et al.
A model of neurotransmitter release explains why two proteins not needed for membrane fusion in vitro are needed in vivo.
>> *Perspective p. 406*

REPORTS

425 Diisopropylammonium Bromide Is a High-Temperature Molecular Ferroelectric Crystal
D.-W. Fu et al.
An organic molecular crystal is found to have ferroelectric properties comparable to those of barium titanate.
>> *Perspective p. 401*

429 A Radically Configurable Six-State Compound
J. C. Barnes et al.
An interlocked-rings topology stabilizes a wide range of collective oxidation states in a metal-free organic compound.
>> *Perspective p. 404*

433 Identification of the Long-Sought Common-Envelope Events
N. Ivanova et al.
A model suggests that an intermediate class of stellar outbursts results from interaction between two stars in a close binary.

436 Synchronous X-ray and Radio Mode Switches: A Rapid Global Transformation of the Pulsar Magnetosphere
W. Hermsen et al.
The detection of synchronized switches in the radio and x-ray pulse properties of a pulsar challenges pulsar emission theories.

440 To Favor Survival Under Food Shortage, the Brain Disables Costly Memory
P.-Y. Plaçais and T. Preat

443 Fasting Launches CRTC to Facilitate Long-Term Memory Formation in *Drosophila*
Y. Hirano et al.
Different types of memory interact in fed versus starved states to promote survival-oriented behavior.

446 The Human THAP9 Gene Encodes an Active *P*-Element DNA Transposase
S. Majumdar et al.
The human THAP9 protein can mediate transposon jumping in both human and fruit fly genomes.

448 Germline DNA Demethylation Dynamics and Imprint Erasure Through 5-Hydroxymethylcytosine
J. A. Hackett et al.
Rare loci that escape epigenetic reprogramming in mammalian germ cells may underlie transgenerational epigenetic inheritance.

452 Actin, Spectrin, and Associated Proteins Form a Periodic Cytoskeletal Structure in Axons
K. Xu et al.
Superresolution microscopy reveals a membrane cytoskeleton in neurons comprising rings of actin separated by spectrin.

456 Comparative Analysis of Bat Genomes Provides Insight into the Evolution of Flight and Immunity
G. Zhang et al.
The analysis of two bat genomes suggests that adaptations to flight involved changes in DNA repair and innate immunity.

460 Tunable Signal Processing Through Modular Control of Transcription Factor Translocation
N. Hao et al.
A yeast protein transforms stress signals into distinct dynamic responses according to the timing and strength of inputs.

464 An Actin-Dependent Step in Mitochondrial Fission Mediated by the ER-Associated Formin INF2
F. Korobova et al.
Actin filaments between the endoplasmic reticulum and mitochondria promote mitochondrial fission.

SCIENCE (ISSN 0036-8075) is published weekly on Friday, except the last week in December, by the American Association for the Advancement of Science, 1200 New York Avenue, NW, Washington, DC 20005. Periodicals Mail postage (publication No. 484460) paid at Washington, DC, and additional mailing offices. Copyright © 2013 by the American Association for the Advancement of Science. The title SCIENCE is a registered trademark of the AAAS. Domestic individual membership and subscription (51 issues): $149 ($74 allocated to subscription). Domestic institutional subscription (51 issues): $990; Foreign postage extra: Mexico, Caribbean (surface mail) $55; other countries (air assist delivery) $85. First class, airmail, student, and emeritus rates on request. Canadian rates with GST available upon request, GST #1254 88122. Publications Mail Agreement Number 1069624. **Printed in the U.S.A.**

Change of address: Allow 4 weeks, giving old and new addresses and 8-digit account number. **Postmaster:** Send change of address to AAAS, P.O. Box 96178, Washington, DC 20090–6178. **Single-copy sales:** $10.00 current issue, $15.00 back issue prepaid includes surface postage; bulk rates on request. **Authorization to photocopy** material for internal or personal use under circumstances not falling within the fair use provisions of the Copyright Act is granted by AAAS to libraries and other users registered with the Copyright Clearance Center (CCC) Transactional Reporting Service, provided that $30.00 per article is paid directly to CCC, 222 Rosewood Drive, Danvers, MA 01923. The identification code for *Science* is 0036-8075. *Science* is indexed in the *Reader's Guide to Periodical Literature* and in several specialized indexes.

CREDIT: (BOTTOM) MARK J. COSTELLO

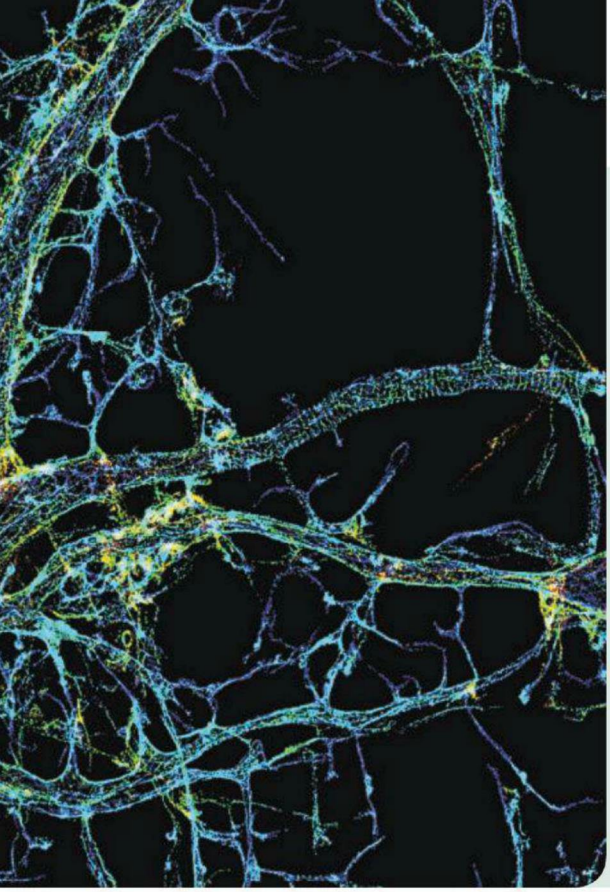

CREDITS (TOP TO BOTTOM): KE XU, GUISHENG ZHONG, STEVEN WANG AND XIAOWEI ZHUANG AT HARVARD UNIVERSITY AND HHMI; JAMES C. LOMBARDI JR.

<< Axonal Actin

How actin is organized in the axons and dendrites of neurons is largely unknown. **Xu *et al.*** (p. 452, published online 13 December) imaged actin in axons and dendrites using stochastic optical reconstruction microscopy. Surprisingly, while actin in dendrites formed long filaments, the actin in axons was organized into evenly spaced ringlike structures at the axon circumference. Spectrin, which is known to interact with actin to form a membrane cytoskeleton in erythrocytes, formed periodic structures that alternated with those of actin. This actin-spectrin cytoskeletal structure might give mechanical support to axons and could also organize other membrane proteins.

Proton Still Too Small

Despite a proton's tiny size, it is possible to measure its radius based on its charge or magnetization distributions. Traditional measurements of proton radius were based on the scattering between protons and electrons. Recently, a precision measurement of a line in the spectrum of muonium—an atom consisting of a proton and a muon, instead of an electron—revealed a radius inconsistent with that deduced from scattering studies. **Antognini *et al.*** (p. 417; see the Perspective by **Margolis**) examined a different spectral line of muonium, with results less dependent on theoretical analyses, yet still inconsistent with the scattering result; in fact, the discrepancy increased.

Hunger and Memory

During starvation, are all brain functions slowed down, or are specific functions disabled to save energy? **Plaçais and Preat** (p. 440) investigated how the brain of *Drosophila* deals with severe resource limitation. The brain cut selected expenses to reduce the threat to survival and switched off the formation of aversive long-term memory that depends on costly protein synthesis. However, **Hirano *et al.*** (p. 443) focused on mild food-deprivation, which actually enhanced long-term memory formation. Presumably, improved memory should enhance survival when competing for limited food. After longer food deprivation, enhancement of aversive long-term memory decreased, while that of appetitive long-term memory remained high: Presumably, as starvation nears, it becomes more important to pursue food at all costs, and so appetitive memory takes precedence over aversive memories.

Environmentally Friendly Ferroelectrics

Ferroelectrics—which are widely used as piezo elements, sensors, and actuators—maintain charge polarization even in the absence of an external electric field. The best ferroelectric properties are found in perovskites such as barium titanate (BTO) and lead zirconate titanate; however, environmentally friendly, lead-free alternatives are highly desirable. **Fu *et al.*** (p. 425; see the Perspective by **Bonnell**) find that the organic molecular crystal diisopropylammonium bromide has ferroelectric properties comparable to those of BTO and may represent a viable alternative to perovskites.

Radically Organic

Metals such as manganese are relatively stable over a wide range of oxidation states. In contrast, purely organic compounds are rarely susceptible to incremental addition or removal of electrons without accompanying fragmentation or coupling reactions. **Barnes *et al.*** (p. 429; see the Perspective by **Benniston**) report a catenane (a compound comprising interlocked rings) in which the topological structure stabilizes six different states that successively differ by the presence or absence of one or two electrons in the framework. The hepta-oxidized state proved remarkably resilient to oxygen exposure.

Bat Genomes

Bats are of great interest because of their ability to fly and as hosts for infectious disease. **Zhang *et al.*** (p. 456, published online 20 December) sequenced the genomes of two distantly related bat species, David's Myotis and Black flying fox. Analysis of the two genomes revealed likely changes that accompanied the evolution of bats, including selection for increased expression of genes involved in the oxidative phosphorylation pathway needed to generate the energy required for flight. Furthermore, while some immune genes have been lost, others are under positive selection, which may potentially explain bats' status as viral reservoirs.

When Stars Get Too Close

Stellar outbursts used to come in two classes: supernovae and novae, the complete explosions and the thermonuclear runaways on the surface of evolved stars, respectively. Over the past two decades a class of stellar outbursts emerged with luminosities between those of novae and supernovae— intermediate-luminosity red transients (ILRTs). **Ivanova *et al.*** (p. 433) propose that these ILRTs are the signature of common envelope events in which a lower-mass star in a close binary system is engulfed by matter transferred from its more massive and more evolved companion star.

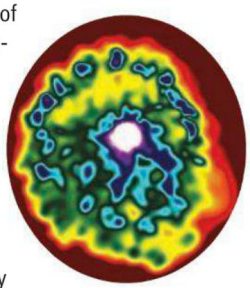

Masterminding Mitochondrial Fission

Mitochondria are highly dynamic and undergo fusion and fission and they move in cells. Defects in mitochondrial dynamics are implicated in many neurodegenerative diseases. Recent findings have suggested that mitochondrial fission occurs preferentially at endoplasmic reticulum (ER) contact sites, with ER circumscribing mitochondria and possibly promoting the constriction of mitochondria during fission. **Korobova *et al.*** (p. 464) now suggest that an ER-localized formin, INF2, is required for mitochondrial fission and that INF2-mediated actin polymerization facilitates mitochondrial constriction.

What — You *Don't* Dip and Read™?!

Do less and get more from your ELISAs

- Quantitate 96 protein samples in 15 minutes, not hours
- Take advantage of a 4-log dynamic range and dilute less
- Run automated assays without wash steps or overnight incubations
- Analyze crude samples with less prep
- Get information-rich direct binding data, not end-point results
- Develop new assays in a few hours, not weeks

The Octet® Platform

Octet Systems with Dip and Read assays.
No hassle, label-free ELISAs.

fortéBIO
A Division of Pall Life Sciences

PALL Life Sciences

www.fortebio.com

Fast. Accurate. EASY.

AAAS *Travels*

Lake Baikal

Discover Moscow, Star City & the Blue Eye of Siberia!

June 21–July 3, 2013

Discover the enchanting Kremlin, visit Star City, explore Irkutsk... the "Paris of Siberia." At Lake Baikal, we board the *M/V Vampilov*, venturing more than 250 miles up Lake Baikal—the Russian "Galapagos Islands." This is the oldest and deepest lake in the world, storing nearly 20% of the fresh-water on earth. It contains more than 1,500 species unique to Baikal. Experience the delights of Moscow and Siberia! $5,995 + air.

For a detailed brochure, please call (800) 252-4910

All prices are per person twin share + air

BETCHART EXPEDITIONS Inc.

17050 Montebello Rd, Cupertino, CA 95014
Email: AAASInfo@betchartexpeditions.com
www.betchartexpeditions.com

STAY INFORMED! STAY CONNECTED!

Get more from your AAAS membership

Are you currently registered to receive e-mails from AAAS and *Science*?

E-mail is the primary way that AAAS communicates with our members about AAAS programs, new member benefits, invitations to special events, and, of course, the latest news and research being published in *Science*.

Sign up today to receive e-mails from AAAS and ensure that you are getting the most out of your membership and *Science* subscription.*

To get started visit: **promo.aaas.org/stayconnected** You'll need your AAAS Member number. Find it above your name on your *Science* mailing label.

Don't miss a thing. Sign up for e-mail communications from AAAS today!

Science AAAS

*AAAS follows CAN-SPAM and European Safe Harbor guidelines for protecting your privacy. We will never sell your e-mail address and you can opt-out of receiving e-mails at any time.

Norman R. Augustine is the retired chairman and chief executive officer of Lockheed Martin Corporation.

They Never Saw It Coming

RECENTLY, A HIGHLY REGARDED NEWSPAPER PUBLISHER, PERHAPS THINKING OF DINOSAURS WHILE speaking of his own profession, remarked to me that "We are all dead; some of us just don't realize it yet." He is of course not alone in his lament: Remember videocassette recorders, carbon paper, and mechanical typewriters? Various writers have warned that it is not the strongest of the species that survives, or the most intelligent, but rather the one most adaptable to change.

Which brings us to what may be America's greatest asset after its democracy and free enterprise system—and also the most resistant to change: its higher education system. Indeed, with the exception of religious institutions, it is difficult to think of any more intransigent entity. The canonical student, professor, book, blackboard, and piece of chalk have survived for centuries as the ingredients of pedagogy throughout the world.

But then came the technological revolution, accompanied by declining U.S. financial support for higher education and the advent of globalization. Given those pressures, one could postulate that, for example, the university of the future will have no library because students will carry it in their pockets; and that there will be no classes, as adaptive, interactive, computer-taught sessions will have taken their place. Lectures will be provided, courtesy of distance learning, by a few world-class professors located around the globe. Biometric identity verification will permit examinations to be held far away from any campus, with instant grading accomplished by teaching-assistant computers. Universities will operate 12 months a year. Departments will cease to exist and tenure will disappear, the victim of mounting financial pressures. The great state universities, responding to continually reduced government funding, will become quasi-private institutions, with most unfortunately lacking adequate endowments. For-profit firms will be created to conduct examinations based on course material placed online without charge by the world's most renowned universities and will award certificates of completion. Players in intercollegiate athletics will be unionized and highly paid, as are their coaches today, and perform before small crowds that serve as studio audiences for multimedia productions. And many more individuals will be able to afford what passes for a college education.

Awful? Perhaps. Possible? Probably. The lack of face-to-face interactions among students and faculty will certainly diminish the educational experience. But with tuition now ranging from $10,000 to $50,000 per year, all but the wealthiest of parents and students may get used to the idea. Most damaging will be the further bifurcation between the wealthy and the poor, with children in the former group attending the best campus-based institutions that manage to survive and the others relegated to a computer screen. Even today, the best predictor of the extent of a child's education is its parents' educational level (and, implicitly, wealth).

Technology is good, but it is important to control it so as to benefit and not harm higher education. This will require that national leaders recognize the enormous return from investments in research. It will also require state leaders to embrace the huge payoff realizable from supporting higher education. And it will require university leaders to better control the cost of education. Also urgently needed is a rethinking of such matters as the balance of emphasis on research and teaching in our great universities; the balance of academics and intercollegiate athletics; the sustainability of universities serving as a backstop for a failing precollege education system; the efficacy of U.S. immigration policies, particularly as they affect students; and the impact of the 15-hour study-weeks revealed by recent surveys of university students.*

When I became the chief executive officer of a large aerospace company, the Berlin Wall had just collapsed. Had I been told that within 6 years 40% of all the people in the industry and three-fourths of its companies would be gone, I would have said, "Not possible." It happened.

– Norman R. Augustine

10.1126/science.1234998

*National Survey of Student Engagement Annual Results 2012 (http://nsse.iub.edu/html/annual_results.cfm).

CREDITS: (LEFT) CARL COX PHOTOGRAPHY; (RIGHT) ISTOCKPHOTO.COM/G. GRULLON/SCIENCE

EDITED BY KRISTEN MUELLER AND MARIA CRUZ

MATERIALS SCIENCE

Graphene in Color

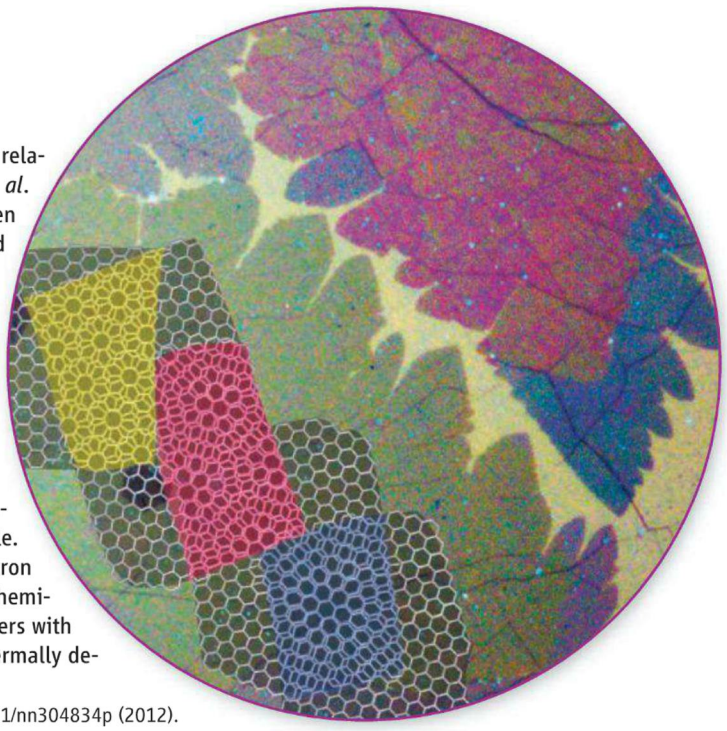

The properties of bilayer graphene films depend on the relative orientation or twist of the two layers. Robinson *et al.* grew single-layer graphene on copper surfaces and then performed two transfers of these films onto silica-coated silicon substrates to create bilayer regions. Because these films are polycrystalline, a variety of twist angles between the layers were created across the surface and resulted in a patchwork of colored regions that appeared red, yellow, or blue. Raman spectroscopy was used to characterize the twist angles; the enhancement of the G peak at ~1600 cm^{-1} occurred at optical excitation wavelengths that differed for the red and yellow regions, and the extent of enhancement corresponded to the deviation of the orientation of the layers from a distinctive critical twist angle. The twist angles were also confirmed by low-energy electron diffraction studies. The coupling could be minimized by chemical functionalization: fluorination of the top graphene layers with XeF_2 quenched the colors, which could be recovered by thermally desorbing the fluorine atoms. — PDS

ACS Nano 10.1021/nn304834p (2012).

DEVELOPMENT

A Positive Conversion

Tracing the pathways that lead to neuronal differentiation is important both for understanding neurodevelopment and because of the implications for developing therapeutics for degenerative diseases such as Parkinson's and Alzheimer's disease. Recent experiments have demonstrated that a group of transcription factors are capable of converting fibroblasts into neuronal cells in vitro and that the process involves microRNAs. To better understand the process, Xue *et al*. studied the role of a particular polypyrimidine-tract–binding protein (PTB) that is repressed during normal brain development by a microRNA, miR-124, and is known to be involved in the regulation of splicing of mRNA. Knockdown of PTB expression in HeLa cells, human embryonic carcinoma stem cells, mouse neural progenitor cells, and primary mouse embryonic fibroblasts induced a neuronal morphology and, for two of the cell types, expression of neuronal markers as well as synaptic activity. PTB not only acts as a target of miR-124, but also serves as a negative regulator of miRNA-124 and other microRNAS. An important consequence of PTB inhibition is the disassembly of the REST complex, which normally acts to silence neuronal genes in non-neuronal cells. Thus, the net result is to change a negative regulatory loop into a positive one and induce neuronal differentiation. — BJ

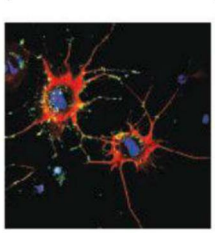

Cell 10.1016/j.cell.2012.11.045 (2013).

GEOLOGY

Flat Weathering

Weathering of silicate minerals is a primary sink for atmospheric CO_2. Much of the focus of recent research has been on the erosion of mountain belts, but as shown by Willenbring *et al.*, areas of lower relief may be more important in global budgets. These authors compiled measurements of denudation rates based on ^{10}Be concentrations in sediments. ^{10}Be is produced by the bombardment of near-surface minerals by cosmic rays; it builds up in stable landscapes and thus tracks both physical erosion and chemical weathering. The authors compared the denudation rates versus overall landscape slopes across nearly 1000 river basins globally and used these data to extrapolate to other areas. Overall, they calculate that about 5 gigatons of sediments are produced each year. Because most of Earth's surface has modest or lower slopes, even though the denudation rate there is relatively low (<10 mm per 1000 years), these areas contribute most of the sediment to the oceans. Thus, these areas, not mountains, may dominate the long-term drawdown of atmospheric CO_2. — BH

Geology 10.1130/G33918.1 (2013).

MATERIALS SCIENCE

Clicking Bones

A challenge in developing drug delivery vehicles or other tissue-specific biomaterials is to find ways to target them to the organs or tissues of interest. Heller *et al.* focused their study on modified dextran polymers, which can form porous nanoscale hydrogel particles. The dextran was initially modified with either alkyne or azide groups, which could then be clicked together within an inverse emulsion. The ratio of the two starting materials was biased to produce gels that had an excess of either alkyne or azide groups to allow for further functionalization of the gels. When injected into mice, unmodified dextran gels primarily accumulated in the liver as well as the lymph nodes, spine, and femur. Further, gels that entered the bone marrow were engulfed by F4/80+ cells. Bisphosphonates have been used to treat osteoporosis and have been coupled to polymers that have shown bone-tissue localization; thus, this group was added via a second click reaction to gels showing excess alkyne groups. Once modified via a second click reaction to show bisphosphonates groups, the nanogel particles showed significantly less uptake by the liver and reduced uptake by the F4/80+ cells. The particles also showed binding to both cortical and trabecular bone lining the marrow cavities. Perhaps more interesting was the overall reduction in F4/80+ cells within the bone marrow, suggesting that they might also provide an anti-osteoporotic effect. — MSL

Adv. Mater. 10.1002/adma201202881 (2012).

CREDITS (TOP TO BOTTOM): J. T. ROBINSON; Y. XUE *ET AL.*, *CELL* **152** (17 JANUARY 2013) © 2013 ELSEVIER INC.

CELL BIOLOGY

Rab-ing Up ER Dynamics

The endoplasmic reticulum (ER) forms a lace-like network throughout the cytoplasm and exhibits a remarkable ability to remodel itself constantly. How the membranes of the ER can grow, fuse, and divide faithfully and efficiently within cells is not altogether clear, although several factors involved in the regulation of ER dynamics have been identified. Intracellular membrane fusion frequently involves members of the Rab GTPase family. English and Voeltz wanted to determine which Rab was involved in ER dynamics. ER vesicles were isolated from *Xenopus* egg extracts and shown to be able to form tubular ER networks in vitro. Although several Rab GTPases were associated with these vesicles, only Rab10 localized to ER-associated structures that could move along microtubules and that appeared to be associated with new ER tubules in mammalian tissue culture cells. Reducing the levels of Rab10 or the expression of a Rab10 mutant reduced the number of ER tubules, because of an impaired ability of dynamic ER tubules to grow from and fuse with other ER membranes. Intriguingly, the Rab10 ER tip structures were also associated with a pair of proteins involved in phospholipid synthesis. — SMH

Nat. Cell Biol. 10.1038/ncb.2647 (2012).

ENVIRONMENTAL SCIENCE

Don't Throw It in the Bin!

Compact fluorescent lamp (CFL) and light-emitting diode (LED) bulbs use between 70 and 85% less energy than traditional incandescent bulbs and have vastly longer lifetimes, providing the potential for substantial energy savings. However, they are much more complex in design than traditional bulbs, with potential adverse environmental impacts similar to those of consumer electronic devices. Lim *et al.* have assessed the environmental and resource depletion impacts from metals in all three types of bulbs, focusing on the bulbs' end of life. The metal content of CFL and LED bulbs was much higher than that of incandescent bulbs, exceeding California's regulatory limits for lead, copper, and zinc in the case of CFL bulbs and for copper and lead in the case of LED bulbs; both types of bulbs would be classified as hazardous waste under U.S. federal and California state regulations. Furthermore, the availability of several metals contained in the bulbs is highly limited. There is thus an urgent need for appropriate waste management, as well as technological development to reduce the content of toxic or rare metals in the bulbs and/or extend bulb lifetimes. — JFU

Environ. Sci. Tech. 10.1021/es302886m (2012).

CREDIT: OLADELE OGUNSEITAN

IMMUNOLOGY

HIV Under Pressure

The RV144 HIV-1 vaccine trial was the first clinically validated preventative vaccine to show efficacy against HIV infection. Since the release of these results, there has been great interest in understanding how protection occurred. Protection correlated with antibodies against the V1 and V2 regions of the gp120 envelope protein of HIV-1. In addition, increased efficacy was seen against virus strains that matched the vaccine strain at V2 residue 169. Liao *et al.* isolated four antibodies from RV144 vaccines that were specific for V2 and residue 169. These antibodies were able to neutralize several lab strains of HIV-1 and could kill $CD4^+$ T cells that were infected with field-isolated strains of the virus. Structural analysis of two of the antibodies, along with a previously described broadly neutralizing antibody that recognizes V2, demonstrated that although the antibodies recognized similar residues of V2, these residues were in very different conformations. Such structural variation suggests that this may be a site of viral vulnerability and implies that the vaccine may have induced immune pressure in this region. — KLM

Immunity 10.1016/j.immuni.2012.11.011 (2013).

DNA Clean & Concentrator™ (DCC™)

DNA Clean-up from Diverse Sources

- ✓ PCR, RE digests, RT reactions, etc.
- ✓ Genomic DNA clean-up
- ✓ PCR Inhibitor removal

Get your DCC™ sample at
www.zymoresearch.com/DCC

ZYMO RESEARCH
The Beauty of Science is to Make Things Simple

www.sciencemag.org

Science

1200 New York Avenue, NW
Washington, DC 20005
Editorial: 202-326-6550, FAX 202-289-7562
News: 202-326-6581, FAX 202-371-9227
Bateman House, 82-88 Hills Road
Cambridge, UK CB2 1LQ
+44 (0) 1223 326500, FAX +44 (0) 1223 326501

Subscription Services For change of address, missing issues, new orders and renewals, and payment questions: 866-434-AAAS (2227) or 202-326-6417, FAX 202-842-1065. Mailing addresses: AAAS, P.O. Box 96178, Washington, DC 20090-6178 or AAAS Member Services, 1200 New York Avenue, NW, Washington, DC 20005

Institutional Site Licenses please call 202-326-6755 for any questions or information

Reprints: Author Inquiries 800-635-7181
Commercial Inquiries 803-359-4578

Permissions 202-326-7074, FAX 202-682-0816

Member Benefits AAAS Travels: Betchart Expeditions 800-252-4910; Apple Store www.store.apple.com/us/go/eppstore/aaas; NASA Federal, 1-888-NASA-FCU (1-888-627-2328) or www.nasafcu.com; Cold Spring Harbor Laboratory Press Publications www.cshlpress.com/affiliates/aaas.htm; GEICO Auto Insurance www.geico.com/landingpage/go51.htm?logo=17624; Hertz 800-654-2200 CDP#343457; Office Depot https://bsd.officedepot.com/portalLogin.do; Seabury & Smith Life Insurance 800-424-9883; Subaru VIP Program 202-326-6417; VIP Moving Services www.vipmayflower.com/domestic/index.html; Other Benefits: AAAS Member Services 202-326-6417 or www.aaasmember.org.

science_editors@aaas.org	(for general editorial queries)
science_letters@aaas.org	(for queries about letters)
science_reviews@aaas.org	(for returning manuscript reviews)
science_bookrevs@aaas.org	(for book review queries)

Published by the American Association for the Advancement of Science (AAAS), *Science* serves its readers as a forum for the presentation and discussion of important issues related to the advancement of science, including the presentation of minority or conflicting points of view, rather than by publishing only material on which a consensus has been reached. Accordingly, all articles published in *Science*—including editorials, news and comment, and book reviews—are signed and reflect the individual views of the authors and not official points of view adopted by AAAS or the institutions with which the authors are affiliated.

AAAS was founded in 1848 and incorporated in 1874. Its mission is to advance science, engineering, and innovation throughout the world for the benefit of all people. The goals of the association are to: enhance communication among scientists, engineers, and the public; promote and defend the integrity of science and its use; strengthen support for the science and technology enterprise; provide a voice for science on societal issues; promote the responsible use of science in public policy; strengthen and diversify the science and technology workforce; foster education in science and technology for everyone; increase public engagement with science and technology; and advance international cooperation in science.

Information for Authors
See pages 752 and 753 of the 10 February 2012 issue or access www.sciencemag.org/about/authors

EDITOR-IN-CHIEF **Bruce Alberts**
EXECUTIVE EDITOR **Monica M. Bradford** NEWS EDITOR **Colin Norman**
MANAGING EDITOR, RESEARCH JOURNALS **Katrina L. Kelner**
DEPUTY EDITORS **R. Brooks Hanson, Barbara R. Jasny, Andrew M. Sugden, Valda J. Vinson**

Editorial senior editors/commentary Lisa D. Chong, Brad Wible; **senior editors** Gilbert J. Chin, Pamela J. Hines, Paula A. Kiberstis (Boston), Marc S. Lavine (Toronto), Beverly A. Purnell, L. Bryan Ray, Guy Riddihough, H. Jesse Smith, Phillip D. Szuromi (Tennessee), Jake S. Yeston, Laura M. Zahn (San Diego); **associate editors** Melissa R. McCartney (Education Projects), Kristen L. Mueller, Jelena Stajic, Sacha Vignieri (Oregon), Nicholas S. Wigginton; **book review editor** Sherman J. Suter; **associate letters editor** Jennifer Sills; **editorial manager** Cara Tate; **senior copy editors** Jeffrey E. Cook, Cynthia Howe, Harry Jach, Lauren Kmec, Barbara P. Ordway, Trista Wagoner; **copy editor** Chris Filiatreau; **senior editorial coordinators** Carolyn Kyle, Beverly Shields; **editorial coordinators** Joi S. Granger, Anita Wynn; **publications assistants** Ramatoulaye Diop, Aneera Dobbins, Jeffrey Hearn, Lisa Johnson, Dona Mathieu, Le-Toya Mayne Flood, Shannon McMahon, Scott Miller, Jerry Richardson, Teresa R. Sakon, Brian White; **editorial assistant** Patricia M. Moore; **executive editorial assistant** Yolanda O'Bannon (San Francisco); **executive assistant** Alison Crawford; **administrative support** Maryrose Madrid

Editorial director, web and new media Stewart Wills; **senior web editor** Sarah Crespi; **web editor** Kerry Klein; **web development manager** Martyn Green; **web developers** Corinna Cohn, Andrew Whitesell

News deputy news editors Robert Coontz, David Grimm (Online), Eliot Marshall, Jeffrey Mervis, Leslie Roberts, Richard Stone, John Travis; **contributing editors** Elizabeth Culotta, Polly Shulman; **news writers** Yudhijit Bhattacharjee, Adrian Cho, Jennifer Couzin-Frankel, Carolyn Gramling, Jocelyn Kaiser, Richard A. Kerr, David Malakoff, Elizabeth Pennisi, Robert F. Service (Pacific NW), Erik Stokstad, Emily Underwood; **web developer** Daniel Berger; **social media strategist** Meghna Sachdev; **intern** Lizzie Wade; **contributing correspondents** John Bohannon, Jon Cohen (San Diego, CA), Ann Gibbons, Sam Kean, Eli Kintisch, Andrew Lawler, Mitch Leslie, Charles C. Mann, Virginia Morell, Gary Taubes; **copy editors** Melissa Raimondi, Kara Estelle, Linda B. Felaco; **administrative support** Scherraine Mack; **bureaus** San Diego, CA: 760-942-3252, FAX 760-942-4979; Pacific Northwest: 503-963-1940

Production director Wendy K. Shank; **assistant manager** Rebecca Doshi; **senior specialists** Steve Forrester, Christopher Redwood, Anthony Rosen; **Preflight director** David M. Tompkins; **manager** Marcus Spiegler; **specialists** Jason Hillman, Tara Kelly

Art director Yael Fitzpatrick; **associate art director** Laura Creveling; **senior illustrators** Chris Bickel, Katharine Sutliff; **illustrator** Yana Hammond; **senior art associates** Holly Bishop, Preston Huey; **art associates** Kay Engman, Garvin Grullón, Chrystal Smith; **photo editor** Leslie Blizard

***Science* International**

Europe (science@science-int.co.uk) **editorial: international managing editor** Andrew M. Sugden; **senior editor/commentary** Julia Fahrenkamp-Uppenbrink; **senior editors** Caroline Ash, Stella M. Hurtley, Ian S. Osborne, Peter Stern; **associate editor** Maria Cruz; **contributing editor** Helen Pickersgill; **editorial support** Rachel Roberts, Alice Whaley; **administrative support** Janet Clements, Jenny Hinson, John Wood; **news: deputy news editor, u.k.** Daniel Clery; **contributing editor, europe** Martin Enserink; **contributing correspondents** Michael Balter (Paris), Kai Kupferschmidt (Berlin), Gretchen Vogel (Berlin)

Asia Japan Office: Asca Corporation, Tomoko Furusawa, Rustic Bldg. 7F, 77 Tenjin-cho, Shinjuku-ku, Tokyo 162-0808, Japan; +81 3 6802 4616, FAX +81 3 6802 4615, inquiry@sciencemag.jp; **contributing correspondents** Dennis Normile [Japan: +81 (0) 3 3391 0630, FAX +81 (0) 3 5936 3531; dnormile@gol.com]; Hao Xin [China: cindyhao@gmail.com]; Mara Hvistendahl [China: mhvisten@aaas.org]; Pallava Bagla [South Asia: +91 (0) 11 2271 2896; pbagla@vsnl.com]

EXECUTIVE PUBLISHER **Alan I. Leshner**
PUBLISHER **Beth Rosner**

Fulfillment Systems and Operations (membership@aaas.org); **customer service supervisor** Pat Butler; **specialists** LaToya Casteel, Michelle Ofordire, April Marshall; **manager, data entry** Mickie Napoleoni; **data entry specialists** Tarrika Hill, JJ Regan, Eva Mae Campbell

Business Operations and Administration director Deborah Rivera-Wienhold; **business systems and financial analysis director** Randy Yi; **manager, fulfillment systems** Frits Buninghe; **systems analyst** Nicole Mehmedovich; **manager, business analysis** Eric Knott; **manager, business operations** Jessica Tierney; **business analysts** Cory Lipman, Celeste Troxler; Christine Wehrli; **financial analyst** Julia Nguyen; **rights and permissions: administrator** Emilie David; **associate** Elizabeth Sandler; **marketing director** Ian King; **marketing managers** Allison Pritchard, Alison Chandler, Julianne Wielga, Samantha Smith; **marketing associates** Aimee Aponte, Mary Ellen Crowley, Elizabeth Sattler, Rebecca Riffkin; **senior marketing executive** Jennifer Reeves; **director, site licensing** Tom Ryan; **director, corporate relations** Eileen Bernadette Moran; **senior publisher relations specialist** Kiki Forsythe; **publisher relations manager** Catherine Holland; **publisher relations, eastern region** Keith Layson; **publisher relations, western region** Ryan Rexroth; **customer relations manager** Iquo Edim; **marketing manager** Christina Schlecht; **marketing associates** Paulina Curto, Mitchell Edmund; **customer relations associate:** Joe Horn; **electronic media: director** Lizabeth Harman; **assistant manager** Lisa Stanford; **production specialists** Antoinette Hodal, Nichele Johnston, Lori Murphy, Kimberly Oster; **web and new media: senior project manager** Trista Smith, **project leader** Luke Johnson **computer specialists** Walter Jones, Kai Zhang, **web developer** Jeremy Bates; **program director, aaas member central** Peggy Mihelich

director, global collaboration, custom publications, advertising Bill Moran
editor, custom publishing Sean Sanders: 202-326-6430
assistant editor, custom publishing Tianna Hicklin 202-326-6463
associate director, collaboration, custom publications/china/taiwan/korea/singapore Ruolei Wu +86-1367-101-5294

Product (science_advertising@aaas.org); **midwest** Rick Bongiovanni: 330-405-7080, FAX 330-405-7081; **east coast/e. canada** Laurie Faraday: 508-747-9395, FAX 617-507-8189; **west coast/w. canada** Lynne Stickrod: 415-931-9782, FAX 415-520-6940; **uk europe/asia** Roger Goncalves: TEL/FAX +41 43 243 1358; **japan,** Makiko Hara: +81 (0) 3 6802 4616, FAX +81 (0) 3 6802 4615; ads@sciencemag.jp; **china/taiwan** Ruolei Wu: +86 1367 1015 294 rwu@aaas.org
worldwide associate director of *Science* Careers Tracy Holmes: +44 (0) 1223 326525, FAX +44 (0) 1223 326532

Classified (advertise@sciencecareers.org); **u.s.: east coast/west coast/south central/south america** Tina Burks: 202-326-6577; **midwest/canada/industry** Allyson Rosen: 202-326-6578; **sales administrator** Marci Gallun; **europe/row sales** Benjamin Asfaha, Lucy Nelson; **sales assistant** Kelly Grace; **japan** Yuri Kobayashi +81 (6) 6627-9250; careerads@sciencemag.jp; **china/taiwan** Ruolei Wu: +86 1367 1015 294 rwu@aaas.org; **advertising support manager** Karen Foote: 202-326-6740; **advertising production operations manager** Deborah Tompkins; **senior production specialist/graphic designer** Amy Hardcastle; **production specialist** Yuse Lajiminmuhip; **senior traffic associate** Christine Hall; **sales coordinator** Shirley Young

AAAS Board of Directors retiring president, chair Nina V. Fedoroff; **president** William H. Press; **president-elect** Phillip A. Sharp; **treasurer** David E. Shaw; **chief executive officer** Alan I. Leshner; **board** May R. Berenbaum, Bonnie L. Bassler, Stephen L. Mayo, Raymond Orbach, Julia M. Phillips, Sue V. Rosser, David D. Sabatini, Inder M. Verma

AAAS
ADVANCING SCIENCE, SERVING SOCIETY

SENIOR EDITORIAL BOARD

A. Paul Alivisatos, *Lawrence Berkeley Nat'l. Laboratory*
Cori Bargmann, *The Rockefeller Univ.*
Ernst Fehr, *Univ. of Zurich*
Erin O'Shea, *Harvard Univ.*
Michael S. Turner, *University of Chicago*

BOARD OF REVIEWING EDITORS

Adriano Aguzzi, *Univ. Hospital Zürich*
Takuzo Aida, *Univ. of Tokyo*
Sonia Altizer, *Univ. of Georgia*
Sebastian Amigorena, *Institut Curie*
Angelika Amon, *MIT*
Kathryn Anderson, *Memorial Sloan-Kettering Cancer Center*
Siv G. E. Andersson, *Uppsala Univ.*
Peter Andolfatto, *Princeton Univ.*
Meinrat O. Andreae, *Max Planck Inst., Mainz*
Paola Arlotta, *Harvard Univ.*
Johan Auwerx, *EPFL*
David Awschalom, *Univ. of California Santa Barbara*
Ben Barres, *Stanford Medical School*
Jordi Bascompte, *Estación Biológica de Doñana, CSIC*
Facundo Batista, *London Research Inst.*
Ray H. Baughman, *Univ. of Texas, Dallas*
David Baum, *Univ. of Wisconsin*
Mark Bear, *Massachusetts Inst. of Technology*
Yasmine Belkaid, *NIAID, NIH*
Philip Benfey, *Duke Univ.*
Stephen J. Benkovic, *Penn State Univ.*
Christophe Bernard, *Aix-Marseille Univ.*
Gregory C. Beroza, *Stanford Univ.*
Gabriele Bergers, *Univ. of California, San Francisco*
Peer Bork, *EMBL*
Bernard Bourdon, *Ecole Normale Superieure de Lyon*
Chris Bowler, *Ecole Normale Supérieure*
Ian Boyd, *Univ. of St. Andrews*
Christian Büchel, *Universitätsklinikum Hamburg-Eppendorf*
Joseph A. Burns, *Cornell Univ.*
William P. Butz, *Population Reference Bureau*
Gyorgy Buzsaki, *New York Univ., School of Medicine*
Mats Carlsson, *Univ. of Oslo*
Mildred Cho, *Stanford Univ.*
David Clapham, *Children's Hospital, Boston*
David Clary, *Univ. of Oxford*
Jonathan D. Cohen, *Princeton Univ.*
Robert Cook-Deegan, *Duke Univ.*
James Collins, *Boston Univ.*
Alan Cowman, *Walter & Eliza Hall Inst.*
Robert H. Crabtree, *Yale Univ.*
Wolfgang Cramer, *Mediterranean Inst. of Biodiversity and Ecology*
Jeff L. Dangl, *Univ. of North Carolina*
Tom Daniel, *Univ. of Washington*
Frans de Waal, *Emory Univ.*
Stanislas Dehaene, *Collège de France*
Robert Desimone, *MIT*
Claude Desplan, *New York Univ.*
Ap Dijksterhuis, *Radboud Univ. of Nijmegen*
Dennis Discher, *Univ. of Pennsylvania*
Gerald W. Dorn II, *Washington Univ. School of Medicine*
Jennifer A. Doudna, *Univ. of California, Berkeley*
Julian Downward, *Cancer Research UK*
Bruce Dunn, *Univ. of California, Los Angeles*
Christopher Dye, *WHO*
David Ehrhardt, *Carnegie Inst. of Washington*
Tim Elston, *Univ. of North Carolina at Chapel Hill*
Gerhard Ertl, *Fritz-Haber-Institut, Berlin*
Barry Everitt, *Univ. of Cambridge*
Paul G. Falkowski, *Rutgers Univ.*
Ernst Fehr, *Univ. of Zurich*
Tom Fenchel, *Univ. of Copenhagen*
Michael Feuer, *The George Washington Univ.*
Alain Fischer, *INSERM*
Susan Fiske, *Princeton Univ.*
Anne C. Ferguson-Smith, *Univ. of Cambridge*
Peter Fratzl, *Max Planck Inst.*
Elaine Fuchs, *Rockefeller Univ.*
Wulfram Gerstner, *EPFL Lausanne*
Andrew Gewirth, *Univ. of Illinois*
Karl-Heinz Glassmeier, *TU Braunschweig*
Elizabeth Grove, *Univ. of Chicago*
Kip Guy, *St. Jude's Children's Research Hospital*
Taekjip Ha, *Univ. of Illinois at Urbana-Champaign*
Christian Haass, *Ludwig Maximilians Univ.*
Steven Hahn, *Fred Hutchinson Cancer Research Center*
Gregory J. Hannon, *Cold Spring Harbor Lab.*
Martin Heimann, *Max Planck Inst., Jena*
Yka Helariutta, *Univ. of Finland*
Isaac Held, *NOAA*
James A. Hendler, *Rensselaer Polytechnic Inst.*
Janet G. Hering, *Swiss Fed. Inst. of Aquatic Science & Technology*
Ray Hilborn, *Univ. of Washington*
Michael E. Himmel, *National Renewable Energy Lab.*
Kai-Uwe Hinrichs, *Univ. of Bremen*
Kei Hirose, *Tokyo Inst. of Technology*
David Hodell, *Univ. of Cambridge*
David Holden, *Imperial College*
Lora Hooper, *UT Southwestern Medical Ctr at Dallas*
Jeffrey A. Hubbell, *EPFL Lausanne*
Thomas Hudson, *Ontario Inst. for Cancer Research*
Ray Huey, *Univ. of Washington*
Steven Jacobsen, *Univ. of California, Los Angeles*
Kai Johnsson, *EPFL Lausanne*
Peter Jonas, *Universität Freiburg*
Matt Kaeberlein, *Univ. of Washington*
William Kaelin Jr., *Dana-Farber Cancer Inst.*
Daniel Kahne, *Harvard Univ.*
Daniel Kammen, *Univ. of California, Berkeley*
Joel Kingsolver, *Univ. of North Carolina at Chapel Hill*
Robert Kingston, *Harvard Medical School*
Roberto Kolter, *Harvard Medical School*
Alberto R. Kornblihtt, *Univ. of Buenos Aires*
Leonid Kruglyak, *Princeton Univ.*
Thomas Langer, *Univ. of Cologne*
Mitchell A. Lazar, *Univ. of Pennsylvania*
David Lazer, *Harvard Univ.*
Virginia Lee, *Univ. of Pennsylvania*
Ottoline Leyser, *Cambridge Univ.*
Olle Lindvall, *Univ. Hospital, Lund*
Marcia C. Linn, *Univ. of California, Berkeley*
Jianguo Liu, *Michigan State Univ.*
Luis Liz-Marzan, *CIC biomaGUNE*
Jonathan Losos, *Harvard Univ.*
Ke Lu, *Chinese Acad. of Sciences*
Christian Lüscher, *Univ. of Geneva*
Laura Machesky, *CRUK Beatson Inst. for Cancer Research*
Anne Magurran, *Univ. of St Andrews*
Oscar Marin, *CSIC & Univ. Miguel Hernández*
Charles Marshall, *Univ. of California, Berkeley*
Chris Marshall, *Inst. of Cancer Research*
Martin M. Matzuk, *Baylor College of Medicine*
C. Robertson McClung, *Dartmouth College*
Graham Medley, *Univ. of Warwick*
Yasushi Miyashita, *Univ. of Tokyo*
Richard Morris, *Univ. of Edinburgh*
Edvard Moser, *Norwegian Univ. of Science and Technology*
Sean Munro, *MRC Lab. of Molecular Biology*
Thomas Murray, *The Hastings Center*
Naoto Nagaosa, *Univ. of Tokyo*
James Nelson, *Stanford Univ. School of Med.*
Daniel Neumark, *Univ. of California, Berkeley*
Timothy W. Nilsen, *Case Western Reserve Univ.*
Pär Nordlund, *Karolinska Inst.*
Helga Nowotny, *European Research Advisory Board*
Luke O'Neill, *Trinity College, Dublin*
Stuart Newman, *New York Medical College*
N. Phuan Ong, *Princeton Univ.*
Joe Orenstein, *Univ. of California, Berkeley & Lawrence Berkeley National Lab*
Stuart H. Orkin, *Dana-Farber Cancer Inst.*
Harry Orr, *Univ. of Minnesota*
Andrew Oswald, *Univ. of Warwick*
Steve Palumbi, *Stanford Univ.*
Jane Parker, *Max-Planck Inst. of Plant Breeding Research*
Donald R. Paul, *Univ. of Texas at Austin*
P. David Pearson, *Univ. of California, Berkeley*
John H. J. Petrini, *Memorial Sloan-Kettering Cancer Center*
Simon Phillpot, *Univ. of Florida*
Joshua Plotkin, *Univ. of Pennsylvania*
Philippe Poulin, *CNRS*
Colin Renfrew, *Univ. of Cambridge*
Trevor Robbins, *Univ. of Cambridge*
Jim Roberts, *Fred Hutchinson Cancer Research Ctr.*
Barbara A. Romanowicz, *Univ. of California, Berkeley*
Jens Rostrup-Nielsen, *Haldor Topsoe*
Mike Ryan, *Univ. of Texas, Austin*
Shimon Sakaguchi, *Kyoto Univ.*
Miquel Salmeron, *Lawrence Berkeley National Lab*
Jürgen Sandkühler, *Medical Univ. of Vienna*
Alexander Schier, *Harvard Univ.*
Randy Seeley, *Univ. of Cincinnati*
Vladimir Shalaev, *Purdue Univ.*
Joseph Silk, *Institut d'Astrophysique de Paris*
Denis Simon, *Arizona State Univ.*
Alison Smith, *John Innes Centre*
Davor Solter, *Inst. of Medical Biology, Singapore*
Peter Sorger, *Harvard Medical School*
John Speakman, *Univ. of Aberdeen*
Allan C. Spradling, *Carnegie Institution of Washington*
Jonathan Sprent, *Garvan Inst. of Medical Research*
Paula Stephan, *Georgia State Univ. and National Bureau of Economic Research*
Elsbeth Stern, *ETH Zürich*
Ira Tabas, *Columbia Univ.*
Yoshiko Takahashi, *Kyoto University*
Sarah Teichmann, *Cambridge Univ.*
John Thomas, *Duke Univ.*
Herbert Virgin, *Washington Univ.*
Bert Vogelstein, *Johns Hopkins Univ.*
Cynthia Volkert, *Univ. of Göttingen*
Bruce D. Walker, *Harvard Medical School*
Douglas Wallace, *Dalhousie Univ.*
Ian Walmsley, *Univ. of Oxford*
David A. Wardle, *Swedish Univ. of Agric Sciences*
David Waxman, *Fudan Univ.*
Jonathan Weissman, *Univ. of California, San Francisco*
Sue Wessler, *Univ. of California, Riverside*
Kathy Willis, *Oxford Univ.*
Ian A. Wilson, *The Scripps Res. Inst.*
Timothy D. Wilson, *Univ. of Virginia*
Rosemary Wyse, *Johns Hopkins Univ.*
Jan Zaanen, *Leiden Univ.*
Kenneth Zaret, *Univ. of Penn. School of Medicine*
Mayana Zatz, *University of Sao Paolo*
Jonathan Zehr, *Univ. of California, Santa Cruz*
Maria Zuber, *MIT*

BOOK REVIEW BOARD

John Aldrich, *Duke Univ.*
David Bloom, *Harvard Univ.*
Angela Creager, *Princeton Univ.*
Richard Shweder, *Univ. of Chicago*
Ed Wasserman, *DuPont*
Lewis Wolpert, *Univ. College London*

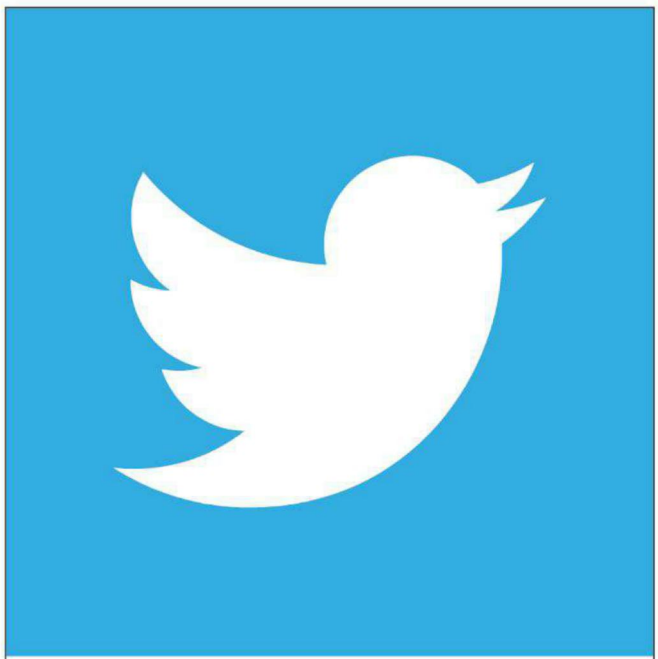

Join the Conversation!

Twitter is a great way to connect with AAAS members and staff about the issues that matter to you most. Be a part of the discussion while staying up-to-date on the latest news and information about your personal member benefits.

Follow us @AAASmember and join the conversation with #AAAS

AAAS MEMBERCENTRAL
MemberCentral.aaas.org

Powder Handling Glove Box used for small-scale handling / weighing of active pharmaceutical ingredients ("API's") in powder form.

Controlled Atmosphere Chambers | PCR (UV) Chambers | Compact Analytical Balance Chamber

Hypoxia Chambers
Anaerobic Chambers
Temperature & Humidity
Nitrogen Dry Box

PCR (UV) Chambers
HEPA Filtered PCR Chamber

Compact Glove Box
HEPA Filtration
Four (4) Standard Sizes
Custom Sizes Available

PLAS ■ LABS, INC.
www.PLAS-LABS.com
800-866-7527

The **Network of Diaspora in Engineering and Science (NODES)** in partnership with **Ireland's Presidency of the European Union** cordially invites interested participants to the

SCIENCE AND ENGINEERING

Join a panel of distinguished guests sharing their perspectives on diaspora networks. Breakout sessions will follow to discuss "IT Platforms and networks for diaspora engagement", "Women diaspora networks", "Funding and diaspora activities" and "Institutional perspectives (Universities, NGO) for diaspora engagement". The event registration is now closed. However, if you and/or the organization you represent want to join the discussion, or to learn more about NODES, please send us an email with your mission statement and a short explanation on how participation in the roundtable will benefit your diaspora engagement efforts at diaspora@aaas.org.

DIASPORA ENGAGEMENT

AAAS | 2013 ANNUAL MEETING

FEBRUARY 14TH • BOSTON, MA

AAAS

AROUND THE WORLD

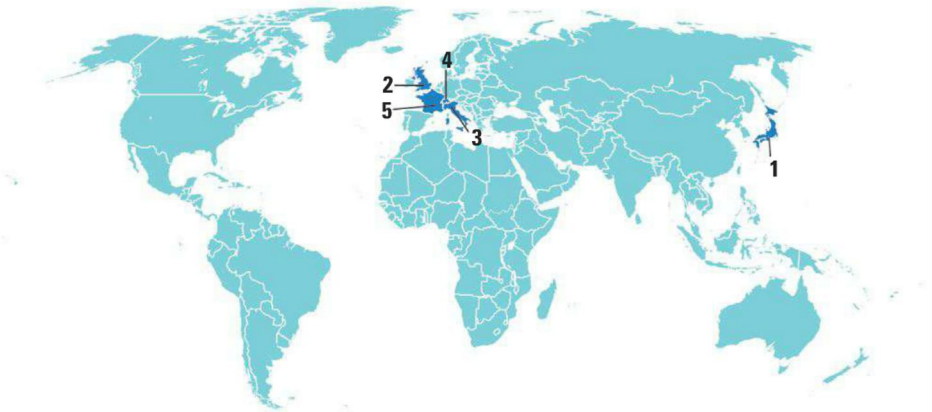

Tokyo, Japan **1**

Stimulus Pushes Japan's Science Spending to Record Level

An economic stimulus package that includes $11 billion worth of science-related spending will—when combined with previously planned spending—bring Japan's national and local government support for research for the fiscal year through March to a record $57 billion. But there are high expectations of an economic payoff.

The stimulus package includes $958 million to upgrade research infrastructure, $107 million for disaster prevention and mitigation studies, $238 million for research on induced pluripotent stem cells and other regenerative therapies, and $437 million for next-generation energy technologies.

The largest item, however, is $2 billion to promote university-industry collaboration, including money to equip universities to conduct industrially relevant research as well as to support actual R&D. "Even though Japan is strong in basic research and funding is increasing, I think it's true that there is little connection to industry," says Kazuhito Hashimoto, a physical chemist at the University of Tokyo. Hashimoto helped take a self-cleaning photocatalytic material from a laboratory discovery to commercial use in building siding and other products.

Culham, U.K. **2**

Fusion Road Map for Europe

The European Fusion Development Agreement has published its road map to move fusion research forward from ITER—a giant international reactor under construction in France that will be the first to produce useful amounts of energy—to an industry-ready prototype fusion power plant by 2050. ITER

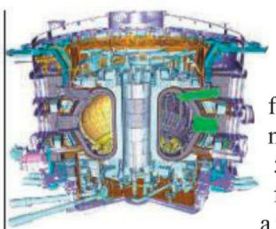

is expected to produce the first net energy gain from fusion: 500 megawatts from a 50 MW input for a few minutes at a time.

The next step will be a prototype power plant dubbed DEMO—but the road map notes a daunting list of technical hurdles to this. Those challenges include more work on how to extract exhaust heat—current designs wouldn't survive the high power and continuous operation of DEMO. Advanced materials able to withstand the intense neutron bombardment from DEMO's reactions will also be needed, along with new ways to use those neutrons to breed more tritium fuel for fusion in the lining of the reactor. With any luck, DEMO might start generating power in the early 2040s. **http://scim.ag/EFDAmap**

Parma, Italy **3**

E.U. Watchdog: Pesticides Threaten Bees

Three pesticides used by European farmers pose an "acute risk" to honey bees, according to the European Food Safety Authority (EFSA). In three studies published last week, EFSA assessed the risks posed to bees by three types of neonicotinoid insecticides: clothianidin, imidacloprid, and thiamethoxam. This family of pesticides has been used by European farmers since the early 1990s and is sold by Syngenta in Basel, Switzerland, and Bayer CropScience in Monheim, Germany. EFSA says none of the three should be used on crops that are attractive to bees, such as maize, rapeseed, or sunflower. Although the study does not link

Osmia ribifloris, a blueberry pollinator.

the pesticides to the collapse of whole bee colonies, the agency's advice could open the door to a neonicotinoid ban in the European Union. **http://scim.ag/beepest**

Geneva, Switzerland **4**

Accord on Global Mercury Limits

After an all-night session that capped 4 years of negotiations, delegates from 140 countries agreed on 19 January to limit mercury pollution. The Minamata Convention—named for a Japanese city where mercury poisoning injured or killed thousands of people—mandates the phase-out of mercury in some batteries, fluorescent lamps, cosmetics, and medical devices by 2020. It sets limits on mercury emissions from coal-fired power plants, waste incineration, and cement factories. Countries with small-scale gold mining must devise strategies to reduce or eliminate mercury use. The treaty allows the use of mercury as a vaccine preservative.

The Zero Mercury Working Group called the treaty a step forward but said controls on the two largest sources of pollution—coal-fired power plants and small-scale gold mining—were disappointingly weak. The treaty will be open for signatures at a meeting in Minamata in October. **http://scim.ag/mercacc**

Grenoble, France **5**

Mathematicians Eye Researcher-Run Publishing

Mathematicians aim to launch a slew of new open access peer-reviewed journals this spring utilizing the software of arXiv, a repository that holds more than half a million preprint articles in mathematics, physics, and other fields. The initiative, called the Episciences Project, is led by Jean-Pierre Demailly, a mathematician at the

CREDITS (TOP TO BOTTOM): USDA; ITER ORGANIZATION 2011; ISTOCKPHOTO.COM

University of Grenoble in France. The aim is for the research community to run its own publishing system, financed by the French government via its Centre for Direct Scientific Communication.

W. Timothy Gowers, a mathematician at the University of Cambridge in the United Kingdom who announced the plans on his blog last Wednesday, is planning to start a journal in additive combinatorics. The idea, he wrote, is that "the parts of the publication process that academics do voluntarily—editing and refereeing—are just as they are for traditional journals, and we do without the parts that cost money, such as copy-editing and typesetting." Gowers, who in January 2012 started a boycott of Amsterdam-based publishing-giant Elsevier that thousands of researchers joined, called for mathematicians to support the effort and suggested "it may later expand into other subjects."

NEWSMAKERS

Three Q's

U.S. Geological Survey (USGS) Director **Marcia McNutt**—a geophysicist who was part of the Obama administration's scientific "dream team"—announced last week that she is leaving her post on 15 February.

Q: What are you proudest of from your time at USGS?

McNutt

M.M.: On a national level, my involvement in *Deepwater Horizon*. [McNutt led the effort to estimate the volume of uncaptured oil from the 2010 spill.] On an institutional basis, it might be [remapping the structure of] USGS … from disciplines that operated like university departments … onto problems that matter, such as energy and minerals, water, climate change, and natural hazards.

Q: And what's your biggest disappointment?

M.M.: We are launching Landsat 8 [on 11 February], but there is still not a plan in place for the continuity of Landsat missions. I think it would just be tragic if what is now a 40-year record of land-use change and climate change were to end with Landsat 8.

Q: Several members of Obama's "dream team" are leaving. What does that mean for the future of science in the administration?

M.M.: It wasn't long until we were hit with things like the oil spill and the Haiti earthquake, and the fact that I already knew people like [Energy Secretary] Steve Chu and [NOAA Administrator] Jane Lubchenco … was such a leg up in getting things done. It wasn't just that it was a team of good scientists, it was a team of people who already had a basis for mutual trust and collaboration. I hope that there will be another dream team that will come in. **http://scim.ag/mcnutt**

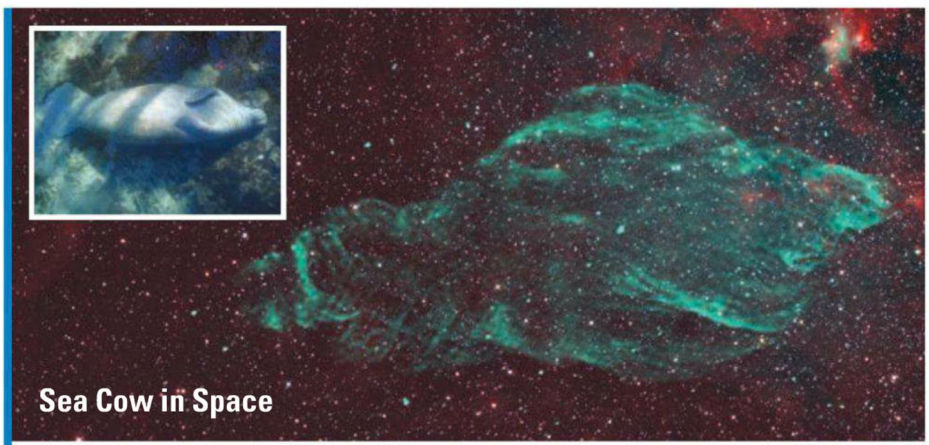
Sea Cow in Space

A distant nebula 18,000 light-years away bears a startling resemblance to Earth's humble manatee—down to the "scars" on its back. Scientists already knew of the giant cloud, called the W50 nebula, which formed when a star went supernova 20,000 years ago. But a new image of it taken by the National Science Foundation's Karl G. Jansky Very Large Array (VLA) has inspired a new name for the object: the Manatee Nebula. The nebula received its new name after someone at the National Radio Astronomy Observatory noticed its resemblance to a manatee floating on its back, flippers over tummy (inset). Bright arcs formed by powerful jets of charged particles in the massive cloud mirror the curved boat propeller scars that the endangered animals often bear. And like its namesake, the Manatee Nebula is a whopper: It's 700 light-years across, one of the biggest supernova remnants ever spotted by VLA.

CREDITS (TOP TO BOTTOM): USGS/WIKIMEDIA COMMONS; (INSET) COURTESY OF TRACY COLSON; NRAO/AUI/NSF; K. GOLAP, M. GOSS, NASA'S WIDE FIELD SURVEY EXPLORER (WISE); HHS/WIKIMEDIA COMMONS

Arthritis Detectives Earn Crafoord Prize

A popular quarry for the modern biologist is the mixture of genes and environment that causes disease. For the discovery of a DNA sequence that, when combined with smoking, dramatically increases the risk of rheumatoid arthritis, three rheumatologists have won the Crafoord Prize in Polyarthritis, which includes SEK 4 million ($614,000).

In the 1980s, **Peter Gregersen**, now at the Feinstein Institute for Medical Research in Manhasset, New York, worked with **Robert Winchester** of Columbia University (and molecular biologist Jack Silver) to sequence variants of human leukocyte antigen genes, which are now linked to autoimmune disease. They identified a stretch of five amino acids shared among HLA gene variants that increased the risk of rheumatoid arthritis.

A team led by **Lars Klareskog**, of the Karolinska Institute in Stockholm, then found that Northern Europeans who have this shared sequence and who smoke are 20 to 40 times more likely to develop the disease, compared with four times more likely with just the DNA.

"It's been a long story," Gregersen says. And many scientists hope to uncover others like it.

FINDINGS

Leprosy Bacterium Reprograms Cells

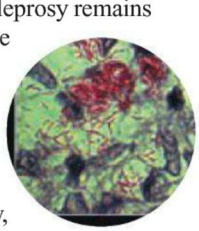

Despite its ancient origins, leprosy remains mysterious—in part because the bacterium that causes leprosy can't be grown in a lab, so it can only be studied in infected humans, armadillos, and genetically engineered mice. Now, a new study in mice shows how the bacterium *Mycobacterium leprae* employs a bit of biological trickery to >>

BY THE NUMBERS

542 Record low number of global guinea worm cases in 2012—good news for the Carter Center's campaign to eradicate the disease, although fighting in Mali might set this back, former President Jimmy Carter noted last week.

14.5% Increase in global measles deaths from 2010 to 2011, according to the World Health Organization, although total measles deaths decreased by 71% from 2000 to 2011.

11 Number of lab-acquired infections reported from 2004 to 2010, according to a first-of-its-kind Centers for Disease Control and Prevention study in *Applied Biosafety*. None were fatal or spread to others.

>>FINDINGS

do its damage: It reprograms certain nerve cells to become like stem cells and uses them to infiltrate the body's muscle and nervous systems.

Biologist Anura Rambukkana of the University of Edinburgh in the United Kingdom and colleagues isolated mice's Schwann cells, which sheathe nerves and help transmit nervous system signals, and infected them with *M. leprae*. The bacteria turned off genes that were expressed in mature Schwann cells and turned on genes associated with earlier stages of cell development—transforming the cells into immature, stemlike cells.

When reintroduced into the mice, some altered cells migrated to muscle tissues, spreading the bacteria. The results suggest that *M. leprae* hijacks Schwann cells so it can use them to infiltrate other tissues in the body, the team reported online last week in *Cell*.

NOTED

>The London headquarters of the Royal Institution—one of the oldest scientific institutions in the world, where Michael Faraday once lectured on electricity—**may be up for sale** for about £60 million ($95 million). Facing financial peril, in 2008 the institution invested in refurbishments, including a restaurant and bar, but failed to recoup those investments.

Dog Domestication Tied To Starchy Diets

The canine's shift from wolf pack to family pet wasn't just about their good behavior. Wolves eat mostly meat, but the first dogs likely dined on roots and cereals, like their human friends—and their genomes reflect that shift. Evolutionary geneticist Erik Axelsson from Uppsala University in Sweden and colleagues compared wolf and dog DNA, looking for regions that were the same in all dogs but variable in wolves; such a lack of variation could indicate that the DNA was important for survival during domestication. Among the more surprising finds were genes for digesting starch. For example, in part depending on the breed, dogs had four to 30 copies of the gene for amylase—(wolves have two copies) and were better at breaking down starch, the researchers reported online this week in *Nature*. "It hints that there are a lot more [genes] to be found that we don't really think about as domestication events," says Elaine Ostrander, a geneticist at the National Human Genome Research Institute in Bethesda, Maryland, who was not connected to the study. **http://scim.ag/dogdomes**

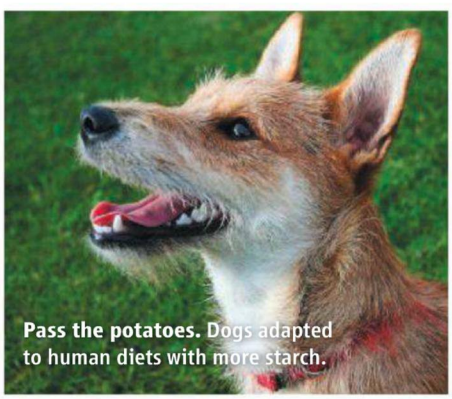

Pass the potatoes. Dogs adapted to human diets with more starch.

Science LIVE

Join us on Thursday, 31 January, at 3 p.m. EST for a live chat **on the science of gun violence. http://scim.ag/science-live**

Random Sample

Pilgrim's Profits

Peaceful pose. An attendee at the 2013 Magh Mela festival.

What's the cost-benefit balance of the world's largest gathering of humans, India's Kumbh Mela? The 3-month-long Hindu festival, held every 12 years, attracts as many as 100 million people to the confluence of the sacred rivers Ganges and Yamuna in Allahabad. On the one hand, there's the potential increase in well-being; for example, computer engineer Ramesh Misra says a ritual bath in the freezing cold water was a "highly fulfilling and blissful" experience that brought him "serenity amidst the seeming superficial chaos."

On the other hand, there are communicable diseases, terrorism, extreme cold, and noise pollution.

For the past 3 years, a team of Indian and British social psychologists have studied the risks and rewards of what they call the "greatest show on Earth." Behavioral psychologist Shruti Tewari of the University of Allahabad teamed up with social psychologist Nick Hopkins of the University of Dundee in the United Kingdom to interview 416 pilgrims to the smaller "Magh Mela" annual festival, which drew about 11 million people to the same spot this year. As a control, the team also interviewed 127 people who live near the festival but did not attend.

The researchers asked the subjects to assess their health and well-being at two times: a month before the festival, and just after it ended. They released their results at a seminar this week at the University of Allahabad. Their conclusion: "an increased sense of well-being" makes the health risks worthwhile.

"Our research shows that people in crowds can form bonds with others, and that this sense of social connection can impact people's identity outside the event," Hopkins says. "It really is time to take crowds—and their positive effects—seriously."

CREDITS (TOP TO BOTTOM): WIKIMEDIA COMMONS; PALLAVA BAGLA

21-gun salute? Customers at a Florida gun shop watch as Barack Obama unveils new firearms proposals.

CREDIT: BRIAN BLANCO/NEWSCOM

PUBLIC HEALTH

Gun Control Agenda Is A Call to Duty for Scientists

When President Barack Obama unveiled an ambitious gun control agenda last week, attention was riveted on his proposals to prevent guns and ammo from falling into the wrong hands. But the administration also moved to get a better understanding of the root causes of gun violence. Declaring the roughly 30,000 firearm-related homicides and suicides each year "a public health crisis," Obama directed the U.S. Centers for Disease Control and Prevention and other agencies to study the causes and prevention of gun violence—ending a 17-year freeze on CDC-sponsored firearms research.

Obama's order is a "startling and wonderful thing," says Stephen Teret, co-director of the Center for Law and the Public's Health at Johns Hopkins University in Baltimore, Maryland. Garen Wintemute, director of the Violence Prevention Research Program at the University of California, Davis, agrees: "Not only will more work get done, but the nature of the work will change dramatically. We'll be able to ask bigger questions."

First, researchers will have to make up for lost time. By the early 1990s, a series of CDC-funded studies had indicated that easy access to guns and keeping firearms at home increases homicide and suicide rates. "The fact that gun ownership was being identified as a risk factor for violent death legitimately raised the possibility" that gun policies might need to change, Wintemute says. The National Rifle Association (NRA) swung into action to stifle that threat. For gun-possession advocates, Wintemute says, "It made perfect sense to try to prevent that evidence from being collected in the first place." Contending that CDC was pursuing a gun control agenda rather than unbiased science, former U.S. Representative Jay Dickey (R–AR), who described himself then as "NRA's point person in Congress," convinced the House to cut $2.6 million from the CDC budget: the precise amount that the agency's National Center for Injury Prevention and Control was slated to spend on gun violence research that year. (In *The Washington Post* last July, Dickey, who lost his House seat in 2000, wrote that he has since become an advocate of research on preventing firearms injuries.)

The 1996 legislation prohibited CDC and the National Institutes of Health from conducting research that might "advocate or promote gun control." Coupled with the funding cut, the proscription cast a pall over the field, Teret says. Although his program has survived on private funding, the CDC ban "was devastating for the field of gun violence prevention," he says. Many young researchers, Teret says, ditched firearms studies in favor of other public health issues.

As a result, from 1996 to 2010, academic papers published on gun violence fell by 60%, according to a review released last week by Mayors Against Illegal Guns, a coalition led by New York Mayor Michael Bloomberg and Boston Mayor Thomas Menino. Today, fewer than a dozen public health researchers in the United States focus primarily on gun-related violence, says Wintemute, who funds his group's research out of his own pocket. CDC and the teams it funded were not the only victims. Beginning in 2003, a series of riders on budget bills called the Tiahrt Amendments restricted the collection and distribution of gun-related crime data by the Department of Justice. Although some restrictions have since been removed, others remain. For example, the Naval Criminal Investigative Service must destroy background checks on gun buyers within 24 hours of using them, and journalists and researchers are not allowed to access data that the agencies collect.

The first agency unfettered by the administration is CDC. Backed by a legal analysis that the 1996 appropriations language does not bar research, Obama last week stated that CDC will immediately start to assess strategies for preventing gun violence and work to identify "the most pressing research questions." He also asked Congress to give CDC an additional $10 million for further research, "including investigating the relationship between video games, media images, and violence." And he called for $20 million to expand the National Violent Death Reporting System from 18 states to all 50 states. That, he said, would help "Americans better understand how and when firearms are used in a violent death and informing future research and prevention strategies."

Some activists assert that research on firearms violence is a low priority. "If there was a public policy benefit to doing it, you'd have researchers doing it just because there was a demand," contends John Lott, an economist and outspoken supporter of gun ownership. And although some studies may be worthwhile, he sees little reason for taxpayers to foot the bill. "It's hard to divorce politics from

the government handing out the money," says Lott, who argues that independent researchers could do it better.

Scientists, for their part, are chomping at the bit to pick up where they left off 17 years ago. "We don't know much of the basic epidemiology of firearm violence," Wintemute says. "What are the risk factors for involvement as a victim or a perpetrator? What distinguishes those who have the same risk factors but don't have the same outcomes?"

Such questions might finally get answered if Congress refrains from imposing new restrictions, says Arthur Kellermann, a firearms researcher at RAND, a Santa Monica, California–based think tank. His work in the 1990s, including a provocative study showing that households with guns had five times greater risk of suicide than those without guns, made Kellermann a "personal lightning rod" for NRA's ire, he says. Two promising research questions, he says, are to probe whether gun safety training programs are effective at reducing firearms injuries and whether it is possible to design handguns that a young child cannot fire. "I would have answered both questions over a decade ago if there had been any support to do it," he says. He and others may finally get that chance.

–EMILY UNDERWOOD

GLOBAL WARMING

Soot Is Warming the World Even More Than Thought

Breathing the sooty plume from a maladjusted diesel engine or a smoldering cooking fire has always been ill-advised. But a new study finds that soot is warming the climate about twice as fast as scientists had estimated.

With roughly 8 million tons of soot produced each year by burning everything from coal in power plants to oil in ship's boilers, that's bad news for the planet. And the same study for the first time points policymakers to the soot sources that will make the best targets for climate regulations. "It's a wonderful study," says atmospheric scientist Susanne Bauer of NASA's Goddard Institute for Space Studies in New York City. "I was waiting a long time for this to come out."

Scientists began the 232-page study—published last week in the *Journal of Geophysical Research: Atmospheres*—4 years ago in response to calls for drastic reductions in emissions of soot, called black carbon in the scientific literature. Soot particles roughly 100 nanometers in diameter were obviously absorbing solar energy and passing it on to the atmosphere, adding to the warming caused by greenhouse gases. But "there wasn't a deep scientific basis" for reducing soot emissions, says the paper's lead author, atmospheric scientist Tami C. Bond of the University of Illinois, Urbana-Champaign. "There was promise, but the science was not completely examined."

That shortcoming has now been remedied. Under the auspices of the International Global Atmospheric Chemistry Project, 31 researchers from nine countries in a range of disciplines came together to assess the climate effects of soot. Working from published field observations, the authors looked at all the effects of soot on the planet's retention of solar energy as well as the effects of other products of soot-producing combustion. They then tried to understand why different researchers got different answers from their climate models. "It's a deeper view," Bond says.

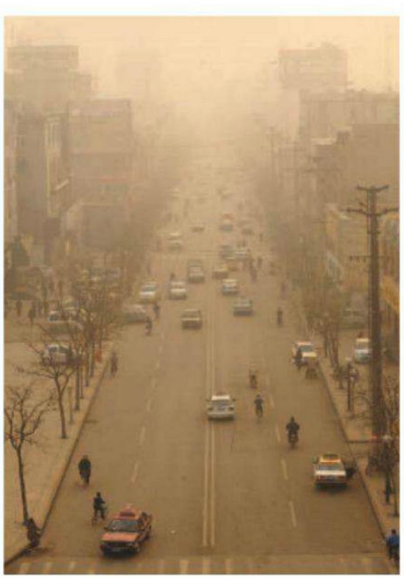

A dark day. Sooty smog is bad for climate—warming it strongly—as well as for people.

CREDIT: PETER PARKS/AFP/GETTY IMAGES

The new, deeper view—which drew 600 comments from 20 peer reviewers—finds a prominent role for soot in global warming. All the ways soot can affect climate—among them by absorbing sunlight, shrinking cloud droplets and thus brightening clouds, and darkening ice and snow—add 1.1 watts per square meter (W/m^2) to the climate system, the study concludes. "That's a big number," Bond says. It puts soot second behind the dominant agent forcing warming, carbon dioxide, which accounts for 1.66 W/m^2. All human-generated climate agents combined—both those that cool climate and those that warm it—account for only an added 1.6 W/m^2. Soot's contribution to the warming is roughly twice as large as estimated in the 2007 assessment made by the Intergovernmental Panel on Climate Change.

But all soot is not created equal, which makes reining in the current warming by reducing soot emissions tricky. Coal burning can produce soot, but it also releases sulfur that goes on to reflect additional sunlight back into space. That tends to cool the planet. Forest and brush fires produce soot, but they also produce microscopic bits of unburned "organic carbon" that can brighten clouds and cool climate.

So spending a lot of money to clean up efficiently burned coal—which produces cooling sulfur but not much warming soot—or to reduce agricultural burning might net little or no reduction in warming. "The findings are both exciting and sobering," Bond says. It is now clear that "you can't just turn off black carbon."

Helpfully, the study points to which soot sources should be cleaned up for the maximum cooling effect on climate. "Diesel engines seem to be at the top of everyone's list," Bond says. Next is coal burned under less than optimum conditions in homes and small industries. But although the 4 billion people burning wood, grass, and dung for energy are clearly endangering their health, much of that burning produces so much organic carbon that cleaning it up probably would not have a dramatic effect on climate.

"This paper has set the bar high for future efforts that address other aspects of policy-relevant science," says atmospheric scientist Joost de Gouw of the National Oceanic and Atmospheric Administration's Earth System Research Laboratory in Boulder, Colorado. "The atmospheric science literature is vast and at times it takes a paper like this to summarize what we know and do not know and to point the way forward."

For soot itself, the remaining work is considerable. The uncertainties calculated in the study are still large. That is due largely to the dearth of data from the major soot-producing regions and to the poorly understood interaction of all kinds of particles with clouds. But then clouds have been the bugaboo of climate scientists for half a century.

–RICHARD A. KERR

EUROPE

'Brussels Ranking' of Universities Off to a Rocky Start

BRUSSELS—At a meeting in Dublin next week, researchers will unveil the details of a new system to grade the world's universities. Backed by millions of euros from the European Union and designed by a group of higher education research centers, the new method is billed as less simplistic and more reliable than existing university rankings, which have long been the subject of fierce criticism.

But the new plan, dubbed U-Multirank, has already aroused controversy. The League of European Research Universities (LERU), which includes some of Europe's top schools, says its 21 members won't provide data. That could seriously undermine the new project. "It's difficult to run a ranking if people are boycotting," says Alex Usher, president of Higher Education Strategy Associates in Toronto, Canada. The ranking's developers have also struggled to bring U.S. and Chinese universities on board, casting further doubt on the usefulness of the data.

Critics of current ranking systems—which include the Academic Ranking of World Universities, better known as the Shanghai ranking, and the *Times Higher Education* World University Rankings—argue that these charts rely on indirect, sometimes inadequate indicators, and that the aggregated scores, based on subjective weights for each indicator, are meaningless (*Science*, 24 August 2007, p. 1026). Some also complain that the rankings are biased toward research in the natural sciences.

Low scores for European universities have only fueled frustrations; now, for instance, only nine E.U. universities are listed in Shanghai's top 50, compared with 36 from the United States. In 2008, France's government championed the creation of a more sophisticated alternative, which has since been led by the Centre for Higher Education (CHE) in Gütersloh, Germany, and the Center for Higher Education Policy Studies at the University of Twente in the Netherlands.

U-Multirank is inspired by a popular CHE ranking of German universities and a clear departure from existing global efforts. Instead of focusing on research quality, it will assess universities more broadly, comparing research reputation, teaching quality, ties with the local community, international orientation, and success in tech transfer. And instead of publishing a single ranking that aggregates indicators using preassigned weights, U-Multirank will let users select their own criteria, providing data and graphs on dozens of measures. The system relies on a range of sources, including bibliometric databases, student surveys, and data provided by the universities themselves, for instance on student/staff ratios or gender balance.

After a 2-year pilot involving 159 universities, U-Multirank will now expand to at least 500 institutions. The first batch of data, in physics, business, mechanical engineering, and electrical engineering, will be collected this year and published in 2013; computing, social sciences, and the humanities may follow. U-Multirank is set to receive €2 million from the European Union in 2013–14.

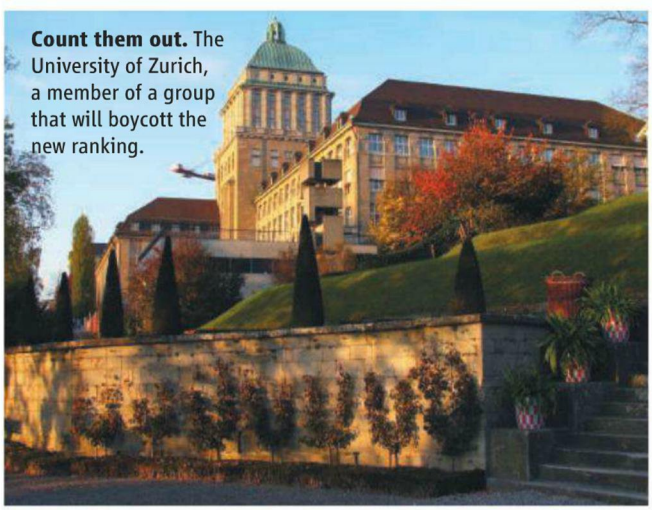

Count them out. The University of Zurich, a member of a group that will boycott the new ranking.

LERU, which includes university heavyweights like Cambridge and Oxford—ranked fifth and tenth respectively, on the Shanghai chart—initially welcomed the idea, albeit cautiously. In a 2010 LERU paper, Geoffrey Boulton from the University of Edinburgh in the United Kingdom said that U-Multirank could provide an "antidote to single monotonic lists." But more recently, the group has slammed the project as unnecessary and poorly designed. The pilot has shown the data collection to be a huge burden on universities, LERU claims, and some statistics—such as graduate employment—are hard to compare from one country to another. Universities could also be tempted to manipulate data to improve their scores, LERU Secretary-General Kurt Deketelaere says.

CHE researcher Gero Federkeil says the pilot study helped test and refine indicators. "To ensure that the data are comparable, you need to give universities very precise [indicator] definitions," he says. Federkeil is aware that universities could cheat but says there will be checks and controls; for example, U-Multirank will look for outliers and check for country-specific inconsistencies. Federkeil is hoping to clear up what he calls "misunderstandings" about U-Multirank, and to get LERU back on board.

The European University Association, which unites about 850 universities, declined to say whether it would advise its members to participate. U-Multirank is taking a risk by asking the universities to supply data themselves, Usher says. "You open the process to hijacking by people who don't want to play ball," he says. "If that happens, I'm not sure the ranking will have credibility with consumers."

Producing a truly global list may prove another headache. Of 24 U.S. universities selected for the pilot project, only four confirmed participation, and just one submitted data. Participation in China was equally low. That is no surprise, Usher says. He recalls a 2008 speech by Valérie Pécresse, then France's higher education minister, who argued for "an objective, well thought-out European ranking, that will let [European] universities shine worldwide." "It was perceived as an E.U. instrument," Usher says. The rankers have tried to address that concern but admit they won't achieve global coverage in the short-term.

Ellen Hazelkorn, vice president for research and enterprise at the Dublin Institute of Technology and an expert on rankings, calls the low international take-up "disappointing." She praises U-Multirank as an ambitious attempt to go beyond single definitions of quality and says it could be a valuable tool to promote the merits of higher education in Europe. "It's a huge undertaking and an important contribution to the debate," Hazelkorn says.

–TANIA RABESANDRATANA

Tania Rabesandratana is a writer based in Brussels.

CREDIT: ROLAND FISCHER/WIKIMEDIA COMMONS

Forbidden fruit. Mapping along the Altyn Tagh fault in Xinjiang (*left*) got Ramón Arrowsmith's team in hot water with local authorities.

FIELD RESEARCH

Foreigners Run Afoul of China's Tightening Secrecy Rules

SHANGHAI, CHINA—In August 2007, J. Ramón Arrowsmith set out for China's far west on what should have been a routine geophysics expedition. Working with Chinese and U.S. colleagues, Arrowsmith, a geologist at Arizona State University, Tempe, spent 20 days in Xinjiang Uyghur Autonomous Region's Altun Mountain Nature Reserve, near Tibet, mapping landforms to trace how earthquakes move along the Altyn Tagh fault. Little did they know that a few months earlier, China's Ministry of Land and Resources had issued a decree forbidding foreigners from using some methods of gathering topographic data.

Leaving the reserve, the team was intercepted by local authorities and brought to a hotel for questioning. Their handheld GPS devices and 1:100,000-scale topographic maps drew particular scrutiny, Arrowsmith says. He had never been similarly hassled over fieldwork in Ethiopia, India, Kyrgyzstan, and other sites. They were grilled for a week, during which they made frantic efforts to sort things out with colleagues in Beijing. The researchers were never charged with a crime, but their data and equipment were seized. That November, after what Arrowsmith calls "a fair amount of apology" from the scientists, they got their belongings back.

As Arrowsmith's group learned the hard way, the Chinese government is curtailing the ability of foreign researchers to conduct fieldwork in China. Between 2006 and 2011, authorities pursued nearly 40 illegal mapping and surveying cases, according to state press reports. Several have involved scientists, one of whom is serving a long prison sentence. The terrain is likely to get even more treacherous: Last year, China's State Bureau of Surveying and Mapping (SBSM) revealed plans to revise its Surveying and Mapping Law, which governs all geospatial and mapmaking activities. Revisions under discussion may not take effect until 2017. But they are expected to further constrain activities of foreign scientists who need to map coordinates and use GPS devices in China—and could scare off Chinese collaborators.

China heads a list of countries that are cracking down on the collection and possession of geographic data. India restricts GPS use in sensitive regions such as Kashmir, and a draft bill in Pakistan would require anyone engaged in mapping to register with the government. But in terms of scientific impact, China's policies are particularly worrisome, says Peter Molnar, a geophysicist at the University of Colorado, Boulder. Among nations that offer exceptional fieldwork opportunities, he says, China and the hardships it presents to foreign researchers make it "one of the most restrictive countries in the world."

Genuine security risk?

China has long kept a wary eye on geographic data. In the 1990s, foreigners were not allowed to possess certain geologic maps, says David Rowley, a geologist at the University of Chicago in Illinois who studies the evolution of Tibetan topography. But such restrictions were easily circumvented. Chinese collaborators kept restricted maps and let their foreign counterparts look at them. Working in China "was a pain," Rowley recalls, but "in the end, we did have access." The regulations "were not big obstacles," agrees Molnar, who speculates that that could be because few scientists knew about them.

As advances in technology have simplified mapping and made detailed geographic information readily accessible, the government has tightened the screws. Since at least 2007, it has been effectively illegal for foreigners to operate a GPS device in China. International brands of cameras with GPS capabilities have been rigged to avoid displaying coordinates if the user is in China, says Stefan Geens, an analyst in Stockholm who studies networked digital maps and geospatial imagery.

Google Earth is another prime target. A Wikileaks cable released in 2010 showed that in 2006, the Chinese government unsuccessfully lobbied the U.S. embassy in Beijing to pressure Google to reduce image resolution of certain Chinese locations. The Chinese version of Google Maps, along with other mapping programs available in China, suppresses latitude and longitude. "They've gone out of their way to shield coordinates,"

CREDITS: RAMÓN ARROWSMITH AND ZACK WASHBURN (2)

Geens says. And in March 2007, the land ministry decree forbade foreigners from carrying out surveys or making "electronic navigation maps." Rowley says: "It is getting more and more difficult for foreigners to do research in geology in China."

An official at SBSM declined to comment. But a recent *China Daily* article states that bureau officials aim to "intensify efforts to crack down on illegal foreign surveying activities" for the purpose of "defending national security and interests." Xu Deming, vice minister of land and resources, told the state-run newspaper *Legal Daily* last September that key concerns include Internet mapping programs, location-based mobile applications, and remote sensing capabilities. "The risks to geographic information security have steadily grown as the collection, transmission, and use of geographic information has become easier," Xu stated.

Critics argue that the tightening policies are anachronistic and ineffective. The GPS restrictions, for example, exist even as more and more cars and mobile phones are GPS-enabled. "The barn door has been left open and the horses have left," Geens says.

Authorities routinely cite the regulations as grounds for hauling in scientists and tour operators. Enforcement appears to be most aggressive in western China, where ethnic tensions, natural resource extraction, and military bases abound. For example, in September 2008, Xinjiang authorities confiscated GPS devices from two British students studying earthquake dynamics and fined them each $1450. Other cases include two Japanese scholars fined and deported in 2006 for mapping the locations of an airport and water facilities, and a U.S. tour operator fined for logging points in two GPS receivers in 2011.

But the most chilling cautionary tale is that of imprisoned Chinese-American geologist Xue Feng.

Arbitrary and confusing

Xue entered a graduate program in geology at the University of Chicago in the 1990s. Among all the students that Rowley, Xue's doctoral adviser, has worked with, Xue ranked "near the top," he says. But with a wife and two children to support, Xue was looking for stability after earning his Ph.D. in 1998. He took a job with the oil industry research firm IHS upon graduation.

Xue, 47, was assigned to IHS's Houston office and tasked with obtaining data from his native China, where a burgeoning oil industry was in the midst of a restructuring that had exposed valuable data. In 2005, he brokered the purchase of coordinates of more than 30,000 Chinese oil wells. IHS sells such information from around the world to firms bidding for oil rights and looking to perform due diligence on a site, Rowley says. Xue subsequently left IHS for another firm. On a trip to China in November 2007, he was detained by security officials; the seemingly innocuous data on oil wells had been classified retroactively as a state secret.

Xue, who holds a U.S. passport, spent nearly 3 years in detention before he was sentenced. During that time, according to accounts he gave U.S. consular officers, authorities burned his arms with lighted cigarettes, struck him with an ashtray, and coerced him into signing false documents. At a trial in July 2010, he was sentenced to 8 years in prison for trafficking in state secrets. Appeals from President Barack Obama, former U.S. ambassador to China Jon Huntsman, and current ambassador Gary Locke may have helped Xue win a minor sentence reduction last summer, says John Kamm, executive director of the San Francisco, California–based human rights organization Dui Hua Foundation. But Xue's wife and children have been left with limited means of support, says Rowley, who created a Web page devoted to the case. He asserts that the well locations are harmless and that much of the information Xue obtained could be reconstructed from published maps.

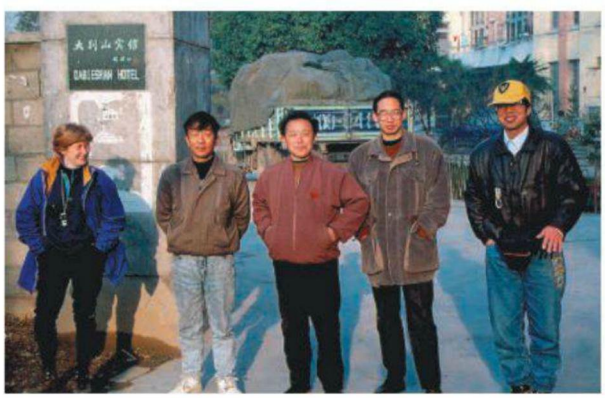

Happier days. Xue Feng (*far right*) was one of David Rowley's top students before his activities in China landed him in prison.

CREDIT: COURTESY OF DAVID ROWLEY/THE UNIVERSITY OF CHICAGO

The restrictions also affect Chinese researchers who have remained in their homeland. Wang Jun, a paleobotanist at the Chinese Academy of Sciences' Nanjing Institute of Geology and Palaeontology, says he is regularly called in for questioning by local police when in the field with foreign partners, even when "our joint field research has nothing to do with surveying and mapping." The regulations have created administrative headaches for local collaborators, who can spend months seeking permission for fieldwork.

U.S. scientists must make sure that both they and their Chinese counterparts fully understand the relevant regulations, says David Fountain, director of the tectonics program at the U.S. National Science Foundation (NSF). Any fallout for breaching a regulation "could be more significant for the collaborators than it is for the U.S. scientists," he warns. Chinese scientists are often slapped with hefty fines—Arrowsmith's partners during his 2007 trip were fined several thousand dollars—and some will ask up front if their Western colleagues can cover any penalties, says Bill Chang, former NSF Beijing representative.

Following Arrowsmith's 2007 trip, which NSF funded, the agency distributed an unofficial translation of the land ministry decree that the team had run afoul of. But that document leaves many questions unanswered. Scientists remain uncertain about whether they are allowed to jot down coordinates in a field notebook or use a GPS-enabled iPhone. Enforcement is piecemeal as well. The decree sets a maximum fine of $4800 for violations, but some researchers have been hit up for $12,900, according to NSF, and the current Surveying and Mapping Law, last updated in 2002, sets a maximum penalty of $80,400. "The rules are confusing," Chang says. Most of the violations publicized so far have involved geospatial research in Xinjiang. Working in Tibet, meanwhile, has become "almost impossible," Rowley says.

Punishment for possessing state secrets—Xue's conviction—is another murky legal area. Each ministry maintains its own list of secrets, Kamm says. "Scientists and researchers should find out what's on the list of ministries with whom they have or will have dealings," he says. He notes that penalties for violating secrecy laws have gotten harsher in the past few years.

Arrowsmith continues to venture into the field in China, in part because its hundreds of active faults "offer excellent datasets for future research." But for many other scientists who rely on geospatial data, China is sliding down the list of attractive destinations. If scientists "have a choice between China and some other place," Chang says, "they factor in all these issues."

–MARA HVISTENDAHL

Shaking Up Science

Two journal editors take a hard look at honesty in science and question the ethos of their profession

FERRIC FANG AND ARTURO CASADEVALL ARE AN UNLIKELY DUO. They live a continent apart and barely speak on the phone. ("There were a couple of times that I failed to immediately recognize his voice," Fang admits.) Fang grew up in Los Angeles, the son of a doctor, and attended Harvard University. Casadevall fled Cuba for the United States at 11, was reunited with his family in New York, and never left. He enrolled at Queens College of the City University of New York because the first year there was free and worked at McDonald's and as a bank teller to earn spending money. "I never thought about a career in science," Casadevall says. "I didn't know you could get paid to do research."

Despite their differences, they rose on parallel tracks through the ranks of microbiology and immunology, running large labs and securing tenure and various accolades at the University of Washington, Seattle, (Fang) and the Albert Einstein College of Medicine in the Bronx, New York (Casadevall). They were acquaintances, having bumped into each other a handful of times, but nothing more.

Disenchantment brought them together almost 5 years ago. Their own achievements aside, the two had nagging worries about what they saw as an unwelcome transformation in academic science. Discovery for its own sake was being sidelined by a push to publish in high-impact journals. Funding was scarcer than ever. Scientists focused on narrow fields and often couldn't communicate their professional passions at a cocktail party.

None of this is new. But Fang and Casadevall decided to try to do something about it—to recapture what brought them to science in the first place, the thrill of the chase, of being part of something bigger than oneself. They wanted to ask: Are we doing science the best way we can? And if not, what's in our power to change?

The partnership

"The 99%, the majority of scientists, are really driven by fear," Fang says. Wonkish and graying at the temples, he's sitting one November morning in a Philadelphia coffee shop with music blaring, steps from the University of Pennsylvania, where he's just given a talk on nitric oxide and bacteria. As often happens these days, the researchers with whom he met preferred to discuss something else: the toxic mix of pressure to score the next grant or the next publication, and high rates of bad scientific behavior, which Fang has been studying in depth.

Fang and Casadevall came together in 2008. Fang was, and still is, editor-in-chief of *Infection and Immunity*, a journal published by the American Society for Microbiology (ASM). Casadevall was an editor there as well. (He was subsequently asked to head up a new ASM publication, *mBio*.) "I realized that I had this privilege of writing opinion pieces," Fang says. "I started badgering my editors for ideas" about the state of science. "The one who stepped forward was Arturo."

The two quickly recognized a hunger for leadership in the area. One of their first commentaries, published in early 2009 and titled "NIH Peer Review Reform—Change We Need, or Lipstick on a Pig?" explored scientists' dependence on grants to pay their salaries and questioned whether proposed changes to peer review at the National Institutes of Health (NIH) would make much difference. "We started getting wonderful feedback about these essays," Fang says. "Very few people wanted to write a letter to the journal, but they were happy to write to [us]."

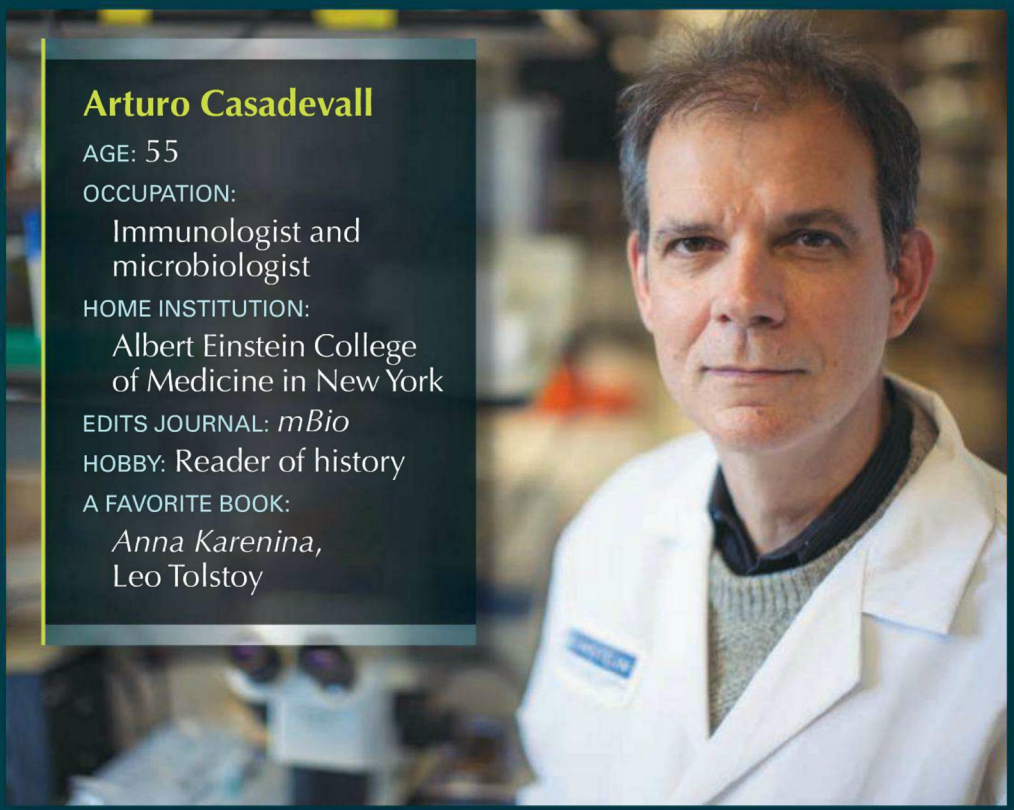

Arturo Casadevall

AGE: 55

OCCUPATION: Immunologist and microbiologist

HOME INSTITUTION: Albert Einstein College of Medicine in New York

EDITS JOURNAL: *mBio*

HOBBY: Reader of history

A FAVORITE BOOK: *Anna Karenina*, Leo Tolstoy

CREDIT: ALBERT EINSTEIN COLLEGE OF MEDICINE

One note came from Hawley Montgomery-Downs, a sleep researcher at West Virginia University in Morgantown. At the time, her tenure was contingent on securing two major NIH grants. She had submitted 10 failed applications in 3 years and was subsisting on number 11, a modest research award. "I have great results … but no time to publish them," she wrote to Fang and Casadevall. "I am not an emotional person, but after reading your commentary I put my head down on my desk and cried. Your article confirmed all the rumors and affirmed that the situation is 'not just me.' "

Montgomery-Downs, who allowed *Science* to quote from her letter, told Fang in November that although she was awarded tenure, none of her grant applications since then had been successful.

Inspired by letters like this one, Casadevall and Fang kept pushing forward. As drafts of their editorials flew from coast to coast by e-mail, a deep friendship developed. "I found a great comrade in arms," Casadevall says over a recent brunch of eggs and toast at a diner near New York's Times Square. "Whenever there's a disagreement, I always defer to Ferric. He's always right."

"We really see eye to eye, but Arturo is the poet and I'm the prose," Fang says. Casadevall massages the words, and Fang crunches the numbers. After several joint essays ruminating on peer review, basic science, and how research is characterized, Fang was working in his office early one evening when he received an unsettling e-mail that would send the two on a different path.

Online
sciencemag.org
Podcast interview with author Jennifer Couzin-Frankel (http://scim.ag/pod_6118).

"We are writing to inform you that in regard to the manuscript indicated below, which was published in the [sic] *Infection and Immunity*, we found repeated use of the same figures within the manuscript as well as the use of figures used in other manuscripts," wrote a dean at the University of the Ryukyus in Okinawa, Japan. Unbeknownst to Fang, the university had been investigating dozens of papers by virologist Naoki Mori following a tip from another journal.

Infection and Immunity had published six of Mori's papers. Three more appeared in ASM's *Journal of Virology*. Digital data experts at ASM performed a pixel by pixel analysis of the figures and came to the same unfortunate conclusion as the university. Mori agreed to retract the papers.

Fang was shaken by the experience. The image manipulation was uncovered almost by chance—a peer reviewer for the journal *Blood* happened to recognize some figures as having been previously published, setting off an inquiry. Until then, Fang had operated under the assumption that science, as many like to say, is self-correcting. Suddenly he realized that probably wasn't the case. "There's a lot of science out there that hasn't been corrected," he now believes.

Still, many journal editors encounter research misconduct during their tenure. Why did the Mori case drive Fang in an obsessive new direction? "So what's wrong with me?" he asks, echoing the question back. "It's not with me. The problem," he says tongue-in-cheek, "is with Arturo."

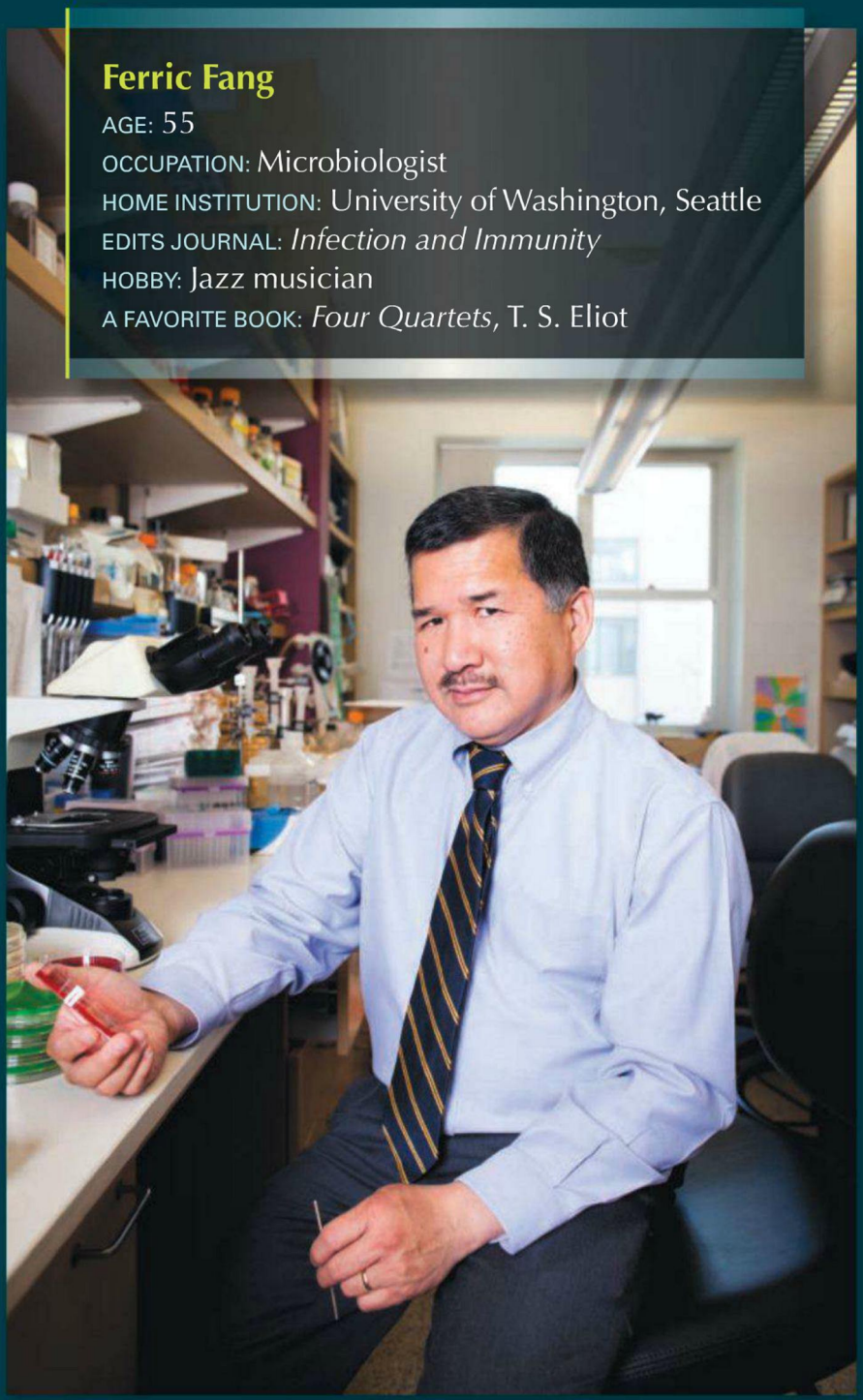

Ferric Fang
AGE: 55
OCCUPATION: Microbiologist
HOME INSTITUTION: University of Washington, Seattle
EDITS JOURNAL: *Infection and Immunity*
HOBBY: Jazz musician
A FAVORITE BOOK: *Four Quartets*, T. S. Eliot

CREDIT: PHOTO BY MATTHEW RYAN WILLIAMS

The problem

Casadevall's worldview is shaped by his experience as a Cuban exile and gratitude for his own good fortune. His father, an attorney who spent time in a Cuban prison camp and was deemed unqualified to practice law in the United States, encouraged Casadevall to develop a trade that could transfer across national borders. When New York University admitted him off the waitlist to its M.D./Ph.D. program in 1979, he was startled to learn that the stipend he would receive was

greater than what he'd been earning at four jobs combined. He asked to enroll in June rather than September partly to start drawing that paycheck. The school agreed.

Like Fang, Casadevall began his scientific career full of idealism. But as time passed, he grew troubled by the reluctance of scientists to study how they perform their craft—the science of science, as it were. "We don't look at our own belly button," he says. There's virtually no information about questions he considers critical to running an efficient research enterprise. Are prizes helpful or harmful to science in general? What's the optimal size of a lab? How common is research misconduct?

> "We don't look at our own belly button."
> —Arturo Casadevall

Casadevall and Fang chose to tackle the last question first. And they hit upon a rich source of data to help them: the scientific literature, including a treasure trove of high-profile papers and retractions spanning decades.

The two first explored whether there was any connection between a journal's impact factor—a ranking based on citations of papers published there—and its retraction rate. They speculated that the more prestigious a journal, the more likely scientists might be to cut corners, or even fudge data, to get their work published in it. They searched the biomedical literature database PubMed for retractions in journals with a range of impact factors and found a robust correlation. The pair published their "retraction index" in *Infection and Immunity* in August 2011.

They weren't the first to uncover this connection, but the paper made a splash: The retraction index was republished in newspapers and magazines worldwide, including this one. In April 2012, *The New York Times* featured Fang and Casadevall's work on retractions, further elevating their profile.

Their next project was more ambitious. The pair wanted to quantify scientific misconduct as best they could in the published literature. For assistance they recruited R. Grant Steen, a medical writer in North Carolina. Snatching time in airports, on airplanes, and after

> "The 99%, the majority of scientists, are really driven by fear."
> —Ferric Fang

hours, they assembled an enormous Excel file of every retraction they could find in PubMed, more than 2000 dating back to 1977.

They cross-referenced many retractions with other sources, such as reports from the U.S. Office of Research Integrity (ORI), which investigates misconduct. The three attributed about 67% of all the retractions to scientific misconduct, including fraud and plagiarism. The results were published in October 2012 in the *Proceedings of the National Academy of Sciences*.

"We never anticipated that the problem was going to be so widespread, ever," says Casadevall, who'd expected honest errors to explain the vast majority of retractions. "We need to clean up our act."

Retractions remain rare, at about one out of every 10,000 papers. But "even a single retracted paper for fraud can be very damaging to the credibility of science," Fang says. The actual problem rate is much higher." Backing him up is a 2009 paper in *PLOS ONE* that examined 21 surveys of research misconduct. Pooling the data, the author, an Italian researcher at the University of Edinburgh in the United Kingdom named Daniele Fanelli, concluded that 14% of scientists said that they knew of a colleague who had falsified data. About 2% admitted committing misconduct themselves.

The drivers

Fang and Casadevall have given much thought to what's behind bad behavior. Both now detect signs of a system they consider flawed. For example, faculty applicants to their respective departments are invited for interviews only if they've been first authors on a publication in a high-profile journal. "We defer to the editors of *Science* and *Nature* to tell us what's good," Casadevall laments. These days, "you get a finding and the whole discussion is not about the finding, it's where you're going to publish."

An underlying issue is funding. Fang's father, a physician-scientist working in the 1960s, told him that back then, half or more of grants were funded. "He always felt that the challenge in science was science itself," Fang says. "The level of competition has changed dramatically. … If you talk to any student or postdoc, they'll say the picture they're getting, the name of the game, is to get money." Sitting on promotion and tenure committees, Fang has watched colleagues pay "lip service" to teaching and quality of science, but the real yardstick is the applicant's funding levels. In part, this is because universities now depend heavily on "soft money"—grant funding—to support their own infrastructure.

"The most productive scientists are still worried because they have a lot of mouths to feed," Fang says. Fear struck him a few years ago when his own funding situation grew dire and half a dozen individuals in his lab were at risk of losing their jobs. They were saved—for the moment—by support from the federal stimulus package. "It's all about money," Fang says. "How can you be sure that you get money?" The answer comes back to publications—and sometimes skirting the rules to get them.

Fang began his journey with Casadevall thinking cheaters were inherently different from the rest of us. Now, he appreciates how a toxic environment can subtly encourage bad behavior. One influence has been the writings of Dan Ariely, a social scientist at Duke University in Durham, North Carolina, who studies cheating. "We have a tendency to point fingers, we have a tendency to identify some people and say, 'These are bad people,' " Ariely says. But "it's unrealistic to create a system that tempts people and expect them to behave very well." Ariely cites an example from his own history: As a teenager, he was badly burned and spent years receiving treatment. One of his favorite physicians pressured him to tattoo the right side of his face to give the appearance of stubble, which had been erased by the burns. "And then I found out I was going to be the third patient in the paper," Ariely says, and that the doctor needed a critical mass of volunteers in order to publish his research. "This was an amazing physician who took great care of me for 3 years, … but at that moment, he wanted the paper out."

This week, Fang and Casadevall published their latest missive in *mBio*: With Joan Bennett, a prominent microbiologist at Rutgers University in New Brunswick, New Jersey, they analyzed ORI reports to determine whether men were found guilty of misconduct to a disproportionate degree. At the senior level, the gender imbalance was dramatic. The three reviewed the ORI files of 72 faculty members,

and only nine of them were women. That's one-third of what one would predict based on female representation in the life sciences. Among trainees, the gap narrowed. Fang and Casadevall speculate that the inclination of male principal investigators to cheat tracks the increased likelihood of men to engage in risky behavior, well documented in the social science literature. Younger scientists—male and female—may cheat to please their boss, or because of pressure to arrive at certain results.

"Scientists love to think that they are totally objective," when in fact they're often not, Bennett says. "I think it's very important to look at these questions."

Fang and Casadevall admit that they're trapped in the system that troubles them. "I think it's crazy to focus so much on impact factors," Fang says. "But I have a postdoc right now who has a great story, and we're going to try to submit his paper to *Nature*. … I see the rules as they are, and I'm not going to sacrifice his career." At the same time, the two are trying to modulate how they run their labs and mentor their students. Casadevall, ever the broad thinker, urges lab members to read widely outside their field. Fang has postdocs working on multiple projects at once, with the hope that something will pan out and they'll be under less pressure. Fang's partnership with Casadevall has also changed how he'd react to fraud in his own lab. If a trainee faked data, Fang says, "I would question myself, that I had failed strategically and not created the right environment for them, and they felt afraid of failure."

Despite the stresses they face, most scientists, of course, don't cheat. Even as Fang looks inward and contemplates sweeping changes to the system, he doesn't absolve individuals who succumb to its temptations. At ASM, Fang worried about trusting Mori's work in the future, and argued that he should be barred from publishing ever again in ASM journals. He was outvoted in favor of a 10-year ban.

> "We defer to the editors of *Science* and *Nature* to tell us what's good."
>
> —Arturo Casadevall

The solutions

With every joint publication on the state of science—they have 14 so far—Fang and Casadevall see more hunger in the community to hash out these topics. Casadevall travels constantly. He spent parts of October and November in Michigan, London, Paris, and Chile. Everywhere, the conversation was the same.

Scientists, especially younger ones, "feel powerless," he says. "The older group is worried, surprised" by the misconduct findings.

> "It's unrealistic to create a system that tempts people and expect them to behave very well."
>
> —Dan Ariely, Duke University

Fang and Casadevall find themselves in increasing demand. Fang participated in a roundtable on scientific integrity last month at the National Academy of Sciences in Washington, D.C. Together they're writing an article for *Scientific American Mind* on cheating.

Fang and Casadevall have heard concerns from researchers that their work will be used to discredit science. It's been cited on anti-science blogs, like those questioning the safety of vaccines or the role of human activities in climate change. While they've considered the risks, "I think we need to have this conversation to try and make science better," Fang says.

Casadevall favors a more generalized science education, rather than the extreme specialization that now occurs in graduate school. An enthusiastic reader of history, he points out that in the 19th century and before, scientists such as Isaac Newton and Gottfried Leibniz were philosophers first and scientists second. He's in discussions with Albert Einstein College of Medicine about "putting the Ph"—philosophy—"back in Ph.D.," and launching a graduate track that includes training in epistemology and metaphysics—or as Casadevall puts it, "How do you know what you know?" and "How much can you push your lab?"

He's also disillusioned by peer review, which he believes yields endless demands to add data to a paper without necessarily improving it. At the open access journal Casadevall runs, *mBio*, the rule is that papers are either accepted or rejected, period.

Fang and Casadevall know that they can't come up with all of the answers. Rather, their goal is to start a conversation and hope others identify solutions. "We have to somehow change the incentives," says economist Paula Stephan of Georgia State University in Atlanta. Her book, *How Economics Shapes Science*, examines the ways in which scientists and institutions compete for resources and rewards. "Historically, a lot of the criticism [of the scientific enterprise] … comes from people outside science," says Stephan, who met Casadevall and Fang at a Health Research Alliance event in Washington, D.C., last year. Although she doesn't agree with them on everything, "it's very exciting when you see people like the two of them, who are editors of journals, really beginning to question the system."

Casadevall and Fang are shifting gears now, moving away from misconduct and into other issues that may prove tougher to tackle quantitatively. Casadevall hypothesizes that prizes are detrimental to science, because they foster a "winner take all" system and reward cutthroat behavior, rather than cooperation that might better advance knowledge. He is currently cataloguing all the Nobel prizes and assessing which were said to have left out potential awardees. Fang is considering using data from ASM journals to ask how often peer review changes the substance of a paper. "We are going to continue to take on question after question," Casadevall says.

Meanwhile, the two must stay abreast of their day jobs: Editing a journal each, running large labs, in Fang's case directing a bustling clinical laboratory, and in Casadevall's sitting on a national biodefense advisory post. When Casadevall worries that he's stretched too thin, his 89-year-old mother, who lives in Queens, urges him onward. "She assures me there will come a day when nobody's going to invite me anywhere. … She says to me, 'Don't turn down an invitation.' " He grins. "If my mom tells me to do it, I'll do it."

Then Casadevall, his glasses folded neatly and hanging from his shirt collar, turns serious. "I really do think that what Ferric and I try to do may be the most important thing I do in my life," he says. Others, he knows, will keep building the edifice of science. These two want to shake its modern foundations.

–JENNIFER COUZIN-FRANKEL

Eating Was Tough For Early Tetrapods

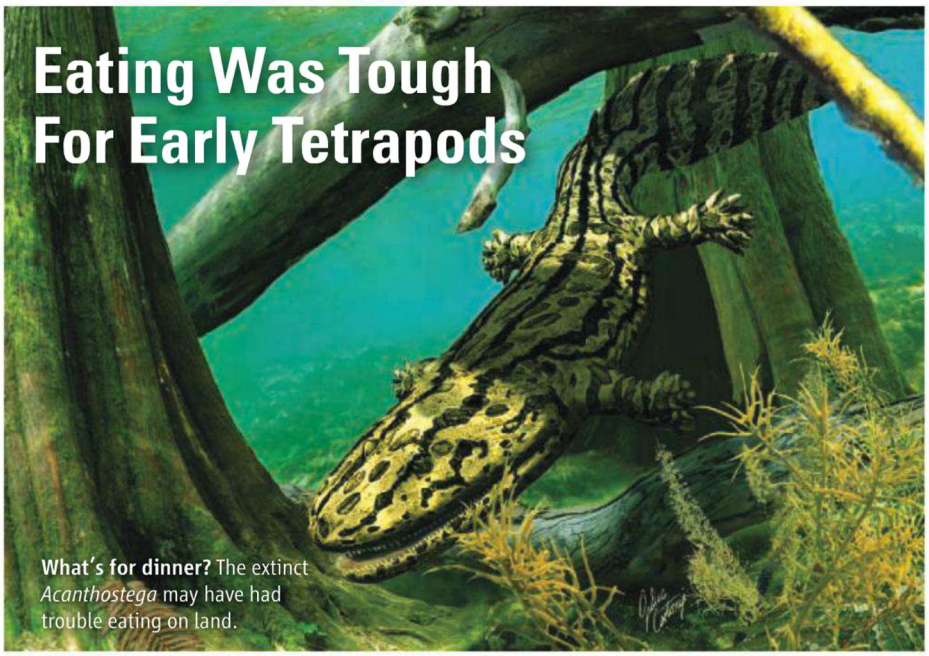

What's for dinner? The extinct *Acanthostega* may have had trouble eating on land.

While a fin-to-limb transition made possible the first steps on land for vertebrates 390 million years ago, it took a long time for ancient tetrapods to leave behind their aquatic ways and become true landlubbers. After that initial landfall, another 80 million years went by before tetrapods developed jaws adapted for terrestrial feeding, according to Philip Anderson, an evolutionary paleobiologist at the University of Massachusetts, Amherst, who presented a survey of fossils from this time period at the meeting.

Those early tetrapods must have had a hard time figuring out how to swallow terrestrial food, if another study presented at the meeting is any guide. That work described the great lengths that some modern fish must go to catch and eat prey out of water. "That's something that paleontologists have not thought about too much," says Alice Gibb, a functional morphologist at Northern Arizona University in Flagstaff. The combination of paleontology and functional morphology evidence shows "that the switch [to eating on land] was awfully hard," concludes Richard Blob, an evolutionary biomechanist at Clemson University in South Carolina.

Vertebrates were among the last animals to crawl onto land. Which locomotor changes enabled this move "is pretty well resolved," says Michael Coates, a vertebrate paleontologist at the University of Chicago in Illinois. But understanding what and how the first four-legged vertebrates ate "is somewhat in its infancy," says Miriam Ashley-Ross, a functional morphologist at Wake Forest University in Winston-Salem, North Carolina.

Some researchers have argued that the first tetrapods were quick to exploit land-based food; others are not sure whether these animals were "surf" or "turf" eaters. Anderson began to wonder about the transition to terrestrial diets 2 years ago, after an initial survey of fossils confirmed that the lower jaws of early tetrapods were very fishlike. He and his colleagues have now extended that work, in all measuring jaws from 97 genera dating from the Devonian 416 million years ago through the early Permian, 295 million years ago. The fossils included classic early tetrapods such as *Acanthostega* and *Tiktaalik*, some closely related fish, ancestral amphibians, and some later evolving reptilelike and mammal-like species. Early tetrapods had elongated jaws, like those in their fish ancestors. But about 80 million years into their evolution, shorter, deeper jaws appeared, Anderson found. These stronger jaws would have been better able to munch on vegetation, he notes.

Early on in tetrapod evolution, "big changes are going on elsewhere in anatomy and the jaws lurch into changing later on," Coates says. During that period, the researchers suggest, these animals may have made brief forays onto land but hunted in the water.

With fishlike mouths, early tetrapods would have faced a difficult task eating on land. Underwater, fish usually rely on suction to draw food into their mouths and swallow. To generate enough inward force in less dense air, a fish—or early tetrapod—would have to expand its mouth 28 times faster, Sam Van Wassenbergh, a biomechanist at the University of Ghent in Belgium, reported at the meeting. And even then, because air is so much less viscous, the air flow might not be enough to draw in prey. Moreover, most fish mouths face forward to grab food items suspended straight ahead in water, not food laying below on the ground.

Many modern terrestrial tetrapods have solved their swallowing problem by having tongues do the job. But Van Wassenbergh started thinking about how early tetrapods might have dined on land after he studied the eel catfish, which lives in the muddy swamps of tropical Africa. It has a tiny head and a long body with no paired fins. When he filmed this fish in 2006, he determined that the secret to its success to capturing insects on land was arching the front end of its body to position the mouth directly over the prey. Once the food is captured, the catfish quickly slips back into the water; only there, where it can take in water to wash down the prey, can it swallow, Van Wassenbergh said.

More recently, he has turned to mudskippers, 15-centimeter-long fish commonly found in the mud in mangrove swamps. In contrast to the eel catfish, the mudskipper has big paired fins and doesn't have to go back into the water with each mouthful of prey.

Mudskippers solve the swallowing problem by carrying water with them, Van Wassenbergh reported. His studies revealed that these fish fill their mouths with water before emerging onto land. They scoot along with their fins, then bend their head down to grab the food. As they do this, they compress the sides of the mouth, moving the water forward and, sometimes, forcing water out as they grab the prey. Instantly, the fish sucks the water back in. That mouthful of water enables them to swallow and keep hunting.

Fossils rarely preserve evidence of the muscles and cartilage connecting bones, and the dearth of such soft tissue data makes it difficult to know how exactly early tetrapods could maneuver their jaws or swallow. But although these animals lacked the complex mouths of mudskippers, Van Wassenbergh "showed that it is possible for something to come up on land and still use the fish suction system," Anderson says. That's certainly food for thought for those trying to reconstruct the life of early tetrapods.

CREDIT: JULIUS T. CSOTONYI

Nervous System May Have Evolved Twice

Biologists have long assumed that the neuron—with its axon, synapses, long processes called dendrites, and a suite of nerve-specific proteins—is the epitome of a specialized cell and thus likely to have evolved only once in the history of life. But a newly sequenced genome of a comb jelly, an ocean-going predator sometimes confused with traditional jellyfish, threatens to upend this view.

The DNA data put these invertebrates, also known as ctenophores, on a different, older branch of the tree of life from that of other organisms with complex nervous systems. This new placement will be controversial, but it suggests to some researchers that nervous systems arose twice. Indeed, the ctenophore's nervous system does appear to be different from those of other animals because its genome lacks genes for proteins that are considered essential to nervous system development and function. "All the things that are fundamental to [a nervous system] are missing in ctenophores," says Casey Dunn, an evolutionary biologist at Brown University.

Leonid Moroz, a neurobiologist at the University of Florida's Whitney Laboratory for Marine Bioscience in St. Augustine, and his colleagues study ctenophores and other invertebrates belonging to animal groups that arose early in the history of life. Comb jellies have an elementary brain and true nerve cells linked by complex synapses to muscles. In contrast, some of the other groups, like jellyfish and other cnidarians, simply have nets of nerve cells and no real brain—and sponges have no nerve cells to speak of.

Some analyses have indicated that ctenophores branched off on the tree of life late, just before all the bilateral animals; other data have them branching off earlier, alongside jellyfish; and at least one controversial study has them arising even before sponges, considered by some to be the most basal multicellular animals.

Moroz and his colleagues recently sequenced the genome of the comb jelly *Pleurobrachia bachei*. Comparing this genome with those of other organisms, Moroz's team concludes that ctenophores split off early, perhaps even before sponges and another odd group called placozoans, which also have no neurons. In this arrangement of the tree of life, if there were a single origin of the nervous system, sponges and placozoans would have had to discard nerve cells and other neural attributes, Moroz told the meeting. More likely, he argued, ctenophores evolved a nervous system after they split off from other animals and became predators, and then another nervous system arose separately, after the sponges and placozoans split off, in the branch leading to cnidarians and bilateral animals.

Independently, researchers at the National Human Genome Research Institute (NHGRI) in Bethesda, Maryland, have deciphered the genome of another ctenophore, and they made the data available to Moroz and others. At the meeting, NHGRI geneticist Andy Baxevanis said their analysis did not completely confirm Moroz's basal placement of ctenophores. However, other evidence suggests an independent origin of the ctenophorean nervous system. Both sequenced comb jellies lack *Hox* genes, which are considered crucial for patterning the developing nervous system in other animals. Also, the molecules in the *P. bachei* synapses are different from those in the nervous systems of other organisms, including jellyfish, Moroz reported. Ctenophores lack the neurotransmitter serotonin, for example. "There are many ways to skin a cat and there are many ways to make a neuron," he says.

Chris Lowe, an evolutionary developmental biologist from Stanford University's Hopkins Marine Station in Pacific Grove, California, welcomes the new sequence data and Moroz's conclusion about the independent evolution of the nervous system. "It's great that he's bringing up these issues," Lowe says. Ctenophores are so different from other organisms in their genetic makeup that "they well may have a nervous system that is totally independent." **–ELIZABETH PENNISI**

CREDIT: LEONID MOROZ

Smart jelly. Ctenophores may have independently evolved a nervous system.

Snapshots From the Meeting >>

Shedding light on how moths track flowers blowing in the wind. Like hummingbirds, hawkmoths hover as they feed on nectar and pollen, so they must track a flower's motion in a breeze to stay with it. Simon Sponberg, a neuromechanist at the University of Washington, Seattle, wondered how moths were able to follow a flower in dim light, because these insects tend to forage at dusk and dawn. By studying the moths' aerial responses to robotic flowers swaying at different speeds in different light levels, he has determined that the moth brain can function even in dim conditions because it takes more time to gather light and produce an image. This adaptation becomes a liability when the flower oscillates more than twice per second, as the moth can't keep up, he reported at the meeting. But Sponberg's high-speed videos of actual flowers blowing in the wind show that blooms typically oscillate more slowly than that. "The moth was free to make this adaptation without having to make a trade-off," Sponberg said. "It tracks at relevant frequencies and doesn't care about what happens" at faster frequencies.

Calcified seaweed bucks the waves with joints. Typically attached to rocks in the surf, coralline algae earned their name because their fronds are calcified, like a coral. Compared with other intertidal algae, such as *Mazzaella flaccida* with its rubbery fronds, these hand-sized seaweeds look quite fragile. Actually, the opposite is true, Mark Denny, a biomechanist of Stanford University's Hopkins Marine Station in Pacific Grove, California, reported at the meeting. His team had previously found that *Mazzaella* can withstand a very powerful single wave, but not repeated battering. In contrast, the coralline alga *Calliarthron cheilosporioides* is "indefatigable," Denny says. He simulated an aquatic battering by gluing the algae to a computer-operated device that repeatedly pulled and released tension on it. The algae often lasted a million cycles before tearing apart and one specimen didn't break after 51 million pulls on it. The algae's secret: The fronds periodically have one-cell-thick joints where the cells are like cables—attached at the top and bottom to the calcified parts but not to each other. Thus, if one cell in a joint fails, the fatigue doesn't spread to the rest, Denny reported. This property may explain why coralline algae dominate the most wave-swept shores, he notes. **–E. P.**

Dead-animal stories
395

Organic options for ferroelectrics
401

LETTERS

edited by Jennifer Sills

Accidental Island Voyagers

THE PERSPECTIVE "MEDITERRANEAN ISLAND VOYAGES" (A. SIMMONS, 16 November 2012, p. 895) is predicated on the widely stated assumption that hominin remains on an island are evidence of intentional voyaging across the seas. Seafaring ability is generally linked to tool use, high cognitive functioning, language, and cooperative behavior. The idea that islands can only be reached after construction and use of watercraft, as assumed by Simmons, is thus very important in relation to our understanding of the timing of development of complex cognition in hominins, especially given the early occupation of Flores Island. However, we feel that the assumption is unsafe; island colonization could occur if humans are carried out to sea by a tsunami, tropical storm, or flash-flooding river and then washed up together on an island.

There are 6000 to 10,000 inhabited islands in the Pacific alone. Although such an event may be unlikely for any particular island, with many islands and frequent storms and tsunamis, it may occasionally have happened.

GRAEME D. RUXTON[1]* AND DAVID MARK WILKINSON[2]

[1]University of St Andrews, St Andrews, KY16 9AX, UK. [2]Natural Science and Psychology, Liverpool John Moores University, Byrom Street, Liverpool, L3 3AF, UK.

*To whom correspondence should be addressed. E-mail: gr41@st-andrews.ac.uk

Response

RUXTON AND WILKINSON INTIMATE THAT EARLY HUMANS MAY HAVE washed up on islands like coconuts (*1*). They are correct to point out that not all sea voyages need be intentional, nor do they necessarily have to be made in seacraft. There are many cases showing that animals can be accidental voyagers, hitching rides on natural rafts or driftwood. This certainly could pertain to unfortunate humans caught up in the types of aquatic catastrophes Ruxton and Wilkinson envision. I do not deny the possibility of accidental island landings by

theBUZZ

Skin-Deep Learning

In his Editorial "Failure of skin-deep learning" (7 December 2012, p. 1263), B. Alberts lamented the lack of in-depth learning in today's U.S. schools. Readers wrote in to add their experiences.

A selection of your thoughts:

I encouraged my son to take biology as a freshman in high school, and the experience had the opposite effect from what I had hoped for—it turned him off sciences permanently. The textbook was just as you describe—full of biochemical detail from mitochondrial function to the Krebs cycle—impossible to comprehend without biochemistry. It becomes a vocabulary memorization experience rather than science.

—Miriam Meisler

Fortunately, in the New South Wales, Australia education system, there are no mandated textbooks for any high school science course…. While there is an emphasis on a thematic, in-depth approach as proposed by Editor-in-Chief Bruce Alberts, there is concern among some science educators that not enough emphasis is made on students learning basic facts. In the same way that mathematics students find algebra difficult without a rote-learned knowledge of the times table, it is difficult to develop an understanding of chemical processes involved in water pollution without factual knowledge of elements, compounds, mixtures, chemical reactions, and their symbolic representations….The challenge is developing a balance between learning facts and applying them to learning activities reflecting real-world issues…..

—Stephen Kirk

…There are colleagues who believe that you can educate future generations of systems biologists at the undergraduate/graduate level by teaching them a balanced mix of biology and hard sciences (computer sciences, physics, math, engineering, etc.). But I wonder if we could extend Alberts' argument to saying that unless you go seriously deep into biology and any of the above (which may be humanly impracticable), you'll be creating jacks of all trades, masters of none….

—Mariano Loza-Coll

Bruce Alberts was able to fully exploit his college experience because of the knowledge that he had absorbed from his high school courses, much of it gained through memorization….[T]he goal of memorization never is to be an end in itself. It lays a foundation, a platform from which increasingly wider and deeper learning can take off.

—Ann Agee

… I think we can easily incorporate a current events section in many middle school and high school curricula that would teach kids that science is more than memorizing enzyme names and the spelling of the names of bacteria.

—Andrew Malaby

I don't believe that just zooming in is a way of improving learning. Sometimes you have to see the forest to understand the tree….

—Daniel Ricciardi

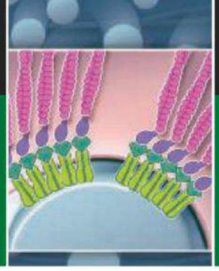

Sensing 3D
402

IBI Prize Essay
408

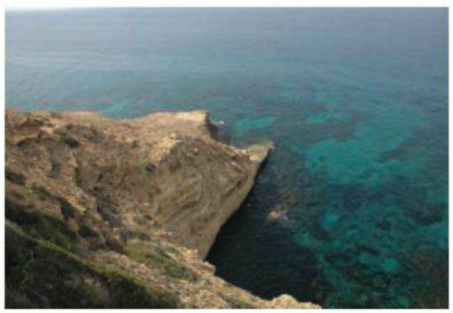

CREDIT: ALAN SIMMONS

small numbers of humans, but in terms of archaeological visibility, these would be very difficult to document.

It is unlikely but within the realm of possibility that accidents could account for some of the early remains I noted. There is even an interesting literature, generally dismissed by contemporary anthropology, proposing that premodern hominins, or "aquatic apes" (*2*–*5*), may have been well adapted to water environments.

However, as Ruxton and Wilkinson note, we are dealing with issues of scale. The nature of the archaeological record requires a search for patterns. When numerous examples of a particular cultural period are found within a restricted area (islands in this case), a considerable population might be inferred. This is unlikely to be the case in the accidental scenario. Furthermore, one must take into account the likelihood of viable groups in such accidental scenarios. Although it is not impossible that both men and women could be swept away to islands by natural events, it seems unlikely that sustainable rates would be high even if they survived their time adrift.

Finally, in my later examples (the Neolithic), there is no doubt that actual colonization was occurring. For example, the Neolithic colonists of Cyprus arrived with a full suite of domestic plants and animals, and quickly established permanent villages. Such intentionality could not have been accidental.

ALAN SIMMONS

Department of Anthropology, University of Nevada, Las Vegas, Las Vegas, NV 89154, USA. E-mail: simmonsa@unlv.nevada.edu

References

1. H. Harries, *Bot. Rev.* **44**, 265 (1978).
2. E. Morgan, *The Aquatic Ape Hypothesis* (Souvenir, London, 1997).
3. M. Vergaegen, S. Munro, *HOMO-J. Comp. Hum. Biol.* **62**, 237 (2011).
4. S. Munro, M. Verhaegen, in *Was Man More Aquatic in the Past?* M. Vaneechoutte, A. Kuliuka, M. Verhaegen, Eds. (Bentham Science Publishers, Oak Park, IL, 2011).
5. R. Wrangham *et al.*, *Am. J. Phys. Anthropol.* **140**, 630 (2009).

Letters to the Editor

Letters (~300 words) discuss material published in *Science* in the past 3 months or matters of general interest. Letters are not acknowledged upon receipt. Whether published in full or in part, Letters are subject to editing for clarity and space. Letters submitted, published, or posted elsewhere, in print or online, will be disqualified. To submit a Letter, go to www.submit2science.org.

Extend Data Exclusivity to Save Drug Development

IN HIS PERSPECTIVE "CAN INTELLECTUAL PROPerty save drug development?" (26 October 2012, p. 483), G. A. FitzGerald points out that the "vertically" integrated pharmaceutical companies—those that encompass everything from discovery through marketing—are disappearing because they are not able to develop new products fast enough. As one possible solution, FitzGerald suggests changing to a more collaborative model that focuses less on discovery and more on sharing data. I would like to offer a simpler solution.

The contraction of the pharmaceutical industry over the past decade has given contract research organizations access to development expertise for a wide variety of drugs. This has facilitated the creation of modular (as opposed to vertically integrated) for-profit companies focused on new ideas. The main limitation to the success of these endeavors is the availability of capital that could move projects into the later-stage clinical trials, where the main cost of bringing a drug to market correctly sits. A simple solution to this obstacle would be to change the data exclusivity laws, rather than changing the intellectual property system.

In 1984, the Hatch-Waxman Act gave the FDA the power to give up to 5 years exclusivity for compounds approved for a first use in humans. This provided an incentive to companies to develop potentially useful medicines even if the compounds did not have sufficient coverage as intellectual property. Because of the rising costs of development, this is no longer an adequate incentive. Modifying this law to give longer data exclusivity would facilitate the funding of later-stage development for the best compounds, irrespective of the primary intellectual property. Moreover, if this authority were provided in a way that empowered the regulators to enforce Phase IV (post-approval) studies, tweaking this law would have the added benefit of making better data available to the market for analysis of new products.

JERRY RAYMOND COLCA

Administration, Metabolic Solutions Development Company, Kalamazoo, MI 49001, USA. E-mail: jcolca@msdrx.com

TECHNICAL COMMENT ABSTRACTS

Comment on "Radiative Absorption Enhancements Due to the Mixing State of Atmospheric Black Carbon"

Mark Z. Jacobson

Cappa *et al.* (Reports, 31 August 2012, p. 1078) suggest that black carbon (BC) in a mixture absorbs only ~6% more sunlight than when volatile chemicals are evaporated from the mixture, and state that "many climate models may overestimate warming by BC." However, the authors misinterpret at least some model results and omit optical focusing at high relative humidity and of involatile components. Thus, their conclusion about model error is not demonstrated.

Full text at http://dx.doi.org/10.1126/science.1229920

Response to Comment on "Radiative Absorption Enhancements Due to the Mixing State of Atmospheric Black Carbon"

Christopher D. Cappa, Timothy B. Onasch, Paola Massoli, Douglas R. Worsnop, Timothy S. Bates, Eben S. Cross, Paul Davidovits, Jani Hakala, Katherine Hayden, B. Tom Jobson, Katheryn R. Kolesar, Daniel A. Lack, Brian M. Lerner, Shao-Meng Li, Daniel Mellon, Ibraheem Nuaaman, Jason Olfert, Tuukka Petäjä, Patricia K. Quinn, Chen Song, R. Subramanian, Eric J. Williams, Rahul A. Zaveri

Jacobson argues that our statement that "many climate models may overestimate warming by BC" has not been demonstrated. Jacobson challenges our results on the basis that we have misinterpreted some model results, omitted optical focusing under high relative humidity conditions and by involatile components, and because our measurements consist of only two locations over short atmospheric time periods. We address each of these arguments, acknowledging important issues and clarifying some misconceptions, and stand by our observations. We acknowledge that Jacobson identified one detail in our experimental technique that places an additional constraint on the interpretation of our observations and reduces somewhat the potential consequences of the stated implications.

Full text at http://dx.doi.org/10.1126/science.1230260

PSYCHOLOGY

Making Sense of Rising IQ Scores

Andreas Schleicher

Science has few more controversial topics than human intelligence and, in particular, the relative influence of nature and nurture on IQ scores. Part of the problem is that IQ test scores are only ordinal and lack the properties of true ratio scales: No IQ test has ever classified anyone as gifted or normal. We do that by administering the test to a standardized sample and then classifying individuals based on test performance relative to that sample. That does not make such tests useless, because much of what people want to know about intelligence is comparative in nature. Parents want to know whether their child is bright enough, compared with other children, to outcompete them to get into medical school. But the ordinal nature of IQ scales leads to debate about the interpretation of the measures obtained: When IQ scores increase, some claim that intelligence has risen. Others claim that standards must have been lowered, and behind the suspicion that better results reflect lowered standards is often a belief that intelligence cannot be raised. Even more controversy results from IQ tests not being "factor invariant." Although they rank individuals consistently by their mastery of tasks representing cognitive complexity at any point in time, over successive generations IQ scores have evolved quite differently across different dimensions of IQ tests.

Those psychometricians who only trust measures that are factor invariant will not be swayed by James Flynn's *Are We Getting Smarter?* any more than by his original discovery that over recent decades average IQs around the world have been rising at the rate of 0.3 points a year (the "Flynn effect"). However, those accepting intelligence as a multidimensional construct, the different aspects of which interact with social developments (and Flynn makes a compelling case for that), will find the book an eye-opener. Flynn (University of Otago) makes sense of the rise in IQ scores and explores what this tells us about shifts in habits of minds and our society.

Are We Getting Smarter?
Rising IQ in the Twenty-First Century
by James R. Flynn
Cambridge University Press, Cambridge, 2012. 324 pp. Paper, $22, £16.99, C$22.95. ISBN 9781107609174.

In fact, he shows that much of the value of IQ measures lies in them not being factor invariant. From 1973 to 2000, American 4th and 8th graders have made significant gains in mathematics, putting young children of 2000 at the 68th percentile of their parents' generation. But the gains drop to zero by 12th grade. Flynn resolves that puzzle by relating these results to differential trends in IQ scores: The lack of gains on an IQ test for the kind of mind comfortable with mathematics signals why, by 12th grade, students cannot do algebra and geometry any better than their parents' generation. Signs of improved performance in terms of children becoming better at mastering the computational skills emphasized at young ages are therefore deceptive, as they fade away when being able to think with numbers becomes more important than the mechanics of arithmetic. Similarly, today's children may learn to master basic reading skills at a younger age, but they are no better prepared for reading more demanding adult literature. These findings provide very important insights for educators.

Flynn identifies the Industrial Revolution and its longer-term outcomes—such as more formal schooling, more cognitively demanding jobs, cognitively challenging leisure, and richer interaction between parents and children—as the ultimate cause of IQ gains. Driven mainly by changes in the world of work, adults have expanded their active vocabularies, and more people can read serious literature if they care to do so. Schoolchildren have no greater fund of culturally valued information, but adults do. Both have responded successfully to the greater complexity of contemporary everyday life, including its visual culture and its demands for faster information processing, but neither has become substantially more at ease with numbers. Both have become accustomed to using logic not only on the concrete but also on abstractions. These considerations lead Flynn to suggest that the large gap in average IQ scores between the developed and developing world will close sooner or later. Universal education will instill the level of logical thinking and abstraction that IQ tests require, and one- or two-child families with richer parent-child interaction approach a point beyond which parents will drive children crazy.

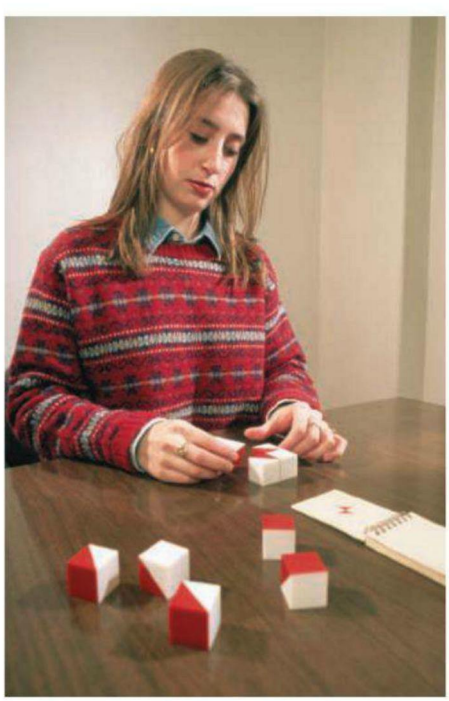

CREDIT: RICHARD T. NOWITZ/CORBIS

Perhaps the book's most interesting contribution lies in integrating the perspectives of psychometrics, cognitive history, and brain physiology. Flynn discusses how intelligence can act like a highly correlated set of abilities on one level (when individual differences are measured), like a set of functionally independent abilities on another level, and like a mix on a third (the brain, whose structure and operations underlie what people do on the former two levels): Performance differences between individuals are correlated primarily in terms of the cognitive complexity of the tasks involved. Various real-world skills show different trends over time as a result of shifting social priorities. And localized neural clusters develop differently as a result of specialized cognitive exercise. Rather than any single perspective, it is the integration of all that explains changes in IQ scores. For example, Flynn illustrates that it is not higher IQ scores but sociology of the family that explains the remarkable academic achievements of Chinese-Americans, whose parents mold children having a passion for educational excellence.

Flynn's analysis has major implications beyond the ways in which we design opportunities for learning throughout life. Failing to understand that IQ scores are meaningless unless we know the test used and when it was normed can make the execution of capital offenders a lottery in which death verdicts are decided by which test they happened to take

The reviewer is at the Directorate for Education, Organisation for Economic Co-operation and Development, 2 rue André Pascal, 75775 Paris Cedex 16, France. E-mail: andreas.schleicher@oecd.org

as schoolchildren or what population they are compared with. If you take a test with current norms and your IQ is 70, you are considered mentally retarded and therefore saved from execution. But if you are unlucky enough to take a test with norms 20 years out of date, the very same performance will yield an IQ of 76, and you will be executed.

So, do IQ gains mean that we are more intelligent than our ancestors? If the question is whether we have better brain potential at conception, the answer is no. Too few generations have passed for natural selection to have had any meaningful impact. But if the questions are "Do we live in societies that pose a wider range of cognitive problems than our ancestors encountered?" and "Have we developed new cognitive skills and the brain physiology that can deal with those problems?" the answer seems yes.

10.1126/science.1232678

MUSEUMS

Charismatic Dead Megafauna

Karen A. Rader

The personification of well-known, singular animals has become a deeply entrenched cultural practice (*1*), perhaps (for the scientifically minded) reaching a postmodern pinnacle with Dolly, the world's first cloned mammal, or Knut, the polar bear raised by zookeepers after being rejected by his mother at birth. Both creatures died (relatively) young but their remains now live on—at, respectively, the Museum of Scotland and the Berlin Natural History Museum. Why and how animals like Dolly and Knut end up in museums—and what museum curators, taxidermists, and visitors make of them once they do—is the central question of *The Afterlives of Animals*.

The Afterlives of Animals
A Museum Menagerie
Samuel J. M. M. Alberti, Ed.
University of Virginia Press, Charlottesville, VA, 2011. 255 pp. $35. ISBN 9780813931678.

In some ways, the set of essays represents a synthesis of editor Samuel Alberti's own interests and academic experience. A historian of Victorian science who has studied natural history museums, he now directs the museum of London's Royal College of Surgeons. Thus, Alberti approaches charismatic dead megafauna on display as both scholar and practitioner—collecting and chronicling their unique stories for posterity while also looking for ways to classify, curate, and make meaning of these beastly narratives.

The individual contributors provide carefully researched "animal biographies" of different specimens. The "afterlives" of the title refers to the complex material, scientific, and cultural trajectories that animals travel when, reborn as specimens, they are collected, preserved, and often put on display. Many of the animals in the book come from the Manchester Museum (where Alberti formerly worked), but other institutions are also represented. Despite the volume's largely Anglo-European focus, one of its strengths is the diversity of scholarly and career backgrounds brought to bear on its inquiry. Writing from their individual disciplinary perspectives, historians, journalists, anthropologists, museum curators, and archeozoologists collectively reveal how "many animals … refuse to be constrained by their zoological classification."

For those animals that were displayed and anthropomorphized in life, personhood (perhaps not surprisingly) continued to be afforded in death. Readers learn how several prominent dead zoo animals—such as the Indian elephant Maharajah, star of a 19th-century Manchester traveling menagerie, and Alfred the Gorilla, one of early-20th-century Bristol's biggest media icons—were revived by museum exhibits. Although their fame waxed and waned (and their spatial centrality to visitors' experiences was not always prominent), as taxidermy or skeletal mounts star animals could successfully become both representative specimens in and mascots of their respective scientific institutions. Other animal luminaries, such as the Hanoverian royalty's many zebra or the London Zoo's giant panda Chi-Chi, live on primarily as emblematic spectacles. Deeply intertwined with the fates of human actors, "the Queen's Ass" became a cultural motif in ballads and broadsheets and on art gallery walls, and the beloved Chinese bear, the face of the World Wildlife Fund.

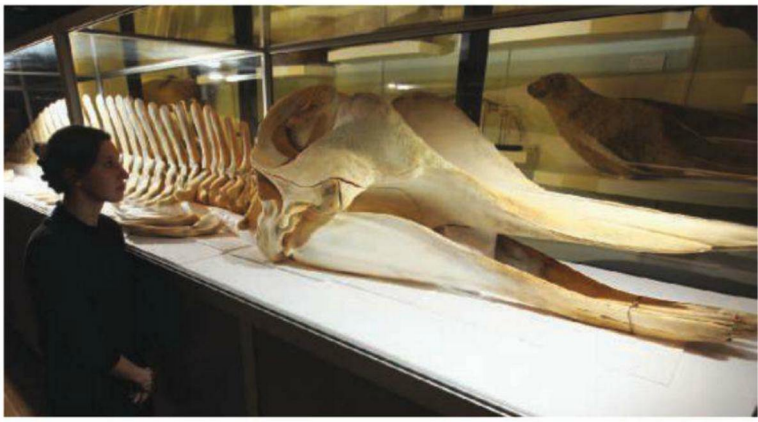

Sad souvenir. The skeleton of the 2006 Thames River whale, a northern bottlenose whale (*Hyperoodon ampullatus*), on display at the Natural History Museum at Tring.

Many more anonymous animal specimens occupy space in museum drawers or in the possession of private collectors. Some of their afterlives are documented and discussed as a kind of a cautionary tale about "the limits of a single biogeographical study." Trophy mounts in hunters' collections, like those in habitat group exhibits, have always required taxidermic preparation, but their importance is linked less to the scientific re-presentation of a wild animal life than to the autobiography of their owners. In turn, the study skins of a female hen harrier (Glasgow's Hunterian Museum and Art Gallery) and the "Manchester mandrill" may be less charismatic and attractive than their front-of-the-house companions, but their tales speak to the value of type specimens for reconstructing the shared environmental and cultural histories of animals.

A few of the essays deal more directly with some important political and ethical issues raised by these animal narratives. Preserved dogs (e.g., the Siberian husky Balto at the Cleveland Museum of Natural History) and iconic whale skeletons (e.g., that of the whale that swam up the Thames and died in 2006) are "sad souvenirs" of animal lives that have ended. Such creatures prompted Henry David Thoreau to confess: "I hate museums; there is nothing so weighs upon my spirit. They are the catacombs of nature." But the re-imagination and re-presentation of animals in the museum space has the potential, Alberti optimistically concludes, "to engage audiences" right where they already are: thinking about nature in relation to culture.

References and Notes

1. For a media analysis of this phenomenon, see (*2*).
2. E. Gouabalt, A. Dubied, C. Burton-Jeangros, *Humanimalia* **3**, 77 (2011).

10.1126/science.1232259

The reviewer is at the Science, Technology, and Society Program, Virginia Commonwealth University, Richmond, VA 23284–2001, USA. E-mail: karader@vcu.edu

CREDIT: OLI SCARFF/GETTY IMAGES

SCIENCE EDUCATION

Science Learning Progressions

New science education standards build upon research-based cognitive models of how learning unfolds over time.

Ravit Golan Duncan[1]* and Ann E. Rivet[2]

Guided by the 2011 U.S. National Research Council framework for science education (*1*), the most recent draft of the Next Generation Science Standards (NGSS) is briefly open for public comment (*2*). Key goals of this effort (*3*) include (i) reducing coverage to a select set of "big ideas" (e.g., atomic molecular theory, biodiversity, energy); (ii) providing a progression to facilitate coherence in learning of these ideas over the course of schooling; and (iii) promoting a practice-oriented approach to inquiry-based science learning.

This reform of standards is meant not merely to update content, but to shift the way U.S. kindergarten through high school (K–12) science education is conceptualized and implemented. The NGSS reflect an evolved vision of inquiry-based learning, emphasizing science as a knowledge-building endeavor. An improvement over prior science education standards (*4*), the NGSS are embedded in learning progressions (LPs)—research-based cognitive models of how learning of scientific concepts and practices unfolds over time. This stresses coherence in the conceptual growth of scientific reasoning across grades.

We discuss the theory and implications of the LP approach underlying the NGSS. We highlight key features of LPs and examine some challenges that accompany development and validation of these constructs.

Reframing the Science Content

Embodying a developmental approach to learning, LPs describe paths by which students might develop more sophisticated ways of reasoning over extended periods of time (*5*–*7*). LPs begin with consideration of learners' prior knowledge and build toward targeted learning goals through carefully designed instruction. These progressions define intermediate levels in students' understanding, derived, where possible, from research on student learning.

A feature of LPs, reflected in the NGSS's guiding framework (*1*), is that core disciplinary concepts are built and refined through engagement with the practices of scientific inquiry. The framework views scientific inquiry as a theory-building enterprise that uses systematic and evidence-based approaches to create models that explain the world around us (*8*). Scientists develop these models within a community with socially constructed and continually negotiated epistemological norms regarding what is knowable, how best to come to know it, and what counts as knowing (*9*). Such norms, often implicit, guide core scientific practices such as research design, data analysis, modeling, and argumentation and are thus critical to the development of valid and reliable scientific knowledge. The trio of concepts, practices, and epistemology is at the heart of the efforts to revise K–12 science standards.

The educational system includes LPs, classroom and large-scale assessments, and the curricula and instruction that drive learning. Assessment plays a major role in the development, validation, and use of LPs. Progressions in turn can inform science standards and are implemented through curricula and classroom instruction. Much of the research on LPs is in its infancy, and current models are largely conjectural owing to gaps in the research base. Nevertheless, they offer a productive starting place for developing standards, curricula, and assessments.

Leveraging Stepping-Stone Ideas

LPs differ from current descriptions of scope and sequence in two important ways. First, to the extent possible, they are grounded in research regarding how students actually come to understand core ideas in science rather than relying solely on normative knowledge in the domain. This is critical because intermediate steps in a LP may include understandings that vary from the canonical knowledge of science. Second, as opposed to adding more information or details over time, LPs focus on deepening understandings and developing increased complexity, applicability, and epistemological rigor with each learning opportunity.

Stepping-stone understandings on the LP path toward targeted knowledge in a domain can be substantially different from accepted scientific concepts. For example, at the middle school–level, students should understand genetic information as specifying the structure (and consequently, the function) of proteins (*10*). Such a conception, while grossly incomplete, is a highly productive intermediary that allows students to explain how genes bring about their observable effects. Similarly, establishing weight as a property of matter is important in early grades, necessary to understanding that even invisible things (e.g., gases and atoms) have weight (*11*). This targeted understanding conflates weight with a more scientific notion of mass, but serves as a productive step toward developing a full understanding of the particulate nature of matter in later grades. The term "mass" is meaningless to young learners and using it does not help them understand this concept.

It is important to differentiate between scientifically inaccurate ideas that are conceptually unproductive and understandings that are inaccurate, yet productive, and that can foster learning of more sophisticated understandings.

Although inaccurate understandings can be conceptually productive stepping stones, the extent to which these should be reflected in standards and curricula is controversial. Developers are reluctant to present wrong ideas in standards, and teachers are concerned about teaching them (*12*). It is important to differentiate between scientifically inaccurate ideas that are conceptually unproductive and understandings that are inaccurate, yet productive, and that can foster learning of more sophisticated understandings. The former are simply wrong; the latter can be seen as incomplete, overly simplistic, or tied to only a few limited contexts. LPs suggest productive—yet at times inaccurate—and understandings that are important building blocks in the learning process. We believe it is counterproductive to shy away from such inaccuracies in the development of standards, assessments, and curricula. Conversely, stan-

[1]Graduate School of Education, Rutgers University, New Brunswick, NJ 08901, USA. [2]Teachers College, Columbia University, New York, NY 10027, USA.

*Author for correspondence. E-mail: ravit.duncan@gse.rutgers.edu

dards and curricula should set as goals such stepping-stone ideas and clearly articulate the basis for their conceptual usefulness.

Challenges to Assessment

When compared with traditional content-centered scope and sequence, LPs present advantages and challenges to the development and use of science assessments at both local and national scales. LPs can inform the design of assessments that capture the nature of students' developing understandings in nuanced ways, as opposed to simply whether or not they "got it." Likewise, assessments play a critical role in informing the development, validation, and use of individual LPs. Such assessments can detect the range of students' abilities, or levels of sophistication, as well as the appropriateness of particular assessment items for evaluating different student groups (*13*, *14*).

However, the process of developing assessment measures to diagnose levels of student reasoning on a LP presents challenges. Students at the high end of a LP tend to demonstrate reasoning that is robust and consistently applied to diverse assessment tasks. Students at the beginning of a LP typically perform poorly across items (*15*). Yet, at intermediate levels of a LP, students' levels of understanding may vary from item to item because their developing knowledge is not robust enough to be consistently applied to diverse situations and phenomena. Therefore, assessments need to attend to the context and features of items and how these are correlated with intermediary steps in a LP. We believe this is a challenging, yet tractable, problem addressed through partnerships of learning scientists, psychometricians, and assessment experts.

Content, Epistemology, and Practices

The LP approach emphasizes science as a theory-building social enterprise steeped in practices and epistemological norms. This perspective is dramatically different from the outmoded stepwise scientific method that is still the predominant focus of science instruction (*16*). For example, students frequently identify hypotheses to test, but these are not grounded in any model of the phenomenon under study. Experimental heuristics, such as "vary-one-thing-at-a-time," are used by students in an epistemological vacuum without consideration of the relevance of variables to the theoretical model. When students engage in developing explanations they commonly do not use evidence to support their arguments and rarely entertain more than one plausible explanation (*17*). Science education should instead engage students in the practices of scientific theory development. Students should generate evidence-based explanations and critique alternative explanations as part of a knowledge-building community with agreed-upon epistemological norms akin to those used by scientists (*18*).

Consequently, a LP perspective contends that all three aspects of deep understanding—content, practices, and epistemology—need to be inherently and consistently integrated throughout instruction across all grades (*1*). For instance, when learning about variation, a concept fundamental to understanding evolution, second graders can measure and model data of variation (practice) across multiple populations and develop a sense of what counts as valid and significant measures of variation (epistemology) (*19*). High school students can develop understanding of natural selection (content), argue about which of several potential environmental pressures are driving selection (practice), and identify what counts as credible evidence about the causal relation between the pressure and the adaptive trait (epistemology) (*20*). Helping students develop scientific knowledge that merges content, practice, and epistemology requires that they develop the knowledge for themselves, see its utility, and practice applying it across a range of contexts (*21*, *22*).

Yet, the NGSS's push to intertwine practices with content and epistemological perspectives across the curriculum is replete with tensions and trade-offs. Questions remain regarding the most appropriate and effective ways to concurrently develop these aspects of scientific reasoning. Most research has (by necessity) elected to place one aspect in the foreground, with some focusing more on content while others focus more on practices and epistemology. We do not yet clearly understand how development of a specific practice affects, and is affected by, development of particular content understandings. It is likely that specific "big ideas" pair better with some practices than with others. Ongoing research is developing ways of theorizing about and examining these interactions and their effect on developing holistic understandings of science.

Engaging the Scientific Community

Given the time-consuming and resource-intensive nature of LP research, only a limited array of fully developed exemplar LPs exists to inform conversations about educational policy, curriculum, and assessment. Little is known about how existing LPs interact within and across disciplines. For example, there are several LPs that together describe development of the big idea of atomic-molecular theory across segments of the kindergarten through college continuum. Yet, stitching these discrete progressions into a coherent trajectory that spans schooling is not trivial. The field has yet to examine how cross-cutting big ideas, such as energy, develop concurrently within progressions across the biological, physical, and earth sciences. That being said, efforts around LPs build on available research in cognition and learning (*23*) and can help us make informed conjectures regarding the most productive directions for science standards, curriculum, and assessment.

As the NGSS come into play (with targeted completion in 2013), it is important for the scientific community to be partners in the dialogue, even as we are mindful of the promises and pitfalls of LPs and their translation into standards. Scientists need to be aware of the long view taken by this approach and the conceptual role of simplified stepping-stone ideas in the learning process.

References and Notes

1. National Research Council, *A Framework for K–12 Science Education: Practices, Crosscutting Concepts, and Core Ideas* (National Research Council, Washington, DC, 2011).
2. Next Generation Science Standards, www.nextgenscience.org.
3. B. Alberts, *Science* **329**, 491 (2010).
4. National Research Council, *National Science Education Standards* (National Research Council, Washington, DC, 1996).
5. T. Corcoran, F. A. Mosher, A. Rogat, *Learning Progressions in Science: An Evidence-Based Approach to Reform* (Center on Continuous Instructional Improvement, Teachers College, Columbia Univ., New York, 2009).
6. R. G. Duncan, C. Hmelo-Silver, *J. Res. Sci. Teach.* **46**, 606 (2009).
7. R. A. Duschl, H. A. Schweingruber, A. W. Shouse, Eds., *Taking Science to School: Learning and Teaching in Grades K-8* (National Research Council, Washington, DC, 2007).
8. R. N. Giere, *Philos. Sci.* **71**, 742 (2004).
9. P. Kitcher, *The Advancement of Science* (Oxford Univ. Press, New York, 1993).
10. R. G. Duncan, A. D. Rogat, A. Yarden, *J. Res. Sci. Teach.* **46**, 655 (2009).
11. M. Wiser, C. Smith, S. Doubler, in (*23*), pp. 359–403.
12. J. Foster, M. Wiser, in (*23*), pp. 435–460.
13. A. E. Rivet, K. A. Kastens, *J. Res. Sci. Teach.* **49**, 713 (2012).
14. M. Wilson, *Constructing Measures: An Item Response Modeling Approach* (Erlbaum, Mahwah, NJ, 2005).
15. J. T. Steedle, R. J. Shavelson, *J. Res. Sci. Teach.* **46**, 699 (2009).
16. C. A. Chinn, B. A. Malhotra, *Sci. Educ.* **86**, 175 (2002).
17. L. K. Berland, B. J. Reiser, *Sci. Educ.* **93**, 26 (2009).
18. M. Ford, *Sci. Educ.* **92**, 404 (2008).
19. R. Lehrer, L. Schauble, *Sci. Educ.* **96**, 701 (2012).
20. W. Sandoval, *Sci. Educ.* **89**, 634 (2005).
21. D. C. Edelson, *J. Res. Sci. Teach.* **38**, 355 (2001).
22. A. E. Rivet, J. S. Krajcik, *J. Res. Sci. Teach.* **45**, 79 (2008).
23. A. Alonzo, A. Gotwals, Eds., *Learning Progressions in Science: Current Challenges and Future Directions* (Sense Publishers, Rotterdam, Netherlands, 2012).

10.1126/science.1228692

STRUCTURAL BIOLOGY

Membrane Protein Twists and Turns

Membrane proteins undergo complex distortions and rearrangements as they are inserted into the membrane.

James U. Bowie

The more than 300 unique structures of membrane proteins solved to date (*1*) provide atomic-level insights into how membrane proteins can facilitate the highly specific and rapid passage of various molecules across the membrane. Only the most jaded scientist could fail to marvel at the molecular elevator that delivers aspartate across the membrane (*2*) or the protein finger that kicks maltose out of its binding pocket during transport (*3*). The structural bonanza has also provided important insights into the feats of molecular gymnastics that allow correct folding of the polypeptide in the membrane. Yet the structural complexity of membrane proteins raises many thorny folding questions that need to be answered.

In 1990, Popot and Engelman proposed that the hydrophobic transmembrane helices are first established across the bilayer and then assemble to form the final three-dimensional bundle (*4*). This model may apply in simple cases, but as a ClC chloride channel structure (see the figure, panel A) (*5*) makes clear, the pathway for membrane protein folding can be much more complicated. The ClC structure is not a neat bundle of rigid, membrane-spanning helices. Some helices break in the middle and change direction; others begin and end within the core of the membrane. For such structures, it is hard to envision completely separate topology and folding stages. In the following, I highlight some of the protein-folding events that must occur during or after insertion into the membrane, treated in order of increasing degrees of complexity.

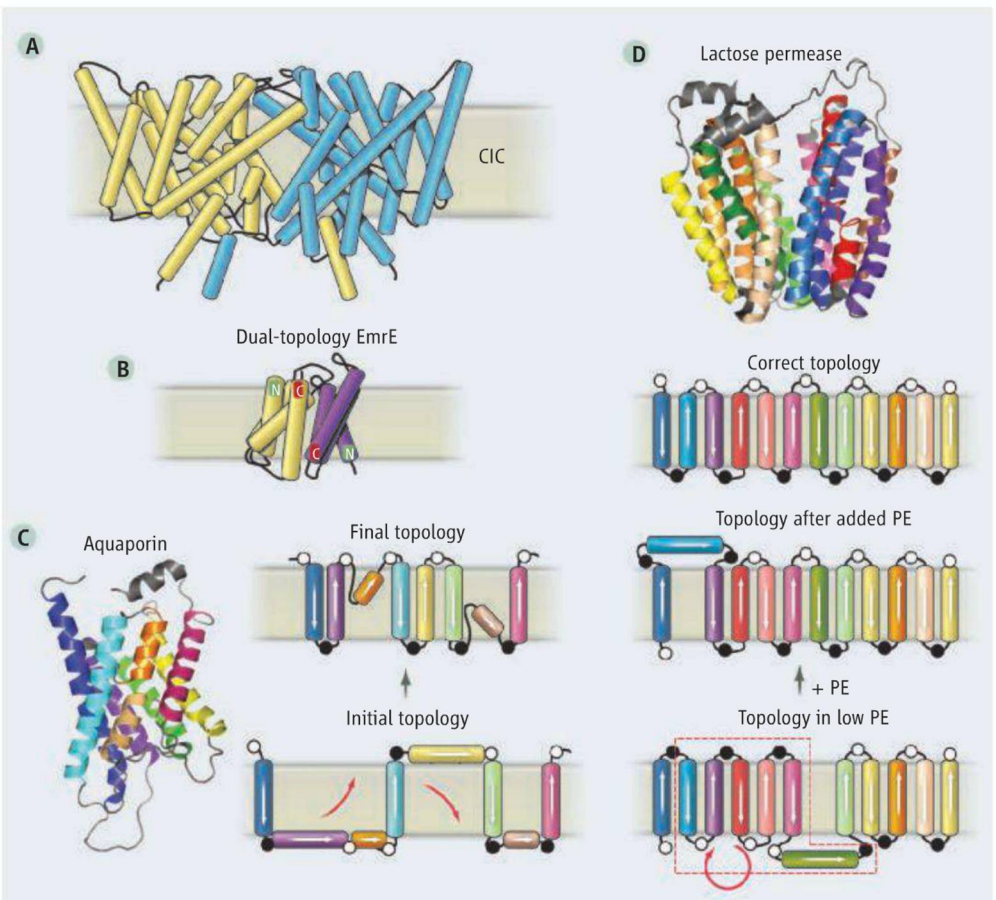

Complex membrane protein folding. (**A**) The ClC chloride channel, which consists of two subunits, has a complex arrangement of helices. (**B**) The EmrE protein has two identical subunits with completely inverted topology. (**C**) The topology of aquaporin 1 changes before and after insertion into the membrane. The red arrows highlight the direction of helix rearrangements. Several helices must either insert into the membrane or flip orientations. (**D**) Topology rearrangements in lactose permease with varying lipid composition. The helices that undergo topology rearrangements in the distinct lipid environments are circled in the dashed red box.

The first level of complexity is helix distortion. High-resolution structures show that most transmembrane helices are not straight, canonical α helices, but rather contain frequent bends and kinks. This is a surprise, because the backbone hydrogen bonds should be quite stable in a lipid bilayer and might be expected to favor rigid, canonical α helices. So how do they bend?

Many kinks occur at proline residues, which cannot exist in a canonical α helix because of steric restrictions, but many kinks do not involve proline. Moreover, even at proline kinks, the proline is not necessarily required for bending (*6*). Recent work suggests that the backbone hydrogen bonds in transmembrane helices can readily shift partners to accommodate bends with minimal energy cost (*7*). As a result, the helices may bend easily to maximize interactions with the rest of the structure. The helices seem to be so malleable that subtle local sequence determinants can create stable helix bending, as recently shown by the kinked transmembrane helix structure of amyloid precursor protein (*8*).

The second level of folding complexity is so-called reentrant segments that plunge deeply into the membrane region and then loop back out on the same side; many of these features occur in the ClC structure shown in panel A of the figure. The reentrant seg-

Department of Chemistry and Biochemistry, UCLA-DOE Institute of Genomics and Proteomics, and Molecular Biology Institute, University of California, Los Angeles, Los Angeles, CA 90095, USA. E-mail: bowie@mbi.ucla.edu

ments require breaking of the helices, which exposes backbone hydrogen bond donors and acceptors. The hydrogen bonding potential can be satisfied by water penetrating into the protein core or other polar side chains within the polypeptide. But how do the reentrant loops get there in the first place? Studies of aquaporin 1 folding suggest that during protein synthesis, the loops initially form extramembrane segments that later dip into the protein (*9*). It seems clear that folding and reentrant loop insertion are coupled events, but the mechanism remains unknown.

Perhaps the most surprising complexity of membrane protein folding is seen in dual-topology proteins (*10*). Some transporters, exemplified by the multidrug transporter EmrE (*11*), have two identical subunits with completely inverted topology (see the figure, panel B). How can an identical sequence adopt two completely opposite topologies? One possibility is that the sequence information is perfectly balanced, so that the polypeptide has a 50:50 shot at either topology as the protein is being synthesized. This seems like a tall order for evolution to fulfill, however. Even a modest energy imbalance would lead to a lot of orphan polypeptide chains without a partner.

Another possibility is that the entire subunit can flip in the membrane after synthesis. Flipping could continue until the chain found its appropriate partner, allowing a perfect balance of topologies. But how likely is it that an entire polypeptide could flip in the membrane? It is actually not so farfetched. Seppälä *et al*. have shown that a positively charged residue at the carboxyl terminus of EmrE can define its topology (*12*). Even when they added an extra transmembrane helix at the end of EmrE, the last residues of the new helix were found to influence topology. This implies that transmembrane helices must still be able to flip after the ribosome has finished making the protein. Lu *et al*. have reported a similar phenomenon for aquaporin 1 insertion (*9*). This protein initially inserts with an incorrect topology and then rearranges to the correct topology late in its biosynthesis (see the figure, panel C). Thus, topology can remain malleable until the protein becomes folded.

How might topology flipping occur? It is possible that unknown folding chaperones catalyze topology rearrangements. Candidates for chaperone functions are accessory proteins that associate with the core translation and insertion machinery during membrane protein insertion (*13*).

However, protein chaperones may not be needed. Dowhan and co-workers have shown that dramatic topology rearrangements can occur in lipid bilayers (*14*). In particular, the topology of half of lactose permease is completely flipped when the membranes of *Escherichia coli* are depleted of phosphotidylethanolamine (PE) lipids (see the figure, panel D). The topology can be flipped back dramatically (but not completely corrected) by reintroducing PE. This topology flipping of lactose permease can occur in a pure lipid membrane background, indicating that accessory proteins are not necessarily required (*15*). These results suggest that a capacity for topology flipping is an intrinsic property of some polypeptides.

The occurrence of dramatic topology rearrangements during folding of membrane proteins demands mechanistic understanding. To study the physical chemistry of this process requires purified and topologically trapped intermediates and methods to trigger folding in a controlled manner. Such systems would allow the kinetics and possibly the thermodynamics of the process to be studied. The pioneering experiments with lactose permease suggest that it should be possible to develop these experimental systems.

References and Notes

1. S. H. White, *Protein Sci.* **13**, 1948 (2004).
2. N. Reyes, C. Ginter, O. Boudker, *Nature* **462**, 880 (2009).
3. M. L. Oldham, D. Khare, F. A. Quiocho, A. L. Davidson, J. Chen, *Nature* **450**, 515 (2007).
4. J. L. Popot, D. M. Engelman, *Biochemistry* **29**, 4031 (1990).
5. R. Dutzler, E. B. Campbell, M. Cadene, B. T. Chait, R. MacKinnon, *Nature* **415**, 287 (2002).
6. S. Yohannan, S. Faham, D. Yang, J. P. Whitelegge, J. U. Bowie, *Proc. Natl. Acad. Sci. U.S.A.* **101**, 959 (2004).
7. Z. Cao, J. U. Bowie, *Proc. Natl. Acad. Sci. U.S.A.* **109**, 8121 (2012).
8. P. J. Barrett *et al*., *Science* **336**, 1168 (2012).
9. Y. Lu *et al*., *Mol. Biol. Cell* **11**, 2973 (2000).
10. M. Rapp, E. Granseth, S. Seppälä, G. von Heijne, *Nat. Struct. Mol. Biol.* **13**, 112 (2006).
11. E. A. Morrison *et al*., *Nature* **481**, 45 (2012).
12. S. Seppälä, J. S. Slusky, P. Lloris-Garcerá, M. Rapp, G. von Heijne, *Science* **328**, 1698 (2010).
13. J. Luirink, Z. Yu, S. Wagner, J.-W. de Gier, *Biochim. Biophys. Acta* **1817**, 965 (2012).
14. W. Dowhan, M. Bogdanov, *Annu. Rev. Biochem.* **78**, 515 (2009).
15. X. Wang, M. Bogdanov, W. Dowhan, *EMBO J.* **21**, 5673 (2002).

Acknowledgments: I thank members of my lab for helpful comments. This work was supported by NIH grant R01GM063919.

10.1126/science.1228655

STRUCTURAL BIOLOGY

(Pseudo-)Symmetrical Transport

Structural symmetry plays a key role in the membrane gating function of transporter proteins.

Lucy R. Forrest

Most walls incorporate some way of getting through them, such as a gate, a revolving door, or an airlock. The airlock concept is also used in moving cargo across cell membranes, for example, for intake of nutrients or expulsion of toxins, which is often an uphill battle against a concentration gradient. Nature fights this battle using membrane-embedded proteins called transporters. These proteins can alternate between at least two preferred conformations. In one of those conformations, the cargo diffuses in and binds to its binding site. The first door then shuts and the other opens, providing unhindered access to the other side of the membrane. Recent studies suggest a key role for structural symmetry in this process.

Any given cell contains dozens of different transporters, each with its own preferred substrate, relying on various energy sources. One class of transporters uses the energy released by a chemical reaction, such as adenosine triphosphate hydrolysis. A second class, the secondary transporters, uses downhill diffusion of one molecule to power the uphill work for another. For example, nutrient/metabolite transporters enable a cell to take up a nutritious substrate against its concentration gradient and, after consuming it, allow the waste to diffuse back out.

The rules of transport in transporters, including the airlock-like alternating-access mechanism, have long been known. Only in the past decade, however, has a clear picture of the structures of these proteins been unveiled, thanks to x-ray crystallography (*1*). A recurring theme in these struc-

Computational Structural Biology Group, Max Planck Institute of Biophysics, Max-von-Laue-Strasse 3, 60438 Frankfurt am Main, Germany. E-mail: lucy.forrest@biophys.mpg.de

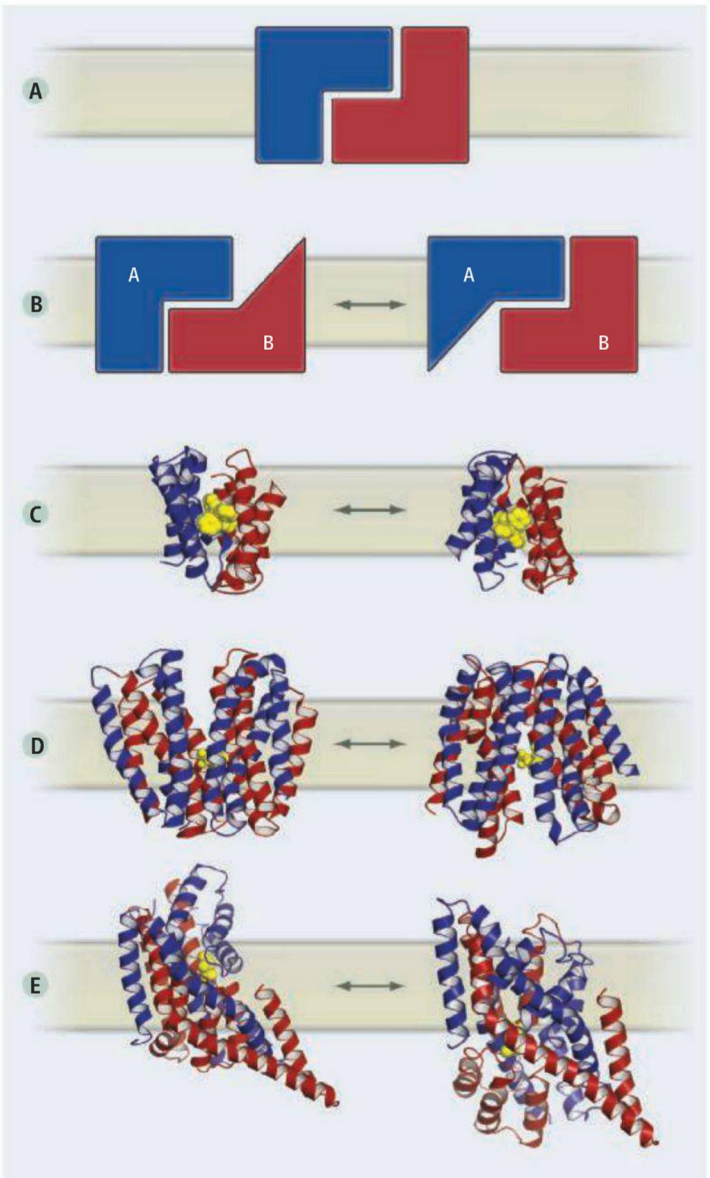

Membrane-embedded airlocks. (**A**) Inverted-topology repeats with similar structures can form channels through the membrane. (**B**) In transporters, the difference between the two halves creates an asymmetry in the overall protein structure, resulting in opening of the outer or inner gate. (**C**) In the antiparallel form of the dimeric transporter EmrE, the outside-open structure (left) has the same energy as the inside-open structure (right, same structure rotated 180°). (**D**) In lactose permease, the repeated elements of the protein are part of a continuous polymer chain and are intertwined. As in EmrE, the two halves appear to alternate between two distinct conformations. (**E**) Exchange between the two conformations of the aspartate transporter, Glt_{Ph}, involves a dramatic elevator-like movement of the substrate across the membrane.

tures, particularly of secondary transporters, is the presence of internal pseudosymmetry of sets of membrane-spanning helices. Sometimes the repeats are arranged in a circular symmetry. However, most transporter architectures have a pseudo-two-fold symmetry, with the two halves of the protein related by an axis running along the plane of the membrane. The two inverted halves are usually intricately intertwined, like clasped hands with interlocking fingers.

Such inverted repeat elements are not unique to secondary transporters. Another set of membrane proteins, called channels, also include these arrangements. Duplication in this case may be a conservative solution to forming a continuous pathway across the membrane, because it results in two half-channels made from similar components that line the axis of the symmetry (see the figure, panel A). However, the inverted repeat elements of secondary transporter structures differ from those of channels: In any given conformation, whether open to the outside or to the inside of the cell, the repeated elements have slightly different arrangements (see the figure, panel B). These differences lead to the structural asymmetry that is required if one door is to be open while the other is closed.

This concept has been illustrated for several different transporter architectures (*2*–*7*) using a modeling strategy that involves swapping the three-dimensional structures of the two repeated halves, starting with the structure of a transporter with one door open. Using homology modeling—in which protein structures are modeled based on known structures of related proteins—the structure of one half of the transporter is used as the template onto which the sequence of the other half is threaded. The result is a three-dimensional model of the same transporter but with the other door open (see the figure, panels C to E).

Different aspects of these models have been experimentally corroborated (*3*–*5*). An inward-facing conformation predicted for an aspartate transporter, for instance, was captured by introducing sulfhydryl groups at specific positions in the protein and reacting them with mercury ions (*8*). The structure of this trapped state was then determined by x-ray crystallography (see the figure, panel E).

Other informative approaches include engineering fluorescent or paramagnetic probes onto the protein surface and measuring their proximity by fluorescence resonance energy transfer (FRET) or electron spin resonance (EPR). Such data have shown that the intracellular water-exposed loops of the lactose permease transporter are closer together (*9*) in one of the airlock states than in the other airlock state known from x-ray crystallography (see the figure, panel D), consistent with predictions based on the inverted-topology repeats (*3*). Other studies measure the accessibility of putative substrate pathways as indicated by the reactivity of engineered sulfhydryl groups to chemical modification or cross-linking (*2*, *4*). Repeating these measurements with different substrates, state-specific inhibitory compounds, or antibodies provides insights into conformational changes during transport.

The transporters mentioned so far comprise a single continuous protein chain, with different amino-acid sequences in the two repeated elements. A much simpler transporter, EmrE, has two identical chains, which according to available structural data (*10*, *11*) are arranged in opposite directions in the membrane. Biochemical analyses suggest that the protein normally prefers to function with the two halves parallel in the membrane (*12*). Nevertheless, the antiparallel form provides a useful case study, because the two chains form slightly different structures in this arrangement (see the figure, panel C) (*10*, *11*). Nuclear magnetic resonance (NMR) studies suggest that EmrE exchanges between two degenerate (that is, same-energy) states (*13*). By interchanging between these conformations, the transporter opens either its outer or inner door. Because both shapes are similar in energy, the protein avoids the need for additional energy input beyond that typically gained from binding.

Will all pseudosymmetric transporters function this way, and if not, how much do the amino acid sequences of the two halves have to differ before the principle of degenerate states breaks down? Different transporters sharing the same overall architecture may connect their states via different types of movements (*14*), although the key factors underlying these distinctions remain incompletely understood. It also remains unclear where the boundary lies between channels (with similar repeat structures) and transporters (with alternating repeat conformations). A notable case is the CLC protein family, which includes both channels and transporters for chloride. Structural and spectroscopic approaches such as EPR, NMR, and FRET should help to elucidate the distinctions between CLC transporters and CLC channels.

How did transporters evolve such complex intertwined polymeric chains? Did they start as transporters made of dimers of adjacent units like EmrE and then begin to swap segments? Hints of these evolutionary pathways have been obtained, for example, by comparison of membrane proteins sequences (*15*). Similar studies using more sensitive sequence comparison methods to scan ever-growing sequence databases, combined with structural analysis of the identified proteins, should provide important insights into this intriguing evolutionary process.

References

1. O. Boudker, G. Verdon, *Trends Pharmacol. Sci.* **31**, 418 (2010).
2. T. J. Crisman, S. Qu, B. I. Kanner, L. R. Forrest, *Proc. Natl. Acad. Sci. U.S.A.* **106**, 20752 (2009).
3. S. Radestock, L. R. Forrest, *J. Mol. Biol.* **407**, 698 (2011).
4. M. Schushan *et al.*, *J. Biol. Chem.* **287**, 18249 (2012).
5. J. Liao *et al.*, *Science* **335**, 686 (2012).
6. L. Kowalczyk *et al.*, *Proc. Natl. Acad. Sci. U.S.A.* **108**, 3935 (2011).
7. R. Mancusso, G. G. Gregorio, Q. Liu, D.-N. Wang, *Nature* **491**, 622 (2012).
8. N. Reyes, C. Ginter, O. Boudker, *Nature* **462**, 880 (2009).
9. I. Smirnova *et al.*, *Proc. Natl. Acad. Sci. U.S.A.* **104**, 16504 (2007).
10. S. J. Fleishman *et al.*, *J. Mol. Biol.* **364**, 54 (2006).
11. Y.-J. Chen *et al.*, *Proc. Natl. Acad. Sci. U.S.A.* **104**, 18999 (2007).
12. I. Nasie, S. Steiner-Mordoch, A. Gold, S. Schuldiner, *J. Biol. Chem.* **285**, 15234 (2010).
13. E. A. Morrison *et al.*, *Nature* **481**, 45 (2011).
14. C. Perez, C. Koshy, Ö. Yildiz, C. Ziegler, *Nature* **490**, 126 (2012).
15. J. S. Lolkema, A. Dobrowolski, D.-J. Slotboom, *J. Mol. Biol.* **378**, 596 (2008).

10.1126/science.1228465

MATERIALS SCIENCE

Ferroelectric Organic Materials Catch Up with Oxides

An organic salt displays ferroelectric properties comparable to those of barium titanate but should be easier to process in device fabrication.

Dawn A. Bonnell

In a ferroelectric material, electric dipoles inherent in the atomic structure (such as might form between cations and anions) can couple with each other so that they align in parallel, creating domains of aligned dipoles. The dipoles, and consequently the domains, can reorient and align with the applied electric field. After the discovery of ferroelectricity in barium titanate ($BaTiO_3$) (*1*), ferroelectric device applications developed (*2*), such as the storage of charge in ferroelectric capacitors used in dynamic random access memories. One drawback of oxide materials is that they are not as simple to process into films as organic materials, but typically ferroelectric organic materials have not had comparable properties. On page 425 of this issue, Fu *et al.* (*3*) present compelling evidence for a molecular compound that can rival ferroelectric oxides.

Department of Materials Science and Engineering, University of Pennsylvania, Philadelphia, PA 19104, USA. E-mail: bonnell@lrsm.upenn.edu

Recent advances in materials processing and nanoscale probes have led to exciting scientific and technical opportunities involving ferroelectric materials. New compounds have been discovered in which the electric dipoles couple to magnetic fields (*4*). Thin-film growth processes are used to engineer lattice strain in ferroelectric films, which controls dipole alignment and phase transition temperatures, and even induces ferroelectricity in normally nonferroelectric compounds (*5*). The advent of nanoscale probes has enabled patterning of ferroelectric domains for nanolithography and high-density memory applications (*6*–*8*). Current and emerging applications range from video game memory chips to medical imaging and new strategies for water splitting and solar energy harvesting.

Both the scientific advances and the applications have been based primarily on $BaTiO_3$ and related oxide materials such as $PbTiO_3$ and $Pb_xZr_yTiO_3$. This class of materials exhib-

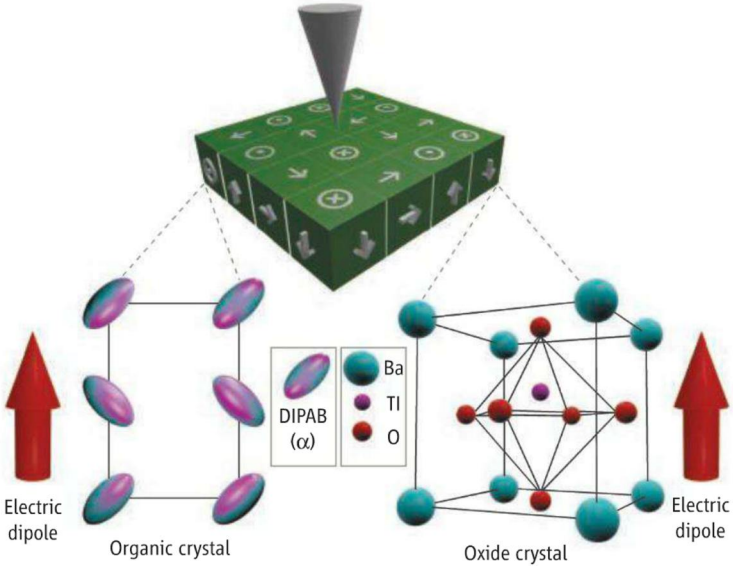

The lineup in ferroelectrics. The origin of electric dipoles in organic and oxide crystals is illustrated. In the organic compound DIPAB reported by Fu *et al.*, molecular units (represented by the purple ellipse) contain atoms with negative and positive partial charge separated over the length of the unit. In oxides, the negative (O) and positive ions (Ba, Ti) are positioned such that a dipole exists in the unit cell. Domains of dipoles aligned in the same direction form with orientations determined by the underlying atomic structure. An external electric field applied locally with a tip or macroscopically with an electrode causes the domains to reorient. Domain properties can be imaged with a scanning probe.

IMAGE COURTESY OF STEPHEN NONNENMANN

its high spontaneous polarization (the polarization present with no electric field applied), high dielectric constant, and high polarization saturation (the maximum that can be achieved with an applied field), as well as stability at room temperature. The limitation of these materials is that they are expensive to produce in the forms necessary for current and next-generation devices, and they often contain environmentally unfriendly elements such as lead.

It has been nearly a century since ferroelectricity was discovered in organic compounds, but during the intervening years, none of these materials exhibited the properties or the stability of the order of those of oxides. Being guided by the principles of atomic structure and symmetry, Fu *et al*. considered molecular structures that met the structural requirements for the presence of ferroelectricity and imposed a further constraint of a high melting point. They came upon diisopropylammonium bromide (DIPAB), which has the additional advantage that it can be processed from aqueous solutions. Using comprehensive crystallographic analysis and theory, they showed that the compound occurs in two polymorphs, and that one of these, the α phase, is ferroelectric and stable over a wide temperature range (77 to 416 K) of interest for many applications (see the figure).

The authors used several approaches to characterize the ferroelectric properties of DIPAB. The spontaneous polarization measured directly by electric field cycling was higher than that of other molecular compounds by a factor of 4 and, remarkably, matched that of $BaTiO_3$. The dielectric constant for DIPAB (measured at 400 Hz) was higher than those of polymer ferroelectric compounds by a factor of 10 and remained relatively high even at 1 MHz. Finally, the coercive field for DIPAB, which dictates the amount of voltage required to reorient the electric dipoles (and which should be low for energy-efficient applications), was one-hundredth that for polymers and half that for $BaTiO_3$. The properties of DIPAB considerably surpass those observed for other organic materials and approach or match those of the ferroelectric oxides.

The dipole coupling that is the basis of ferroelectricity is an intrinsically local phenomenon. The dipoles are separated by and interact across distances of 0.4 to 1 nm, depending on the compound; the domains of aligned dipoles have sizes ranging from nanometers to micrometers. Thus, spatially localized measurements of ferroelectric behavior are essential. Fortunately, a toolbox of local-property probes is now available to characterize properties at these length scales (*9*). Fu *et al*. used a variant, piezoresponse force microscopy, to map the domain orientations and determine the ferroelectric properties of individual domains, illustrating the insight gained from local analysis.

This combination of ferroelectric phase stability and outstanding properties suggests that DIPAB may replace oxides in some applications, with benefits in terms of ease of processing and sustainability. Further, the surprisingly strong ferroelectric behavior in this organic compound suggests a reconsideration of the generality of charge interactions that underlie related properties. Other properties, notably piezoelectricity and electrostriction, are manifestations of charge interactions in structures and are well known in solids. Recently, evidence of all three of these properties has been observed on local scales in components of biological or physiological materials (*10*, *11*), so perhaps ferroelectric coupling is an important part of some biological processes. In that case, the highly functional DIPAB may be the bridge in understanding between coupling in oxides and that in complex soft materials.

References

1. H. D. Megaw, *Nature* **155**, 484 (1945).
2. J. F. Scott, *Science* **315**, 954 (2007).
3. D.-W. Fu *et al*., *Science* **339**, 425 (2013).
4. J. Wang *et al*., *Science* **299**, 1719 (2003).
5. D. Schlom *et al*., *Annu. Rev. Mater. Res.* **37**, 589 (2007).
6. D. Li, D. A. Bonnell, *Annu. Rev. Mater. Res.* **38**, 351 (2008).
7. S. Kalinin *et al*., *Adv. Mater.* **16**, 795 (2004).
8. J. F. Scott, C. A. Paz de Araujo, *Science* **246**, 1400 (1989).
9. D. A. Bonnell *et al*., *Rev. Mod. Phys.* **84**, 1343 (2012).
10. S. V. Kalinin *et al*., *Annu. Rev. Mater. Res.* **37**, 189 (2007).
11. Y. Liu, Y. Zhang, M. J. Chow, Q. N. Chen, J. Li, *Phys. Rev. Lett.* **108**, 078103 (2012).

10.1126/science.1232939

CELL BIOLOGY

Deconstructing Dimensionality

How do cells sense a three-dimensional environment?

Martin A. Schwartz[1] and Christopher S. Chen[2]

Cells were first cultured in glass dishes over a century ago (*1*, *2*), a technology still used with only minimal changes. Yet, cells on glass or tissue culture plastic, so-called two-dimensional (2D) culture, often fail to reflect in vivo function. The ability to grow cells within extracellular matrix (ECM) gels (3D culture) was a major advance that recapitulated in vivo cellular behaviors, ranging from differentiated function to maintenance of stem cell niches (*3*–*5*). The question of how cells distinguish between 2D and 3D environments to determine gene expression, cell behavior, and morphogenesis is of much interest to cell biologists and tissue engineers. However, cells do not sense "dimensionality" directly as an independent variable; rather, it is ascertained through its effects on various cell processes.

Epithelial cells inside ECM gels typically form tubes or spheres with hollow cores (*5*, *6*), and thus differ topologically from monolayer cultures. One key consequence of this reorganization is the size of the compartments (see the figure). Cells in a 3D environment usually polarize with a basal compartment facing the gel and an enclosed apical compartment that is quite small, often comparable to the combined volume of the cells themselves (*7*). Apically secreted factors are therefore highly concentrated compared to those secreted in 2D cultures, and paracrine effects are magnified. Ions can also be secreted in a polarized manner—in kidney tubule cells, for example, this leads to differences in electrolyte composition. As membrane receptor localization is often polarized, accessibility of autocrine factors to receptors can modulate cell responses as well.

[1]Cardiovascular Research Center, Yale School of Medicine, 300 George Street, New Haven, CT 06511, USA. [2]Department of Bioengineering, University of Pennsylvania, Philadelphia, PA 19104, USA. E-mail: martin.schwartz@yale.edu; chrischen@seas.upenn.edu

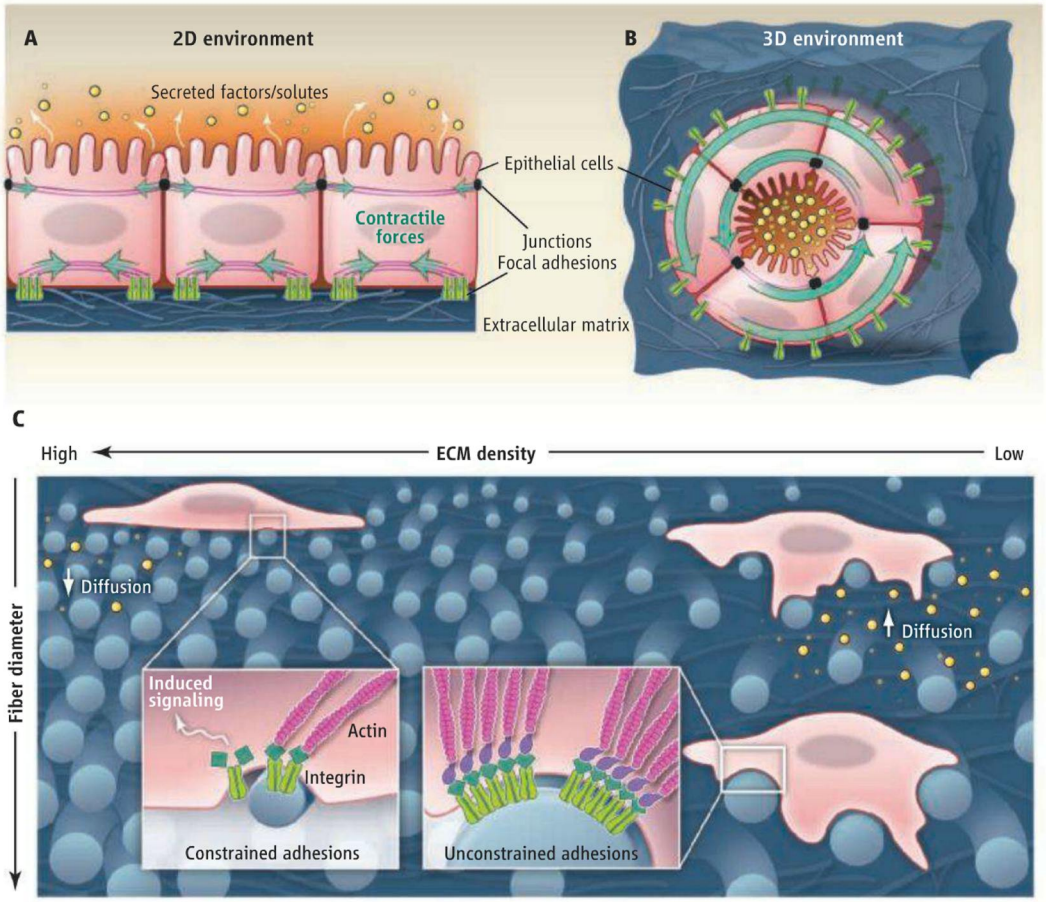

Independent variables. (**A**) Cells on a rigid planar surface organize focal adhesions and actin stress fibers at the basal surface of the cell and transfer contractile forces to the surface and to other cells. Apical domains face the medium where secreted factors are diluted; basal domain faces the ECM-coated surface. (**B**) Cells in 3D culture form a spherical acinus or tube with a curved surface. Curvature and soft matrix materials limit formation of actin stress fibers. The apical domain faces a small interior compartment where secreted factors can be highly concentrated. Mechanical tension can be transmitted through cell-cell junctions to generate hoop stresses around the whole structure. (**C**) ECM fibers control cell behavior through differences in density and fiber diameter. These variables influence cell protrusions, diffusion of solutes, and the local clustering and force transmission by integrins that bind to the ECM.

Topographical differences in ECM proteins also can modulate cell responses. In either 2D or 3D environments, ECM constituents can be arranged into fibrils that are thick, thin, long, or short (or uniformly coated on a solid support) (*8*, *9*). This organization can affect curvature of the plasma membrane and the clustering and organization of membrane receptors, as well as alter mechanical forces at the cell-ECM interface. Additionally, the spacing between fibers, determined by ECM density, can influence whether a cell forms a relatively planar interface with a fiber mat, crawls inside the ECM and is surrounded with fibers, or adopts some intermediate state in which it extends processes into the pores of the matrix (*8*).

The difference in curvature between cells in flat monolayers versus spheroids or tubules also affects cell functions. Although the radius of curvature is too large to affect cell structures at the nanoscale [for example, the binding of Bin/amphiphysin/Rvs (BAR) domain proteins to membranes (*10*)], changes in curvature at the micrometer scale can control the assembly of large cytoskeletal structures such as focal adhesions (which link actin filaments to the adhesions) or microtubules. Curvature may also influence cell-cell and cell-matrix interactions through changes in the size of the domains and the distribution of mechanical forces. For example, cells in a tube or acinus can undergo apical contraction to decrease the structure's radius. They can also experience "hoop" stresses around the entire structure. This distribution of forces throughout the structure creates opportunities for multicellular morphogenetic movements such as sprouting or invagination (*11*). Moreover, the size and curvature of the apical and basal domains are also variable in a 3D ECM, which influence contractility and cytoskeletal organization within these regions. By contrast, forces experienced by cells in 2D are ultimately resisted in only one domain (basal) by the stiffness of the substratum, thereby limiting such effects.

The degree to which the ECM resists deformation from cell-generated tractions (ECM rigidity or stiffness) modifies the structure and dynamics of the cell-ECM adhesions, which subsequently influences cell signaling and behavior (*12*). Although this is true for both 2D and 3D cultures, sensing ECM rigidity differs depending on how the ECM is presented. In 2D, cells experience tractions primarily as shear stresses on their basal surface, whereas cells in a 3D environment experience both planar stresses and stresses that are perpendicular to the cells' basal surface. There are also substantial differences in the mechanics of synthetic gels used to model stiffness effects in 2D settings as compared to natural ECMs (*13*). Such gels exhibit linear elastic behavior, whereas the fibrillar nature of natural ECMs give rise to complex nonlinear elastic behavior with appreciable viscous components. These physical differences could influence how cells respond to their environment.

For cells in 2D culture, apical-basal polarity is essentially fixed by having the solid support below and the medium above. Cells in 3D gels initially have ECM on all sides. Epithelial and endothelial cells create their polarity, reorganizing into structures that generally have the basal domain facing the ECM and a fluid-filled apical compartment inside (*6*, *7*). This arrangement can be reversed by suitable manipulations (*14*), indicating that polarity is a regulated variable. Mesenchymal cells also organize differently. In 2D they are forced into an epithelial state where apical and basal domains differ. However, in 3D culture, they contact ECM on all sides without evident apical-basal polarity (*15*). Binding ECM on the apical domain triggers different responses than at the basal domain—for example, there are distinct effects on gene expression, cytoskeletal organization, and even cell survival (*16*–*18*).

CREDITS: K. SUTLIFF/*SCIENCE*; IMAGE COURTESY OF STEPHEN NONNENMANN

Transport of soluble components differs between 2D and 3D environments. In 2D, solutes undergo free diffusion through the medium and convective mixing, leading to their rapid distribution. Three-dimensional matrices eliminate convection and restrict the diffusion of large molecules (*19*). ECM components also bind many soluble molecules, including most growth factors, which further slows their transport but can also concentrate them within the microenvironment. All of these factors reduce transport rates such that some solutes could take days to reach embedded cells.

Cells can freely spread, migrate, and rearrange on a 2D surface because there is no constraint in the plane of the substrate, whereas in a 3D matrix, cells have to either squeeze through pores or degrade the matrix to spread or migrate (*8*). Such constraints affect the speed of migration in 3D, which could alter cell signaling triggered by the assembly of new cell-matrix adhesions. Furthermore, such constraints can lead to an apparent paradox in which increasing cross-linking of a matrix enhances cell spreading and motility by increasing substrate stiffness; cross-linking cells into a 3D matrix is likely to retard spreading and motility by making it harder for cells to degrade ECM components and move through the environment.

Cells can only sense their surroundings over a limited distance, essentially a single cell length. Thus, "dimensionality" per se is not a single variable that can be sensed on a cellular scale. Identifying the mechanisms by which cells assess the nature of their environment will advance basic cell biology and facilitate the development of synthetic matrices (*20*) for specific tissue engineering applications.

References

1. A. Carrel, *J. Exp. Med.* **15**, 516 (1912).
2. R. G. Harrison, *J. Exp. Zool.* **17**, 521 (1914).
3. E. Santos, R. M. Hernández, J. L. Pedraz, G. Orive, *Trends Biotechnol.* **30**, 331 (2012).
4. G. Benton, J. George, H. K. Kleinman, I. P. Arnaoutova, *J. Cell. Physiol.* **221**, 18 (2009).
5. B. Weigelt, M. J. Bissell, *Semin. Cancer Biol.* **18**, 311 (2008).
6. G. E. Davis *et al.*, *Cell. Mol. Biol.* **288**, 101 (2011).
7. L. M. McCaffrey, I. G. Macara, *Trends Cell Biol.* **21**, 727 (2011).
8. K. Wolf, P. Friedl, *Trends Cell Biol.* **21**, 736 (2011).
9. J. S. Harunaga, K. M. Yamada, *Matrix Biol.* **30**, 363 (2011).
10. B. J. Peter *et al.*, *Science* **303**, 495 (2004).
11. G. M. Odell, G. Oster, P. Alberch, B. Burnside, *Dev. Biol.* **85**, 446 (1981).
12. D. E. Discher, P. Janmey, Y. L. Wang, *Science* **310**, 1139 (2005).
13. C. Storm, J. J. Pastore, F. C. MacKintosh, T. C. Lubensky, P. A. Janmey, *Nature* **435**, 191 (2005).
14. K. D. Liu *et al.*, *Am. J. Physiol. Renal Physiol.* **293**, F1633 (2007).
15. E. Cukierman, R. Pankov, D. R. Stevens, K. M. Yamada, *Science* **294**, 1708 (2001).
16. X. Chen, S. L. Thibeault, *Tissue Eng. Part A* **18**, 2528 (2012).
17. Y. K. Wang, H. H. Lin, M. J. Tang, *Am. J. Physiol. Cell Physiol.* **280**, C1440 (2001).
18. R. Eisen, S. Walid, D. R. Ratcliffe, G. K. Ojakian, *Am. J. Physiol. Cell Physiol.* **290**, C1297 (2006).
19. A. S. Hoffman, *Adv. Drug Deliv. Rev.* **54**, 3 (2002).
20. M. P. Lutolf, J. A. Hubbell, *Nat. Biotechnol.* **23**, 47 (2005).

10.1126/science.1233814

CHEMISTRY

Corralling Positively Charged Molecular Radicals

Linked organic rings can form highly charged molecular and radical ions with unusual stability.

Andrew Benniston

At the outset, the idea of forcing together multiple positive charges onto an organic molecule and ending up with a stable interlocked supramolecular structure seems destined for failure. Columbic repulsion forces usually extract an energetic penalty on adding an additional charge onto a highly charged molecule, and the organic radicals that would form with stepwise charge addition are likely to be unstable. On page 429 of this issue, Barnes *et al.* (*1*) show that counterintuitive thinking about this problem can reap rewards. They show that a [2]catenane molecule, in which two identical rings interlock noncovalently like links of a chain (*2*), displays a rich vein of electrochemical responses. This homocatenane (HC) can stabilize organic radicals and bear up to eight positive charges.

[2]Catenanes have been viewed as curiosity structures of interest mainly for their topology; like the links of a chain, the components can only be separated by breaking one of the rings. Over many years, examples of molecular-based [2]catenane structures have emerged based on neutral components, using either hydrogen bonding (*3*), anion recognition (*4*), or cation binding (*5*) to template their formation. Previous work by Stoddart's group focused on the tetracationic bipyridinium (blue box), as shown in the figure, to form interlocked structures with highly electron-donating crown ethers (*6*).

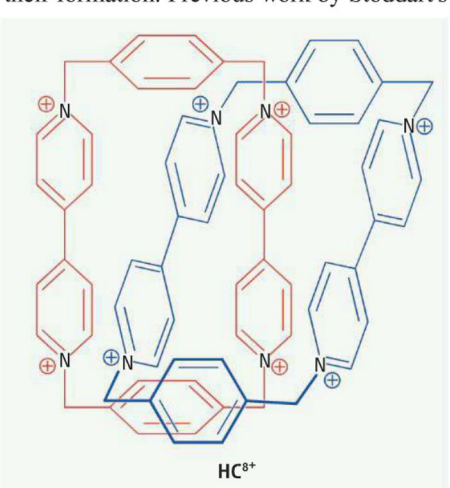

Charging ahead. The molecular structure is shown of the octacationic [2]catenane produced by Barnes *et al.*, which was characterized by proton nuclear magnetic resonance spectroscopy.

In essence, the approach of Barnes *et al.* forces together the two "blue box" structures depicted in the figure, and a total of eight positive charges can be localized on the structure when it is oxidized electrochemically in solution. Because HC^{8+} contains such a high charge and suffers high Coulombic repulsion, it is not surprising that it was not isolated as a solid. However, it was fully characterized in solution by proton nuclear magnetic resonance spectroscopy. The as-prepared state of the [2]catenane is actually an equilibrium mixture containing HC^{6+} (diradical) and HC^{7+} (monoradical).

Two points are noteworthy. One is that the electrons are spin-paired in the diradical and form a singlet state. The other is that the radical HC^{7+} is stable and was isolated as a single crystal for x-ray structural analysis. Organic radicals are usually highly energetic and short-lived because they can readily react with one another to form dimmers. Thus, the capture of HC^{7+} in the solid state is very

School of Chemistry, Newcastle University, Newcastle upon Tyne, NE1 7RU UK. E-mail: andrew.benniston@newcastle.ac.uk

unusual. Nature has used the complex structure of enzymes to stabilize radicals. Here, Barnes *et al*. have demonstrated a topological control of the reactivity for a radical. A series of controlled electrochemical steps can reduce the [2]catenane structure and eventually yield the fully neutral species. Again, it was possible to isolate and structurally characterize several of the intermediates.

The molecular [2]catenane reported by Barnes *et al*. represents a multiple electron storage module, and is at least on par with the universally used C_{60} electron acceptor. The basic *N*,*N*′-dimethyl-4,4′-bipyridinium cation (viologen) is often used in artificial photosynthesis applications. Perhaps the [2]catenane may play a future role in this area, capitalizing on its multiple electron storage capacity, or in other applications that take advantage of stored electrons.

References

1. J. C. Barnes *et al*., *Science* **339**, 429 (2013).
2. G. Schill, *Catenanes, Rotaxanes and Knots* (Academic Press, New York, 1971).
3. E. R. Kay, D. A. Leigh, *Top. Curr. Chem.* **262**, 133 (2005).
4. M. S. Vickers, P. D. Beer, *Chem. Soc. Rev.* **36**, 211 (2007).
5. J. P. Sauvage, *Acc. Chem. Res.* **23**, 319 (1990).
6. D. B. Amabilino, J. F. Stoddart, *Chem. Rev.* **95**, 2725 (1995).

10.1126/science.1233633

PHYSICS

How Big Is the Proton?

Precise spectroscopic measurements of muonic hydrogen reveal a proton radius appreciably different from the currently accepted value.

Helen S. Margolis

As the simplest possible atom, comprising a single proton and a single electron, hydrogen has played a central role in the development of modern physics. For example, the observation in 1947 of the $2S\text{-}2P_{1/2}$ energy level splitting, now termed the Lamb shift, stimulated the development of the theory of quantum electrodynamics (QED). Hydrogen and other, more exotic two-body atomic systems continue to provide fertile testing grounds for fundamental physical theories and are still yielding surprises, as demonstrated by the experiments reported by Antognini *et al*. on page 417 of this issue (*1*). By using laser spectroscopy to study two transitions in muonic hydrogen (in which the electron is replaced by its heavier cousin, the muon), they determine a value for the root-mean-square charge radius of the proton that differs appreciably from the latest (2010) CODATA recommended value (*2*).

The CODATA value is based on data from two types of experiment: electron-proton scattering and high-resolution spectroscopy of atomic hydrogen. Electron-proton scattering experiments provide the most direct way of determining the proton size, but are complex to analyze. The proton charge density falls off approximately exponentially with distance from the center, leading to a strong dependence of the root-mean-square radius on the tail of this charge distribution. As discussed in a recent reanalysis of the globally available electron-proton scattering data (*3*), this cannot be determined with high accuracy from the experiments.

Transition frequencies in atomic hydrogen depend on the proton size because the electric field within the proton differs from that produced by a point charge. The effect is small, but detectable due to the accuracy with which optical frequencies can be measured (*4*). The hydrogen transition frequencies also depend on the Rydberg constant, but by studying more than one transition, it is possible to extract both the proton charge radius and the Rydberg constant from the measurements, assuming that the theory of QED is correct (*5*).

Antognini *et al*. have obtained a far more precise measurement of the proton charge radius by laser spectroscopy of muonic hydrogen. The muon has the same charge as the electron, but a mass about 207 times greater, meaning that it spends a much larger fraction of the time within the proton charge distribution. Consequently, its energy levels are much more sensitive to the proton size than are those of the hydrogen atom.

The new experiment is an extension of previous work by the same international collaboration (*6*), which found that the proton charge radius as determined from spectroscopy of a single component of the 2S-2P transition in muonic hydrogen differed from the 2006 CODATA value by almost 5 standard deviations. This unexpected result has triggered much debate over the past 2 years, but the origin of the discrepancy has not yet been identified.

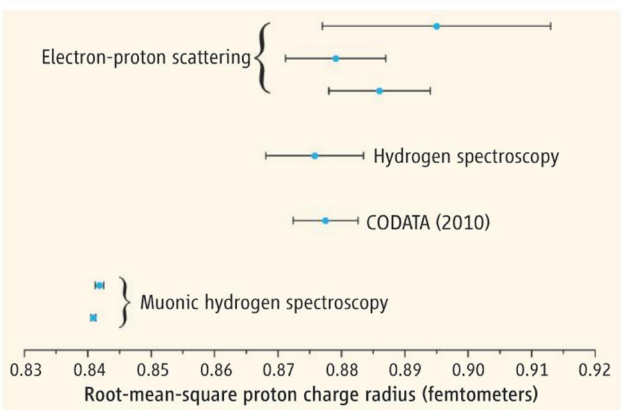

Measuring up. Values of the root-mean-square proton charge radius determined by different methods. The discrepancy between the 2010 CODATA value and the muonic hydrogen results is clear.

The experimental procedure used by Antognini *et al*. is broadly similar to that employed previously, but with the important difference that two transition frequencies are measured rather than one. In this way, a value for the proton charge radius can be extracted that does not rely on a theoretical prediction of the 2S hyperfine splitting, removing a possible source of error in the previous measurements. An improved data analysis procedure has also been developed, resulting in a value for the proton charge radius with an uncertainty 40% lower than the earlier measurement. The discrepancy between the muonic hydrogen result and the CODATA value remains, however, with the difference now being 7 standard deviations (see the figure).

This new result can be expected to stimulate further efforts to understand the reasons for the discrepancy. One area for investigation will undoubtedly be the complex QED calculations required to extract the proton size from the spectroscopic measurements. Numerous terms in the equations linking the measured transition frequencies to the proton size have already been checked and

National Physical Laboratory, Teddington, Middlesex TW11 0LW, UK. E-mail: helen.margolis@npl.co.uk

additional correction terms evaluated, but so far none of this work has identified a problem.

Another possibility is an unidentified source of systematic error in one of the experiments. Although muonic hydrogen is very challenging to study experimentally, the high sensitivity of the transition frequencies to the proton size means that measurements only have to be made to 4 to 5% of the transition linewidth. For the hydrogen spectroscopy, by contrast, it is necessary to measure to a much smaller fraction of the linewidth, and so detailed modeling of the lineshapes is required. This introduces a potential source of systematic error that might be uncovered by new experiments that aim to make improved measurements of the Rydberg constant (*7*–*9*).

New insight may also come from other measurements involving spectroscopy of other two-body atomic systems—muonic deuterium and muonic helium ions. If the results of these experiments turn out to reinforce the proton size puzzle, then it could become necessary to question the foundations of the world's most precise and best-tested fundamental physical theory, QED itself.

References and Notes

1. A. Antognini *et al.*, *Science* **339**, 417 (2013).
2. P. J. Mohr, B. N. Taylor, D. B. Newell, *Rev. Mod. Phys.* **84**, 1527 (2012).
3. I. Sick, *Prog. Part. Nucl. Phys.* **67**, 473 (2012).
4. C. G. Parthey *et al.*, *Phys. Rev. Lett.* **107**, 203001 (2011).
5. F. Biraben, *Eur. Phys. J. Spec. Top.* **172**, 109 (2009).
6. R. Pohl *et al.*, *Nature* **466**, 213 (2010).
7. J. L. Flowers, P. E. G. Baird, L. Bougueroua, H. A. Klein, H. S. Margolis, *IEEE Trans. Instrum. Meas.* **56**, 331 (2007).
8. O. Arnoult, F. Nez, L. Julien, F. Biraben, *Eur. Phys. J. D* **60**, 243 (2010).
9. J. N. Tan, S. M. Brewer, N. D. Guise, *Phys. Scr.* **T144**, 014009 (2011).

Acknowledgments: Supported by the UK Department for Business, Innovation and Skills under the National Measurement System Electromagnetics and Time program.

10.1126/science.1233202

NEUROSCIENCE

Chaperones That SNARE Neurotransmitter Release

A new model for neurotransmitter release may be relevant for membrane fusion reactions in general.

Frederick M. Hughson

The cellular machinery of neurotransmitter release is well known, but the precise molecular mechanism has long been elusive (*1*). Its basic features are clear enough: Neuron firing causes the intracellular Ca^{2+} concentration to rise, triggering the fusion of synaptic vesicles carrying neurotransmitter molecules with the plasma membrane. Fusion is mediated by SNARE [soluble *N*-ethylmaleimide–sensitive factor (NSF) attachment protein (SNAP) receptor] proteins and a Ca^{2+} sensor (synaptotagmin) in a process that has been reproduced in vitro using artificial membrane vesicles (liposomes) and purified proteins. A conundrum has, however, remained: In vitro fusion does not depend critically on two additional proteins—Munc13 and Munc18—that are essential for synaptic vesicle fusion in vivo. On page 421 of this issue, Ma *et al.* (*2*) report a modified in vitro fusion assay that depends not only on SNAREs and synaptotagmin-Ca^{2+}, but also on both Munc13 and Munc18. The results identify a mechanistic role for Munc13 and Munc18 and force reconsideration of the fundamental model for SNARE assembly.

The SNARE machinery includes one protein (synaptobrevin) on the synaptic vesicle and two proteins (syntaxin and SNAP-25) on the target plasma membrane. These vesicle (v-) and target membrane (t-) SNAREs assemble to form ternary complexes that bridge the two membranes and mediate fusion. Fusion is greatly accelerated by synaptotagmin-Ca^{2+}. These features are recapitulated in vitro by fluorescence-based assays that monitor the fusion of liposomes bearing v- and t-SNAREs.

Because a fully assembled SNARE complex is extremely stable, the process of SNARE assembly exerts a substantial pulling force on the two apposed membranes (*3*). Partial SNARE complexes are less stable and prone to nonproductive side reactions. To appreciate these side reactions, it is helpful to note that the core of the fully assembled SNARE complex is a simple bundle of four long α helices. One helix is contributed each by synaptobrevin and syntaxin, and two helices by SNAP-25. A well-characterized side reaction results in the formation of a four-helix bundle with two syntaxins and one SNAP-25, leaving no place for the v-SNARE synaptobrevin. Another potential side reaction has SNAP-25 donating only one of its helices to each of two t-SNARE complexes, producing a tangle of partly assembled components.

Mitigating these side reactions has been important in developing liposome fusion assays that dissect the molecular mechanisms underlying neurotransmitter release. For example, to prevent formation of dead-end 2:1 syntaxin–SNAP-25 complexes, a small soluble piece of synaptobrevin has been used as a "placeholder" (*4*). The placeholder peptide is subsequently displaced during the SNARE assembly reaction that leads v-liposomes (containing synaptobrevin) and t-liposomes (containing SNAP-25 and syntaxin) to fuse (*5*). Adding synaptotagmin-Ca^{2+} to this assay greatly increases the rate of fusion (*6*). Troubling, however, is that in vitro, fusion does not depend on the presence of either Munc18 or Munc13, both of which are essential for synaptic vesicle docking and/or fusion in vivo.

Ma *et al.* propose that Munc13 and Munc18 are chaperones that solve the SNARE side reaction problem in vivo (see the figure). Munc18 (also called neuronal Sec1) forms a tight complex with syntaxin, clamping it in a closed conformation that is unable to bind other SNAREs (*7*). Why, then, is Munc18 essential for neurotransmitter release? Might one of its roles be to protect syntaxin from side reactions, serving as a chaperone that guides syntaxin into productive, membrane-bridging SNARE complexes? Munc18 can indeed accelerate the fusion of v- and t-liposomes (*8*). Furthermore, Munc13, a synaptic vesicle "priming" protein, catalyzes the transition from syntaxin-Munc18 complexes to fully assembled v/t-SNARE complexes (syntaxin–SNAP-25–synaptobrevin) (*9*). Although the Munc13 experiments were performed using soluble SNAREs lacking membrane anchors, the results raised the exciting possibility that Munc13 is needed in vivo to extract syntaxin from the grip of Munc18.

Department of Molecular Biology, Princeton University, Princeton, NJ 08544, USA. E-mail: hughson@princeton.edu

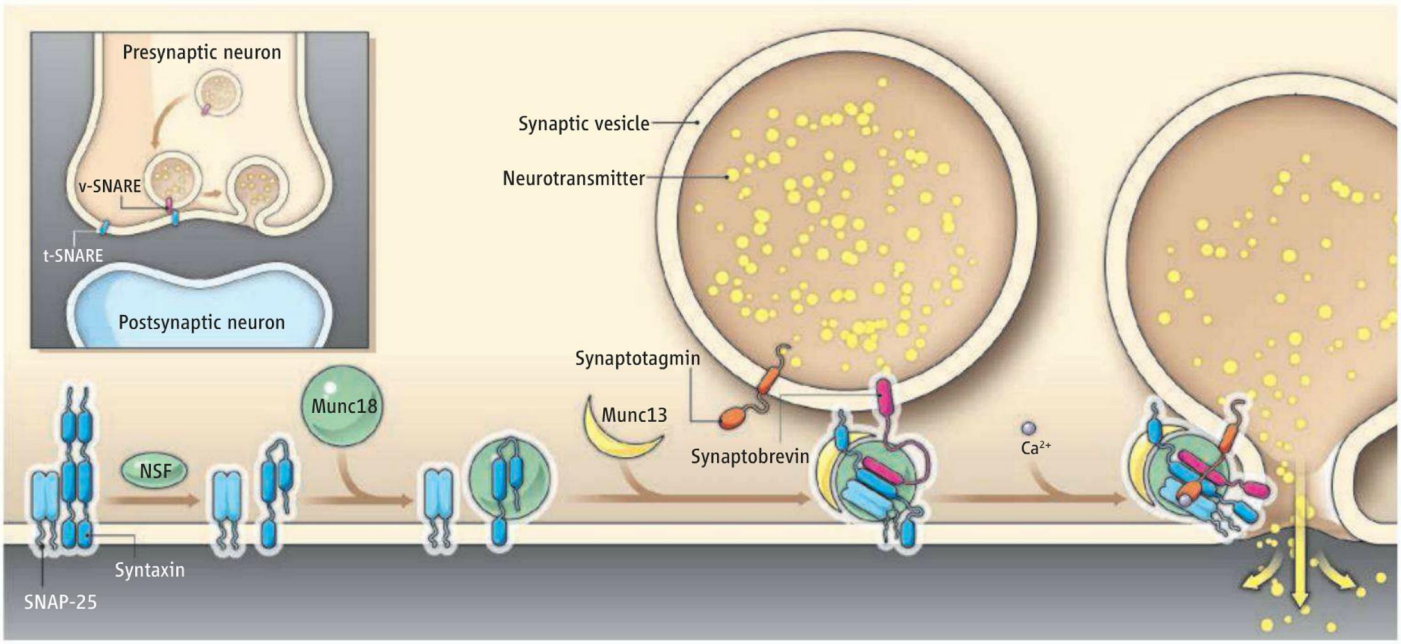

CREDIT: Y. HAMMOND/*SCIENCE*

A model with Muncs. Syntaxin, freed by NSF from nonproductive complexes (as shown) binds in a closed conformation to Munc18. Munc13 chaperones the assembly of ternary v/t-SNARE complexes that contain syntaxin, SNAP-25, and synaptobrevin. Synaptotagmin-Ca^{2+} is required for efficient membrane fusion.

Ma *et al*. explored the possibility that syntaxin-Munc18 complexes (rather than syntaxin–SNAP-25 complexes, which are vulnerable to side reactions) represent the physiologically relevant starting point for SNARE assembly and membrane fusion. The authors devised a scheme for generating syntaxin-Munc18 liposomes, as the traditional detergents used for making v- and t-liposomes caused syntaxin and Munc18 to dissociate. No fusion was observed when syntaxin-Munc18 liposomes and v-liposomes were mixed, even after the addition of the missing SNARE (SNAP-25) and synaptotagmin-Ca^{2+}. Thus, Munc18 indeed prevents syntaxin from entering into SNARE complexes and therefore inhibits membrane fusion. Strikingly, the further addition of Munc13 resulted in rapid liposome fusion. It is presumably the ability of Munc13 to catalyze the entry of Munc18-bound syntaxin into SNARE complexes that underlies its strong stimulatory effect on the rate and extent of membrane fusion in this new reconstitution system.

The pathway proposed by Ma *et al*. has the additional virtue of protecting proper SNARE complexes from disassembly chaperones. The extreme stability of fully assembled SNARE complexes, while critical for their membrane fusion activity, means that spontaneous SNARE disassembly is imperceptibly slow (*10*). Cells therefore express an AAA+ family protein, NSF, which consumes adenosine triphosphate (ATP) to drive SNARE complex disassembly. Remarkably, the reconstitution system of Ma *et al*. operates efficiently in the presence of NSF and ATP. Presumably, the Munc18-Munc13 route to SNARE assembly provides a protected pathway for productive SNARE complex formation even in the presence of the SNARE disassembly machinery. This suggests that assembly and disassembly chaperones function in alternation to catalyze cycles of membrane fusion and SNARE recycling. The disassembly chaperone NSF may play additional roles; for example, it may disentangle syntaxin that is trapped in dead-end side reaction products, thereby allowing Munc18 to bind and protect it.

The findings of Ma *et al*. will undoubtedly influence efforts to understand other intracellular membrane fusion reactions. For example, Munc13 is structurally similar to subunits of assemblies belonging to the complexes associated with tethering containing helical rods (CATCHR) family (*11*), which operate in various intracellular trafficking pathways to orchestrate SNARE assembly (*12*). Even where CATCHR complexes are not involved, there is reason to believe that a Munc13-like function is operating. The data are perhaps most compelling for yeast vacuole-vacuole fusion. In this case, both membranes contain identical complements of SNAREs; that is, both v- and t-SNAREs are present on each of the two fusing membranes. Disassembling "cis" v/t-SNARE complexes and guiding their reassembly into "trans" (membrane-bridging) v/t-SNARE complexes requires both NSF and the multisubunit homotypic fusion and vacuole protein sorting (HOPS) complex (*13*). Notably, HOPS contains a subunit homologous to Munc18; its other subunits may perform the Munc13 role. We thus seem poised on the brink of major breakthroughs in our mechanistic understanding not only of neurotransmitter release, but of intracellular membrane docking and fusion reactions more generally, with chaperones of both the assembly and disassembly variety taking center stage.

References

1. R. Jahn, D. Fasshauer, *Nature* **490**, 201 (2012).
2. C. Ma, L. Su, A. B. Seven, Y. Xu, J. Rizo, *Science* **339**, 421 (2013).
3. Y. Gao *et al*., *Science* **337**, 1340 (2012).
4. A. V. Pobbati, A. Stein, D. Fasshauer, *Science* **313**, 673 (2006).
5. J. M. Hernandez *et al*., *Science* **336**, 1581 (2012).
6. M. C. Chicka, E. Hui, H. Liu, E. R. Chapman, *Nat. Struct. Mol. Biol.* **15**, 827 (2008).
7. K. M. S. Misura, R. H. Scheller, W. I. Weis, *Nature* **404**, 355 (2000).
8. J. Shen, D. C. Tareste, F. Paumet, J. E. Rothman, T. J. Melia, *Cell* **128**, 183 (2007).
9. C. Ma, W. Li, Y. Xu, J. Rizo, *Nat. Struct. Mol. Biol.* **18**, 542 (2011).
10. D. Fasshauer, W. Antonin, V. Subramaniam, R. Jahn, *Nat. Struct. Biol.* **9**, 144 (2002).
11. W. Li *et al*., *Structure* **19**, 1443 (2011).
12. I. M. Yu, F. M. Hughson, *Annu. Rev. Cell Dev. Biol.* **26**, 137 (2010).
13. J. Mima, C. M. Hickey, H. Xu, Y. Jun, W. Wickner, *EMBO J.* **27**, 2031 (2008).

10.1126/science.1233801

IBI* SERIES WINNER

Keeping an Eye on Biology

Genomics Explorers, an IBI prize–winning module, engages students with bioinformatics and molecular research.

Susan R. Singer,[1]*§ Jodi A. Schwarz,[2] Cathryn A. Manduca,[3] Sean P. Fox,[3] Ellen R. Iverson,[3] Benjamin J. Taylor,[4]† Steven B. Cannon,[5] Gregory D. May,[6]‡ Sonja L. Maki,[1] Andrew D. Farmer,[6] Jeffrey J. Doyle[7]

Genomic data sets offer opportunities for students to generate original findings without expensive laboratory equipment, extending the benefits of undergraduate research to the classroom (*1*–*4*). Yet, working with data sets online can frustrate biology students who may miss connections to fascinating biological questions. Integrating organismal and molecular biology with bioinformatics can enhance student learning. We have developed a program in genomics, adapted for a plant (*Chamaecrista fasciculata*) and an animal (*Aiptasia pallida*), designed to support student learning with a Web-based guide (http://serc.carleton.edu/exploring_genomics/index.html) (see the first chart).

Curriculum development began with a collaborative effort, "Teaching Big Science at Small Colleges," to develop, assess, and share inquiry-based, integrated instructional units (I[3]Us) in genomics (http://serc.carleton.edu/genomics/index.html) (*5*). All I[3]Us are aligned with the evidence-based design principles described in *America's Lab Report* (*6*). Incorporating our own genomics research on nonmodel organisms resulted in our learning module, Genomics Explorers (*7*). Students ask questions on several levels of biological organization, from genes to genomes to organisms to evolution and environment (see the second chart).

Students initially worked with whole-transcriptome data from individuals with schizophrenia, shared by our collaborators at the National Center for Genome Resources. Despite the human interest factor, students were quickly lost in a sea of nucleotides without a biological context and were frustrated trying to use the available bioinformatics tools. Classroom observers noted that, rather than asking questions at the level of whole transcriptomes, students defaulted to a strategy of hunting for a single, often poorly chosen, gene. Conceptual understanding is particularly challenging for undergraduates dealing with very small or very large scales (*8*). We realized it was essential to guide student learning of both the biology and the bioinformatics.

We shifted to our own research organisms and developed a module introducing students to questions about interactions between organisms and their environments. We illustrate our approach with *Chamaecrista*. Students explore both the living organism and large data sets that are less abstract than DNA sequences. They use a photoperiod calculator to compare the flowering time of *Chamaecrista* from different latitudes (data available in the Explorer) with flowering time for perennial lilacs (*Syringa*) in a public phenology data set. After contrasting flowering time and latitude for the two plants, students generate explanations. In the second activity, students encounter whole-transcriptome data sets from *Chamaecrista* and are asked to formulate questions that can be addressed by comparing transcriptomes from different *Chamaecrista* ecotypes and organs at different stages of development.

To support students in developing and answering questions with transcriptomes, we organized our Web site around genomics problem-solving strategies. Our goal is to have students concurrently use science practices and biological concepts, a more effective approach than separating them (*9*). The site provides local data access and links to tools. For example, *Chamaecrista* transcriptome and genome sequence data are searchable on the *Chamaecrista* Genomics Explorer with a local BLAST search. Although the integrated approach supported students as they explored

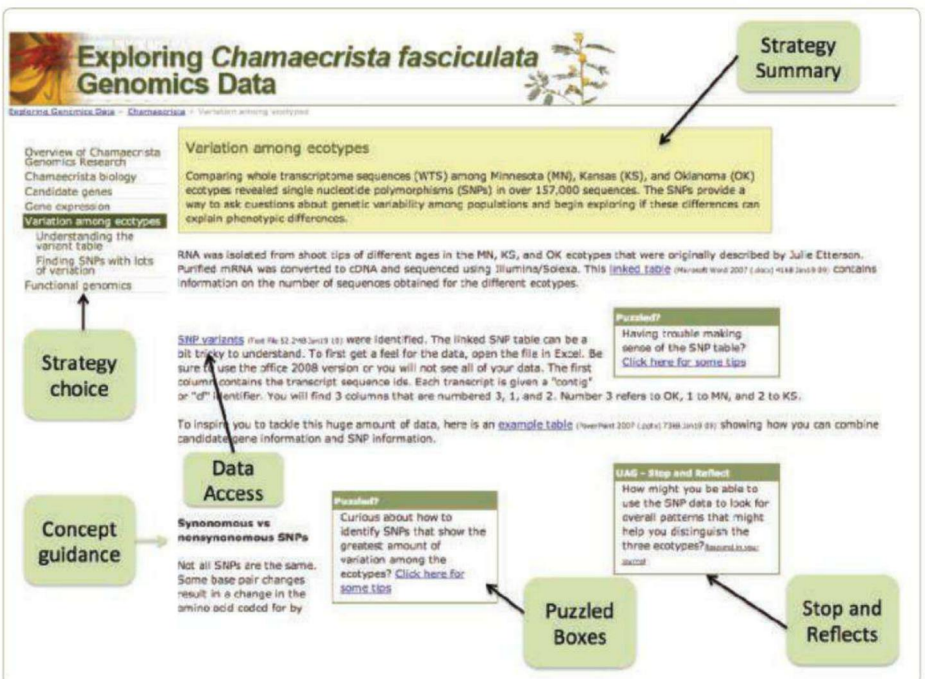

***Chamaecrista* Genomics Explorer supports problem solving.** The Explorer guides students to choose as a starting point: a literature-based entry to the biology of *Chamaecrista*, a candidate gene approach, or variation among three known ecotypes (a SNP-based approach). Links to tools and data are available centrally and as students need them. We include concept guidance, "Puzzled?" boxes that link to hints where our study shows that students frequently get stuck, and "Stop and Reflect" boxes that encourage both reflection and higher-order cognitive thinking. Reflecting on a lab learning experience has been shown to enhance student understanding of the nature of science (*6*).

[1]Department of Biology, Carleton College, Northfield, MN 55057, USA. [2]Department of Biology, Vassar College, Poughkeepsie, NY 12604, USA. [3]Science Education Resource Center, Carleton College, Northfield MN 55057, USA. [4]Department of Entomology, University of Wisconsin, Madison WI 53706, USA. [5]U.S. Department of Agriculture Agricultural Research Service, Iowa State University, Ames, IA 50010, USA. [6]National Center for Genome Resources, Santa Fe, NM 87505, USA. [7]Department of Plant Biology, Cornell University, Ithaca, NY 14853, USA.

*IBI, *Science* Prize for Inquiry-Based Instruction; www.sciencemag.org/site/feature/data/prizes/inquiry/. †Present address: Anoka Technical College, Anoka, MN 55303, USA. ‡Present address: Dupont Pioneer, Johnston, IA 50131, USA. §Author for correspondence. E-mail: ssinger@carleton.edu (SRS).

the different strategies (fig. S1), the lack of a central resource for data and tools was frustrating. In response, we added tool and data pages in the main selection menu.

Interacting with the Web site in one or two laboratory sessions allows students to revise their questions and explore multiple strategies. At the end of each session, students (either individually or in teams) briefly present their findings and next question to the entire lab, which encourages collaboration. We added visualization tools to support students in making comparisons among data sets, including mapping the transcriptome onto the soybean (*Glycine max*) genome.

In a third activity, students shift to a molecular lab experience, conducting expression analyses by isolating RNA and performing semiquantitative or quantitative polymerase chain reaction (PCR). Students have found nonsynonymous, single-nucleotide polymorphisms (SNPs) among ecotypes and then used restriction digests of their PCR products to determine whether the SNP was valid or an artifact of sequencing. Some chose to sequence their PCR products, providing additional information and validation for their work. If cost is a barrier, students can design functional genomics experiments without actually conducting them.

Groups present their experimental plans to the class for critique, and collaboration among groups is encouraged. Often, a whole class experiment emerges addressing a more comprehensive question. For example, several groups can collectively investigate the relative effects of different temperatures and photoperiods on the developmental expression of one or more genes of interest in two different ecotypes. The process is designed so students own their questions.

Students make their thinking visible with short presentations on their experimental questions and findings, lab notebook records, a final presentation and paper, and a model for the effects of genes and environment on flowering time (fig. S2). Each group produces a paper focused on their research question that includes an investigation seeking patterns at the level of the transcriptomes, not simply individual genes. Peer and instructor feedback is provided each week, and the final paper must address the points raised.

Genomic Explorers enables students to identify a research strategy and to use bioinformatics tools for investigation, without relying on the instructor for assistance. Off-loading the basic instruction to the Web site creates space for the in-depth conversations among students and the instructor on the nature of research and biology that typically arise during a traditional undergraduate research experience.

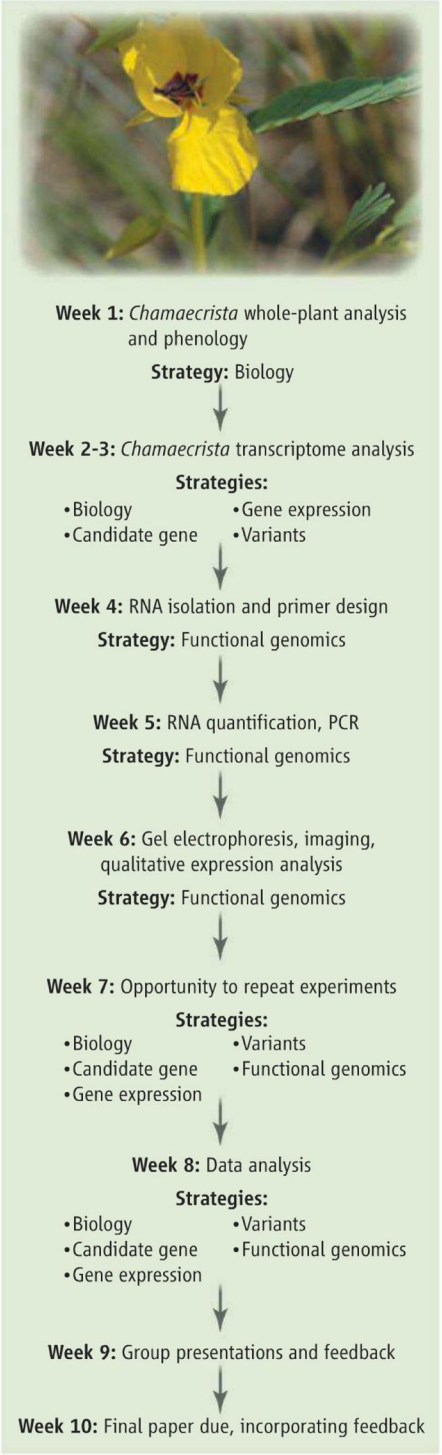

PHOTO CREDIT: SEAN FOX; AUTHOR PHOTOS: SARA RUBINSTEIN, JERRY CALVIN, SEAN FOX, SEAN FOX, SEAN FOX, BENJAMIN TAYLOR, DAN KUESTER, GREGORY MAY, ANDREW FARMER, KATHY BERARD, JANE DOYLE, SONJA MAKI

Flow of *Chamaecrista* instructional modules.

About the authors

Shown left to right and top to bottom: Susan Singer, Jodi Schwarz, Cathy Manduca, Sean Fox, Ellen Iverson, Benjamin Taylor, Steven Cannon, Greg May, Andrew Farmer, Sonja Maki, and Jeff Doyle.

References and Notes

1. D. Lopatto, *Science in Solution: The Impact of Undergraduate Research on Student Learning* (Research Corporation for Science Advancement, Tucson, AZ, 2009).
2. S. Laursen, A.-B. Hunter, E. Seymour, H. Thiry, G. Melton, *Undergraduate Research in the Sciences* (Jossey-Bass, San Francisco, CA, 2010).
3. American Association for the Advancement of Science (AAAS), *Vision and Change in Undergraduate Biology Education: A Call to Action* (AAAS, Washington, DC, 2011).
4. C. A. Wei, T. Woodin, *CBE Life Sci. Educ.* **10**, 123 (2011).
5. L. M. Banta *et al.*, *CBE Life Sci. Educ.* **11**, 203 (2012).
6. S. R. Singer, M. L. Hilton, H. A. Schweingruber, Eds., *America's Lab Report: Investigations in High School Science* (National Academies Press, Washington, DC, 2005).
7. S. R. Singer *et al.*, *Plant Physiol.* **151**, 1041 (2009).
8. S. R. Singer, N. R. Nielsen, H. A. Schweingruber, Eds., *Discipline-Based Education Research: Understanding and Improving Learning in Undergraduate Science and Engineering Education* (National Academies Press, Washington, DC, 2012).
9. National Research Council, *A Framework for K–12 Science Education: Practices, Crosscutting Concepts, and Core Ideas* (National Academies Press, Washington, DC, 2011).

10. Our work was supported by NSF DEB 0746571 and DUE 0837375 to S.R.S. S.R.S. and J.A.S. thank the Carleton and Vassar students who participated in our study. S.R.S. and J.A.S. developed the curriculum and participated in the biology and education research analyses. S.P.F. created the Web site infrastructure and aided in classroom observation and research analysis, along with C.A.M., E.R.I., and B.J.T. S.R.S., S.B.C., G.D.M., S.L.M., A.D.F., and J.J.D. contributed to the *Chamaecrista* research, including sequencing and assembling the *Chamaecrista* transcriptome. Institutional review Board approval 08-09 006 (Carleton and Vassar Colleges).

Supplementary Materials
www.sciencemag.org/cgi/content/full/339/6118/408/DC1

10.1126/science.1229848

Testing the waters. Melting sea ice is opening a Northern bonanza for oil, rare earths, and even fish—but is the United States ready?

ARCTIC DEVELOPMENT

Warming Climate Exposes Resources—and Risks—in the Far North

Five years ago, a pair of mini-submarines descended to the seabed below the North Pole, where the crews planted a rust-proof, titanium Russian flag. The timing and the powerful symbolism of the move provoked a global storm: With climate change melting the Arctic ice and exposing a potential trove of natural resources, would the region become a flashpoint for geopolitical conflict?

At a recent AAAS forum, experts downplayed the risk suggested by that made-for-headlines event. Diplomacy and cooperation are already reducing the risks of Arctic conflict, they said. Of far greater concern is that U.S. policy and diplomacy may be unprepared as accelerating climate change opens a new era in Arctic development, threatens indigenous populations, and destabilizes climate patterns worldwide.

The decline in the Arctic's summer ice cover is "definitely outpacing what a lot of our worst-case climate models have been suggesting would happen…as we continue to warm the planet," said Julienne Stroeve, a researcher based at the U.S. National Snow & Ice Data Center in Boulder, Colorado. "The changes are happening a lot faster than expected, and there are a lot of implications for governance and exploration."

"I don't think we have a strategy, an agreed-to national plan," added Heather A. Conley, senior fellow and director of the Europe Program at the Center for Strategic and International Studies in Washington, D.C. "How much are we going to develop the Arctic? How much are we going to protect it?...We're going to be testing the system across the Arctic and testing international cooperation to make sure that we can work together and not at cross-purposes."

Conley and Stroeve joined Jed Hamilton, senior research consultant for ExxonMobil, at the 10 December event at AAAS. The forum, moderated by NPR science correspondent Richard Harris, was sponsored by the American Chemical Society, Georgetown University's Program on Science in the Public Interest, and the AAAS Office of Government Relations.

Since the end of the Cold War in the early 1990s, the Arctic has been more a forum for international cooperation than for military competition. "We aren't seeing great tension. In fact, 2 years ago, Norway and Russia after 40 years [of dispute] agreed on their border in the Arctic," Conley said. "We're seeing cooperation between nations on search and rescue, oil spills and response—they're trying to address the transformation.

"I've disappointed a lot of journalists when I've told them we aren't seeing the militarization of the Arctic," she added.

In her view, the greater concern is the apparent lack of policy preparation by the United States for changing conditions in the region. Melting sea ice may mean more commerce, mining, and tourism, but infrastructure ranging from lodging to search and rescue facilities and hospitals is lacking.

In the future, Conley said, "you're going to see the Arctic as a public-private partnership, where the private sector is going to have to join with the government" in sharing data, assessing needs, and building international networks.

The receding sea ice would seem especially alluring to oil and gas companies. The U.S. Geological Survey has concluded that about a quarter of the Earth's remaining hydrocarbon potential lies in the Arctic. And indeed, there are ambitious efforts to assess and tap oil and natural gas reserves in the oceans off of Alaska, Canada, Greenland, and Siberia.

But Hamilton said that these projects still face enormous challenges: Severe winter weather, including crushing sea-surface ice floes; technical and engineering challenges in getting the crude or gas to refineries and to market; and huge production and transportation costs.

ExxonMobil and its partners are beginning development of a 1-billion-barrel oil field off the northeast coast of Canada, he said, but "it will take us 5 years and north of $10 billion to develop that field."

The oil will be extracted over a period of 40 years, he added, "and when all is said and done and people have spent their entire careers on that project, that 40 years of production will satisfy 12 days of world demand right now."

Even as policy begins to focus on these regional opportunities, the climate is continuing to warm, largely as a result of global greenhouse gas emissions. According to current estimates, 1.9 trillion metric tons of carbon are held in Arctic soils, and as those soils warm, they will begin to release that carbon into the atmosphere. That could become a massive new driver for climate change.

There are already some indications that the receding sea ice has a dangerous impact on global climate, Stroeve said. The difference in temperatures between the Arctic and equator plays a central role in global circulation of air and ocean currents. As the Arctic

CREDIT: JEREMY POTTER NOAA/OAR/OER

warms, she noted, the circulation may slow down—with powerful effects.

"We've been noticing that by warming up the Arctic, you actually allow these sorts of extreme conditions to persist longer—droughts, floods," Stroeve said. "They're moving more slowly in the atmosphere, so they can stay around in a region longer and cause more extreme events."

These are urgent concerns and, in Stroeve's view, they require further research and ambitious action by lawmakers and policymakers. Public support for action will be crucial, and a key element of Arctic policy and development must assure the rights of indigenous people.

"How do you balance between wanting to access the economic development with the rights of indigenous people and their control over that [development]?" Conley asked. "There are people whose lives and food security are being deeply impacted by this transformation. This affects societies, it affects ways of life." *–Edward W. Lempinen*

SCIENCE POLICY

S&T Policy Fellows Celebrate 40 Years

Growing impact. The 2012–2013 class of Fellows is the largest yet for the influential AAAS program.

CREDIT: AAAS SCIENCE & TECHNOLOGY POLICY FELLOWSHIPS

In 1973, the first class of AAAS Science & Technology Policy Fellows was dispatched to Washington, D.C. The seven select scientists and engineers were the vanguard of a movement that, four decades later, has grown to more than 2500 researchers who provide unmatched expertise to address public science issues.

"Scientists are trained to be able to quantify uncertainty," said Jessica Tuchman Mathews, president of the Carnegie Endowment for International Peace and a member of the 1973 class. "And since that's so much of what Congress has to do, it's an incredibly valuable set of skills."

In a series of interviews conducted to commemorate the program's 40th anniversary, Mathews and other top-level alumni said the Fellowships have had a dramatic effect on their careers. [Watch all of the 40th-anniversary interviews at www.aaas.org/go/fellowsvideo.] They also feel that the program has had a transformative impact on U.S. and global science policy.

In recent years, S&T Fellows have helped to set up a digital library for Iraqi scientists, provided key data to support the Endangered Species Act, contributed to a federal task force on global climate change adaptation, and worked on recovery and reconstruction projects in Haiti just weeks after the country's devastating January 2010 earthquake.

The Fellows' work has been good for science in many ways, said Kerri-Ann Jones, assistant U.S. secretary of state for oceans and international environmental and scientific affairs, and a 1985–86 Diplomacy Fellow. "As scientists became more informed of budget processes and other things, I think they became more active about championing investments in research and development."

"One of the exciting things about the program," agreed Fellowships Director Cynthia Robinson, "is that all of those individuals have taken the experience they've had in Washington D.C.… to engage in the work that they've done throughout the rest of their careers." *–Carla Schaffer and Edward W. Lempinen*

AAAS

Call for Nomination of 2013 Fellows

AAAS Fellows who are current members of the Association are invited to nominate members for election as Fellows. A member whose efforts on behalf of the advancement of science or its applications are scientifically or socially distinguished, and who has been a continuous member for the 4-year period leading up to the year of nomination, may by virtue of such meritorious contribution be elected a Fellow by the AAAS Council.

A nomination must be sponsored by three previously elected AAAS Fellows (who are current in their membership), two of whom must have no affiliation with the nominee's institution.

Nominations undergo review by the steering groups of the Association's sections (the chair, chair-elect, retiring chair, secretary, and four members-at-large of each section). Each steering group reviews only those nominations designated for its section.

Names of Fellow nominees who are approved by the steering groups are presented to the Council for election.

Nominations with complete documentation must be received by 17 April 2013. Nominations received after that date or nominations that are incomplete as of the deadline will not move forward, but may upon request be held for the following year.

Complete instructions and a copy of the nomination form are available at www.aaas.org/aboutaaas/fellows/instructions.shtml. To request a hard copy of the nomination form, please contact the AAAS Executive Office, 1200 New York Avenue, NW, Washington, DC, 20005, USA; at 202-326-6468; or at kobrien@aaas.org.

AAAS
ADVANCING SCIENCE, SERVING SOCIETY

Results of the 2012 Election of AAAS Officers

Following are the results of the 2012 election. Terms begin on 19 February 2013.

General Election
President: Gerald R. Fink
Board of Directors: Claire M. Fraser; Elizabeth F. Loftus
Committee on Nominations: Judy R. Franz; Barbara J. Grosz; Peter S. Kim; Mario J. Molina

Section on Agriculture, Food, and Renewable Resources
Chair Elect: Sally Mackenzie
Member-at-Large of the Section Committee: Pamela C. Ronald
Electorate Nominating Committee: Mary Susan Moran; Linda L. Walling

Section on Anthropology
Chair Elect: Nina G. Jablonski
Member-at-Large of the Section Committee: George R. Milner
Electorate Nominating Committee: Agustín Fuentes; Lisa Sattenspiel
Council Delegate: Clark Spencer Larsen

Section on Astronomy
Chair Elect: Robert P. Kirshner
Member-at-Large of the Section Committee: Edward L. (Ned) Wright
Electorate Nominating Committee: Edmund Bertschinger; Margaret Meixner
Council Delegate: Eugene H. Levy

Section on Atmospheric and Hydrospheric Sciences
Chair Elect: Antonio J. Busalacchi, Jr.
Member-at-Large of the Section Committee: Ana P. Barros
Electorate Nominating Committee: Diane M. McKnight; Patricia K. Quinn

Section on Biological Sciences
Chair Elect: Dennis J. Thiele
Member-at-Large of the Section Committee: Bonnie Bartel
Electorate Nominating Committee: Tom Curran; Suzanne Sandmeyer
Council Delegate: James R. Broach; Judy Callis; Lynn Cooley; Jessica Gurevitch; George A. O'Toole; Nancy C. Walworth

Section on Chemistry
Chair Elect: Thomas E. Mallouk
Member-at-Large of the Section Committee: Susannah Scott
Electorate Nominating Committee: Shelia S. David; David A. Wink
Council Delegate: Judith N. Burstyn; Marisa C. Kozlowski; Donna J. Nelson

Section on Dentistry and Oral Health Sciences
Chair Elect: Luisa Ann DiPietro
Member-at-Large of the Section Committee: Ichiro Nishimura
Electorate Nominating Committee: Paulette Spencer; Thomas E. Van Dyke

Section on Education
Chair Elect: Cathryn A. Manduca
Member-at-Large of the Section Committee: Melanie M. Cooper
Electorate Nominating Committee: Penny J. Gilmer; Ramon E. Lopez

Section on Engineering
Chair Elect: Nicholas A. Peppas
Member-at-Large of the Section Committee: Ilesanmi "Ade" Adesida
Electorate Nominating Committee: William E. Bentley; Edmund G. Seebauer

Section on General Interest in Science and Engineering
Chair Elect: Terry Devitt
Member-at-Large of the Section Committee: Mariette DiChristina
Electorate Nominating Committee: Lynn E. Elfner; Katherine E. Rowan

Section on Geology and Geography
Chair Elect: William H. Schlesinger
Member-at-Large of the Section Committee: Stephen G. Wells
Electorate Nominating Committee: Mary Anne Holmes; Paul L. Koch
Council Delegate: Ben A. van der Pluijm

Section on History and Philosophy of Science
Chair Elect: Anita Guerrini
Member-at-Large of the Section Committee: Diana Kormos Buchwald
Electorate Nominating Committee: Richard M. Burian; John Dupré

Section on Industrial Science and Technology
Chair Elect: Steven W. Popper
Member-at-Large of the Section Committee: Gary L. Messing
Electorate Nominating Committee: Paul S. Drzaic; Edmund G. Seebauer

Section on Information, Computing, and Communication
Chair Elect: J.J. Garcia-Luna Aceves
Member-at-Large of the Section Committee: William Gropp
Electorate Nominating Committee: Tom M. Mitchell; Peter Norvig

Section on Linguistics and Language Science
Chair Elect: Sandra Chung
Member-at-Large of the Section Committee: Carol A. Padden
Electorate Nominating Committee: Mark C. Baker; James Pustejovsky

Section on Mathematics
Chair Elect: David M. Bressoud
Member-at-Large of the Section Committee: Susan Friedlander
Electorate Nominating Committee: Susanne C. Brenner; Barbara Lee Keyfitz
Council Delegate: Deborah F. Lockhart

Section on Medical Sciences
Chair Elect: Karen H. Antman
Member-at-Large of the Section Committee: Scott D. Emr
Electorate Nominating Committee: Jeffrey I. Cohen; Joseph Loscalzo

Section on Neuroscience
Chair Elect: Pat Levitt
Member-at-Large of the Section Committee: Joshua R. Sanes
Electorate Nominating Committee: William Mobley; Peter L. Strick
Council Delegate: Harry T. Orr

Section on Pharmaceutical Sciences
Chair Elect: Deanna L. Kroetz
Member-at-Large of the Section Committee: Kathleen M. Giacomini
Electorate Nominating Committee: Stephen V. Frye; Margaret O. James

Section on Physics
Chair Elect: Susan N. Coppersmith
Member-at-Large of the Section Committee: Don Q. Lamb
Electorate Nominating Committee: David D. Awschalom; Sharon C. Glotzer
Council Delegate: Arthur Bienenstock; Philip W. Phillips

Section on Psychology
Chair Elect: James L. McClelland
Member-at-Large of the Section Committee: Lynne M. Reder
Electorate Nominating Committee: Morton Ann Gernsbacher; Judith F. Kroll

Section on Social, Economic, and Political Sciences
Chair Elect: Barbara Boyle Torrey
Member-at-Large of the Section Committee: Elizabeth Cooksey
Electorate Nominating Committee: Kaye Husbands Fealing; Ronald R. Rindfuss

Section on Societal Impacts of Science and Engineering
Chair Elect: James R. Fleming
Member-at-Large of the Section Committee: Caroline S. Wagner
Electorate Nominating Committee: Jennifer Sue Bond; Stephen D. Nelson

Section on Statistics
Chair Elect: David L. DeMets
Member-at-Large of the Section Committee: Joan F. Hilton
Electorate Nominating Committee: James L. Rosenberger; Bin Yu

Can We Name Earth's Species Before They Go Extinct?

Mark J. Costello,[1]* Robert M. May,[2] Nigel E. Stork[3]

Some people despair that most species will go extinct before they are discovered. However, such worries result from overestimates of how many species may exist, beliefs that the expertise to describe species is decreasing, and alarmist estimates of extinction rates. We argue that the number of species on Earth today is 5 ± 3 million, of which 1.5 million are named. New databases show that there are more taxonomists describing species than ever before, and their number is increasing faster than the rate of species description. Conservation efforts and species survival in secondary habitats are at least delaying extinctions. Extinction rates are, however, poorly quantified, ranging from 0.01 to 1% (at most 5%) per decade. We propose practical actions to improve taxonomic productivity and associated understanding and conservation of biodiversity.

Why is discovering species important? Species provide the most practical metric for distinguishing habitats and tracking progress in exploring Earth's biodiversity. They are as fundamental to biology as elements are to chemistry and particles to physics and are the first step in exploring biology. Once species are described, more detailed studies can look at populations and genetic and biochemical diversity. Species inventories draw attention to where taxonomic effort will discover most new species, including resources and ecosystems. Having a standard list of species names is essential for quality assurance in biological and ecosystem sciences and natural resource management. Another reason to discover species is to improve understanding of which and how many species will become extinct.

A meeting of conservation biologists or ecologists is hardly complete without worries about extinction rates, that many millions of species are yet to be discovered, and that the taxonomic workforce is decreasing. We contend that at least two of these three concerns are mistaken. We do not dispute that we are in a human-caused mass extinction phase with many species committed to extinction, but actual extinctions have been fewer than arguably expected. With a realistic surge of effort, most species could be named within the present century. Recent analyses have narrowed estimates of how many species may now live on Earth, but estimates of extinction rates are less quantifiable, varying by a factor of more than 100. In this review, we compare recent estimates of species richness and extinction rates on Earth in the context of trends in the size and distribution of the taxonomic workforce. We suggest actions that would enable most species on Earth to be named in this century and that could be achieved at less cost than efforts to discover life on other planets.

What Species Are Known

The incomplete Catalogue of Life (*1*) currently lists >1.3 million species, and an expert-validated inventory of an anticipated 230,000 marine species is more than 95% complete (*2*). These inventories try to account for known synonyms (species described more than once), but more are being created as taxonomic revisions remove others (*3*). Reconciling synonyms may take decades. For example, 93% of all cetacean names are synonyms (i.e., 9 out of 10) (*4*); more than 80% of names in some alga genera (*5*); 32% for insects (*6*); 33% to 88% for groups of seed plants (*7*); 38% for world mollusks, 50% for marine fish, and 81% for freshwater fish in Europe (*8*); and 40% for all marine species (*2*). Thus, we consider 20% of the currently estimated 1.9 million described species to be undiscovered synonyms, reducing this to 1.5 million valid described species (*8*).

The Unknown Species

Modern estimates of eukaryotic (nonbacterial) species on Earth have ranged from 2 million to 100 million (*8*). Recent studies have provided a firmer basis for debate about global species richness, because they are based on broad-scale empirical data and new statistical models that provide confidence limits (*9*). Mora *et al.* extrapolated the rate of discovery of selected higher taxa to predict 8.7 million (±1.3 million SE) eukaryotic species globally, of which 25% (2.2 million ± 0.18 million standard error) were marine (*10*); Costello *et al.* used rates of description of 1/3 of named species to predict a total of 0.3 million marine and 1.7 million terrestrial species (*8*). These approaches and expert opinion estimated that 0.3 to 0.7 and 0.7 to 1.0 million marine species may exist, respectively (*2*). Another model applied to species description rates for 112,000 species of plants predicted that 30% more remained to be discovered, whereas experts estimated 18% (*11*). In addition, modeling of uncertainty of the number of species of arthropods on tropical trees suggested that there may be 6.1 to 7.8 million terrestrial arthropod species (90% confidence intervals of 3.6 to 13.7 million) (*12*, *13*). Collectively, these new estimates suggest that there is likely to be ~5 ± 3 million species on Earth. Previous estimates of 30 to 100 million based on potential deep-sea diversity and estimates of insect host specificity now seem highly unlikely (*8*, *12*).

How Many Taxonomists?

If we narrowly define taxonomists as the people describing species new to science, then—contrary, for example, to statements made to a U.K. House of Lords committee (*14*)—recent decades have had two to three times as many taxonomists as before the 1960s (*8*). This is true for a range of groups and regions [e.g., (*8*, *11*, *15*)] and is supported by an increasing number of publications describing new species in all regions of the world (Fig. 1A). A survey of literature and institutions using a broad definition of a taxonomist estimated that there may be 30,000 to 40,000 worldwide (*16*). During the period 2000 to 2009, more than 8600 people described 30,484 species in the terrestrial and marine databases analyzed by Costello *et al.* (*8*). That 166,000 species were described in this period indicates that there may be 47,000 taxonomists describing species new to science. However, overall there are fewer species being described per author, suggesting that it may already be harder to discover new species (*8*, *11*, *15*). This apparent decline in species per author does not appear to have been due to an increasing proportion of people who only describe one or two species in their lifetimes. For example, over the past century, 42 to 44% of authors described only one marine species per decade (*2*), and the skewness of the frequency distribution of terrestrial and marine species described per author has not shown any trend (*8*).

The impression that the number of taxonomists was declining may be because taxonomists tend to be best known when near retirement and because of the dilution of traditional taxonomy among new biology specializations. For example, there was a 12% decline in traditional taxonomic expertise in the Natural History Museum (NHM) (London) over 15 years as they were replaced by specialists in molecular biology (*17*). There is no evidence that most taxonomists are near retirement in any country. In 1999, marine

[1]Leigh Marine Laboratory, University of Auckland, Post Office Box 349, Warkworth, New Zealand. [2]Department of Zoology, University of Oxford, South Parks Road, Oxford OX1 3PS, UK. [3]Environmental Futures Centre, School of Environment, Griffith University, 170 Kessels Road, QLD 4111, Brisbane, Australia.

*To whom correspondence should be addressed. E-mail: m.costello@auckland.ac.nz

taxonomists in Europe had a median age of 40 to 44 years and an average age of 47 (*18*). In Canada, the median age of taxonomic experts was 39, with an average of 36 (*19*), whereas in the United Kingdom, 57% were in their 40s or 50s (*17*).

Where Are The Taxonomists?

The numbers of taxonomists may be decreasing in some institutions of the countries that formerly led the field of taxonomy [e.g., (*14*)], but not for South America, at least (*20*). The increasing number of taxonomists is partially due to the increase in taxonomists based in South America and Asia (Fig. 1B). For example, 80% of 1200 people requesting insect specimens from NHM during 1986 to 1991 and 78% of 271 institutions borrowing plant specimens from Kew in 1989 were from Europe and North America (*21*). However, only 51% of 5148 authors of papers in *Zootaxa* from 2001 to 2008 were from the same regions (*22*). The proportion of authors of papers describing new species from these regions decreased similarly from 72% to 68% to 56% per decade, although the actual number of publications increased (Fig. 1). This increase in the proportion of taxonomists based in the Southern Hemisphere and Asia-Pacific region is appropriate because most species occur in these regions (*8*, *23*, *24*).

Extinction Rates?

Certified extinctions in better known groups of vertebrates have been at rates comparable to the mass extinctions in the geological past [e.g., (*25*, *26*)]. However, there is evidence that contemporary extinctions have not been as high as some had predicted (*27*), for several reasons: effective conservation efforts (*28*, *29*); species surviving in managed landscapes (e.g., agricultural, secondary forest) (*30*); and "extinction debt" (*31*). Although retention of pristine environments is essential for the conservation of some locally endemic species (*32*, *33*), more than half of forests in the tropics are secondary forest (*30*). Conservation can take advantage of this delayed extinction to protect key environments and restore habitats and populations. More than 90% of the mammals and birds that have gone extinct recently (within 500 years) were hunted by humans and associated species, particularly those introduced to islands with predator-naive endemic species (*34*), and present threats to marine species are still almost entirely from hunting.

How to extrapolate from the extinct and currently most threatened species to all species is uncertain because: (i) the risk of extinction varies between taxa (*26*, *35*), (ii) future extinctions may be more driven by habitat and environmental change, and (iii) surviving species may be more resilient by occupying secondary habitats and/or at low population sizes. Only <5% of all known species have been assessed for extinction risk (*36*). Most current models predict <5% extinction per decade (*25*–*27*), although the impact of climate change on extinctions is particularly uncertain because species may adapt and/or adjust their distribution (*37*, *38*). Although marine species may be able to adapt their distribution to climate (temperature) change more easily than terrestrial species (*39*), climate-change induced acidification, stratification, and deoxygenation are the kind of changes that contributed to mass marine extinctions millions of years ago. Thus, global-scale environmental change presents an even greater risk of an anthropogenic mass extinction event than the causes of the recent directly human-mediated extinctions. Another concern is that local threats, such as habitat loss, hunting, and harvesting, are now acting synergistically with climate change (*35*, *40*).

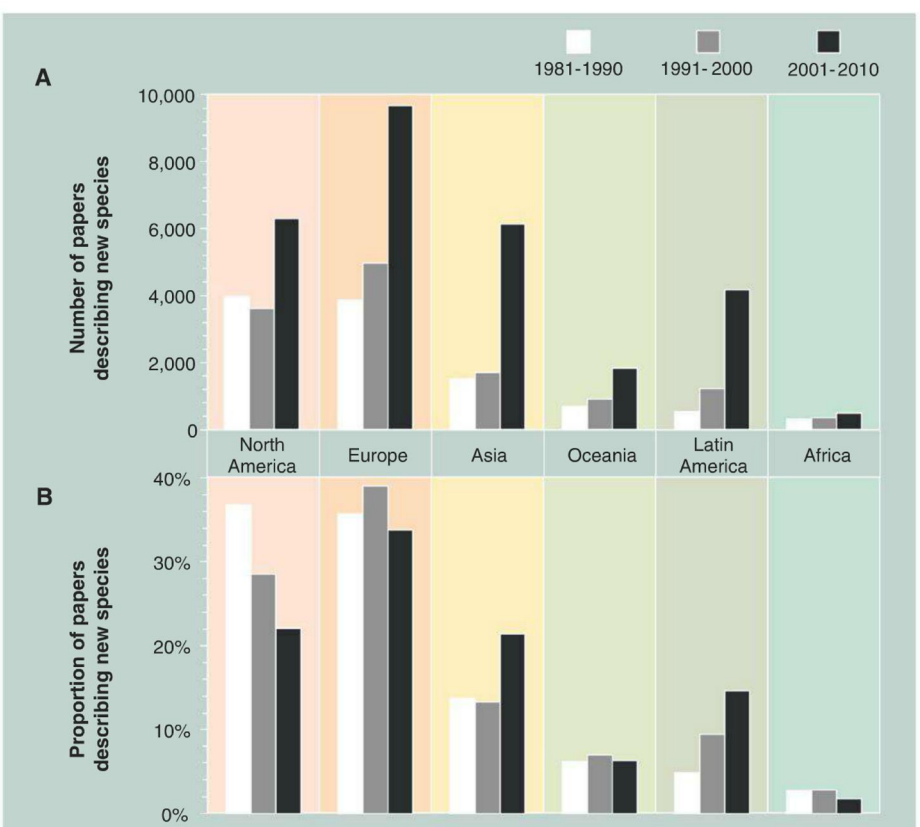

Fig. 1. (**A**) The number of papers describing species new to science increased in all geographic regions from 1981 to 1990 (white bar), to 1991 to 2000 (gray bar), and 2001 to 2010 (black bar) (n = 10,819, 12,703, and 28,596 publications, respectively). (**B**) However, the proportion of papers from North America decreased, and the proportion from Asia and Latin America increased. Data compiled from the Web of Science and Zoological Record by Lohrmann *et al.* (*58*).

Species Description Versus Extinction Rates

Current taxonomic effort has described an average of 17,500 species per year over the past decade, rising above 18,000 per year since 2006 (*41*). At this rate of description, if there are 2 million species on Earth then most will have been described by 2040; if 5 million, by the year 2220 (Fig. 2). If description rates are increased to 20,000 species per year, then 3.5 million will be described by 2100. It may get harder to discover new species as most are found, but this may be offset by proportionally more taxonomic effort in less studied localities and taxa.

If extinction rates are as high as 5% per decade, then regardless of how many species exist on Earth, more than half will be extinct within 150 years. If most species are unknown to science, then their extinction will also be unknown, further compromising estimates of extinction rates. However, at the rates considered more realistic (i.e., <1% per decade) (*27*), the rate of species description greatly outpaces extinction rates whether there are 2 or 10 million species on Earth. However, in contrast to the relatively constant rate of species description in recent decades, actual extinction rates may become nonlinear if their causes act synergistically.

Increasing Taxonomic Productivity

Taxonomic productivity could be enhanced through several activities (Table 1). The Convention on Biological Diversity has responded to the need for taxonomy by establishing the Global Taxonomy Initiative (GTI), which has assessed countries' taxonomic needs and proposed strategies to increase taxonomic effort (*42*). Indeed, we may now be in the greatest period of biological discovery. Thus, there is no

justification for believing that discovering species is fruitless because so few have been described, there are insufficient taxonomists, and so many species are or soon will be extinct [e.g., (*43*, *44*)].

The infrastructures for publishing taxonomic information and data exist and can continue to improve, while their archival requirements are not especially demanding (*45*). Standardized species distribution data can be published and integrated through the Global Biodiversity Information Facility, Ocean Biogeographic Information System, and associated databases; authoritative species inventories through scholarly databases that are part of Species 2000 and the World Register of Marine Species (*1*, *4*); and wider biodiversity information through numerous web sites and content aggregators that are online and open-access. The bottleneck in making progress is not technology; it is having enough people involved and their activities coordinated, and historic knowledge captured in open-access online databases. The U.S. National Science Foundation's Partnerships for Enhancing Expertise in Taxonomy research program was a pioneer in this field but has not been replicated in Europe or elsewhere (*46*).

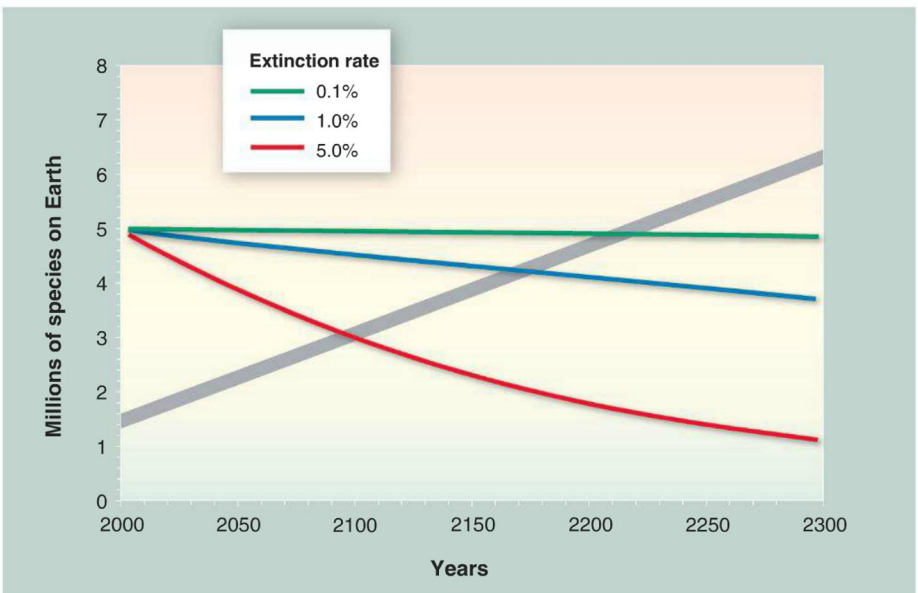

Fig. 2. Comparison of the number of species left to describe if decadal extinction rates are at 0.1% (green line), 1% (blue line), or 5% (red line) with the number of described species (gray line) if the past decade's average of 16,000 species per year continues.

Table 1. Actions to increase the species description rates and taxonomic efficiency.

Publication process
• More taxonomic revisions of species groups so as to recognize synonyms and clarify their relationships
• Reduce the time in prepublication peer review and editing
• More rapid publication through immediate online publication when a paper is accepted
• Mandatory online registration of new species
Online open-access databases
• Completion of expert-validated open-access inventories of all described species on Earth, linked to literature, distribution, and other information by cooperatives of taxonomists
• Greater online interoperability between publications, databases, and scholarly Web sites so that authoritative information is more easily detected
• Open access to taxonomic literature that helps identify species and recognize undescribed species
Specimen collection, description, and curation
• Coordinated field sampling for species in geographic areas and habitats that are likely to add substantially to the world's collections
• Recognizing that no country can have experts in all taxa, proactive international cooperation should facilitate exploration, discovery, and description of new species
• Use of digital imaging and molecular technologies to accelerate the description of species
• Increased availability and access to museum and herbarium specimens, particularly type specimens through exchanges, loans, and on-line imaging; increased support for taxonomists to visit collections and other taxonomists
Global coordination and resources
• Global coordination among the scientific community, both professional and amateur, to share knowledge and fill gaps in expertise
• New appointments of taxonomists in countries with rich diversity
• Financial support from government and nongovernment sources to support open access to taxonomic publications and scholarly databases and fill gaps in expertise.

Is Discovering All Species Practical?

If each species is considered a book of knowledge for which we lack a title page, then we need to catalog 0.5 to 6.5 million more books. Ten times more books are already in the U.S. Library of Congress, and each book may have taken as much or more effort to produce as one species description. But many people write books, not just those who are employed to do so. Opening up taxonomic literature to the public, as is already the case for birds [e.g., (*47*)], mammals, fish, flowering plants, butterflies, and some other invertebrates, will help more people study and discover species (Table 1). Already, half of all new species of European animals, including the less charismatic species, are being described by amateurs (*48*). The increasing accessibility of information through the Internet and mobile telephones is already providing new opportunities to aid species identification.

As fewer species remain to be discovered, it will become harder to maintain the rate of discovery without the assistance of a larger community of observers. New molecular methods of discriminating species will help this process of classification—including recognition of sibling and synonymous species—but will not necessarily increase the rate of description (*49*, *50*). Greater accessibility of species descriptions will help reduce the creation of synonyms. Because of synonymies, revisions of previously described species are as critical to estimating global species richness as are descriptions of new species. There is some evidence that fewer synonyms are being created (*2*), but this may also reflect the time lag to recognize them. Immediate online publication accelerates access to species information without the need to wait for the print issue of the journal (*51*). Some have questioned the need for prior peer review in taxonomy because its absence will speed up publication [e.g., (*52*)], and others (*53*) have proposed a more radical open-access Internet-based "publish-as-you-go" model whereby a species' information would be online before its formal naming.

Recognizing that almost all science journals are now published online, the codes of botanical and zoological nomenclature now accept descriptions of new species in publications in electronic-only journals that have an International Standard Serial or Book Number (ISSN or ISBN) and are preferably archived on different continents in electronic and print form (*54*, *55*).

New scientific names for fungi will be registered in MycoBank. Names of bacteria were effectively standardized in 1980, and new names must be published in the *International Journal of Systematic and Evolutionary Microbiology*. Such coordination and standardization of species nomenclature is critical to minimize confusion and must be supported (*52*). The convergence of expert-edited and automated tools for linking with publications could further help quality assurance in taxonomy. For example, by cross-linking authoritative online species databases (e.g., Global Species Databases in Species 2000 and World Register of Marine Species) to species names in publications (e.g., Biodiversity Heritage Library and Index of Organism Names) and registration systems (e.g., MycoBank and ZooBank).

The scale of this taxonomic challenge must not be underestimated. A 1-month survey of seabed in New Caledonia found 127,652 specimens and 2738 species of mollusks, of which 80% were new to science (*56*). A sample of 24,000 specimens of insects from the canopy of 10 trees in Borneo took 2 years to sort to 5000 morphospecies and included 739 morphospecies of chalcid wasps from 1455 specimens (*57*). Most species are rare and, not surprisingly, most described species are only known from single specimens and localities [e.g., (*6*)]. The museums and herbaria of the world probably contain more than 400 million specimens, with millions more in other collections—perhaps several billion in all (*52*). Marine taxonomists estimated that there were 65,000 undescribed marine species in collections (*2*), suggesting that about 0.5 million unnamed species may already be in collections. A full-time taxonomist might examine a few thousand specimens, and describe a hundred species, a year. Thus, the equivalent of 500 taxonomists over 10 years is needed to describe this backlog of undescribed species in collections, and this effort needs to be complemented by new field expeditions.

Conclusion

The estimates of how many species are on Earth (5 ± 3 million) are now more accurate than the moderate predictions of extinction rates (0.01 to 1% per decade). The latter suggest 500 to 50,000 extinctions per decade if there are 5 million species on Earth. Our review suggests that currently species are more likely to be described than become extinct, but this may change if extinction rates increase. We endorse the recommendations of Wheeler *et al.* (*52*) to improve taxonomic effort. They estimate US$0.5 to $1 billion per year would provide a tenfold increase in global taxonomic effort globally and result in the description of all species within 50 years.

The United Nations ended the 2011 Year of Biodiversity with a declaration that we are in the Decade of Biodiversity. As part of the convention and GTI, most countries have repeatedly agreed to cooperate to discover all biodiversity, and databases now provide metrics of progress and effort (e.g., species described, number of authors involved, and locations with data). This knowledge underpins assessments [e.g., International Union for Conservation of Nature and Natural Resources (IUCN) Red Lists] that produce increasingly accurate figures on what species exist on Earth, their distribution, and the threats to their survival.

Society should be concerned with the loss of biodiversity, in terms of habitats, species, and natural resources, just as it is with human health along with food and water supply and the quality of people's lives. All of these are interconnected. Overestimates of how many species may exist on Earth and the rates of extinction are self-defeating because they can make attempts to discover and conserve biodiversity appear hopeless. As we show here, they are also inaccurate, and more taxonomic resources will reap benefits in the discovery and conservation of life on Earth. Taxonomists are not in danger of extinction. They are increasing in numbers and will become more in demand as more species mean more diagnostic challenges to discriminate species, whether they are pests, pathogens, food, ecological keystone, or endangered species. We believe that with modestly increased effort in taxonomy and conservation, most species could be discovered and protected from extinction.

References and Notes

1. F. A. Bisby *et al.*, Eds., *Species 2000 & ITIS Catalogue of Life: 2010, Annual Checklist*, CD-ROM (Species 2000, Reading, UK, 2011).
2. W. Appeltans *et al.*, *Curr. Biol.* **22**, 2189 (2012).
3. A. R. Solow, L. A. Mound, K. J. Gaston, *Syst. Biol.* **44**, 93 (1995).
4. M. J. Costello *et al.*, *PLoS ONE*, **8**, e51629 (2013).
5. R. A. Andersen, *Biodivers. Conserv.* **1**, 267 (1992).
6. N. E. Stork, in *Biodiversity II*, M. L Reaka-Kudla, D. E. Wilson, E. O. Wilson, Eds. (Joseph Henry Press, Washington DC, 1997), pp. 41–68.
7. R. Govaerts, *Taxon* **52**, 583 (2003).
8. M. J. Costello, S. P. Wilson, B. Houlding, *Syst. Biol.* **61**, 871 (2012).
9. M. J. Costello, S. P. Wilson, *Glob. Ecol. Biogeogr.* **20**, 319 (2011).
10. C. Mora, D. P. Tittensor, S. Adl, A. G. B. Simpson, B. Worm, *PLoS Biol.* **9**, e1001127 (2011).
11. L. N. Joppa, D. L. Roberts, S. L. Pimm, *Proc. Biol. Sci.* **278**, 554 (2011).
12. A. J. Hamilton *et al.*, *Am. Nat.* **176**, 90 (2010).
13. A. J. Hamilton *et al.*, *Am. Nat.* **177**, 544 (2011).
14. House of Lords, Systematics and taxonomy: Follow-up. Science and Technology Committee, 5th Report of Session 2007-08 (The Stationery Office, London, 2008).
15. L. N. Joppa, D. L. Roberts, S. L. Pimm, *Trends Ecol. Evol.* **26**, 551 (2011).
16. F. Haas, C. L. Häuser, in *Success stories in implementation of the programmes of work on dry and sub-humid lands and the Global Taxonomy Initiative: Abstracts of poster presentations at the 11th meeting of the Subsidiary Body on Scientific, Technical and Technological Advice on the Convention on Biological Diversity, Montreal* (CBD Technical Series no. 21, 2005), pp. 87–89.
17. G. A. Boxshall, D. Self, UK taxonomy and systematics review—2010, Natural Environment Research Council; www.nerc.ac.uk/research/programmes/taxonomy/events/review.asp (accessed 20 November 2012) (2011).
18. M. J. Costello, P. Bouchet, C. S. Emblow, A. Legakis, *Mar. Ecol. Prog. Ser.* **316**, 257 (2006).
19. T. E. Lovejoy *et al.*, *Canadian Taxonomy: Exploring Biodiversity, Creating Opportunity* (Council of Canadian Academies, Ottawa, 2010).
20. M. R. de Carvalho *et al.*, *Science* **307**, 353b (2005).
21. K. J. Gaston, R. M. May, *Nature* **356**, 281 (1992).
22. Z.-Q. Zhang, in *Systema Naturae 250: The Linnaean Ark*, A. Polaszek, Ed. (CRC Press, Taylor & Francis Group, Boca Raton, FL, 2010), pp. 95–107.
23. N. E. Stork, *Biol. J. Linn. Soc. Lond.* **35**, 321 (1988).
24. M. J. Costello *et al.*, *PLoS ONE* **5**, e12110 (2010).
25. R. M. May, J. H. Lawton, N. E. Stork, in *Extinction Rates*, J. H. Lawton, R. M. May, Eds. (Oxford Univ. Press, Oxford, 1995), pp. 1–24.
26. H. M. Pereira *et al.*, *Science* **330**, 1496 (2010).
27. N. E. Stork, *Biodivers. Conserv.* **19**, 357 (2010).
28. M. Hoffmann *et al.*, *Science* **330**, 1503 (2010).
29. N. S. Sodhi, R. Butler, W. F. Laurance, L. Gibson, *Trends Ecol. Evol.* **26**, 585 (2011).
30. R. L. Chazdon *et al.*, *Conserv. Biol.* **23**, 1406 (2009).
31. D. Tilman, R. M. May, C. L. Lehman, M. A. Nowak, *Nature* **371**, 65 (1994).
32. L. Gibson *et al.*, *Nature* **478**, 378 (2011).
33. T. J. Davies *et al.*, *PLoS Biol.* **9**, e1000620 (2011).
34. J. E. M. Baillie *et al.*, *A Global Species Assessment* (IUCN, Gland, Switzerland, and Cambridge, UK, 2004).
35. B. W. Brook, N. S. Sodhi, C. J. A. Bradshaw, *Trends Ecol. Evol.* **23**, 453 (2008).
36. IUCN, *IUCN Red List of Threatened Species: Version 2011.2*; www.iucnredlist.org (accessed 28 November 2011).
37. R. T. Corlett, *Trends Ecol. Evol.* **26**, 606 (2011).
38. T. D. Dawson, S. T. Jackson, J. L. House, I. C. Prentice, G. M. Mace, *Science* **332**, 53 (2011).
39. W. W. L. Cheung *et al.*, *Fish Fish.* **10**, 235 (2009).
40. N. E. Stork *et al.*, *Conserv. Biol.* **23**, 1438 (2009).
41. Q. D. Wheeler, S. Pennak, *2011 State of Observed Species*, International Institute for Species Exploration; retrieved from http://species.asu.edu/SOS, 20 February 2012 (2012).
42. Secretariat to the Convention on Biological Diversity, "Guide to the Global Taxonomy Initiative," Convention on Biological Diversity Technical Series No. 30 (2010).
43. J. D. Thomas, in *Biodiversity II*, M. L. Reaka-Kudla, D. E. Wilson, E. O. Wilson, Eds. (Joseph Henry Press, Washington DC, 1997), pp. 357–369.
44. M. J. Benton, *When Life Nearly Died: The Greatest Mass Extinction of All Time* (Thames & Hudson Ltd., London, 2008).
45. C. S. Parr, R. Guralnick, N. Cellinese, R. D. M. Page, *Trends Ecol. Evol.* **27**, 94 (2012).
46. F. Boero, *Trends Ecol. Evol.* **16**, 266 (2001).
47. W. M. Hochachka *et al.*, *Trends Ecol. Evol.* **27**, 130 (2012).
48. B. Fontaine *et al.*, *PLoS ONE* **7**, e36881 (2012).
49. F. Boero, *Diversity* **2**, 115 (2010).
50. W. N. Eschmeyer, R. Fricke, J. D. Fong, D. Polack, *Zootaxa* **2525**, 19 (2010).
51. Z-Q. Zhang, *Zootaxa* **2768**, 1 (2011).
52. Q. D. Wheeler *et al.*, *Syst. Biodivers.* **10**, 1 (2012).
53. D. R. Maddison, R. Guralnick, A. Hill, A.-L. Reysenbach, L. A. McDade, *Trends Ecol. Evol.* **27**, 72 (2012).
54. S. Knapp, J. McNeill, N. J. Turland, *PhytoKeys* **6**, 5 (2011).
55. International Commission on Zoological Nomenclature, *Zootaxa* **3450**, 1 (2012).
56. P. Bouchet, P. Lozouet, P. Maestrati, V. Heros, *Biol. J. Linn. Soc. Lond.* **75**, 421 (2002).
57. N. E. Stork, *Biol. J. Linn. Soc. Lond.* **35**, 321 (1988).
58. V. Lohrmann, K. Vohland, M. Ohl, C. Häuser, Taxonomische Forschungin Deutschland: Eine Übersichtsstudie, Museum für Naturkunde, Berlin; http://biodiversity.de/images/stories/Downloads/taxo-studie-01-2012.pdf (accessed 20 November 2012) (2012).

Acknowledgments: We thank A. Hamilton (University of Melbourne), W. Appeltans (International Oceanographic Commission, United Nations Educational, Scientific, and Cultural Organization), B. Houlding and S. Wilson (Trinity College, Dublin), D. Costello, and V. Lohrmann (Museum für Naturkunde, Berlin) for helpful discussion.

10.1126/science.1230318

Proton Structure from the Measurement of 2S-2P Transition Frequencies of Muonic Hydrogen

Aldo Antognini,[1,2]* François Nez,[3] Karsten Schuhmann,[2,4] Fernando D. Amaro,[5] François Biraben,[3] João M. R. Cardoso,[5] Daniel S. Covita,[5,6] Andreas Dax,[7] Satish Dhawan,[7] Marc Diepold,[1] Luis M. P. Fernandes,[5] Adolf Giesen,[4,8] Andrea L. Gouvea,[5] Thomas Graf,[8] Theodor W. Hänsch,[1,9] Paul Indelicato,[3] Lucile Julien,[3] Cheng-Yang Kao,[10] Paul Knowles,[11] Franz Kottmann,[2] Eric-Olivier Le Bigot,[3] Yi-Wei Liu,[10] José A. M. Lopes,[5] Livia Ludhova,[11] Cristina M. B. Monteiro,[5] Françoise Mulhauser,[11] Tobias Nebel,[1] Paul Rabinowitz,[12] Joaquim M. F. dos Santos,[5] Lukas A. Schaller,[11] Catherine Schwob,[3] David Taqqu,[13] João F. C. A. Veloso,[6] Jan Vogelsang,[1] Randolf Pohl[1]

Accurate knowledge of the charge and Zemach radii of the proton is essential, not only for understanding its structure but also as input for tests of bound-state quantum electrodynamics and its predictions for the energy levels of hydrogen. These radii may be extracted from the laser spectroscopy of muonic hydrogen (μp, that is, a proton orbited by a muon). We measured the $2S_{1/2}^{F=0}$-$2P_{3/2}^{F=1}$ transition frequency in μp to be 54611.16(1.05) gigahertz (numbers in parentheses indicate one standard deviation of uncertainty) and reevaluated the $2S_{1/2}^{F=1}$-$2P_{3/2}^{F=2}$ transition frequency, yielding 49881.35(65) gigahertz. From the measurements, we determined the Zemach radius, r_Z = 1.082(37) femtometers, and the magnetic radius, r_M = 0.87(6) femtometer, of the proton. We also extracted the charge radius, r_E = 0.84087(39) femtometer, with an order of magnitude more precision than the 2010-CODATA value and at 7σ variance with respect to it, thus reinforcing the proton radius puzzle.

As the simplest of all stable atoms, hydrogen (H) is unique in its use for comparison between theory and experiment of bound-state energy level structures. Observation of the simple Balmer series in the H emission spectrum inspired the Bohr atomic model and quantum mechanics. More precise measurements of the first Balmer line revealed a splitting of the $n = 2$ states (n is the principal quantum number) arising from the electron's magnetic moment (spin-orbit interaction). Such data represented the crucial validation of the Dirac equation. However, further direct investigation of the hydrogen $2S_{1/2}$-$2P_{1/2}$ energy splitting (Lamb shift) and the 1S hyperfine splitting (HFS) in 1947 by means of microwave spectroscopy revealed a small deviation from the prediction of the Dirac equation. This fueled the development of quantum electrodynamics (QED). Precision measurements of H transition frequencies have been pursued in the past 40 years by laser spectroscopy. In spite of the considerable advances in both experimental (spectroscopy) and theoretical (bound-state QED) accuracy, the comparison between theory and experiment has been hampered by the lack of accurate knowledge of the proton charge and magnetization distributions. The proton structure is important because an electron in an S state has a nonzero probability to be inside the proton. The attractive force between the proton and the electron is thereby reduced because the electric field inside the charge distribution is smaller than the corresponding field produced by a point charge. Thus, the measured transition frequencies depend on the proton size.

Although the shifts of the energy levels associated with the proton finite size are small, it is the 1 to 2% relative uncertainty of the proton charge radius, r_E (*1*–*3*), and Zemach radius, r_Z (*4*, *5*), respectively, that presently limit the theoretical predictions of the Lamb shift and the HFS in H. The Zemach radius reflects the spatial distribution of magnetic moments smeared out (convoluted) by the charge distribution of the proton.

Historically, these radii were derived from measurements of the differential cross section in elastic electron-proton scattering. An independent and more precise determination of these radii can be achieved by laser spectroscopy of the exotic "muonic hydrogen" atom, μp (*6*). Such atoms are formed by a proton and a negative muon, μ^-, a particle whose mass, m_μ, is 207 times that of the electron, m_e. Its atomic energy levels are affected by the finite size of the proton charge distribution (neglecting higher moments of the charge distribution and higher orders in α) by

$$\Delta E_{\text{finite size}} = \frac{2\pi Z\alpha}{3} r_E^2 |\Psi(0)|^2 \qquad (1)$$

where $\Psi(0)$ is the atomic wave function at the origin, α the fine structure constant, and $Z = 1$ the proton charge. For S states, $|\Psi(0)|^2$ is proportional to m_r^3, with $m_r \approx 186 m_e$ being the reduced mass of the μp system. The muon Bohr radius is 186 times smaller than the electron Bohr radius in H, resulting in a strongly increased sensitivity of μp to the proton finite size.

We have recently performed the measurement of the $2S_{1/2}^{F=1}$-$2P_{3/2}^{F=2}$ transition (Fig. 1 C) in μp, which led to a determination of r_E with a relative accuracy $u_r = 8 \times 10^{-4}$ (*6*). Yet the r_E value obtained is seven standard deviations smaller than the world average (*7*) based on H spectroscopy and elastic electron scattering. This discrepancy has triggered a lively discussion addressing the accuracy of these experiments, bound-state QED, the proton structure, the Rydberg constant (R_∞), and possibilities of new physics.

Principle and measurements. The principle of the muonic hydrogen Lamb shift experiment is to form muonic hydrogen in the 2S state (Fig. 1A) and then measure the 2S-2P energy splitting (Fig. 1C) by means of laser spectroscopy (Fig. 1B) using the setup sketched in Fig. 2 (*6*).

Negative muons from the proton accelerator of the Paul Scherrer Institute, Switzerland, are stopped in H_2 gas at 1 hPa and 20°C, where highly excited μp atoms ($n \approx 14$) are formed. Most of these deexcite quickly to the 1S ground state (*8*), but ~1% populate the long-lived 2S state (Fig. 1A), whose lifetime is ~1 μs at 1 hPa (*9*). A 5-ns laser pulse with a wavelength tunable from 5.5 to 6 μm (*10*, *11*) illuminates the target gas volume, about 0.9 μs after the muon reached the target. On-resonance light induces 2S → 2P transitions, which are immediately followed by 2P → 1S deexcitation via 1.9-keV K_α x-ray emission (lifetime τ_{2P} = 8.5 ps). A resonance curve is obtained by measuring the number of 1.9-keV x-rays in time coincidence with the laser pulse (i.e., within a time window of 0.900 to 0.975 μs after the muon entry into the target) as a function of the laser wavelength. The 75-ns width of this window corresponds to the confinement time of the laser light within the multipass mirror cavity surrounding the gas target.

We have measured the two 2S-2P transitions depicted in Fig. 1C, one from the singlet state with frequency $\nu_s = \nu(2S_{1/2}^{F=0} - 2P_{3/2}^{F=1})$ and wavelength $\lambda_s \cong 5.5$ μm and the other from the triplet state with $\nu_t = \nu(2S_{1/2}^{F=1} - 2P_{3/2}^{F=2})$ and $\lambda_t \cong 6.0$ μm. For the latter, we present an updated analysis of the data presented in (*6*).

[1]Max-Planck-Institut für Quantenoptik, 85748 Garching, Germany. [2]Institute for Particle Physics, Eidgenössische Technische Hochschule (ETH) Zürich, 8093 Zürich, Switzerland. [3]Laboratoire Kastler Brossel, École Normale Supérieure, CNRS and Université Pierre et Marie Curie (UPMC), 75252 Paris, CEDEX 05, France. [4]Dausinger and Giesen GmbH, Rotebühlstraße 87, 70178 Stuttgart, Germany. [5]Departamento de Física, Universidade de Coimbra, 3004-516 Coimbra, Portugal. [6]I3N, Departamento de Física, Universidade de Aveiro, 3810-193 Aveiro, Portugal. [7]Physics Department, Yale University, New Haven, CT 06520–8121, USA. [8]Institut für Strahlwerkzeuge, Universität Stuttgart, 70569 Stuttgart, Germany. [9]Ludwig-Maximilians-Universität, Munich, Germany. [10]Physics Department, National Tsing Hua University, Hsinchu 300, Taiwan. [11]Département de Physique, Université de Fribourg, 1700 Fribourg, Switzerland. [12]Department of Chemistry, Princeton University, Princeton, NJ 08544–1009, USA. [13]Paul Scherrer Institute, 5232 Villigen-PSI, Switzerland.

*To whom correspondence should be addressed. E-mail: aldo@phys.ethz.ch

Figure 3 shows the two measured μp resonances. Details of the data analysis are given in (*12*). The laser frequency was changed every few hours, and we accumulated data for up to 13 hours per laser frequency. The laser frequency was calibrated [supplement in (*6*)] by using well-known water absorption lines. The resonance positions corrected for laser intensity effects using the line shape model (*12*) are

$$\nu_s = 54611.16(1.00)^{stat}(30)^{sys}\text{GHz} \quad (2)$$

$$\nu_t = 49881.35(57)^{stat}(30)^{sys}\text{GHz} \quad (3)$$

where "stat" and "sys" indicate statistical and systematic uncertainties, giving total experimental uncertainties of 1.05 and 0.65 GHz, respectively. Although extracted from the same data, the frequency value of the triplet resonance, ν_t, is slightly more accurate than in (*6*) owing to several improvements in the data analysis. The fitted line widths are 20.0(3.6) and 15.9(2.4) GHz, respectively, compatible with the expected 19.0 GHz resulting from the laser bandwidth (1.75 GHz at full width at half maximum) and the Doppler broadening (1 GHz) of the 18.6-GHz natural line width.

The systematic uncertainty of each measurement is 300 MHz, given by the frequency calibration uncertainty arising from pulse-to-pulse fluctuations in the laser and from broadening effects occurring in the Raman process. Other systematic corrections we have considered are the Zeeman shift in the 5-T field (<60 MHz), AC and DC Stark shifts (<1 MHz), Doppler shift (<1 MHz), pressure shift (<2 MHz), and black-body radiation shift (<<1 MHz). All these typically important atomic spectroscopy systematics are small because of the small size of μp.

The Lamb shift and the hyperfine splitting. From these two transition measurements, we can independently deduce both the Lamb shift ($\Delta E_L = \Delta E_{2P_{1/2}-2S_{1/2}}$) and the 2S-HFS splitting (ΔE_{HFS}) by the linear combinations (*13*)

$$\frac{1}{4}h\nu_s + \frac{3}{4}h\nu_t = \Delta E_L + 8.8123(2)\text{meV}$$

$$h\nu_s - h\nu_t = \Delta E_{HFS} - 3.2480(2)\text{meV} \quad (4)$$

Finite size effects are included in ΔE_L and ΔE_{HFS}. The numerical terms include the calculated values of the 2P fine structure, the $2P_{3/2}$ hyperfine splitting, and the mixing of the 2P states (*14*–*18*). The finite proton size effects on the 2P fine and hyperfine structure are smaller than 1×10^{-4} meV because of the small overlap between the 2P wave functions and the nucleus. Thus, their uncertainties arising from the proton structure are negligible. By using the measured transition frequencies ν_s and ν_t in Eqs. 4, we obtain (1 meV corresponds to 241.79893 GHz)

$$\Delta E_L^{exp} = 202.3706(23)\text{ meV} \quad (5)$$

$$\Delta E_{HFS}^{exp} = 22.8089(51)\text{ meV} \quad (6)$$

The uncertainties result from quadratically adding the statistical and systematic uncertainties of ν_s and ν_t.

The charge radius. The theory (*14*, *16*–*22*) relating the Lamb shift to r_E yields (*13*):

$$\Delta E_L^{th} = 206.0336(15) - 5.2275(10)r_E^2 + \Delta E_{TPE} \quad (7)$$

where E is in meV and r_E is the root mean square (RMS) charge radius given in fm and defined as $r_E^2 = \int d^3r\, r^2\, \rho_E(\boldsymbol{r})$ with ρ_E being the normalized proton charge distribution. The first term on the right side of Eq. 7 accounts for radiative, relativistic, and recoil effects. Fine and hyperfine corrections are absent here as a consequence of Eqs. 4. The other terms arise from the proton structure. The leading finite size effect $-5.2275(10)r_E^2$ meV is approximately given by Eq. 1 with corrections given in (*13*, *17*, *18*). Two-photon exchange (TPE) effects, including the proton polarizability, are covered by the term $\Delta E_{TPE} = 0.0332(20)$ meV (*19*, *24*–*26*). Issues related with TPE are discussed in (*12*, *13*).

The comparison of ΔE_L^{th} (Eq. 7) with ΔE_L^{exp} (Eq. 5) yields

$$r_E = 0.84087(26)^{exp}(29)^{th}\text{ fm} = 0.84087(39)\text{ fm} \quad (8)$$

This r_E value is compatible with our previous μp result (*6*), but 1.7 times more precise, and is now independent of the theoretical prediction of the 2S-HFS. Although an order of magnitude more precise, the μp-derived proton radius is at 7σ variance with the CODATA-2010 (*7*) value of $r_E = 0.8775(51)$ fm based on H spectroscopy and electron-proton scattering.

Magnetic and Zemach radii. The theoretical prediction (*17*, *18*, *27*–*29*) of the 2S-HFS is (*13*)

$$\Delta E_{HFS}^{th} = 22.9763(15) - 0.1621(10)r_Z + \Delta E_{HFS}^{pol} \quad (9)$$

where E is in meV and r_Z is in fm. The first term is the Fermi energy arising from the interaction between the muon and the proton magnetic moments, corrected for radiative and recoil contributions, and includes a small dependence of $-0.0022r_E^2$ meV = −0.0016 meV on the charge radius (*13*).

The leading proton structure term depends on r_Z, defined as

$$r_Z = \int d^3r \int d^3r' r' \rho_E(\boldsymbol{r})\rho_M(\mathbf{r} - \mathbf{r}') \quad (10)$$

with ρ_M being the normalized proton magnetic moment distribution. The HFS polariz-

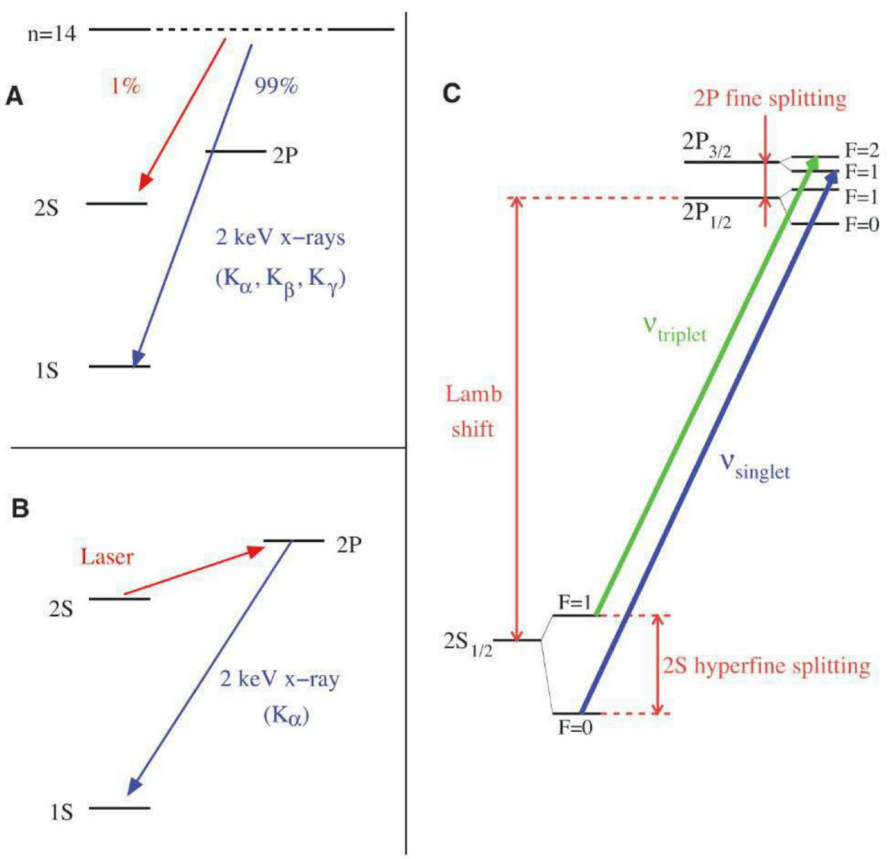

Fig. 1. **(A)** Formation of μp in highly excited states and subsequent cascade with emission of "prompt" $K_{\alpha,\beta,\gamma}$. **(B)** Laser excitation of the 2S-2P transition with subsequent decay to the ground state with K_α emission. **(C)** 2S and 2P energy levels. The measured transitions ν_s and ν_t are indicated together with the Lamb shift, 2S-HFS, and 2P-fine and hyperfine splitting.

ability contribution $\Delta E_{HFS}^{pol} = 0.0080(26)$ meV is evaluated by using measured polarized structure functions (*28*, *29*).

Comparison of ΔE_{HFS}^{th} (Eq. 9) with ΔE_{HFS}^{exp} (Eq. 6) yields

$$r_Z = 1.082(31)^{exp}(20)^{th}\ \text{fm} = 1.082(37)\ \text{fm} \quad (11)$$

This value has a relative accuracy of $u_r = 3.4\%$, limited by our measurements, and is compatible with both $r_Z = 1.086(12)$ fm (*4*) and $r_Z = 1.045(4)$ fm (*5*) from electron-proton scattering and $r_Z = 1.047(16)$ fm (*30*) and $r_Z = 1.037(16)$ fm (*31*) from H spectroscopy. The agreement between the muonic and the other r_Z values implies agreement between predicted and measured 2S-HFS.

By knowing r_Z and r_E, it is possible to extract the magnetic RMS radius when models for charge ρ_E and magnetization distributions ρ_M are assumed. Use of a dipole model for both, with the muonic values for r_E and r_Z, yields $r_M = 0.87(6)$ fm, in agreement with recent results from electron scattering $r_M = 0.803(17)$ fm (*1*, *32*), $r_M = 0.867(28)$ fm (*2*), and $r_M = 0.86(3)$ fm (*33*).

The proton-size puzzle. The origin of the large discrepancy between our r_E and the CODATA value is not yet known (*34*). The radius definitions used in H and μp spectroscopy and in scattering are consistent (*35*). Various studies have confirmed the theory of the μp Lamb shift and in particular the proton-structure contributions. The extracted r_E value changes by less than our quoted uncertainty for various models of the proton charge distribution (*36*).

Solving the proton radius puzzle by assuming a large tail for the proton charge distribution (*37*) is ruled out by electron-proton scattering data (*5*, *38*, *39*) and by chiral perturbation theory (*40*). The possibility that we performed spectroscopy on a three-body system such as a *pp*μ-molecule or a μ*pe*-ion instead of a "bare" μp atom (*41*) has been excluded by three-body calculations (*42*).

The ΔE_{TPE} between the muon and a proton with structure is evaluated by using the doubly virtual Compton amplitude, which, by means of dispersion relations, can be related to measured proton form factors and spin-averaged structure functions. Part of a subtraction term needed to remove a divergence in one Compton amplitude is usually approximated by using the one-photon on-shell form factor (*19*). A possible large uncertainty related with this approximation has been emphasized in (*26*, *43*), but this possibility has been strongly constrained by heavy-baryon chiral perturbation theory calculations (*25*).

R_∞ is necessary to extract r_E from the measured 1S-2S transition frequency in H (*44*). Hence, several new atomic physics experiments aim at an improved determination of R_∞, checking also for possible systematic shifts in previous R_∞ determinations in H.

Recent electron-proton scattering measurements yielded $r_E = 0.879(9)$ fm (*1*) and $r_E = 0.875(11)$ fm (*2*), in disagreement with our result. The extraction of r_E from elastic electron-proton scattering requires extrapolation of the measured electric form factor to zero momentum transfer, $Q^2 = 0$. This extrapolation has been investigated in detail (*45*). A global fit of proton and neutron form factors based on dispersion relations and the vector-dominance model gives $r_E = 0.84(1)$ fm (*33*), in agreement with our value, albeit with a larger χ^2 than the phenomenological fits (*1*).

The r_E value from μp could deviate from the values from electron-proton scattering and H spectroscopy if the muon-proton interaction differs from the electron-proton interaction. The window for such "new physics" is small given the multitude of low-energy experimental constraints coming from hydrogen, muonium, and μSi spectroscopy; electron and muon g-2 measurements; meson decays; neutron scattering; and searches for dark photons, etc. [(*46*) and references therein]. Nevertheless, models with new force carriers of MeV-mass have been proposed that could explain the r_E puzzle without conflicting with other experimental observations (*46*, *47*).

Conclusions. We have presented a measurement of the $2S_{1/2}^{F=0}$-$2P_{3/2}^{F=1}$ transition in μp and a reanalysis of the $2S_{1/2}^{F=1}$-$2P_{3/2}^{F=2}$ transition (*6*). Summing and subtracting these two measurements leads to an independent assessment of the 2S-HFS

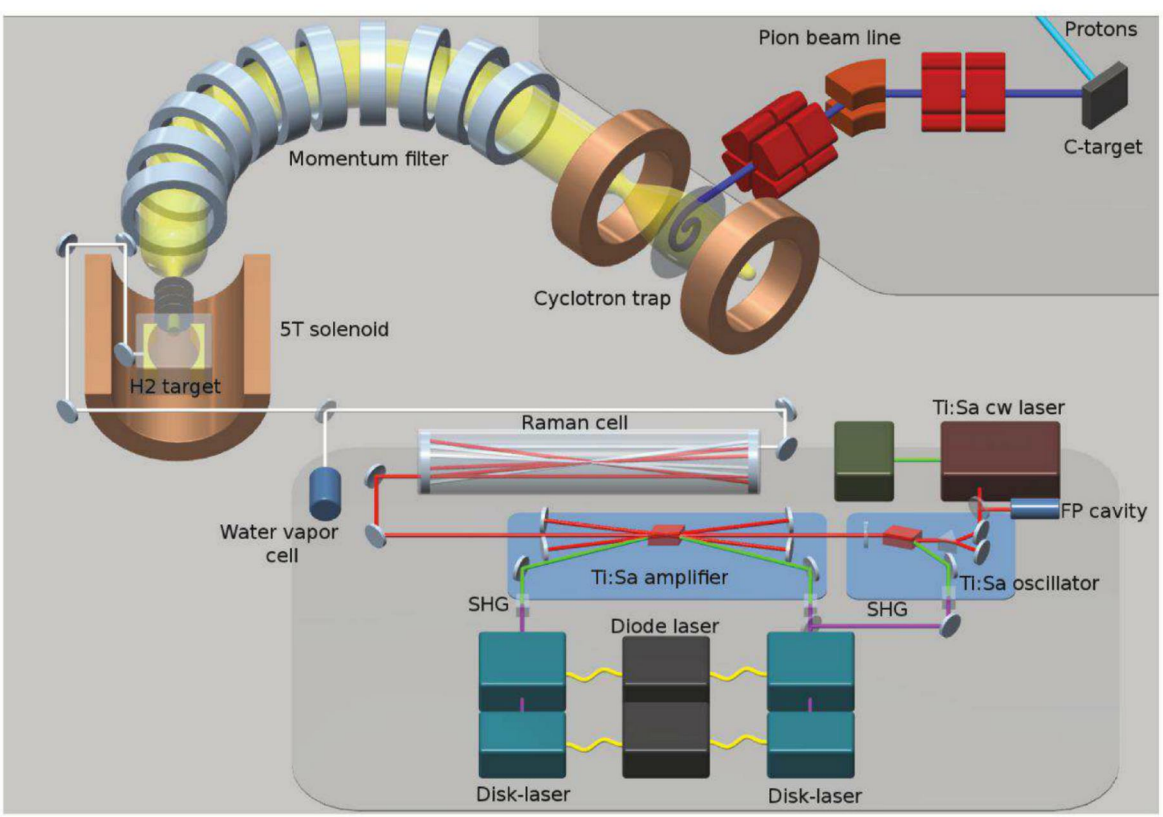

Fig. 2. Experimental apparatus. Accelerator-created negative pions are transported to the cyclotron trap. Here they decay into MeV-energy muons, which are decelerated by a thin foil placed at the trap center. The resulting keV-energy muons leave the trap and follow a toroidal magnetic field of 0.15 T (acting as a momentum filter) before entering a 5-T solenoid where the hydrogen target is placed. A muon entrance detector provides a signal that triggers the laser system. About 0.9 μs later, the formed μp is irradiated by the laser pulse to induce the 2S-2P transition. Such a short delay is achieved by the continuous 1.5-kW pumping of two Q-switched disk lasers operating in prelasing mode (*8*). The disk-laser pulses are frequency doubled [second harmonic generation (SHG)] and used to pump a Ti:Sa laser. The Ti:Sa oscillator is seeded by a stabilized continuous-wave Ti:Sa laser, and the emitted red pulses of ~700-nm wavelength and 5-ns length are well suited for efficient Raman conversion to 5.5 - 6 μm via three Stokes shifts in hydrogen gas at 15 bar (*9*). These pulses are then injected into a multipass cavity surrounding the hydrogen gas target. Absolute calibration from 5.5 to 6 μm was performed by water vapor spectroscopy.

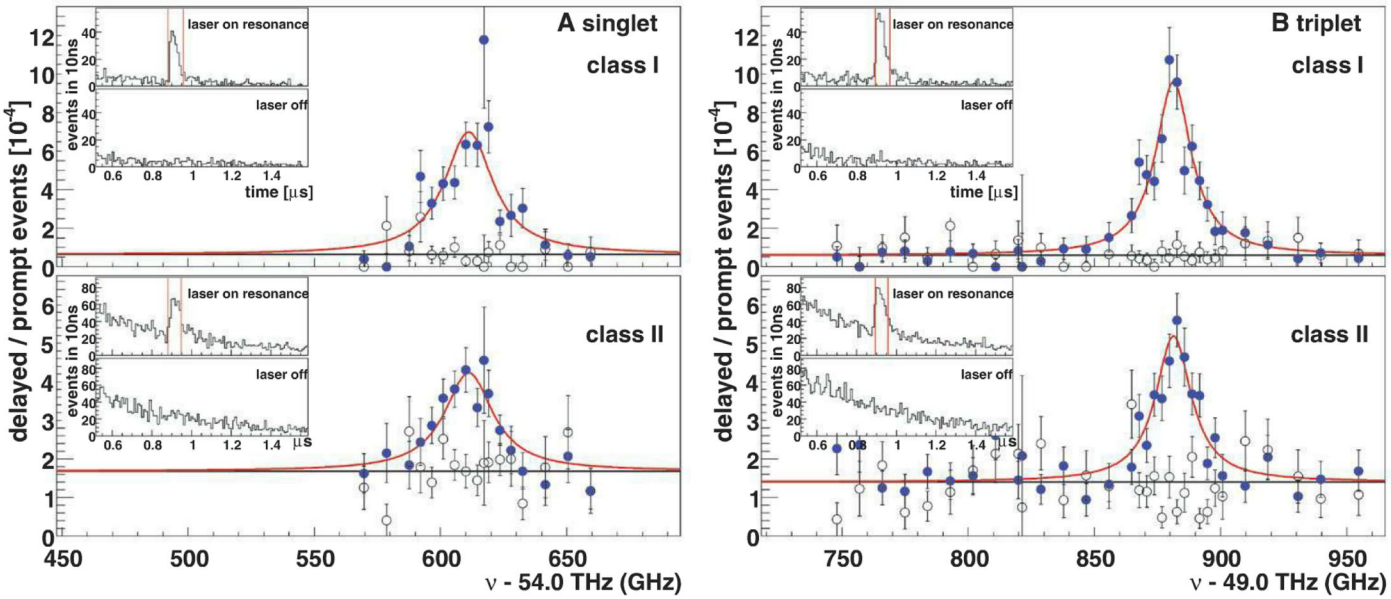

Fig. 3. Muonic hydrogen resonances (solid circles) for singlet ν_s (**A**) and triplet ν_t (**B**) transitions. Open circles show data recorded without laser pulses. Two resonance curves are given for each transition to account for two different classes, I and II, of muon decay electrons (*12*). Error bars indicate the standard error. (Insets) The time spectra of K_α x-rays. The vertical lines indicate the laser time window.

and the "pure" 2S-2P Lamb shift. By comparison with theoretical predictions, two proton-structure parameters are determined: $r_E = 0.84087(39)$ fm and $r_Z = 1.082(37)$ fm. These radii play a crucial role in the understanding of the atomic hydrogen spectrum (bound-state QED). They also provide information needed to test quantum chromodynamics in the nonperturbative region.

Subtracting the H(1S) and H(2S) Lamb shifts, computed by using the muonic r_E, from the measured 1S−2S transition frequency in H gives $R_\infty = 3.2898419602495(10)(25) \times 10^{15}$ Hz/c. The first uncertainty of 1.0 kHz/c and the second of 2.5 kHz/c originate from the uncertainties of the muonic r_E and QED theory in H, respectively. This R_∞ deviates by −115 kHz/c, corresponding to 6.6 standard deviations, from the CODATA (*7*) value but is six times more precise (relative accuracy of $u_r = 8 \times 10^{-13}$).

Our value of the proton charge radius $r_E(p)$ can be used to determine a new deuteron charge radius, $r_E(d)$, by using the accurately measured isotope shift of the 1S-2S transition in H and D (*48*). From equation 4 of (*48*)

$$r_E^2(d) - r_E^2(\mathrm{p}) = 3.82007(65)\ \mathrm{fm}^2 \quad (12)$$

we obtain a precise value of the deuteron RMS charge radius

$$r_E(d) = 2.12771(22)\ \mathrm{fm} \quad (13)$$

in agreement with $r_E(d) = 2.130(10)$ fm (*49*) from electron-deuteron scattering but more than an order of magnitude more precise. The CODATA (*7*) value $r_E(d) = 2.1424(25)$ fm is in disagreement, because it is dominantly based on the 7σ discrepant $r_E(p)$ value of CODATA combined with Eq. 12. The Lamb shift in muonic deuterium μd can provide an independent $r_E(d)$ value.

References and Notes

1. J. C. Bernauer *et al.*, *Phys. Rev. Lett.* **105**, 242001 (2010).
2. X. Zhan *et al.*, *Phys. Lett. B* **705**, 59 (2011).
3. P. G. Blunden, I. Sick, *Phys. Rev. C Nucl. Phys.* **72**, 057601 (2005).
4. J. Friar, I. Sick, *Phys. Lett. B* **579**, 285 (2004).
5. M. O. Distler, J. C. Bernauer, T. Walcher, *Phys. Lett. B* **696**, 343 (2011).
6. R. Pohl *et al.*, *Nature* **466**, 213 (2010).
7. P. J. Mohr, B. N. Taylor, D. B. Newell, *Rev. Mod. Phys.* **84**, 1527 (2012).
8. R. Pohl, *Hyperfine Interact.* **193**, 115 (2009).
9. R. Pohl *et al.*, *Phys. Rev. Lett.* **97**, 193402 (2006).
10. A. Antognini *et al.*, *IEEE J. Quantum Electron.* **45**, 993 (2009).
11. A. Antognini *et al.*, *Opt. Commun.* **253**, 362 (2005).
12. Materials and methods are available as supplementary materials on *Science* Online.
13. A. Antognini *et al.*, *Ann. Phys.*, published online 31 December 2012 (10.1016/j.aop.2012.12.003).
14. K. Pachucki, *Phys. Rev. A* **53**, 2092 (1996).
15. A. P. Martynenko, *Phys. Atomic Nuclei* **71**, 125 (2008).
16. U. D. Jentschura, *Ann. Phys.* **326**, 500 (2011).
17. E. Borie, *Ann. Phys.* **327**, 733 (2012).
18. E. Borie, http://arxiv.org/abs/1103.1772v6 (2012).
19. K. Pachucki, *Phys. Rev. A* **60**, 3593 (1999).
20. M. I. Eides, H. Grotch, V. A. Shelyuto, *Phys. Rep.* **342**, 63 (2001).
21. S. G. Karshenboim, E. Y. Korzinin, V. G. Ivanov, V. A. Shelyuto, *JETP Lett.* **92**, 8 (2010).
22. S. G. Karshenboim, V. G. Ivanov, E. Y. Korzinin, *Phys. Rev. A* **85**, 032509 (2012).
23. U. D. Jentschura, *Phys. Rev. A* **84**, 012505 (2011).
24. C. E. Carlson, M. Vanderhaeghen, *Phys. Rev. A* **84**, 020102 (2011).
25. M. C. Birse, J. A. McGovern, *Eur. Phys. J. A* **48**, 120 (2012).
26. R. J. Hill, G. Paz, *Phys. Rev. Lett.* **107**, 160402 (2011).
27. A. P. Martynenko, *Phys. Rev. A* **71**, 022506 (2005).
28. C. E. Carlson, V. Nazaryan, K. Griffioen, *Phys. Rev. A* **83**, 042509 (2011).
29. E. Cherednikova, R. Faustov, A. Martynenko, *Nucl. Phys. A.* **703**, 365 (2002).
30. A. V. Volotka, V. M. Shabaev, G. Plunien, G. Soff, *Eur. Phys. J. D* **33**, 23 (2005).
31. A. Dupays, A. Beswick, B. Lepetit, C. Rizzo, D. Bakalov, *Phys. Rev. A* **68**, 052503 (2003).
32. J. C. Bernauer *et al.*, *Phys. Rev. Lett.* **107**, 119102 (2011).
33. I. T. Lorenz, H.-W. Hammer, U. Meißner, *Eur. Phys. J. A* **48**, 151 (2012).
34. R. Pohl, R. Gilman, G. A. Miller, K. Pachucki, http://arxiv.org/abs/1301.0905 (2013).
35. U. D. Jentschura, *Eur. Phys. J. D* **61**, 7 (2011).
36. J. D. Carroll, A. W. Thomas, J. Rafelski, G. A. Miller, http://arxiv.org/abs/1108.2541v1 (2011).
37. A. De Rújula, *Phys. Lett. B* **697**, 26 (2011).
38. J. L. Friar, I. Sick, *Phys. Rev. A* **72**, 040502 (2005).
39. I. C. Cloët, G. A. Miller, *Phys. Rev. C Nucl. Phys.* **83**, 012201(R) (2011).
40. A. Pineda, *Phys. Rev. C Nucl. Phys.* **71**, 065205 (2005).
41. U. D. Jentschura, *Ann. Phys.* **326**, 516 (2011).
42. J.-P. Karr, L. Hilico, *Phys. Rev. Lett.* **109**, 103401 (2012).
43. G. A. Miller, A. W. Thomas, J. D. Carroll, J. Rafelski, *Phys. Rev. A* **84**, 020101(R) (2011).
44. C. G. Parthey *et al.*, *Phys. Rev. Lett.* **107**, 203001 (2011).
45. R. J. Hill, G. Paz, *Phys. Rev. D* **82**, 113005 (2010).
46. C. E. Carlson, B. C. Rislow, *Phys. Rev. D* **86**, 035013 (2012).
47. B. Batell, D. McKeen, M. Pospelov, *Phys. Rev. Lett.* **107**, 011803 (2011).
48. C. G. Parthey *et al.*, *Phys. Rev. Lett.* **104**, 233001 (2010).
49. I. Sick, D. Trautmann, *Nucl. Phys. A.* **637**, 559 (1998).

Acknowledgments: We thank L. M. Simons, B. Leoni, H. Brückner, K. Linner, W. Simon, J. Alpstäg, Z. Hochman, N. Schlumpf, U. Hartmann, S. Ritt, M. Gaspar, M. Horisberger, B. Weichelt, J. Früchtenicht, A. Voss, M. Larionov, F. Dausinger, and K. Kirch for their contributions. We acknowledge support from the Max Planck Society and the Max Planck Foundation, the Swiss National Science Foundation (projects 200020-100632 and 200021L-138175/1), the Swiss Academy of Engineering Sciences, the Bonus Qualité Recherche de l'Unités de Formations et de Recherche de physique fondamentale et appliquée de l'UPMC, the program PAI Germaine de Staël no. 07819NH du ministère des affaires étrangères France, the Ecole Normale Supérieure (ENS), UPMC, CNRS, and the Fundação para a Ciência e a Tecnologia (FCT, Portugal) and Fundo Europeu De Desenvolvimento Regional (project PTDC/FIS/102110/2008 and grant SFRH/BPD/46611/2008). P.I. acknowledges support by the ExtreMe Matter Institute, Helmholtz Alliance HA216/EMMI. T.N. and R.P. were in part supported by the European Research Council (ERC) Starting Grant no. 279765. A.L.G. received support from FCT through program grant SFRH/BD/66731/2009.

Supplementary Materials

www.sciencemag.org/cgi/content/full/339/6118/417/DC1
Materials and Methods
Supplementary Text
References

11 September 2012; accepted 30 November 2012
10.1126/science.1230016

Reconstitution of the Vital Functions of Munc18 and Munc13 in Neurotransmitter Release

Cong Ma,[1,2,3,4]*† Lijing Su,[2,3,4]* Alpay B. Seven,[2,3,4] Yibin Xu,[2,3,4] Josep Rizo[2,3,4]†

Neurotransmitter release depends critically on Munc18-1, Munc13, the Ca^{2+} sensor synaptotagmin-1, and the soluble *N*-ethylmaleimide–sensitive factor (NSF) attachment protein (SNAP) receptors (SNAREs) syntaxin-1, synaptobrevin, and SNAP-25. In vitro reconstitutions have shown that syntaxin-1–SNAP-25 liposomes fuse efficiently with synaptobrevin liposomes in the presence of synaptotagmin-1–Ca^{2+}, but neurotransmitter release also requires Munc18-1 and Munc13 in vivo. We found that Munc18-1 could displace SNAP-25 from syntaxin-1 and that fusion of syntaxin-1–Munc18-1 liposomes with synaptobrevin liposomes required Munc13, in addition to SNAP-25 and synaptotagmin-1-Ca^{2+}. Moreover, when starting with syntaxin-1–SNAP-25 liposomes, NSF–α-SNAP disassembled the syntaxin-1–SNAP-25 heterodimers and abrogated fusion, which then required Munc18-1 and Munc13. We propose that fusion does not proceed through syntaxin-1–SNAP-25 heterodimers but starts with the syntaxin-1–Munc18-1 complex; Munc18-1 and Munc13 then orchestrate membrane fusion together with the SNAREs and synaptotagmin-1-Ca^{2+} in an NSF- and SNAP-resistant manner.

Neurotransmitter release by Ca^{2+}-triggered synaptic vesicle fusion is crucial for neural function. Key components of the release machinery include (*1*, *2*) (i) the SNAP receptor (SNARE) proteins synaptobrevin, syntaxin-1, and SNAP-25, which form a tight four-helix bundle called the SNARE complex (*3*) that brings the vesicle and plasma membranes together and is key for membrane fusion (*4*–*6*); (ii) *N*-ethylmaleimide sensitive factor (NSF) and soluble NSF adaptor proteins (SNAPs), which disassemble the SNARE complex (*3*) to recycle the SNAREs for another round of fusion (*7*); (iii) the Sec1-Munc18 (SM) protein Munc18-1, which binds to a self-inhibited "closed" conformation of syntaxin-1 (*8*, *9*) and to SNARE complexes (*10*, *11*); (iv) Munc13, which contains a large MUN domain that is critical for release (*12*) and catalyzes opening of syntaxin-1 (*13*); and (v) the Ca^{2+} sensor synaptotagmin-1 (*14*). Despite important advances, a coherent model that integrates the functions of these eight central proteins has not emerged, and it is unclear why neurotransmitter release is totally abrogated in the absence of Munc18-1 and Munc13 (*15*–*17*). Munc18-1 is part of the conserved core fusion machinery (*1*, *2*), and the Munc13 MUN domain is also likely to have a universal function in fusion (*18*, *19*). However, reconstitutions of synaptic vesicle fusion have not explained the functional importance of Munc18-1 and Munc13. The ability of the neuronal SNAREs to induce lipid mixing between liposomes (*20*) can be enhanced by Munc18-1 (*11*), but without requiring Munc13. Similarly, Munc13-4 can enhance lipid mixing by the SNAREs (*21*) in the absence of Munc18-1. Moreover, these studies did not include synaptotagmin-1, which induces efficient fusion of liposomes containing syntaxin-1–SNAP-25 heterodimers with synaptobrevin liposomes in the absence of Munc18-1 and Munc13 (*22*–*26*), despite the essential nature of Munc18-1 and Munc13 for release in vivo.

To resolve this gap between the reconstitution results and the physiological data, we performed reconstitution experiments that included the eight key components of the release machinery and were able to reproduce the functional requirement for Munc18-1 and Munc13.

[1]Key Laboratory of Molecular Biophysics, Ministry of Education, and Institute of Biophysics and Biochemistry, Huazhong University of Science and Technology, Wuhan 430074, China. [2]Department of Biophysics, University of Texas Southwestern Medical Center, 6000 Harry Hines Boulevard, Dallas, TX 75390, USA. [3]Department of Biochemistry, University of Texas Southwestern Medical Center, 6000 Harry Hines Boulevard, Dallas, TX 75390, USA. [4]Department of Pharmacology, University of Texas Southwestern Medical Center, 6000 Harry Hines Boulevard, Dallas, TX 75390, USA.

*These authors contributed equally to this work.
†To whom correspondence should be addressed. E-mail: cong.ma7@gmail.com (C.M.); jose@arnie.swmed.edu (J.R.)

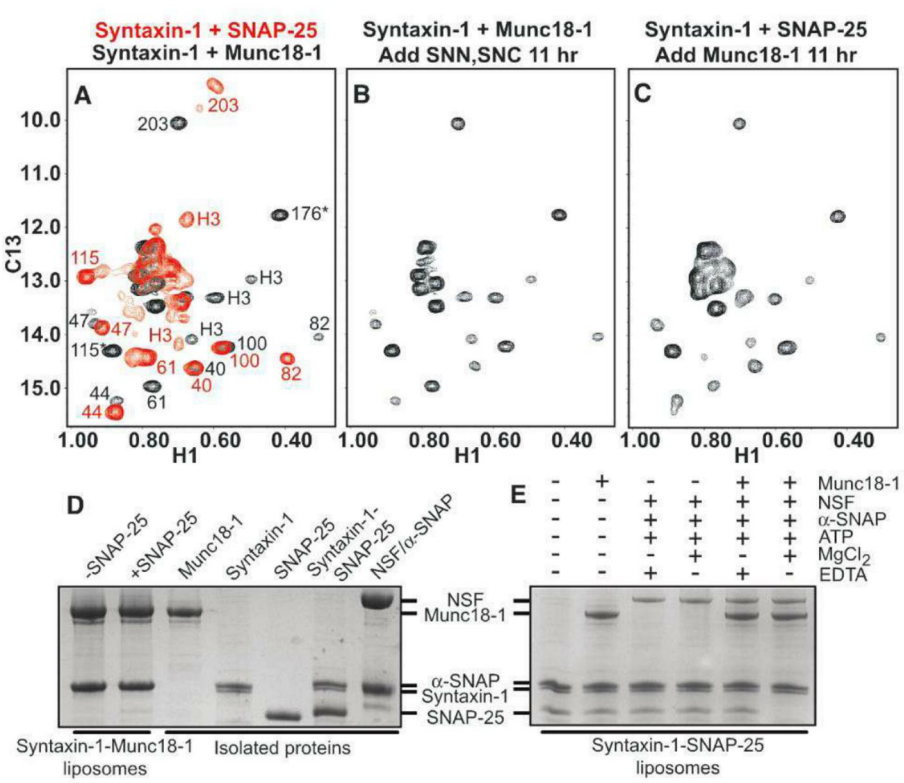

Fig. 1. Munc18-1 displaces SNAP-25 from syntaxin-1. (**A** to **C**) ^{1}H-^{13}C HMQC spectra of ^{2}H-Ile-$^{13}CH_3$–syntaxin-1 (A) bound to Munc18-1 (black) or to SNAP-25 (red); (B) initially bound to Munc18-1 and then incubated with the SNAP-25 SNARE motifs (SNN and SNC) for 11 hours; and (C) initially bound to SNAP-25 and then incubated with Munc18-1 for 11 hours. In (A), the available cross-peak assignments for the syntaxin-1–Munc18-1 complex are indicated in black and those for the syntaxin-1-SNAP-25 complex in red [(*13*) for assignments; H3 identifies the SNARE motif; asterisk indicates tentative assignments]. Because of the 2:1 stoichiometry of the syntaxin-1–SNAP-25 complex, the cross-peak of I203 is double. (**D**) Proteoliposomes containing coexpressed syntaxin-1–Munc18-1 complex were incubated with SNAP-25 or buffer, cofloatation assays were performed, and the top fraction was analyzed by means of SDS–polyacrylamide gel electrophoresis (SDS-PAGE) and Coomassie Blue staining (left two lanes). (**E**) Proteoliposomes containing syntaxin-1 were incubated with Munc18-1, SNAP-25, NSF, α-SNAP, ATP, Mg^{2+}, and/or EDTA as indicated. Cofloatation assays were then performed, and the results analyzed by means of SDS-PAGE and Coomassie Blue staining. The five lanes on the right of (D) show loading controls with soluble proteins.

Munc18-1 displaces SNAP-25 from syntaxin-1. Most attempts to reconstitute synaptic fusion have used liposomes containing syntaxin-1–SNAP-25 heterodimers, assuming that these heterodimers constitute obligatory intermediates and serve as acceptors for synaptobrevin. The syntaxin-1–Munc18-1 complex is commonly assumed to form upstream. To test whether syntaxin-1–SNAP-25 heterodimers can form when starting with the syntaxin-1–Munc18-1 complex, we used ^{1}H-^{13}C heteronuclear multiple quantum coherence (HMQC) nuclear magnetic resonance (NMR) spectra of the syntaxin-1 cytoplasmic region specifically ^{1}H,^{13}C–labeled at Ile methyl groups (^{2}H-Ile-$^{13}CH_3$–syntaxin-1) (Fig. 1A), which allow distinguishing different complexes of syntaxin-1 (*13*). The HMQC spectrum of the ^{2}H-Ile-$^{13}CH_3$–syntaxin-1–Munc18-1 complex was not altered by addition of the SNARE motifs of SNAP-25 (Fig. 1B) even in the presence of the Munc13-1 MUN domain (fig. S1A), which facilitates the transition from the syntaxin-1–Munc18-1 complex to the SNARE complex (*13*). Conversely, incubation of the ^{2}H-Ile-$^{13}CH_3$–syntaxin-1–SNAP-25 complex with Munc18-1 led to the HMQC spectrum characteristic of the ^{2}H-Ile-$^{13}CH_3$–syntaxin-1–Munc18-1 complex (Fig. 1C). Thus, SNAP-25 cannot open the conformation of syntaxin-1 bound to Munc18-1 without synaptobrevin, and Munc18-1 displaces SNAP-25 from syntaxin-1 in solution. The MUN domain accelerated this displacement (fig. S1B), showing that Munc13-1 catalyzes not only the opening (*13*) but also the closing of syntaxin-1.

To analyze the interplay between Munc18-1 and SNAP-25 using full-length syntaxin-1 in a membrane environment, we performed cofloatation assays with liposomes containing coexpressed syntaxin-1–Munc18-1 complex (*27*), which revealed that SNAP-25 does not displace Munc18-1 from membrane-anchored syntaxin-1 (Fig. 1D). In assays with liposomes containing only syntaxin-1, we observed cofloatation of SNAP-25, revealing efficient binding to syntaxin-1 (Fig. 1E and fig. S2). Munc18-1 addition led to cofloatation with the proteoliposomes and only a small decrease in bound SNAP-25 (Fig. 1E), suggesting that most Munc18-1 bound to the syntaxin-1 N-terminal region of the syntaxin-1–SNAP-25 heterodimers (*10*, *11*) without displacing SNAP-25. However, such displacement might have been hindered by the tendency of aggregation of syntaxin-1–SNAP-25 heterodimers, as suggested by gel filtration in detergent (fig. S3). Because NSF–α-SNAP disassemble reconstituted syntaxin-

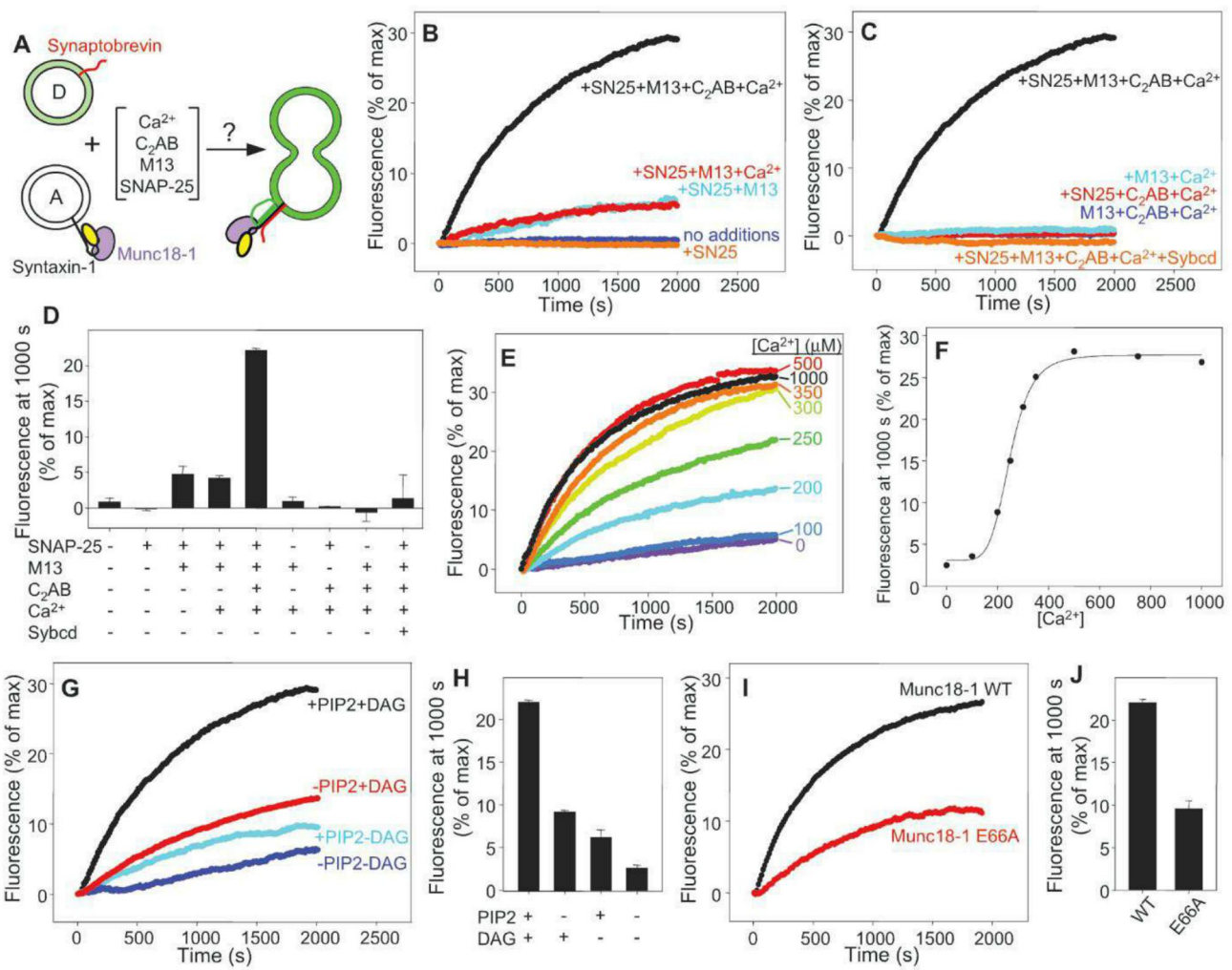

Fig. 2. Requirement of Munc13 for lipid mixing of syntaxin-1–Munc18-1 liposomes with synaptobrevin liposomes. (**A**) Diagram summarizing the lipid mixing experiments, which were performed with acceptor liposomes containing syntaxin-1–Munc18-1 and donor liposomes containing synaptobrevin and NBD-lipids quenched by rhodamine-lipids. (**B** and **C**) Traces showing the lipid mixing observed in the presence of SNAP-25, Munc13-1 C1C2BMUN (M13), synaptotagmin-1 C_2AB fragment (C_2AB), synaptobrevin cytoplasmic domain (Sybcd), and/or 0.5 mM Ca^{2+} in various combinations. The *y* axis represents NBD fluorescence normalized to the maximum fluorescence observed upon detergent addition. (**D**) Quantification of the results obtained in the experiments of (B) and (C). (**E**) Lipid mixing observed in the presence of SNAP-25, C1C2BMUN, and C_2AB fragment as a function of Ca^{2+} concentration. (**F**) Plot of the normalized NBD fluorescence intensity at 1000 s as a function of Ca^{2+} observed in (E). (**G** and **H**) Dependence of lipid mixing on the presence of DAG and/or PIP2 in the acceptor syntaxin-1–Munc18-1 liposomes (G), and quantification of the results (H). (**I** and **J**) Lipid mixing obtained with acceptor liposomes that contained syntaxin-1 bound to wild-type (WT) or E66A mutant Munc18-1 (I) and quantification of the results (J). In (D), (H), and (J), bars represent averages of the normalized NBD fluorescence observed after 1000 s in repeated experiments performed under the same conditions. Error bars represent SDs.

1–SNAP-25 heterodimers (*28*), we tested their effect in the cofloatation assays. Addition of Munc18-1, NSF–α-SNAP, and Mg^{2+}–adenosine 5′-triphosphate (ATP) completely released SNAP-25 from the proteoliposomes, whereas Munc18-1 remained bound, but such release was not observed in the presence of ethylenediaminetetraacetic acid (EDTA) and/or absence of Munc18-1 (Fig. 1E). Thus, disassembly of the syntaxin-1–SNAP-25 heterodimers by NSF–α-SNAP, which requires ATP hydrolysis, allows Munc18-1 to "capture" the syntaxin-1 closed conformation, thus preventing rebinding of SNAP-25 to syntaxin-1.

Reconstitution of Munc18-1– and Munc13-dependent membrane fusion. The above results suggest that the syntaxin-1–Munc18-1 complex is the true starting point for neurotransmitter release, which would explain the critical importance of Munc13 because it mediates syntaxin-1 opening (*13*). To test this notion, we reconstituted syntaxin-1–Munc18-1 complex and synaptobrevin into separate liposome populations and analyzed lipid mixing between them using a 7-nitrobenz-2-oxa-1,3-diazole (NBD) fluorescence dequenching assay (Fig. 2A) (*20*). The fluorescence intensity after 1000 s was used to quantify the results as a compromise measurement that reflects the initial slope and the level of completion of the reaction. To test the effects of synaptotagmin-1 and Munc13, we used a synaptotagmin-1 fragment that contains its C_2 domains (C_2AB fragment) and has been widely used in reconstitution assays (*22*, *24*), and a Munc13-1 fragment that contains its C_1, C_2B, and MUN domains (C1C2BMUN). This fragment was more stable than the MUN domain in the presence of reconstituted proteoliposomes, and inclusion of the C_1 and C_2B domains enabled binding to diacylglycerol (DAG) and phosphatidylinositol-4,5-bisphosphate (PIP2) (fig. S4).

No lipid mixing between synaptobrevin-liposomes and syntaxin-1–Munc18-1 liposomes was observed even after adding SNAP-25, but addition of SNAP-25 and C1C2BMUN yielded some lipid mixing that was increased by the C_2AB fragment in the presence of Ca^{2+} (Fig. 2, B and D). No lipid mixing occurred in the absence of SNAP-25 or C1C2BMUN, and the synaptobrevin cytoplasmic domain inhibited the reaction, demonstrating that lipid mixing was SNARE-dependent and strictly required the Munc13-1 C1C2BMUN fragment (Fig. 2, C and D). The efficiency of lipid mixing had a high cooperativity with Ca^{2+} (Fig. 2, E and F), with a Hill coefficient of 5.9 that resembles values observed in vivo [4 to 5 (*29*)]. Half-maximal efficiency occurred at 250 μM Ca^{2+} (Fig. 2, E and F). For comparison, neurotransmitter release requires 10 to 25 μM Ca^{2+} in the calyx of Held, but higher Ca^{2+} requirements (75 to 300 μM) have been reported for other systems (*29*), and the efficiency of lipid mixing in our reconstitutions is probably limited by a lack of a defined docking mechanism. Lipid mixing was decreased by removal of DAG and PIP2, agents that stimulate release via the Munc13 C_1 and C_2B domains (*30*, *31*), and the decrease was accentuated when both DAG and PIP2 were absent (Fig. 2, G and H, and fig. S4D), suggesting that these lipids play a synergistic role in attracting C1C2BMUN to the membrane and enhancing MUN-domain activity. To establish an additional correlation with physiological data, we tested the effects of a mutation in Munc18-1 (E66A) that decreases neurotransmitter release in neurons by about 50% (*32*). In the mutant, one amino acid was substituted at a certain location; thus, E66A indicates that glutamic acid at position 66 was replaced by alanine. Single-letter abbreviations for the amino acid residues are as follows: A, Ala; C, Cys; D, Asp; E, Glu; F, Phe; G, Gly; H, His; I, Ile; K, Lys; L, Leu; M, Met; N, Asn; P, Pro; Q, Gln; R, Arg; S, Ser; T, Thr; V, Val; W, Trp; and Y, Tyr. Reassuringly, this mutation led to a comparable decrease in lipid mixing (Fig. 2, I and J, and fig. S4D).

To ensure that the observed lipid mixing reflected full fusion, we analyzed content mixing by adapting a method based on sulforhodamine dequenching that allows simultaneous monitoring of lipid mixing from dequenching of DiD lipids (*26*) and optimized liposome preparation for minimal leakiness (fig. S5). When we mixed

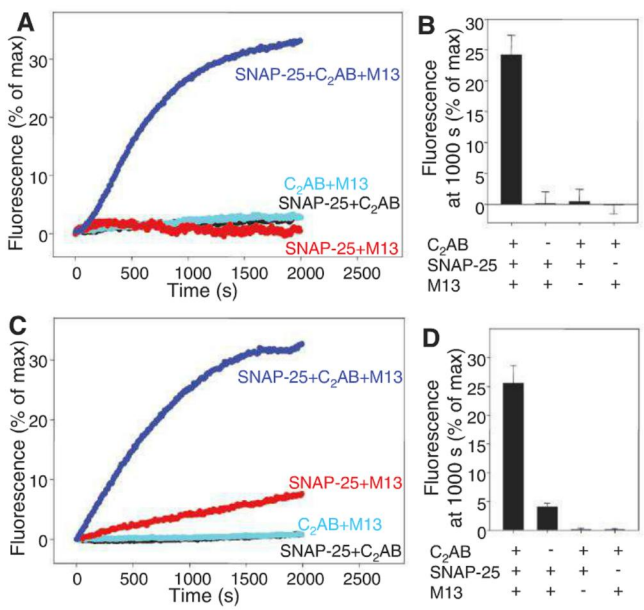

Fig. 3. Content mixing assays with syntaxin-1–Munc18-1 liposomes and synaptobrevin-liposomes. (**A**) Traces showing the content mixing between syntaxin-1–Munc18-1acceptor liposomes and synaptobrevin donor liposomes in the presence of SNAP-25, Munc13-1 C1C2BMUN (M13), and/or synaptotagmin-1 C_2AB fragment (C_2AB) (all in 0.5 mM Ca^{2+}). The donor liposomes contained encapsulated self-quenched sulforhodamine and self-quenched DiD lipids. The *y* axis represents sulforhodamine fluorescence normalized to the maximum fluorescence observed upon detergent addition. (**B**) Quantification of the results obtained in the experiments of (A). (**C** and **D**) Traces showing the lipid mixing observed from DiD fluorescence dequenching in the same experiments (C) and quantification of the results (D). Error bars represent SDs.

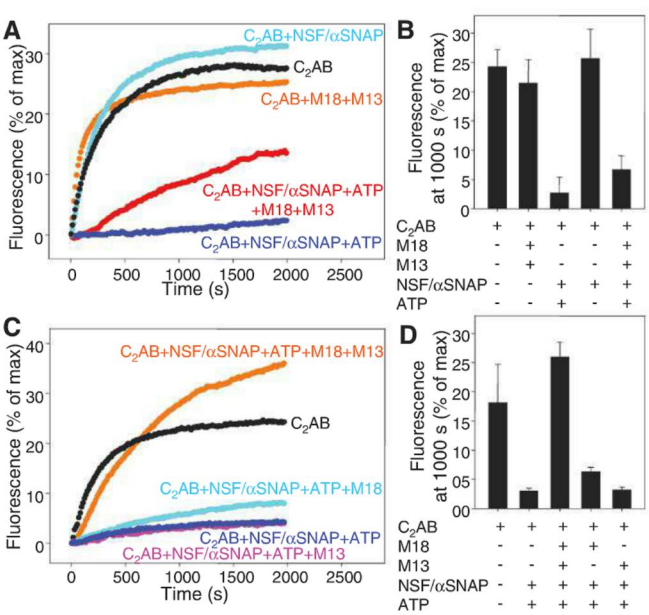

Fig. 4. NSF–α-SNAPs inhibit lipid mixing between syntaxin-1–SNAP-25 liposomes and synaptobrevin-liposomes, and Munc18-1–Munc13-1 activate lipid mixing. (**A**) Traces showing the lipid mixing observed between syntaxin-1–SNAP-25 acceptor liposomes and synaptobrevin donor liposomes containing NBD-lipids quenched by rhodamine-lipids in the presence of Munc18-1 (M18), Munc13-1 C1C2BMUN (M13), synaptotagmin-1 C_2AB fragment (C_2AB), NSF, α-SNAP, and/or Mg^{2+}-ATP in various combinations (all in 0.5 mM Ca^{2+}). The *y* axis represents NBD fluorescence normalized to the maximum fluorescence observed upon detergent addition. (**B**) Quantification of the results obtained in the experiments of (A). (**C**) Lipid mixing experiments performed as in (A) with various additions, all in the presence of 2 μM SNAP-25 excess. (**D**) Quantification of the results of (C). Error bars represent SDs.

synaptobrevin-donor liposomes with acceptor liposomes containing syntaxin-1–Munc18-1 complex, efficient sulforhodamine fluorescence dequenching required SNAP-25, C1C2BMUN, and C_2AB fragment-Ca^{2+} (Fig. 3, A and B). The measured lipid mixing (Fig. 3, C and D) paralleled the NBD dequenching data (Fig. 2, B to D) and was similar to the sulforhodamine dequenching results, although in the absence of C_2AB fragment, there was a small amount of lipid mixing but not sulforhodamine dequenching. The time course of the sulforhodamine fluorescence dequenching in the presence of SNAP-25, C1C2BMUN, and C_2AB fragment-Ca^{2+} closely followed the time course of DiD fluorescence dequenching (fig. S6). Thus, content mixing accompanies lipid mixing in these experiments, which suggests that our system reconstitutes membrane fusion with the three neuronal SNAREs, Munc18-1, and core fragments of Munc13-1 and synaptotagmin-1. However, we cannot rule out that some degree of leakiness may occur during fusion (*27*).

Munc18-1 and Munc13-1 activate membrane fusion inhibited by NSF–α-SNAP. Multiple studies have shown efficient liposome fusion with SNAREs and syntaptotagmin-1 in the absence of Munc18-1 and Munc13-1 (*22–26*). However, these studies used liposomes containing syntaxin-1–SNAP-25 heterodimers and did not incorporate NSF-SNAPs, which inhibit lipid mixing induced by the SNAREs alone because they disassemble the syntaxin-1–SNAP-25 heterodimers (*28*). Because NSF–α-SNAPs facilitate displacement of SNAP-25 from syntaxin-1 by Munc18-1 (Fig. 1E), we hypothesized that Munc18-1 captures the syntaxin-1 released from the syntaxin-1–SNAP-25 heterodimers and, together with Munc13-1, leads to membrane fusion through an NSF–α-SNAP–resistant pathway.

We tested this hypothesis using lipid-mixing assays with liposomes containing syntaxin-1–SNAP-25 heterodimers (separately expressed proteins). As expected, highly efficient lipid mixing between these liposomes and synaptobrevin liposomes was observed in the presence of C_2AB fragment-Ca^{2+} (Fig. 4, A and B). Similar amounts of lipid mixing were observed upon addition of Munc18-1, C1C2BMUN, or NSF–α-SNAP in the absence of ATP, but lipid mixing was almost completely abolished by NSF–α-SNAP in the presence of ATP (Fig. 4, A and B). Some lipid mixing was observed when Munc18-1 and C1C2BMUN were added together with NSF–α-SNAP and ATP (Fig. 4, A and B). We reasoned that an excess of SNAP-25 might assist in lipid mixing-activation by Munc18-1 and C1C2BMUN because free SNAP-25 should favor SNARE complex formation without affecting the rate of syntaxin-1–SNAP-25 dissociation by NSF–α-SNAP. Indeed, lipid mixing was enhanced by increasing SNAP-25 concentrations, saturating at 2 μM (fig. S7). The 2 μM excess SNAP-25 did not affect the overall lipid mixing observed upon addition of only C_2AB fragment-Ca^{2+} (Fig. 4, A and C, black symbols), and NSF–α-SNAP still inhibited lipid mixing strongly in the presence of excess SNAP-25 and the absence of Munc18-1 and C1C2BMUN (Fig. 4, C and D). With 2 μM SNAP-25 excess, Munc18-1 and C1C2BMUN stimulated lipid mixing to levels comparable with those observed without NSF–α-SNAP (Fig. 4, C and D); Munc18-1 alone (but not C12C2BMUN alone) appeared to provide a small amount of activation (Fig. 4, C and D). Activation of lipid mixing by Munc18-1 and C1C2BMUN in NSF–α-SNAP–resistant manner was also observed in the absence of the C_2AB fragment (fig. S8) or using liposomes containing coexpressed syntaxin-1–SNAP-25 heterodimers (fig. S9). Thus, inclusion of NSF–α-SNAP is key to unmask the crucial importance of Munc18-1 and Munc13-1 for membrane fusion in these reconstituted systems.

Discussion. Our results lead us to propose a model of neurotransmitter release (Fig. 5 and fig. S10) that explains the essential roles of Munc18-1 and Munc13 in vivo and postulates that (i) syntaxin-1–SNAP-25 heterodimers constitute "off-pathway" complexes that are disrupted by Munc18-1 and by NSF-SNAPs; (ii) the productive pathway for synaptic vesicle fusion starts with the syntaxin-1–Munc18-1 complex, which may form directly or by displacement of SNAP-25 from syntaxin-1 by Munc18-1, and can be aided by NSF-SNAPs and perhaps by Munc13; (iii) Munc13 opens syntaxin-1 and, together with Munc18-1, forms a template to bring the three

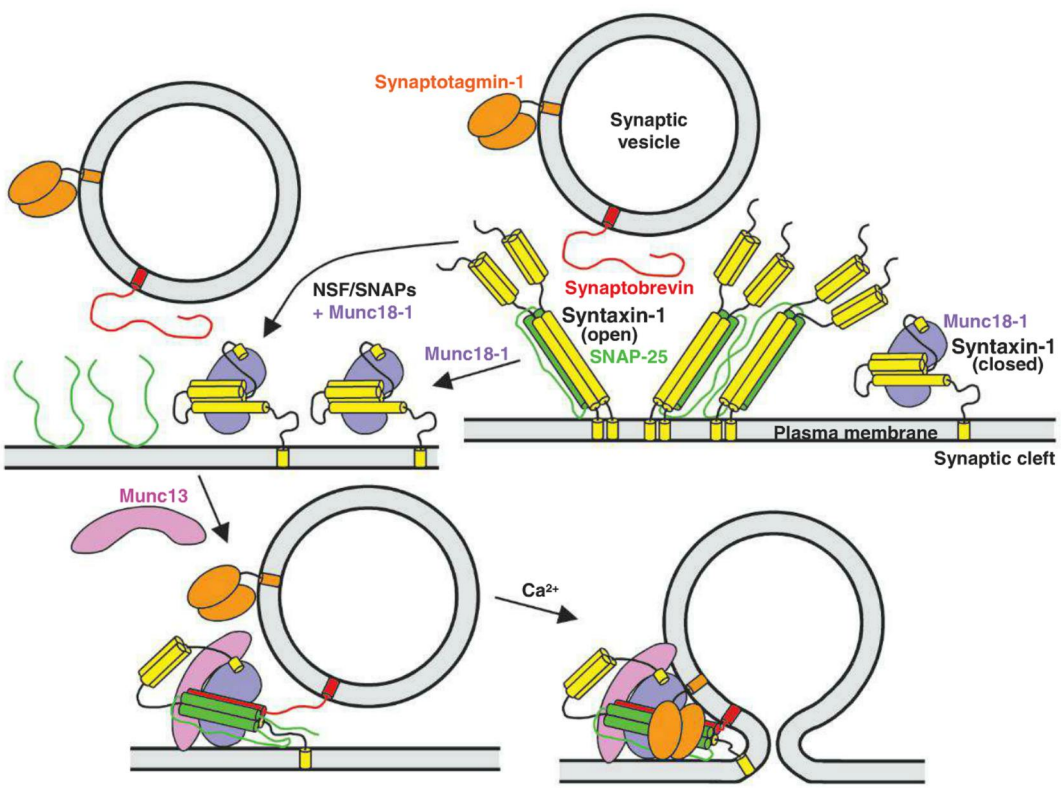

Fig. 5. Model of synaptic vesicle fusion integrating the function of eight major components of the release machinery. In the top right, syntaxin-1 (yellow) is shown in a closed conformation bound to Munc18-1 and in an open conformation bound to SNAP-25. To illustrate the likely heterogeneity of syntaxin-1–SNAP-25 heterodimers, two complexes with 2:1 or 4:2 stoichiometries are shown, but larger complexes bridged by SNAP-25 (not shown) are also likely to exist. The model postulates that the syntaxin-1–SNAP-25 heterodimers are converted to syntaxin-1–Munc18-1 complexes (top left) and that Munc13 helps to open syntaxin-1 and to orchestrate trans-SNARE complex assembly together with Munc18-1, leading to a partially assembled SNARE complex that remains bound to Munc18-1 and Munc13 (bottom left). This state, which may correspond to that of primed synaptic vesicles and cannot be disassembled by NSF-SNAPs, serves as the substrate for synaptotagmin-1-Ca^{2+} to trigger fast synaptic vesicle fusion (bottom right). The arrangement of Munc18-1, Munc13, and synaptotagmin-1 with respect to the SNARE complex is unknown but is drawn to suggest the possibility that the three proteins may bind simultaneously to the SNARE complex and may also help to bridge the two membranes to help induce fusion. The interaction of synaptotagmin-1 with the SNARE complex may occur before Ca^{2+} influx (not shown in bottom left for simplicity).

SNAREs together, initiating trans-SNARE complex assembly in an NSF-SNAP–resistant manner; and (iv) the resulting Munc18-1–Munc13-SNARE assembly underlies the primed state that enables fast membrane fusion through the action of synaptotagmin-1 and Ca^{2+}.

The functional interplay between NSF-SNAPs and Munc18-1–Munc13 uncovered here suggests that in addition to their role in disassembling cis-SNARE complexes, NSF-SNAPs have an important function in guiding the system to the productive pathway by disassembling syntaxin-1–SNAP-25 heterodimers. This feature may arise because syntaxin-1–SNAP-25 heterodimers are heterogeneous and may constitute poor starting points for an exquisitely regulated process such as neurotransmitter release. In contrast, the syntaxin-1–Munc18-1 complex provides a well-defined starting point amenable to tight regulation by several factors, including Munc13 and other active zone proteins (*1*). This productive pathway may also be favored by specific interactions at active zones. Although some of these features are specific to synaptic vesicle fusion, multiple factors besides SNAREs are also required for physiological reconstitution of endosomal (*33*) and vacuolar (*34*) fusion. Moreover, the interplay between Munc18-1–Munc13 and NSF–α-SNAP is reminiscent of results obtained in reconstitutions of yeast vacuolar fusion, which showed that the homotypic fusion and vacuole protein sorting (HOPS) tethering complex orchestrates trans-SNARE complex assembly in an NSF-SNAP–resistant manner (*35*, *36*). It is remarkable that the same task can be performed by Munc18-1 and Munc13, even though HOPS includes an SM protein (Vps33p) and five large subunits without homology to Munc13. Thus, orchestration of SNARE complex assembly without interference from NSF-SNAPs may constitute a general function of SM proteins and associated factors. This notion does not preclude other functions proposed for SM proteins and their cofactors, including the possibility that they cooperate with the SNAREs in exerting force on the membranes to induce fusion (*10*, *37*).

References and Notes

1. J. Rizo, C. Rosenmund, *Nat. Struct. Mol. Biol.* **15**, 665 (2008).
2. T. C. Südhof, J. E. Rothman, *Science* **323**, 474 (2009).
3. T. Söllner, M. K. Bennett, S. W. Whiteheart, R. H. Scheller, J. E. Rothman, *Cell* **75**, 409 (1993).
4. P. I. Hanson, R. Roth, H. Morisaki, R. Jahn, J. E. Heuser, *Cell* **90**, 523 (1997).
5. R. B. Sutton, D. Fasshauer, R. Jahn, A. T. Brunger, *Nature* **395**, 347 (1998).
6. M. A. Poirier *et al.*, *Nat. Struct. Biol.* **5**, 765 (1998).
7. A. Mayer, W. Wickner, A. Haas, *Cell* **85**, 83 (1996).
8. I. Dulubova *et al.*, *EMBO J.* **18**, 4372 (1999).
9. K. M. Misura, R. H. Scheller, W. I. Weis, *Nature* **404**, 355 (2000).
10. I. Dulubova *et al.*, *Proc. Natl. Acad. Sci. U.S.A.* **104**, 2697 (2007).
11. J. Shen, D. C. Tareste, F. Paumet, J. E. Rothman, T. J. Melia, *Cell* **128**, 183 (2007).
12. J. Basu *et al.*, *Nat. Struct. Mol. Biol.* **12**, 1017 (2005).
13. C. Ma, W. Li, Y. Xu, J. Rizo, *Nat. Struct. Mol. Biol.* **18**, 542 (2011).
14. R. Fernández-Chacón *et al.*, *Nature* **410**, 41 (2001).
15. M. Verhage *et al.*, *Science* **287**, 864 (2000).
16. J. E. Richmond, W. S. Davis, E. M. Jorgensen, *Nat. Neurosci.* **2**, 959 (1999).
17. F. Varoqueaux *et al.*, *Proc. Natl. Acad. Sci. U.S.A.* **99**, 9037 (2002).
18. J. Pei, C. Ma, J. Rizo, N. V. Grishin, *J. Mol. Biol.* **391**, 509 (2009).
19. W. Li *et al.*, *Structure* **19**, 1443 (2011).
20. T. Weber *et al.*, *Cell* **92**, 759 (1998).
21. K. L. Boswell *et al.*, *J. Cell Biol.* **197**, 301 (2012).
22. M. C. Chicka, E. Hui, H. Liu, E. R. Chapman, *Nat. Struct. Mol. Biol.* **15**, 827 (2008).
23. A. Stein, A. Radhakrishnan, D. Riedel, D. Fasshauer, R. Jahn, *Nat. Struct. Mol. Biol.* **14**, 904 (2007).
24. M. Xue, C. Ma, T. K. Craig, C. Rosenmund, J. Rizo, *Nat. Struct. Mol. Biol.* **15**, 1160 (2008).
25. H. K. Lee *et al.*, *Science* **328**, 760 (2010).
26. Diao *et al.*, *eLife* **1**, e00109 (2012).
27. Materials and methods are available as supplementary materials on *Science* Online.
28. T. Weber *et al.*, *J. Cell Biol.* **149**, 1063 (2000).
29. R. Schneggenburger, E. Neher, *Curr. Opin. Neurobiol.* **15**, 266 (2005).
30. J. S. Rhee *et al.*, *Cell* **108**, 121 (2002).
31. O. H. Shin *et al.*, *Nat. Struct. Mol. Biol.* **17**, 280 (2010).
32. F. Deák *et al.*, *J. Cell Biol.* **184**, 751 (2009).
33. T. Ohya *et al.*, *Nature* **459**, 1091 (2009).
34. C. Stroupe, C. M. Hickey, J. Mima, A. S. Burfeind, W. Wickner, *Proc. Natl. Acad. Sci. U.S.A.* **106**, 17626 (2009).
35. J. Mima, C. M. Hickey, H. Xu, Y. Jun, W. Wickner, *EMBO J.* **27**, 2031 (2008).
36. H. Xu, Y. Jun, J. Thompson, J. Yates, W. Wickner, *EMBO J.* **29**, 1948 (2010).
37. J. Rizo, X. Chen, D. Araç, *Trends Cell Biol.* **16**, 339 (2006).

Acknowledgments: We thank Y. Sun for expert technical assistance; Y. Liu for initial efforts to reconstitute syntaxin-1–Munc18-1 complexes; and W. Li, W. Wickner, and M. Brown for fruitful discussions. This work was supported by grant I-1304 from the Welch Foundation (to J.R.), grant 31200618 from the National Science Foundation of China (to C.M.), and grants NS37200 and NS40944 from the NIH (to J.R.).

Supplementary Materials

www.sciencemag.org/cgi/content/full/science.1230473/DC1
Materials and Methods
Figs. S1 to S10
References (*38*–*57*)

19 September 2012; accepted 23 November 2012
Published online 20 December 2012;
10.1126/science.1230473

REPORTS

Diisopropylammonium Bromide Is a High-Temperature Molecular Ferroelectric Crystal

Da-Wei Fu,[1]* Hong-Ling Cai,[1]* Yuanming Liu,[2]* Qiong Ye,[1] Wen Zhang,[1] Yi Zhang,[1] Xue-Yuan Chen,[3] Gianluca Giovannetti,[4,5] Massimo Capone,[4] Jiangyu Li,[2]† Ren-Gen Xiong[1]†

Molecular ferroelectrics are highly desirable for their easy and environmentally friendly processing, light weight, and mechanical flexibility. We found that diisopropylammonium bromide (DIPAB), a molecular crystal processed from aqueous solution, is a ferroelectric with a spontaneous polarization of 23 microcoulombs per square centimeter [close to that of barium titanate (BTO)], high Curie temperature of 426 kelvin (above that of BTO), large dielectric constant, and low dielectric loss. DIPAB exhibits good piezoelectric response and well-defined ferroelectric domains. These attributes make it a molecular alternative to perovskite ferroelectrics and ferroelectric polymers in sensing, actuation, data storage, electro-optics, and molecular or flexible electronics.

Ferroelectrics are multifunctional electroactive materials with a range of applications. Their temperature-dependent spontaneous polarization can be switched by electric field or mechanical forces (*1*–*4*), making them attractive for temperature sensing, data storage, mechanical actuation, and energy harvesting (*5*). They often exhibit tunable dielectric responses and nonlinear electro-optic effects (*6*, *7*) and thus can also be used to manipulate electromagnetic waves (*1*). Ferroelectricity was originally discovered in Rochelle salt (*8*) in 1921 and later in a few other molecular systems (*9*), but the rapid development of ferroelectrics took place only after the discovery of ferroelectricity in perovskite barium titanate (BTO) (*10*) and lead zirconate titanate (PZT) (*11*). Relative to BTO and PZT, most

[1]Ordered Matter Science Research Centre, Southeast University, Nanjing 211189, China. [2]Department of Mechanical Engineering, University of Washington, Seattle, WA 98195, USA. [3]Fujian Institute of Research on the Structure of Matter, Chinese Academy of Sciences, Fuzhou 350002, China. [4]CNR-IOM-Democritos National Simulation Centre and International School for Advanced Studies (SISSA), Via Bonomea 265, I-34136 Trieste, Italy. [5]Institute for Theoretical Solid State Physics, IFW-Dresden, PF 270116, 01171 Dresden, Germany.

*These authors contributed equally to this work.
†To whom correspondence should be addressed. E-mail: xiongrg@seu.edu.cn (R.-G.X.); jjli@u.washington.edu (J.L.)

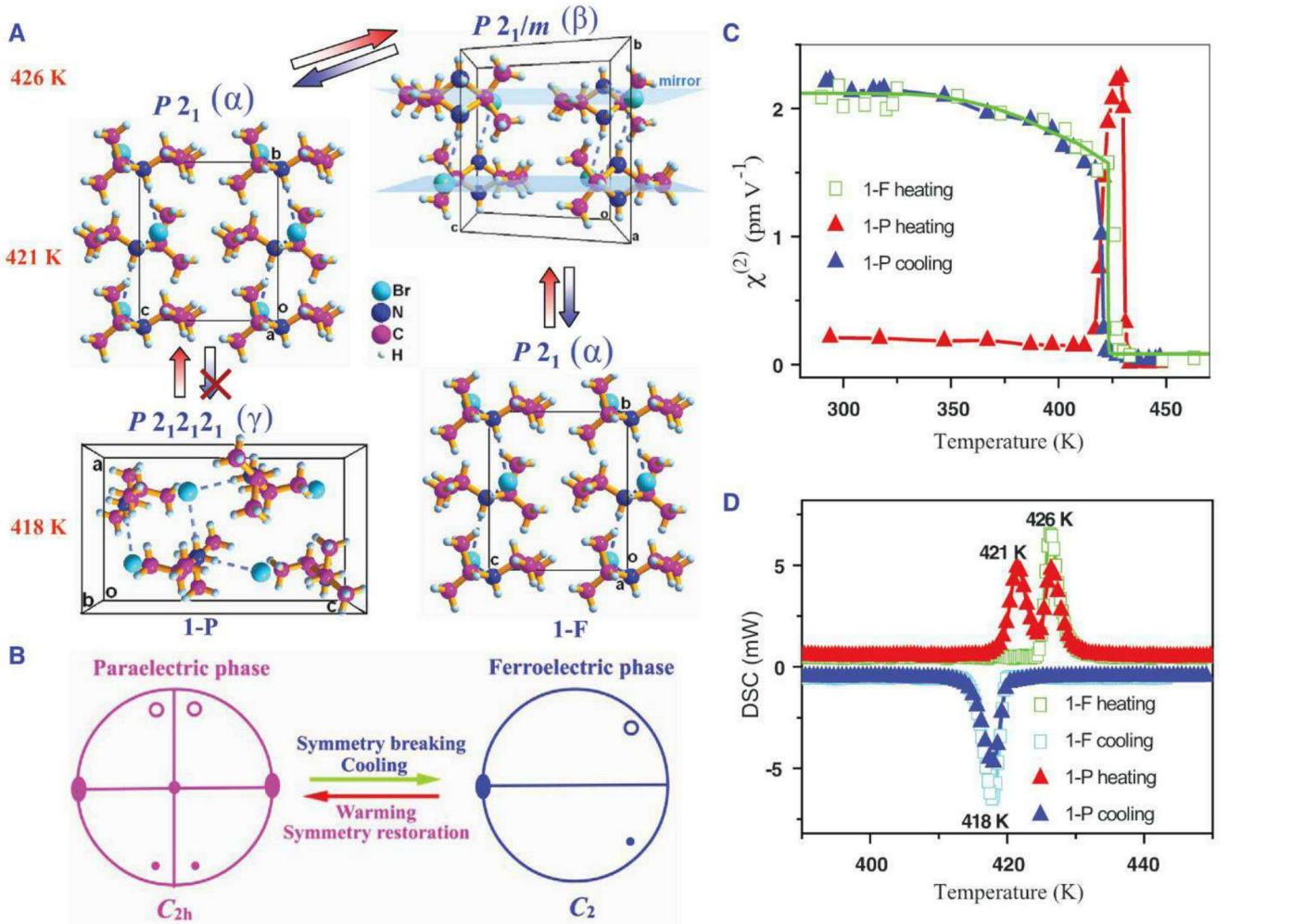

Fig. 1. Structural phase transition of DIPAB polymorphs. (**A**) The phase transition sequence: γ phase (1-P) to α phase at about 421 to 426 K (irreversible); α phase (1-F) to paraelectric β phase at 426 K (reversible). (**B**) Equatorial plane projection of point group of C_2 in the ferroelectric phase and C_{2h} in the paraelectric phase. (**C**) Second-order nonlinear optical coefficient versus temperature, confirming transition sequence seen in (A) and (B). (**D**) DSC data confirming transition sequence seen in (A) and (B).

Fig. 2. Dielectric properties of 1-F measured under different frequencies as a function of temperature. (**A**) Dielectric constant across the Curie point. (**B**) 1/ε′ follows the Curie-Weiss law. (**C**) Dielectric constant away from the Curie point. (**D**) The imaginary part of the dielectric constant.

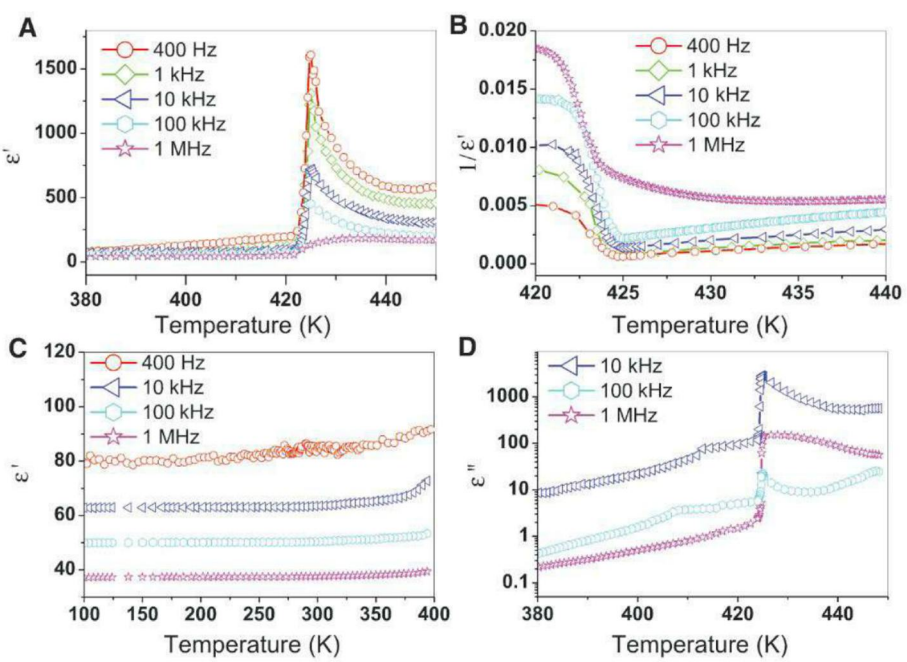

molecular ferroelectrics suffer from low spontaneous polarization (P_s), low melting temperature and phase transition temperature (Curie temperature, T_c), small dielectric constant, and weak piezoelectricity; their advantages include light weight, mechanical flexibility, and environmentally friendly processing as they are lead-free. Ferroelectric polymers such as poly(vinylidene fluoride) (PVDF) and its copolymers (*12*) share some of the drawbacks of molecular ferroelectrics, which limits their applications. The recently reported croconic acid (*6*) has a high spontaneous polarization of around 23 μC cm^{-2}; however, evidence for a ferroelectric phase transition, piezoelectric response, or ferroelectric domains has not been reported. By searching among organic compounds with a polar point group at room temperature and relatively high melting point, we found that diisopropylammonium chloride (DIPAC) is a ferroelectric with spontaneous polarization of 8.2 μC cm^{-2} (*13*). Here, we show that diisopropylammonium bromide (DIPAB), a molecular crystal processed from aqueous solution, possesses ferroelectric properties comparable to those of BTO.

A crystalline sample of DIPAB was grown by slow evaporation of the aqueous solution; the recrystallization of DIPAB yields two different polymorphs (*14*). One (1-F), obtained from methanol, is needle-shaped, whereas the other (1-P), obtained from water or a methanol-water solution, has a block shape (fig. S1). The 1-P form can be easily converted into 1-F by heating for 5 min at about 428 K, and large single crystals of 1-F suitable for dielectric hysteresis loop measurements can be obtained by controlling the cooling rate of the saturated methanol or aqueous solution of DIPAB.

Structure characterization by x-ray diffraction (XRD) (*14*) reveals that 1-F belongs to the monoclinic crystal system at room temperature, with a polar point group C_2 and chiral space group $P2_1$ (*15*) that we refer to as α phase (fig. S2 and table S1), which, in principle, is ferroelectrically active. In contrast, 1-P at room temperature belongs to the orthorhombic crystal system with a nonpolar point group D_2 and a chiral space group $P2_12_12_1$ (γ phase) (fig. S3 and table S2), which is ferroelectrically inactive. When the crystals were heated above 426 K (Fig. 1A), we observed that the nitrogen atoms of both polymorphs entered an apparently disordered state, resulting in a centrosymmetric structure with a nonpolar point group C_{2h} and space group $P2_1/m$ (β phase) (tables S1 and S2). When cooling down to room temperature, the space group of 1-F shifted back to $P2_1$, indicating a reversible phase transition. The space group of 1-P, on the other hand, became $P2_1$ instead of $P2_12_12_1$ upon cooling (Fig. 1A). Notably, a symmetric mirror plane disappeared below 426 K in α-DIPAB (Fig. 1B). Such broken symmetry has been verified by second harmonic generation (SHG) spectra, which are sensitive to the space inversion symmetry and thus are often used to detect ferroelectric transitions (*16*–*19*). The second-order nonlinear optical coefficient $\chi^{(2)}$ of 1-F (Fig. 1C) was close to zero above T_c and increased sharply below T_c, reaching a saturation value approximately twice that of KH_2PO_4 (KDP), a notable nonlinear optic crystal; this finding confirmed that the space inversion symmetry is broken at T_c. In the vicinity of T_c, $\chi^{(2)}$ showed a steplike jump indicating a first-order phase transition. The SHG effect of 1-P, on the other hand, was very weak at room temperature but increased sharply to an intensity very close to that of 1-F at 428 K; this is attributed to a transition from $P2_12_12_1$ to $P2_1$ upon heating. With further temperature increase, $\chi^{(2)}$ dropped rapidly to near zero, indicating transformation to centrosymmetric $P2_1/m$, and the subsequent cooling process revealed a variation of $\chi^{(2)}$ similar to that of 1-F. The SHG spectra thus are fully consistent with the phase transition sequence shown in Fig. 1A.

The phase transition sequences of 1-F and 1-P were further verified by differential scanning calorimetry (DSC) (Fig. 1D). Only one heat anomaly was observed for 1-F (at 418 to 426 K), suggesting a reversible phase transition. The sharp heat anomaly peak and a relatively large thermal hysteresis (8 K) are indicative of a first-order phase transition. This heat anomaly peak also can be observed in the differential thermal analysis (DTA) curve at about 423 K (fig. S4), showing that 1-F decomposes at about 520 K, far beyond T_c (*14*). For the 1-P crystal, there are two peaks, at 421 K and 426 K, in the heating process of the DSC measurement, and there is only one peak at 418 K in the cooling process. This is consistent with the crystal structure characterization and the SHG, and all the data combined suggest that in the heating process, the space group of 1-P is $P2_12_12_1$ below 421 K, possibly $P2_1$ between 421 K and 426 K, and $P2_1/m$ above 426 K, whereas in the cooling process it turns from $P2_1/m$ to $P2_1$ directly at 418 K. This type of polymorphism is rare in ferroelectric systems; consequently, in the temperature range between T_c and the liquid nitrogen boiling temperature, there is only one stable ferroelectric phase for DIPAB. In contrast, there are three ferroelectric phases for BTO in that temperature range. As such, DIPAB possesses one of the highest transition temperatures among molecular ferroelectrics at 426 K and

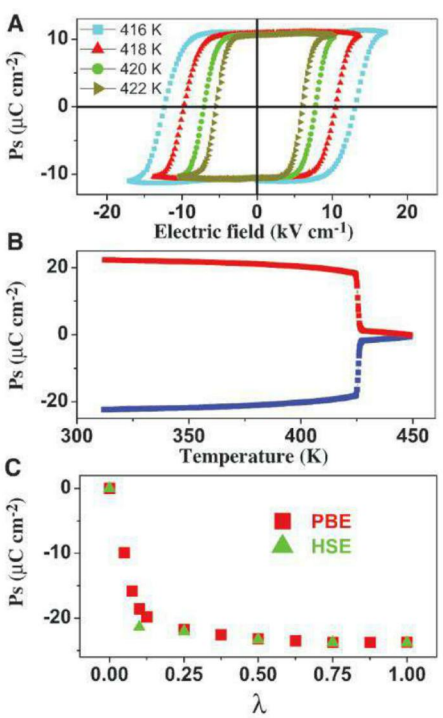

Fig. 3. Ferroelectric properties of 1-F. (**A**) Hysteresis loop measured at different temperatures. (**B**) Spontaneous polarization versus temperature. (**C**) Spontaneous polarization P_s along the path connecting the centrosymmetric $P2_1/m$ (λ = 0) to the experimental polar $P2_1$ structure (λ = 1), calculated from first principles using two different methods.

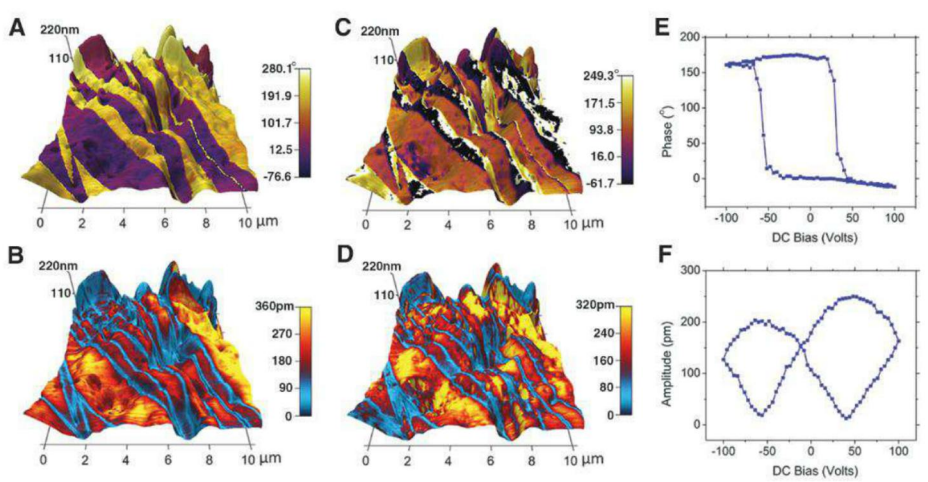

Fig. 4. Piezoresponse force microscopy of 1-F. (**A** and **B**) Phase mapping (A) and amplitude mapping (B) of vertical PFM overlaid on 3D topography. (**C** and **D**) Phase mapping (C) and amplitude mapping (D) of lateral PFM overlaid on 3D topography. (**E**) Phase-voltage hysteresis loop. (**F**) Amplitude-voltage butterfly loop.

has a stable structure in a broad temperature range below T_c, making it attractive for various applications.

A signature of the ferroelectric phase transition is a prominent dielectric anomaly. This is indeed observed at 426 K in the temperature dependence of the dielectric constant of 1-F (Fig. 2A), which shows a peak as high as 1608 at the lowest measured frequency. In the vicinity of T_c, the temperature-dependent permittivity along the polar axis follows the Curie-Weiss law of ferroelectric materials parameterized as $\varepsilon' = C/(T - T_0)$, as shown by the linear relationship between the reciprocal dielectric constant and the temperature in Fig. 2B. The Curie-Weiss constant C, a useful parameter for evaluating the value of P_s, is fitted to be 1.32×10^4 K, considerably higher than the values for ferroelectrics such as KDP (2.9×10^3 K) (*4*), triglycine sulfate (3.2×10^3 K) (*4*), $NaNO_2$ (4.7×10^3 K) (*4*), and DIPAC (8.4×10^3 K) (*13*), but smaller than that of inorganic compounds such as BTO (1.5×10^5 K) (*4*), $PbTiO_3$ (4.1×10^5 K) (*4*), and PZT (1.4×10^5 to 4.2×10^5 K) (*20*). The value of T_0 is estimated to be 416 K, smaller than T_c, indicating a first-order phase transition. In contrast, the temperature-dependent permittivity of 1-P shows an evident yet less prominent dielectric anomaly (fig. S5), which we were unable to fit to a Curie-Weiss form, reflecting its nonferroelectric nature (*14*). Far away from T_c, 1-F has a very large dielectric constant of up to 85 at room temperature measured under 400 Hz (Fig. 2C), an order of magnitude higher than that of polymer ferroelectrics such as PVDF. Even at a frequency of 1 MHz, the dielectric constant remains as high as 38, and its imaginary part ε'' is only 0.2 at 380 K (Fig. 2D), suggesting a small loss tangent of 0.44%. Such a high dielectric constant and low dielectric loss also make DIPAB attractive as a dielectric in capacitors for electric energy storage.

All the evidence points to a ferroelectric phase transition at 426 K in the 1-F polymorph, and indeed a ferroelectric hysteresis loop was recorded using a simple Sawyer-Tower circuit at 25 Hz. On cooling from 438 K, the 1-F loop looks like an open mouth–shaped ellipsoid (fig. S6), indicating paraelectric characteristics with leakage current (*14*). Just below T_c, a typical ferroelectric hysteresis loop emerges (Fig. 3A), confirming the ferroelectricity of α-DIPAB. The coercive field is estimated to be 5.0 kV cm^{-1}, smaller than those of PVDF (500 kV cm^{-1}) (*4*), BTO (10 kV cm^{-1}) (*4*), PZT (20 to 80 kV cm^{-1}) (*21*), and DIPAC (9 kV cm^{-1}) (*13*). The spontaneous polarization measured using a pyroelectric technique (Fig. 3B) reveals a very sharp transition from the paraelectric to the ferroelectric phase in an interval of about 3 K, indicating again a first-order phase transition. P_s is measured to be 23 μC cm^{-2}, compared to 8 μC cm^{-2} for PVDF (*4*), 26 μC cm^{-2} for BTO (*4*), 30 to 55 μC cm^{-2} for PZT (*21*), and 8 μC cm^{-2} for DIPAC (*13*). We also observed that the variation of P_s with respect to temperature is very similar to that of $\chi^{(2)}$, which can be explained from the relationship $\chi^{(2)} = 6\varepsilon_0\beta P_s$ deduced from Landau theory, where β is the high-order dielectric coefficient (*1*, *19*). To verify our measurement of spontaneous polarization, we performed first-principles density functional theory (*22*, *23*) calculations within the generalized gradient approximation to the exchange correlation potential according to the Perdew-Burke-Ernzerhof (PBE) method (*24*) and the Heyd-Scuseria-Ernzerhof hybrid (HSE) functional (*25*). The spontaneous polarization (Fig. 3C) is plotted as a function of the dimensionless variable λ (*14*), which parameterizes the continuous evolution from the centrosymmetric $P2_1/m$ structure (λ = 0), based on a supergroup analysis (*26*), to the experimental polar $P2_1$ structure (λ = 1); the agreement between these two approaches shows the stability and accuracy of the results. For the actual polar structure we obtain a finite polarization of ~23.9 μC cm^{-2}, in agreement with the experimental value. In addition, the abrupt variation of P_s as a function of λ also reflects the first-order phase transition observed in experiments. The calculations suggest that the emergence of the spontaneous polarization is driven by a cooperative atomic distortion at molecular sites that breaks the mirror symmetry plane of each single DIPAB molecule along the *b* axis of Fig. 1A, resulting in an asymmetric arrangement of the charges.

Finally, we used piezoresponse force microscopy (PFM) (*27*, *28*) to measure the local piezoelectric response and the ferroelectric domain structure at the nanoscale. Phase and amplitude mappings obtained with vertical PFM overlaid on three-dimensional (3D) topography (Fig. 4, A and B) correspond well to each other, revealing a ferroelectric domain pattern with alternating bands of upward and downward polarizations separated by domain walls; no crosstalk with topography is observed. The piezoresponse is measured to be as high as 360 pm under only 1 V ac, comparable with most other ferroelectrics, thus confirming its excellent piezoelectricity. Lateral PFM overlaid on 3D topography shows phase (Fig. 4C) and amplitude (Fig. 4D) mappings in good correspondence with the vertical mappings, despite the out-of-plane polarization direction of the sample. This can be understood from the piezoelectric tensor **d** of a C_2 point group, with nonzero d_{22} and d_{25} and spontaneous polarization P_2 (*29*), which induces normal and shear piezoelectric strains simultaneously under an electric field applied along the polar axis, whereas for BTO and PZT with out-of-plane polarization, only normal response is expected from symmetry. In this sense, the terms vertical and lateral PFM are somewhat misleading, and it is more appropriate to describe the data in terms of normal and shear PFM. Switching PFM was also carried out, with dc voltage applied on top of the ac voltage to switch the polarization, resulting in characteristic hysteresis and butterfly loops (Fig. 4, E and F). These findings further confirm the ferroelectricity of the molecular crystal.

References and Notes

1. M. E. Lines, A. M. Glass, *Principles and Applications of Ferroelectrics and Related Materials* (Oxford Univ. Press, New York, 2001).
2. W. Zhang, R. G. Xiong, *Chem. Rev.* **112**, 1163 (2012).
3. W. Eerenstein, N. D. Mathur, J. F. Scott, *Nature* **442**, 759 (2006).
4. S. Horiuchi, Y. Tokura, *Nat. Mater.* **7**, 357 (2008).
5. J. F. Scott, *Science* **315**, 954 (2007).
6. S. Horiuchi *et al.*, *Nature* **463**, 789 (2010).
7. M. Veithen, X. Gonze, P. Ghosez, *Phys. Rev. Lett.* **93**, 187401 (2004).
8. J. Valasek, *Phys. Rev.* **17**, 475 (1921).
9. A. Lurio, E. Stern, *J. Appl. Phys.* **31**, 1125 (1960).
10. H. D. Megaw, *Nature* **155**, 484 (1945).
11. B. Jaffe, R. S. Roth, S. Marzullo, *J. Appl. Phys.* **25**, 809 (1954).
12. A. J. Lovinger, *Science* **220**, 1115 (1983).
13. D.-W. Fu *et al.*, *Adv. Mater.* **23**, 5658 (2011).
14. See supplementary materials on *Science* Online.
15. G. Kociok-Köhn, B. Lungwitz, A. C. Filippou, *Acta Crystallogr. C* **52**, 2309 (1996).
16. J. H. Lee *et al.*, *Nature* **466**, 954 (2010).
17. M. Fiebig, Th. Lottermoser, D. Fröhlich, A. V. Goltsev, R. V. Pisarev, *Nature* **419**, 818 (2002).
18. C. C. Neacsu, B. B. van Aken, M. Fiebig, M. B. Raschke, *Phys. Rev. B* **79**, 100107 (2009).
19. H.-L. Cai *et al.*, *Phys. Rev. Lett.* **107**, 147601 (2011).
20. I. Kanno, Y. Yokoyama, H. Kotera, K. Wasa, *Phys. Rev. B* **69**, 064103 (2004).
21. C. M. Foster *et al.*, *J. Appl. Phys.* **81**, 2349 (1997).
22. G. Giovannetti *et al.*, *Nat. Commun.* **2**, 398 (2011).
23. P. Hohenberg, W. Kohn, *Phys. Rev.* **136** (3B), B864 (1964).
24. J. P. Perdew, K. Burke, M. Ernzerhof, *Phys. Rev. Lett.* **77**, 3865 (1996).
25. J. Heyd, G. E. Scuseria, M. Ernzerhof, *J. Chem. Phys.* **118**, 8207 (2003).
26. E. Kroumova *et al.*, *J. Appl. Cryst.* **34**, 783 (2001).
27. S. V. Kalinin *et al.*, *Annu. Rev. Mater. Res.* **37**, 189 (2007).
28. D. A. Bonnell, S. V. Kalinin, A. L. Kholkin, A. Gruverman, *MRS Bull.* **34**, 648 (2009).
29. J. F. Nye, *Physical Properties of Crystals: Their Representation by Tensors and Matrices* (Oxford Univ. Press, New York, 1985).

Acknowledgments: Supported by NSFC key fund grants 20931002 and 90922005 (R.-G.X.), NSF grant CMMI 1100339 (J.L.), and the European Research Council under starting independent research grant 240524 "SUPERBAD" (M.C. and G.G.). Numerical calculations were performed at CINECA. J.L. and R.-G.X. contributed to the design of the study, analysis of the data, and writing of the paper. D.-W.F. did the sample preparation. H.-L.C. made the dielectric constant and ferroelectric hysteresis loop measurements. Y.L. did the PFM studies. W.Z. wrote parts of the paper. Q.Y. contributed ideas and wrote some key parts of the paper. Y.Z. carried out the powder diffraction studies. X.-Y.C. carried out SHG measurements. G.G. and M.C. made ab initio calculations and wrote part of the manuscript.

Supplementary Materials

www.sciencemag.org/cgi/content/full/339/6118/425/DC1
Materials and Methods
Figs. S1 to S6
Tables S1 and S2
References (*30*–*33*)

4 September 2012; accepted 14 November 2012
10.1126/science.1229675

A Radically Configurable Six-State Compound

Jonathan C. Barnes,[1,5] Albert C. Fahrenbach,[1,5] Dennis Cao,[1,5] Scott M. Dyar,[1] Marco Frasconi,[1] Marc A. Giesener,[1] Diego Benítez,[4] Ekaterina Tkatchouk,[4] Oleksandr Chernyashevskyy,[3] Weon Ho Shin,[5] Hao Li,[1] Srinivasan Sampath,[1,5] Charlotte L. Stern,[1] Amy A. Sarjeant,[1] Karel J. Hartlieb,[1] Zhichang Liu,[1] Raanan Carmieli,[1] Youssry Y. Botros,[1,2,6,7] Jang Wook Choi,[5] Alexandra M. Z. Slawin,[8] John B. Ketterson,[3] Michael R. Wasielewski,[1] William A. Goddard III,[4,5] J. Fraser Stoddart[1,5]*

Most organic radicals possess short lifetimes and quickly undergo dimerization or oxidation. Here, we report on the synthesis by radical templation of a class of air- and water-stable organic radicals, trapped within a homo[2]catenane composed of two rigid and fixed cyclobis(paraquat-*p*-phenylene) rings. The highly energetic octacationic homo[2]catenane, which is capable of accepting up to eight electrons, can be configured reversibly, both chemically and electrochemically, between each one of six experimentally accessible redox states (0, 2+, 4+, 6+, 7+, and 8+) from within the total of nine states evaluated by quantum mechanical methods. All six of the observable redox states have been identified by electrochemical techniques, three (4+, 6+, and 7+) have been characterized by x-ray crystallography, four (4+, 6+, 7+, and 8+) by electron paramagnetic resonance spectroscopy, one (7+) by superconducting quantum interference device magnetometry, and one (8+) by nuclear magnetic resonance spectroscopy.

Typically, organic radicals are unstable species with fleeting lifetimes that make their isolation and characterization a demanding task. The few that are stable, from the triphenylmethyl radical discovered (*1*) by Gomberg in 1900 to the others isolated (*2*–*8*) in the intervening years, generally have structures that raise kinetic barriers (*9*), thus helping to curtail the rates of intermolecular dimerization and/or oxidation of the open-shell centers. Not long after Gomberg's discovery, Michaelis described (*10*, *11*) the redox properties of *N,N′*-dialkyl-4,4′-bipyridinium (BIPY)–based compounds—also known as viologens (*11*, *12*)—and their ability to form radical cations ($BIPY^{\bullet+}$) upon a one-electron reduction. The inter- and intramolecular behavior of these radical cationic $BIPY^{\bullet+}$ compounds was investigated further more than 40 years ago by Kosower (*12*, *13*) and Hünig (*14*), who drew attention to their ability to dimerize in solution—and in so doing form diamagnetic (closed shell) species—a situation they referred to frequently as pimerization. In more recent times, this spin-pairing of radical cation dimers has been stabilized in the supramolecular settings of host-guest systems. For example, Kim (*15*) has demonstrated the enhanced stabilization of *N,N′*-dimethyl-4,4′-bipyridinium radical cations—or, more commonly, methyl viologen ($\mathbf{MV}^{\bullet+}$) radical cations—inside the cavity of cucurbit[8]uril. Likewise, we have observed (*16*) the inclusion of $\mathbf{MV}^{\bullet+}$ inside the cavity of the diradical dication cyclobis(paraquat-*p*-phenylene) (*17*) [$\mathbf{CBPQT}^{2(\bullet+)}$] ring to form a tris(bipyridinium radical cation) inclusion complex.

In the context of mechanically interlocked molecules, and hard on the heels of discovering (*18*, *19*) how both the mixed-valence and radical-cation dimers of tetrathiafulvalene can be stabilized inside the central rings of [3]catenanes, we have reported recently (*20*) on the phenomenon of BIPY-based radical-radical molecular recognition in a tristable [2]rotaxane and subsequently on the templation (*21*) of a [2]rotaxane where the BIPY unit of the respective dumbbell components function as a recognition unit for the $CBPQT^{2(\bullet+)}$ ring. In all of these BIPY-based examples, the stability of the radical cationic state is low and the lifetimes of these radical viologen derivatives is short as a result of oxidation followed closely by decomplexation, as in the case of the [2]pseudorotaxane, or translational motion of the ring in the interlocked system to alleviate any strain that occurs as a consequence of Coulombic repulsion. In the investigation described here, a class of stable organic radicals is introduced as a readily obtainable homo[2]catenane (HC), wherein no relative movements involving the two mechanically interlocked rings occur at room temperature, regardless of the redox state, thus maintaining the ideal geometry for electron transfer in the face of large Coulombic forces. Consequently, the radical trapped within the heptacationic HC is so stable that the compound can withstand being purged with air for several weeks and still retain its radical character. The stability of the open-shell electronic structure is achieved by the close stacking of the BIPY units that is enforced by the mechanical bond formed between the two electron-deficient CBPQT rings immobilized with respect to one another. Indeed, the monoradical heptacation resists complete oxidation to the highly energetic 8+ redox state under ambient conditions as a result of the increased Coulombic repulsions concentrated within such a confined space of just over 1 cubic nanometer.

A recent addition (*21*) to the protocols employed in the template-directed syntheses of mechanically interlocked molecules involves taking advantage of favorable radical-radical interactions that exist between BIPY radical cation dimers. The extent of dimerization is easily controlled by enforcing an N_2 atmosphere and also by moderating the concentrations of the species, typically in CH_3CN solution when dealing with the PF_6^- salt. Beginning with the pairing of two dibromide precursors $\mathbf{DB}^{\bullet+}$, after $\mathbf{DB}^{2+}$ has been reduced in the presence of an excess of Zn dust to give the $(\mathbf{DB}^{\bullet+})_2$ dimer, we have employed (Fig. 1A) this template-directing strategy in the preparation of a homocatenane. Mechanical bond formation is envisaged to begin with the addition of one equivalent of 4,4′-bipyridine to the dimer, closing one ring, and thus producing the intermediate $\mathbf{DB}^{\bullet+}\subset\mathbf{CBPQT}^{2(\bullet+)}$ as an inclusion complex. Addition of a second equivalent of 4,4′-bipyridine to this complex generates the HC, presumably as the tetraradical tetracation $\mathbf{HC}^{4(\bullet+)}$, which is the "as synthesized" purple product before the crude reaction mixture is removed from the N_2 atmosphere.

Upon exposure to air, $\mathbf{HC}^{4(\bullet+)}$ is oxidized and comes to rest as an $\mathbf{HC}^{\bullet7+}/\mathbf{HC}^{2\bullet6+}$ equilibrium mixture, stopping just short of reaching the fully oxidized $\mathbf{HC}^{8+}$. The purple solid was purified by preparative reverse-phase high pressure liquid chromatography (RP-HPLC) and its purity confirmed by analytical HPLC. When $\mathbf{HC}^{\bullet7+}/\mathbf{HC}^{2\bullet6+}$ was examined by high-resolution electrospray ionization mass spectrometry (HR-ESI-MS), peaks were observed for $[M - PF_6]^+$ from $\mathbf{HC}^{\bullet7+}$ and $[M - 2PF_6]^{2+}$ from $\mathbf{HC}^{\bullet7+}$ and $\mathbf{HC}^{2\bullet6+}$. The resonances in the ^{1}H nuclear magnetic resonance (NMR) spectrum of $\mathbf{HC}^{8+}$ (Fig. 1B) were obtained by treating $\mathbf{HC}^{\bullet7+}/\mathbf{HC}^{2\bullet6+}$ with an excess of tris(4-bromophenyl)aminium hexachloroantimonate (**TBPA**•$SbCl_6$) (*22*) and the assignments were confirmed by two-dimensional ^{1}H-^{1}H correlated spectroscopy experiments. For more details of the HPLC (fig. S1), MS (fig. S17), and NMR experiments (fig. S11), see the supplementary materials.

The characterizations (Fig. 2) of the redox states of the HC from electrochemical experiments and electron paramagnetic resonance (EPR) spectroscopy go hand in hand. Figure 2A shows the plot of the current versus potential, which was

[1]Department of Chemistry, Northwestern University, 2145 Sheridan Road, Evanston, IL 60208, USA. [2]Department of Materials Science and Engineering, Northwestern University, 2145 Sheridan Road, Evanston, IL 60208, USA. [3]Department of Physics, Northwestern University, 2145 Sheridan Road, Evanston, IL 60208, USA. [4]Materials and Process Simulation Center, California Institute of Technology, Pasadena, CA 91125, USA. [5]NanoCentury KAIST Institute and Graduate School of EEWS (WCU), Korea Advanced Institute of Science and Technology (KAIST), 373-1 Guseong Dong, Yuseong Gu, Daejeon 305-701, Republic of Korea. [6]Intel Labs, Building RNB-6-61, 2200 Mission College Boulevard, Santa Clara, CA 95054, USA. [7]National Center for Nano Technology Research, King Abdulaziz City for Science and Technology, P.O. Box 6086, Riyadh 11442, Kingdom of Saudi Arabia. [8]EaStCHEM School of Chemistry, University of St Andrews, North Haugh, St Andrews, KY16 9ST, UK.

*To whom correspondence should be addressed. E-mail: stoddart@northwestern.edu

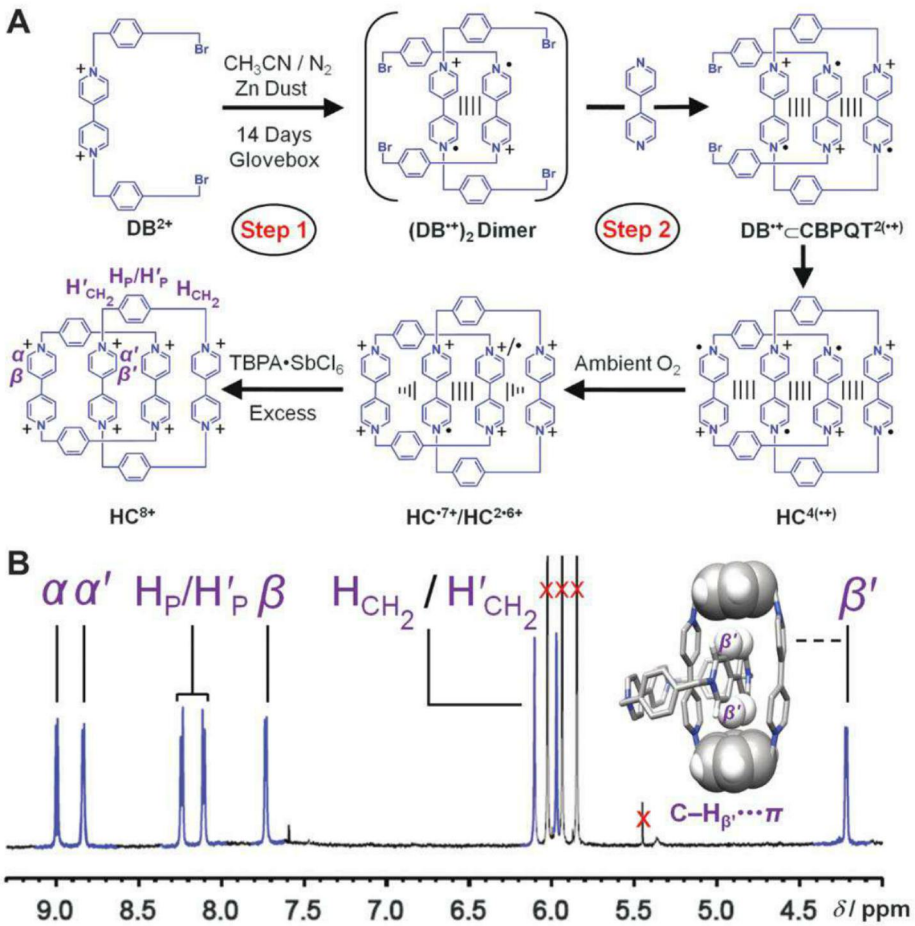

Fig. 1. (**A**) The key posited steps in the synthetic route to $\mathbf{HC^{4(\bullet+)}}$, and ultimately $\mathbf{HC^{8+}}$, involve the reduction (Step 1) of a bisbromomethyl(bis-*p*-benzylbipyridinium) dication, $\mathbf{DB^{2+}}$ to $\mathbf{DB^{\bullet+}}$, which spontaneously forms the $(\mathbf{DB^{\bullet+}})_2$ dimer before its reaction (Step 2) with 4,4′-bipyridine to afford $\mathbf{HC^{4(\bullet+)}}$ through the 1:1 inclusion complex $\mathbf{DB^{\bullet+}\subset CBPQT^{2(\bullet+)}}$ as a templating intermediate. Addition of an aqueous NH_4PF_6 solution converts all of the counterions to PF_6^- ions before exposure of the reaction mixture to air, whereupon $\mathbf{HC^{4(\bullet+)}}$ is oxidized to $\mathbf{HC^{\bullet7+}/HC^{2\bullet6+}}$, which then affords $\mathbf{HC^{8+}}$ upon treatment with tris(4-bromophenyl) aminium hexachloroantimonate (**TBPA**•$SbCl_6$). (**B**) The ^1H NMR spectrum (600 MHz) of $\mathbf{HC^{8+}}$, recorded in CD_3CN at 298 K, reveals resonances for the α, β, H_P and H_{CH2} protons associated with the outside $BIPY^{2+}$ units in addition to resonances for the α′, β′, H'_P and H'_{CH2} protons associated with the inside $BIPY^{2+}$ units. The inset on the right shows the solid-state structure of $\mathbf{HC^{\bullet7+}}$. The three large peaks resonating at ~6 parts per million (ppm) are attributed to NH_4^+ protons.

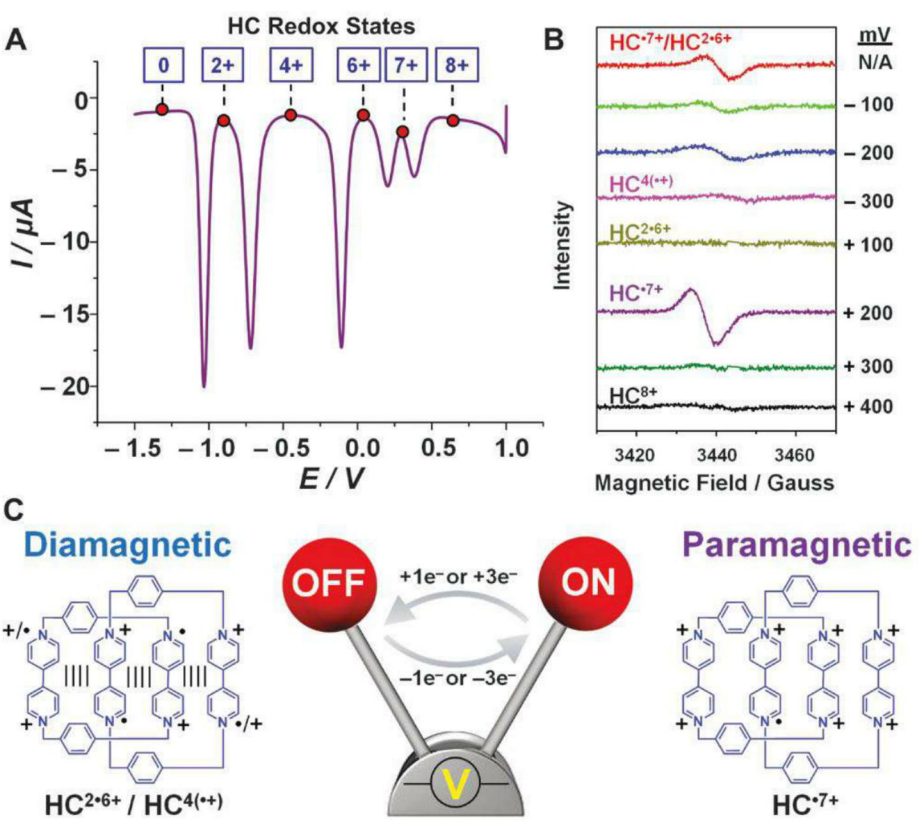

Fig. 2. (**A**) The six redox states of the HC identified by square-wave DPV. (**B**) EPR analysis was performed on a 1-mM sample of the HC, beginning with the starting state (top), where no potential was applied. Bulk electrolysis was then conducted on the sample using the displayed potentials (from top to bottom), and an aliquot was removed for EPR analysis immediately after each electrolysis step. The small signals observed through the sequence of reductions can be attributed to incomplete spin-pairing, deficient bulk electrolysis, or both. (**C**) A graphical representation of the redox switching mechanism between the paramagnetic and diamagnetic states. The paramagnetic $\mathbf{HC^{\bullet7+}}$, corresponding to the "on" state, can be reduced (electro)chemically by adding either one or three electrons to form $\mathbf{HC^{2\bullet6+}}$ or $\mathbf{HC^{4(\bullet+)}}$, respectively. Both of these states—considered as "off" states—are diamagnetic.

obtained by conducting square-wave differential pulse voltammetry (DPV) experiments on the HC in a 1-mM dimethylformamide (DMF) solution [0.1 M tetrabutylammonium hexafluorophosphate ($TBAPF_6$); Ag/AgCl used as reference]. In total, there are five reversible redox processes and six redox states that are accessible (electro)chemically, whereas the remaining three redox states ($HC^{\bullet+}$, $HC^{3\bullet3+}$, and $HC^{3\bullet5+}$) have yet to be observed experimentally. Cyclic voltammetry (CV), which was conducted (fig. S18) at 200 mVs^{-1}, confirmed that all of the redox processes are fully reversible. The electrochemical data highlight the small separation of the 6+ and 7+ reduction potentials in both the CV and DPV experiments, an observation that is consistent with their appearance in the mass spectrometric (fig. S17) and spectroelectrochemical (SEC) (fig. S10) data. The continuous wave (CW) EPR spectra (Fig. 2B) of the HC in DMF (1 mM, 0.1 M $TBAPF_6$; Ag used as pseudoreference) are shown at different potentials during the electrolysis of a 1-mL sample. The lack of hyperfine splitting is indicative of an intramolecular spin exchange mechanism between $BIPY^{\bullet+}$ units (*20*) in the HC. The EPR trace when no potential was applied confirms that the starting state of the HC largely comprises the paramagnetic $\mathbf{HC}^{\bullet7+}$. Electrolysis was performed by holding the displayed potentials for 30 min, beginning with –100 mV. Conversion to $\mathbf{HC}^{4(\bullet+)}$, which was achieved by applying a potential of –300 mV, confirms that it is virtually "EPR silent," indicating that the four radicals are spin-paired and the compound in this redox state is diamagnetic. Shifting the potential to +100 mV to obtain $\mathbf{HC}^{2\bullet6+}$ resulted in little or no signal in the EPR trace, supporting the notion that the bisradical is also spin-paired. Moving the potential to +200 mV and holding it for 30 min led, however, to a dramatic increase in the intensity of the EPR signal as a result of the conversion to the paramagnetic $\mathbf{HC}^{\bullet7+}$.

The difference in signal intensities between the initial and +200 mV EPR traces supports the notion that an equimolar mixture of $\mathbf{HC}^{2\bullet6+}$ and $\mathbf{HC}^{\bullet7+}$ exists in equilibrium in the starting state. This observation is, of necessity, a qualitative one, since it would be inappropriate to try to quantify the spin concentration on account of the varying degrees of spin exchange between the $BIPY^{\bullet+}$ units for the different redox states of HC, not to mention the difficulty in generating exclusively, by electrochemical means, the monoradical state in solution. Increasing the potential in the positive direction to +400 mV resulted in the loss of signal in the EPR spectrum, indicating that $\mathbf{HC}^{\bullet7+}$/$\mathbf{HC}^{2\bullet6+}$ has been oxidized to $\mathbf{HC}^{8+}$. Hence, in the bisradical state, the two electrons are spin-paired and exist as a $(BIPY^{\bullet+})_2$ radical cation dimer. A solid-state CW EPR spectrum was also obtained (fig. S12) using single crystals of $\mathbf{HC}^{\bullet7+}$. The result was close to identical with that obtained in solution for the monoradical, an observation that confirms that the paramagnetism persists in the solid state. The paramagnetic character of the monoradical crystalline material ($\mathbf{HC}^{\bullet7+}$) was verified using superconducting quantum interference device magnetometry, wherein the magnetic susceptibility displayed Curie-like paramagnetic behavior (figs. S13 to S16). The spectro- and electrochemical data, as well as the magnetization results, provide a mechanistic basis for switching (Fig. 2C) between a paramagnetic ($\mathbf{HC}^{\bullet7+}$) "on" state and diamagnetic ($\mathbf{HC}^{4(\bullet+)}$ and $\mathbf{HC}^{2\bullet6+}$) "off" states.

Characterizing the location and delocalization of the radical electrons in the different redox states of the HC is of paramount importance in understanding the relationship between the (super)structure and function. Single-crystal x-ray diffraction analyses (Fig. 3) have been performed on the PF_6^- salts of (i) $\mathbf{HC}^{\bullet7+}$ (Fig. 3A), (ii) $\mathbf{HC}^{2\bullet6+}$ (Fig. 3D), and (iii) $\mathbf{HC}^{4(\bullet+)}$ (Fig. 3G), as well as (iv) the intermediate $\mathbf{DB}^{\bullet+}\subset\mathbf{CBPQT}^{2(\bullet+)}$ (figs. S8 and S9). The overall charge balances in (i), (ii), (iii), and (iv) were established by the presence of seven, six, four, and three PF_6^- ions, respectively. In (i) to (iii), the plane-to-plane distances between each pair of stacked $BIPY^{2+/\bullet+}$ units are highlighted in Fig. 3, A, D, and G. Analysis of the intermediate $\mathbf{DB}^{\bullet+}\subset\mathbf{CBPQT}^{2(\bullet+)}$ reveals that the three $BIPY^{\bullet+}$ units are evenly spaced at 3.40(1) Å apart and the $BIPY^{\bullet+}$ of $\mathbf{DB}^{\bullet+}$ is centered within the cavity of the $\mathbf{CBPQT}^{2(\bullet+)}$ ring. The dihedral angles between the pyridinium rings, which are given below each $BIPY^{\bullet+}$ unit in fig. S8, are sufficiently low to deem the rings coplanar. This flattening effect (*23*, *24*) is characteristic of $BIPY^{\bullet+}$ radical cations. This method of analysis serves as a means of identifying which BIPY units are participating in delocalization of the radical electrons. By applying this approach to the solid-state structures of $\mathbf{HC}^{\bullet7+}$ (Fig. 3A), $\mathbf{HC}^{2\bullet6+}$ (Fig. 3D), and $\mathbf{HC}^{4(\bullet+)}$ (Fig. 3G), it is possible to identify the location of electronic delocalization. In $\mathbf{HC}^{\bullet7+}$ and $\mathbf{HC}^{2\bullet6+}$, the inner $BIPY^{2(\bullet+)/\bullet3+}$ plane-to-plane separation is 3.60(1) Å and the associated dihedral angles are small and similar within $\mathbf{HC}^{2\bullet6+}$ [8.8(1)° and 9.1(1)°] and $\mathbf{HC}^{\bullet7+}$ [1.5(1)° and 0.7(1)°]. These observations suggest that radical electrons are delocalized across the two inner BIPY units, resulting in a spin-paired $(BIPY^{\bullet+})_2$ radical cation dimer for $\mathbf{HC}^{2\bullet6+}$ and a single unpaired

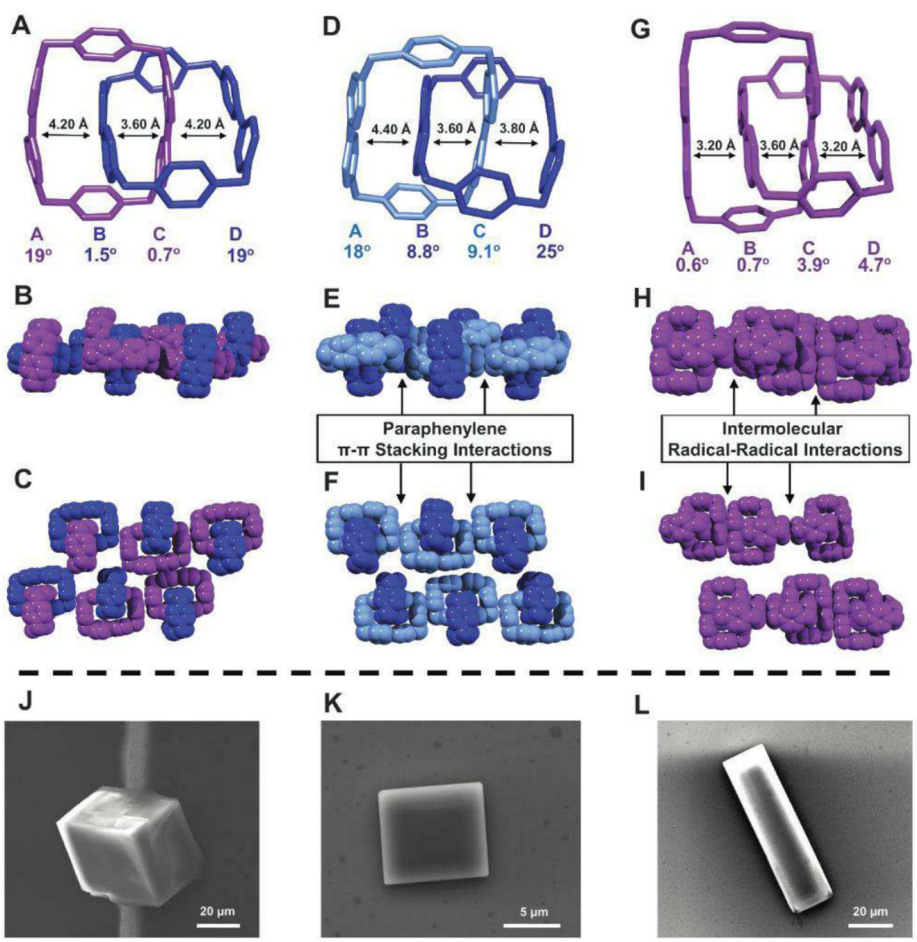

Fig. 3. Stick diagrams and space-filling representations of the x-ray crystal (super)structures of $\mathbf{HC}^{\bullet7+}$ (**A** to **C**), $\mathbf{HC}^{2\bullet6+}$ (**D** to **F**), and $\mathbf{HC}^{4(\bullet+)}$ (**G** to **I**), as well as SEM images (**J** to **L**) of the microscopic crystals that correspond to each redox state. The annotated plane-to-plane distances are those between adjacent $BIPY^{2\bullet+/\bullet+}$ units. The dihedral angles between the pyridinium rings in the $BIPY^{2+/\bullet+}$ units are listed below the stick diagrams [(A), (D), and (G)]. The space-filling representations indicate the packing arrangements of $\mathbf{HC}^{\bullet7+}$, $\mathbf{HC}^{2\bullet6+}$, and $\mathbf{HC}^{4(\bullet+)}$. The PF_6^- counterions were removed for clarity.

spin $(BIPY_2)^{\bullet 3+}$ mixed-valence dimer for $\mathbf{HC}^{\bullet 7+}$, whereas the outer dicationic $BIPY^{2+}$ units possess large dihedral angles (18° to 25°) and are participating very little, if at all, in radical delocalization. By contrast, although the solid-state structural analysis of $\mathbf{HC}^{4(\bullet+)}$ reveals (Fig. 3G) a similar plane-to-plane distance of 3.60(1) Å between the inside $BIPY^{\bullet+}$ units, the distances separating the inside and outside $BIPY^{\bullet+}$ units decrease to 3.20(1) Å—down from a range of 3.80(1) Å to 4.40(1) Å in the case of $\mathbf{HC}^{\bullet 7+}$ and $\mathbf{HC}^{2\bullet 6+}$—causing the width of the $CBPQT^{2(\bullet+)}$ rings themselves to decrease in $\mathbf{HC}^{4(\bullet+)}$. Moreover, all of the $BIPY^{\bullet+}$ units are flattened in $\mathbf{HC}^{4(\bullet+)}$, with their torsional angles all under 5°, an observation that is indicative of tetraradical formation and the complete delocalization of the four radicals between the inside and outside $BIPY^{\bullet+}$ units. Additionally, although the superstructures (Fig. 3, B and C) of $\mathbf{HC}^{\bullet 7+}$ and $\mathbf{HC}^{2\bullet 6+}$ (Fig. 3, E and F) demonstrate a total lack of intermolecular $BIPY^{\bullet+}\cdots BIPY^{\bullet+}$ interactions—leading to the formation of small cubic crystals of $\mathbf{HC}^{\bullet 7+}$ (Fig. 3J) and $\mathbf{HC}^{2\bullet 6+}$ (Fig. 3K) as observed by scanning electron microscopy (SEM)—in the case of the superstructure (Fig. 3, H and I) of $\mathbf{HC}^{4(\bullet+)}$, the individual tetraradicals pack by dint of intermolecular $BIPY^{\bullet+}\cdots BIPY^{\bullet+}$ interactions, resulting in the formation of rectangular needles (Fig. 3L) upon crystallization of $\mathbf{HC}^{4(\bullet+)}$.

The ability to control chemically the redox states, and consequently the morphologies of the crystals, augurs well for the use of the HC in device settings—for example, as semiconducting materials in organic field-effect transistors, wherein the individual $\mathbf{HC}^{4(\bullet+)}$ tetraradicals self-assemble on the surface of an SiO_2 wafer prepatterned with electrodes. Moreover, these geometrical observations, along with EPR and ultraviolet/visible/near-infrared spectroscopic data (fig. S10), suggest that there are varying degrees of electronic coupling between the inside BIPY units in $\mathbf{HC}^{2\bullet 6+}$ and $\mathbf{HC}^{\bullet 7+}$. This type of through-space mixed-valence behavior has been observed and quantified (*25*–*28*) in other organic-based systems. Further investigations into the potential for intramolecular electron transfer are currently under way in order to assign each mixed-valence species quantitatively according to Robin-Day classification (*29*).

Theoretical calculations were performed on the HC using density functional theory (DFT) (*30*) (M06 functional with the 6-311++G** basis set and using Poisson Boltzmann Finite continuum solvation). In the valence bond (VB) description, the tetraradical $\mathbf{HC}^{4(\bullet+)}$ has a singly occupied VB orbital (SOVBO) on each of the four $BIPY^{\bullet+}$ units that combine to form two paired VBs, A-B and C-D, where the four $BIPY^{\bullet+}$ units are labeled A through D as shown in Fig. 3, D and G. With DFT, the four SOVBOs are combined to form two doubly occupied molecular orbitals (MOs), of which the highest occupied (HOMO) is shown in Fig. 4A, and two empty MOs, of which the lowest unoccupied (LUMO) is shown in Fig. 4A. The delocalization of the HOMO between A and B and between C and D indicates the bonding. All of the other eight states outside of $\mathbf{HC}^{4(\bullet+)}$, ranging from $\mathbf{HC}^{0}$ to $\mathbf{HC}^{8+}$, can be visualized as adding or subtracting electrons from these four MOs. For $\mathbf{HC}^{2\bullet 6+}$, the electrons are removed from the SOVBO on A and D, making them doubly charged (stabilized by solvation) so that the doubly occupied HOMO localizes on B and C as in Fig. 4A, with the LUMO on A and D. Removing one more electron to form $\mathbf{HC}^{\bullet 7+}$ leads to the singly occupied MO (SOMO) in Fig. 4A, again on B and C, which becomes the LUMO for $\mathbf{HC}^{8+}$. Additional orbitals are shown in fig. S23.

The theoretical energies (internal energies comparable to enthalpies reported in kcal mol^{-1}) for the process of formation of the uncatenated rings into the (electro)chemically accessible states of the HC were calculated in CH_3CN solution (Fig. 4B) and in the gas phase (Fig. 4C). The results of these calculations indicate that the 8+ redox state is the most energetically unfavorable state, with an energy of 67 kcal mol^{-1} in solution and 619 kcal mol^{-1} in the gas phase, whereas the 7+ redox state has an energy of 17 kcal mol^{-1} in solution and 427 kcal mol^{-1} in the gas phase. These large differences in energy provide some explanation as to why the molecule resists complete oxidation to $\mathbf{HC}^{8+}$, but instead stops at the thermodynamic mixture $\mathbf{HC}^{\bullet 7+}/\mathbf{HC}^{2\bullet 6+}$ under ambient conditions. It is important to note that the 4+ oxidation state is the most thermodynamically stable with an energy of –127 kcal mol^{-1} in CH_3CN, an observation that is consistent with the formation of $\mathbf{HC}^{4(\bullet+)}$ in the proposed mechanism for the synthesis of the HC. Further discussion of the binding energies (table S1) for all of the redox states as well as an accurate prediction of the redox potentials (table S2) can be found in the supplementary materials.

The ease with which this radically configurable homo[2]catenane can be made and its solid-state

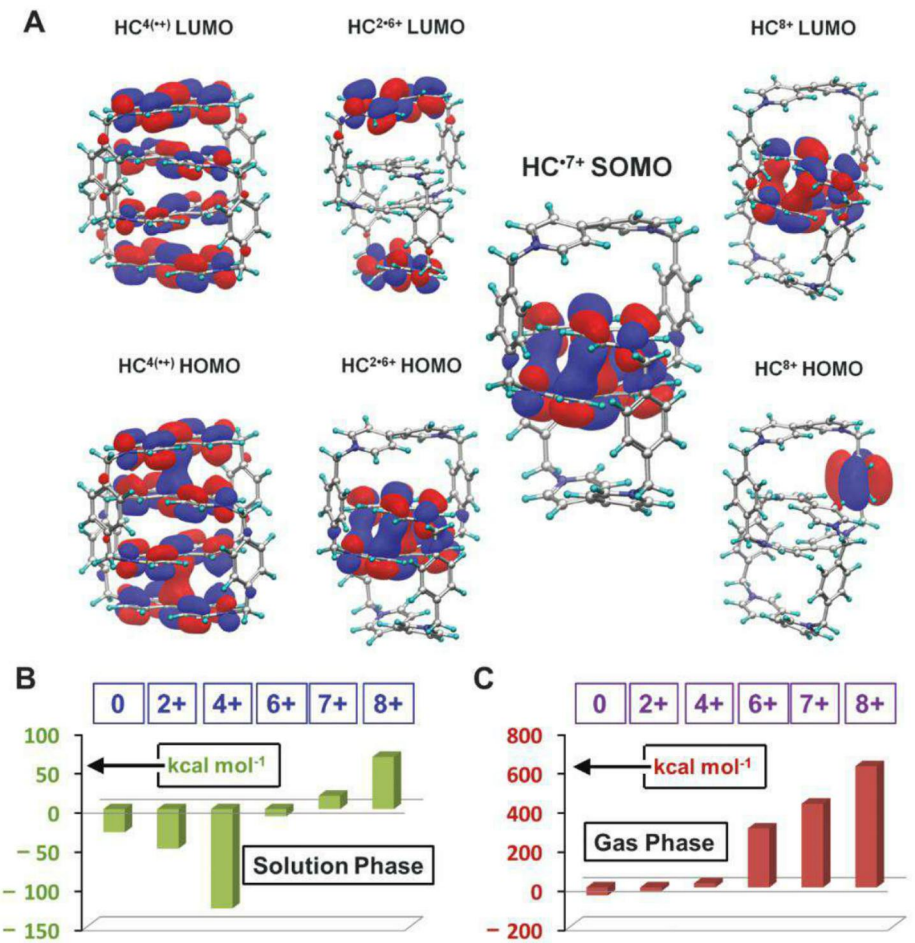

Fig. 4. (**A**) Calculated LUMOs and HOMOs for $\mathbf{HC}^{4(\bullet+)}$, $\mathbf{HC}^{2\bullet 6+}$, and $\mathbf{HC}^{8+}$, along with the SOMO for $\mathbf{HC}^{\bullet 7+}$, reveal similarities in the orbital overlaps for the HOMO of the bisradical hexacation $\mathbf{HC}^{2\bullet 6+}$ and the SOMO of the monoradical heptacation $\mathbf{HC}^{\bullet 7+}$. In both cases, there are orbital overlaps involving the two inside $BIPY^{\bullet+}$ units, supporting the notion of delocalization of the radical electrons across these two units. Although the orbital interactions for the HOMO of $\mathbf{HC}^{4(\bullet+)}$ also indicate electronic delocalization over two $BIPY^{\bullet+}$ units, they occur across both pairs of inside and outside $BIPY^{\bullet+}$ units. (**B** and **C**) Histograms summarizing the calculated binding energies (kcal mol^{-1}) between each ring at all of the (electro) chemically accessible redox states of the homo[2]catenane in CH_3CN (B) and in the gas phase (C).

morphologies controlled, combined with the fact that its monoradical state is stable under ambient conditions, gives this compound great potential for incorporation into organic radical frameworks (*31*, *32*), electronic memory devices (*33*–*35*), semiconductors (*36*), and energy storage devices (*37*).

References and Notes

1. M. Gomberg, *J. Am. Chem. Soc.* **22**, 757 (1900).
2. R. Chiarelli, M. A. Novak, A. Rassat, J. A. Tholence, *Nature* **363**, 147 (1993).
3. A. Rajca, J. Wongsriratanakul, S. Rajca, *Science* **294**, 1503 (2001).
4. S. D. J. McKinnon, B. O. Patrick, A. B. P. Lever, R. G. Hicks, *Chem. Commun.* **46**, 773 (2010).
5. B. D. Koivisto, R. G. Hicks, *Coord. Chem. Rev.* **249**, 2612 (2005).
6. A. W. Cordes, R. C. Haddon, R. T. Oakley, *Adv. Mater.* **6**, 798 (1994).
7. M. E. Itkis, X. Chi, A. W. Cordes, R. C. Haddon, *Science* **296**, 1443 (2002).
8. Y. Morita *et al.*, *Nat. Mater.* **10**, 947 (2011).
9. I. Ratera, J. Veciana, *Chem. Soc. Rev.* **41**, 303 (2012).
10. L. Michaelis, E. S. Hill, *J. Gen. Physiol.* **16**, 859 (1933).
11. L. Michaelis, *Chem. Rev.* **16**, 243 (1935).
12. E. M. Kosower, J. L. Cotter, *J. Am. Chem. Soc.* **86**, 5524 (1964).
13. E. M. Kosower, J. Hajdu, *J. Am. Chem. Soc.* **93**, 2534 (1971).
14. S. Hünig, *Pure Appl. Chem.* **15**, 109 (1967).
15. W.-S. Jeon, H.-J. Kim, C. Lee, K. Kim, *Chem. Commun.* (17): 1828 (2002).
16. A. C. Fahrenbach *et al.*, *J. Am. Chem. Soc.* **134**, 3061 (2012).
17. B. Odell *et al.*, *Angew. Chem. Int. Ed. Engl.* **27**, 1547 (1988).
18. J. M. Spruell *et al.*, *Nat. Chem.* **2**, 870 (2010).
19. A. Coskun *et al.*, *J. Am. Chem. Soc.* **133**, 4538 (2011).
20. A. Trabolsi *et al.*, *Nat. Chem.* **2**, 42 (2010).
21. L. Hao, X.-D. Zheng, T.-B. Lu, *Angew. Chem. Int. Ed.* **49**, 8148 (2010).
22. N. G. Connelly, W. E. Geiger, *Chem. Rev.* **96**, 877 (1996).
23. W. W. Porter 3rd, T. P. Vaid, *J. Org. Chem.* **70**, 5028 (2005).
24. T. M. Bockman, J. K. Kochi, *J. Org. Chem.* **55**, 4127 (1990).
25. D.-L. Sun, S. V. Rosokha, S. V. Lindeman, J. K. Kochi, *J. Am. Chem. Soc.* **125**, 15950 (2003).
26. D. Sun, S. V. Rosokha, J. K. Kochi, *J. Am. Chem. Soc.* **126**, 1388 (2004).
27. S. F. Nelsen, *Chemistry* **6**, 581 (2000).
28. P. Neta, M.-C. Richoux, A. Harriman, *J. Chem. Soc., Faraday Trans. II* **81**, 1427 (1985).
29. M. B. Robin, P. Day, *Adv. Inorg. Chem. Radiochem.* **10**, 247 (1968).
30. Jaguar 7.6, Schrödinger, LLC, New York, NY (2006).
31. D. Maspoch *et al.*, *C. R. Chim.* **8**, 1213 (2005).
32. K. Inoue, H. Iwamura, *J. Am. Chem. Soc.* **116**, 3173 (1994).
33. J. Lee *et al.*, *Angew. Chem. Int. Ed.* **50**, 4414 (2011).
34. C. P. Collier *et al.*, *Science* **289**, 1172 (2000).
35. J. E. Green *et al.*, *Nature* **445**, 414 (2007).
36. H. Usta, A. Facchetti, T. J. Marks, *Acc. Chem. Res.* **44**, 501 (2011).
37. K. Nakahara, K. Oyaizu, H. Nishide, *Chem. Lett.* **40**, 222 (2011).

Acknowledgments: The data reported in this paper are tabulated in the supplementary materials, and the crystallographic parameters of each single crystal were deposited into the Cambridge Crystallographic Data Centre, where they are freely available under reference numbers 855030, 855031, 855032, and 889233. We thank S. Shafaie for his expertise and assistance with high-resolution mass spectrometry, and the Integrated Molecular Structure Education and Research Center at Northwestern University for providing access to equipment for the relevant experiments. Molecular crystal images were produced using the UCSF Chimera package from the Resource for Biocomputing, Visualization, and Informatics at the University of California, San Francisco. The authors acknowledge our joint collaborators Turki S. Al-Saud and M. B. Alfageeh from the King Abdulaziz City of Science and Technology in Saudi Arabia. J.F.S. is supported by the Non-Equilibrium Energy Research Center, which is an Energy Frontier Research Center (EFRC) funded by the U.S. Department of Energy, Office of Basic Energy Sciences (DOE-BES) under award DESC0000989. R.C. is supported by the Argonne-Northwestern Solar Energy Research Center, which is an EFRC funded by DOE-BES under award DE-SC0001059. M.R.W. and S.M.D. are supported by the U.S. National Science Foundation under grant CHE-1012378. J.C.B. was supported by a National Defense Science and Engineering Graduate Fellowship from the U.S. Department of Defense (DOD) and gratefully acknowledges support from the Ryan Fellowship (as does D.C.) awarded under the auspices of the Northwestern University International Institute for Nanotechnology, as well as the DOD award W911NF-10-1-0510 and the DOE-BES under award DE-SC0005462. A.C.F. and D.C. are supported by a Graduate Research Fellowship from the National Science Foundation. M.A.G. was supported by a Summer Undergraduate Research Fellowship from the American Chemical Society. J.F.S., D.B., E.T., and W.A.G. are funded through the Focus Center Research Program Center on Functional Engineered Nano Architectonics. J.F.S. and A.M.Z.S. were supported under the auspices of an international collaboration supported in the United States by the NSF under grant CHE-0924620 and in the United Kingdom by the Engineering and Physical Sciences Research Council under grant EP/H003517/1. J.C.B., A.C.F., D.C., W.A.G., and J.F.S. are also supported by the World Class University program (R-31-2008-000-10055-0) funded by the Ministry of Education, Science and Technology, Republic of Korea.

Supplementary Materials

www.sciencemag.org/cgi/content/full/339/6118/429/DC1
Materials and Methods
Supplementary Text
Schemes S1 and S2
Figs. S1 to S18
Tables S1 to S3
References (*38*–*43*)

6 August 2012; accepted 5 November 2012
10.1126/science.1228429

Identification of the Long-Sought Common-Envelope Events

N. Ivanova,[1]* S. Justham,[2] J. L. Avendano Nandez,[1] J. C. Lombardi Jr.[3]

Common-envelope events (CEEs), during which two stars temporarily orbit within a shared envelope, are believed to be vital for the formation of a wide range of close binaries. For decades, the only evidence that CEEs actually occur has been indirect, based on the existence of systems that could not be otherwise explained. Here we propose a direct observational signature of CEEs arising from a physical model where emission from matter ejected in a CEE is controlled by a recombination front as the matter cools. The natural range of time scales and energies from this model, as well as the expected colors, light-curve shapes, ejection velocities, and event rate, match those of a recently recognized class of red transient outbursts.

Many binary star systems, including X-ray binaries, cataclysmic variables, close double-neutron stars, and the potential progenitors of Type Ia supernovae and short-duration γ-ray bursts, are thought to be formed by common-envelope events (CEEs). Because most stellar-mass binary merger sources for gravitational waves have experienced a CEE in their past, improved knowledge of CEEs should decrease the large uncertainty in theoretically predicted merger rates. However, the short time scale expected for CEEs suggested that we would never directly observe them, allowing us only to draw inferences from the systems produced.

A CEE begins when a binary orbit becomes unstable and decays. This might, for example, be driven purely by tidal forces (i.e., the Darwin instability), although CEEs are more commonly imagined as occurring after a period of rapid mass transfer from one star to the other (*1*). In some cases, the rate of transfer is so high that the receiving star is unable to accrete all the matter without forming a shared common envelope (CE) around the binary. This CE causes drag on one or both stars and hence orbital decay, with orbital energy and angular momentum being transferred to the CE. This may end with a stellar merger or—if the CE is ejected—the binary may survive, typically with a much reduced orbital separation, critical to explaining many observed compact binaries.

When a CEE results in formation of a close binary, it is expected that a substantial proportion of the mass is ejected—typically almost the entire envelope of one of the stars. Some mass can also be ejected in the case of a merger. This partial ejection has two causes (*2*). First, the orbital energy deposited into the CE early in the merger may exceed the binding energy of

[1]Department of Physics, University of Alberta, Edmonton, AB T6G 2E7, Canada. [2]National Astronomical Observatories, The Chinese Academy of Sciences, Beijing 100012, China. [3]Department of Physics, Allegheny College, Meadville, PA 16335, USA.

*To whom correspondence should be addressed. E-mail: nata.ivanova@ualberta.ca

the outer layers. Second, angular momentum transport may be too slow for the angular momentum absorbed by the upper layers of the envelope to be redistributed across the envelope as a whole.

Here we consider the behavior of this ejected matter to try to predict the appearance of CEEs. A situation involving similar physics—Type IIP supernovae—has been studied previously [e.g, (*3*–*5*)]. In that model, as the ejected stellar plasma expands and cools, recombination changes its opacity, leading to the propagation of a photosphere-defining "cooling wave," which moves inward with respect to the mass variable.

For smooth and spherically symmetric ejecta distributions, the model light curve will have a plateau shape: The area of the photosphere is defined by recombination, and so the emitting surface does not grow with the speed at which the ejected matter itself moves. During this phase, whereas material ejected by the CEE will expand with velocity of the order of magnitude of the initial escape velocity, the photospheric radius should appear almost constant. The luminosity L_P of the emission during the plateau (*3*–*5*), rescaled to the likely energy range of CEE, is

$$L_P \approx 1.7 \times 10^4 L_\odot \left(\frac{R_{init}}{3.5R_\odot}\right)^{2/3} \left(\frac{E_k^\infty}{10^{46}\text{erg}}\right)^{5/6} \times \left(\frac{m_{unb}}{0.03M_\odot}\right)^{-1/2} \left(\frac{\kappa}{0.32\ \text{cm}^2\text{g}^{-1}}\right)^{-1/3} \times \left(\frac{T_{rec}}{4500\ \text{K}}\right)^{4/3} \quad (1)$$

where R_{init} is the initial radius, E_k^∞ is the kinetic energy of the unbound mass m_{unb} at late times after escaping the potential well, κ is the opacity of the ionized ejecta, and T_{rec} is the recombination temperature. The duration of the plateau t_P with the same assumptions is

$$t_P \approx 17\ \text{days} \left(\frac{R_{init}}{3.5R_\odot}\right)^{1/6} \left(\frac{E_k^\infty}{10^{46}\text{erg}}\right)^{-1/6} \times \left(\frac{m_{unb}}{0.03M_\odot}\right)^{1/2} \left(\frac{\kappa}{0.32\ \text{cm}^2\text{g}^{-1}}\right)^{1/6} \times \left(\frac{T_{rec}}{4500\ \text{K}}\right)^{-2/3} \quad (2)$$

This model does not depend on the origin of the energy released during the outburst. For Type IIP supernovae, recombination controls the release of the internal energy generated by strong supernova shocks. For CEEs, however, there is no such supernova-provided energy input. Instead, the energy released by recombination itself may dominate the energy budget of many outbursts (*6*). The unbound mass m_{unb} could potentially radiate—simply due to recombination—as much energy as

$$E_{recom} \cong 2.6 \times 10^{46}\text{ergs}(X + 1.5Yf_{He})\frac{m_{unb}}{M_\odot} \quad (3)$$

Here X is the mass fraction of hydrogen and Y is the mass fraction of helium. Hydrogen would initially be ionized in almost all of the likely ejected material from most stars; however, helium may be fully ionized only in some fraction of it, denoted f_{He}. The role of recombination in a CEE has hitherto been debated in the overall energy balance, the controversy arising from whether it can be effectively converted into mechanical energy to help eject the CE (*7*–*9*). This energy budget for the outburst may be increased by the thermal energy of the ejecta. Much of the pre-CEE thermal energy of the ejecta may be expended on adiabatic cooling (*6*). However, the shock heating caused by the CEE could well be substantial in some cases.

To estimate the extent of the parameter space of CEE outbursts, we use the model described above to predict the diversity of real events. We assume that E_k^∞ scales with the gravitational potential at the surface of the primary star (*2*) and use the dimensionless factor ζ to write $E_k^\infty = \zeta(Gm_1^2 f_m)/R_{init}$, where $f_m = m_{unb}/m_1$ is the fraction of the total primary mass m_1 that becomes unbound. From Eqs. 1 and 2, this leads to $L_P \propto (f_m^2 m_1^7 R_{init}^{-1}\zeta^5)^{1/6}$ and $t_P \propto (f_m^2 m_1 R_{init}^2 \zeta^{-1})^{1/6}$. Two families of events seem likely, one for mergers (i.e., $f_m << 1$) and one for CE ejection (i.e., $f_m \leq 1$) (Fig. 1).

In addition to the predicted ranges of outburst energy and duration, this model for CEE outbursts has several noteworthy features. The physics that causes the plateau-shaped light curve should lead to a difference in the phometrically inferred expansion velocity and the actual material velocity (which could be inferred from spectra). The effective photospheric temperature should be ~5000 K for thick ejecta (*4*), and so the outburst color will naturally be red. In addition, once the ejected envelope has fully recombined, the material may suddenly become transparent, unless enough of the ejecta has cooled down sufficiently to produce dust. These characteristics are reminiscent of curious transients with predominantly red spectra that were recently detected in the local universe [e.g., (*10*–*16*, *17*)]. This empirical class has been dubbed luminous red novae (LRNe), a subset of the even more ambiguously defined class of intermediate-luminosity red transients (ILRTs) (*2*). ILRTs cover a wide range of outburst energies, from 10^{45} to a few 10^{47} ergs (brighter than the brightest novae but still fainter than Type Ia supernovae). They are characterized by spectroscopically inferred expansion velocities of 200 to 1000 km/s—much lower than would be expected for novae or supernovae and also markedly different from the photometric expansion velocities (*18*). In addition, some could be seen as red giants within a dozen years after the outburst (*16*, *19*).

It was not known what ILRTs are or whether they have a common cause; several ideas have been suggested (*2*). A model that considered the possibility that LRNe are caused by stellar mergers—a subset of CEEs—has been independently considered several times for different LRN outbursts, though further examinations of outburst features always showed various drawbacks. However, those problematic features do match expectations from our CEE-driven outburst model (*2*).

A particular feature of the LRN outbursts—as opposed to all ILRTs—is the presence of a plateau in their luminosity curves. We compare well-known LRNe (*2*) to the expected CEE diversity in Fig. 1. The agreement is pronounced, especially given the simplicity of the model and the potential complexities it neglects—e.g., how CEE ejecta deviate from spherical symmetry, or how much ζ for mergers might be different from ζ for full envelope ejection (*2*).

M85 OT2006-1 is an LRN with well-known peak luminosity and plateau duration. If the luminosity from M85 OT2006-1 was largely from recombination, ~1.5 $M_\odot$ of plasma would have recombined to provide the observed total energy. This fits with constraints on the progenitor mass ($\leq$2 $M_\odot$) from the stellar population age (*20*). Thus, M85 OT2006-1 plausibly ejected the whole envelope of a low-mass giant. This outburst showed a plateau, with luminosity $\approx 1 \times 10^6$ to 2×10^6 $L_\odot$ (*21*) for $\approx$60 to 80 days, and had expansion velocities of 350 km/s (*14*). Our inferred ejecta mass and the observed expansion velocity indicate a kinetic energy of $\sim 1.8 \times 10^{48}$ erg. Then, $R_{init} = 45\ R_\odot$, self-consistent with our model, gives $L_P \sim 10^6\ L_\odot$ and $t_P \sim 70$ days.

Another recent outburst, V1309 Sco, is similar to, but fainter than, most LRNe, as it radiated away only $\sim 3 \times 10^{44}$ erg during a ~25-day plateau-shaped maximum in the light curve (*19*). The progenitor was a contact binary with a relatively rapidly decaying orbital period of ~1.4 days. After the outburst, the system appeared to be a single star; therefore, this appears to have been a CEE, leading to a merger (*19*). However, several features of the V1309 Sco outburst, in particular the plateau in the light curve and sudden transparency, were difficult to reconcile with prior theoretical expectations for the appearance of a CEE (*2*).

Because the V1309 Sco progenitor was observed in detail, this system is ideal for testing our model. Beginning with the properties of the premerger contact binary (*19*, *22*), we calculated the amount of material that became unbound during the V1309 merger using two methods—simple energy balance using a one-dimensional (1D) stellar code and a set of 3D hydrodynamical simulations (*2*). Both methods predict that a small mass, ~0.03 to 0.08 $M_\odot$, will become unbound. Complete recombination of this ejected mass would provide enough energy ($\geq 7 \times 10^{44}$ ergs)

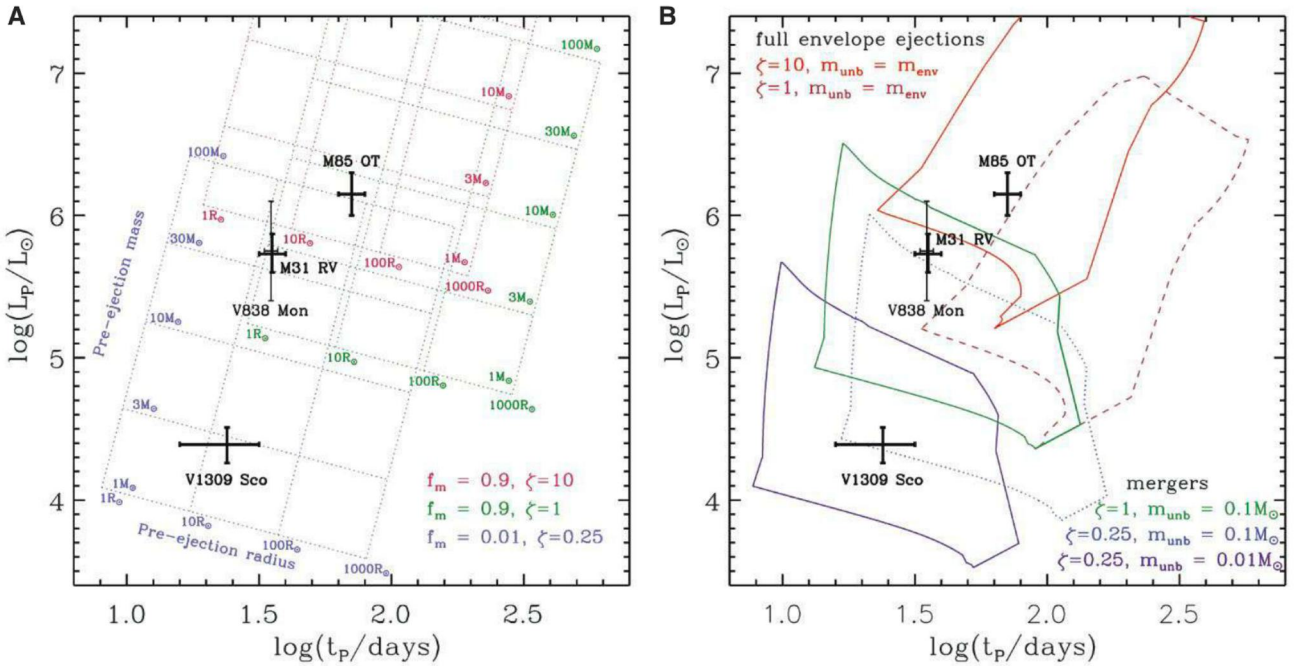

Fig. 1. (Left) Model diversity in the L_P–t_P parameter space is indicated by lines representing constant primary mass and radius. f_m is fractional mass loss and ζ is the kinetic energy at infinity, parametrized as a fraction of the binding energy at the surface of the primary star. Stellar mergers are in a regime of little mass ejection, whereas f_m = 0.9 approximates full envelope ejection. **(Right)** Estimated ranges of the plateau luminosity L_P and duration t_P for primary stars with zero-age main sequence (ZAMS) masses from 1 to 150 $M_\odot$. m_{unb} is the ejecta mass. It is assumed that mergers can happen anytime during the primary star's evolution, whereas full envelope ejection can occur only for post–main-sequence primary stars. We used fitting formulae for stellar evolution (*24*), at $Z_\odot$. In both panels, values for L_P and t_P are marked for the outbursts from V1309 Sco, M85 OT, M31-RV, and V838 Mon.

to explain the total energy output of V1309 Sco. The output of the 3D simulations, combined with Eqs. 1 and 2, predicts plateau durations from 16 to 25 days and plateau luminosities of 1.8×10^4 to 2.2×10^4 $L_\odot$. These values match the observed luminosity ($L_P \sim 2 \times 10^4 L_\odot$) and plateau duration (about 25 days).

Considering the menagerie of theoretically expected outbursts from CEEs, we note that events in the top right of Fig. 1 should be relatively rare [compare with η Car; see (*2*)], and those in the bottom left (stellar mergers) comparatively hard to detect in a magnitude-limited survey. Assuming that the peak luminosity of the outburst is about an order of magnitude higher than L_P, we find that the whole range of L_P and t_P for stellar masses 1 to 150 $M_\odot$ coincides well with the observed domain for luminosities and durations of LRNe suggested in (*23*). We can estimate the rate of CEE-originated outbursts that appear as red transients, by considering what fraction of stars in the galaxy undergo a CEE. We estimate 0.024 such events per year per Milky Way–like galaxy (*2*), of which about half should be more luminous outbursts (results of a CE ejection) and half are lower-luminosity events (powered by stellar mergers). This is consistent with the empirical lower limit for more luminous ILRTs of 0.019 $year^{-1}$ for the Galaxy (*20*), because we do not expect that all luminous ILRTs must be powered by a CEE [though some non-LRN ILRTs, like NGC 300-OT or SN2008S, might potentially also be triggered by CEEs (*2*)].

The question of whether recombination energy can help to unbind a stellar envelope during a CEE is important for understanding the formation and survival of many binary systems (*8*, *9*). Our model suggests that a large fraction of the energy from recombination is commonly radiated away after a CEE. Such luminosity provides a beacon, which helps to illuminate and identify a CE ejection or merger at large distances. The recombination wave also controls the shape of the plateau-shaped light curve of LRNe. We therefore suggest that detecting and characterizing the population of ILRTs will help us understand CEEs.

References and Notes

1. N. Ivanova, *Astron. Soc. Pac. Conf. Ser.* **447**, 91 (2011).
2. Materials and methods are available as supplementary materials on *Science* Online.
3. N. N. Chugai, *Sov. Astron. Lett.* **17**, 210 (1991).
4. D. V. Popov, *Astrophys. J.* **414**, 712 (1993).
5. D. Kasen, S. E. Woosley, *Astrophys. J.* **703**, 2205 (2009).
6. D. Kasen, E. Ramirez-Ruiz, *Astrophys. J.* **714**, 155 (2010).
7. I. Iben Jr., M. Livio, *Publ. Astron. Soc. Pac.* **105**, 1373 (1993).
8. Z. Han, P. Podsiadlowski, P. P. Eggleton, *Mon. Not. R. Astron. Soc.* **270**, 121 (1994).
9. R. F. Webbink, *Astrophys. Space Sci. Libr.* **352**, 233 (2008).
10. J. Mould *et al.*, *Astrophys. J.* **353**, L35 (1990).
11. P. Martini *et al.*, *Astron. J.* **118**, 1034 (1999).
12. H. E. Bond *et al.*, *Nature* **422**, 405 (2003).
13. S. R. Kulkarni *et al.*, *Nature* **447**, 458 (2007).
14. A. Pastorello *et al.*, *Nature* **449**, E1 (2007).
15. H. E. Bond *et al.*, *Astrophys. J.* **695**, L154 (2009).
16. H. E. Bond, *Astrophys. J.* **737**, 17 (2011).
17. M. M. Kasliwal *et al.*, *Astrophys. J.* **730**, 134 (2011).
18. E. Berger *et al.*, *Astrophys. J.* **699**, 1850 (2009).
19. R. Tylenda *et al.*, *Astron. Astrophys.* **528**, A114 (2011).
20. E. O. Ofek *et al.*, *Astrophys. J.* **674**, 447 (2008).
21. A. Rau, S. R. Kulkarni, E. O. Ofek, L. Yan, *Astrophys. J.* **659**, 1536 (2007).
22. K. Stępień, *Astron. Astrophys.* **531**, A18 (2011).
23. A. Rau *et al.*, *Publ. Astron. Soc. Pac.* **121**, 1334 (2009).
24. J. R. Hurley, O. R. Pols, C. A. Tout, *Mon. Not. R. Astron. Soc.* **315**, 543 (2000).

Acknowledgments: N.I. acknowledges support from the Natural Sciences and Engineering Research Council of Canada and Canada Research Chairs Program. S.J. acknowledges support from the Chinese Academy of Sciences and National Natural Science Foundation of China. J.L.A.N. acknowledges support from Consejo Nacional de Ciencia y Tecnología. J.C.L. thanks R. Scruggs for useful discussions. This research has been enabled by the use of computing resources provided by WestGrid and Compute/Calcul Canada as well as the Extreme Science and Engineering Discovery Environment (supported by NSF grant OCI-1053575).

Supplementary Materials

www.sciencemag.org/cgi/content/full/339/6118/433/DC1
Supplementary Text
Figs. S1 to S4
Table S1
References (*25*–*74*)
Movies S1 and S2

4 June 2012; accepted 29 November 2012
10.1126/science.1225540

Synchronous X-ray and Radio Mode Switches: A Rapid Global Transformation of the Pulsar Magnetosphere

W. Hermsen,[1,2]* J. W. T. Hessels,[2,3] L. Kuiper,[1] J. van Leeuwen,[2,3] D. Mitra,[4] J. de Plaa,[1] J. M. Rankin,[2,5] B. W. Stappers,[6] G. A. E. Wright,[7] R. Basu,[4] A. Alexov,[8] T. Coenen,[2] J.-M. Grießmeier,[9,10] T. E. Hassall,[6,11] A. Karastergiou,[12] E. Keane,[13] V. I. Kondratiev,[3,14] M. Kramer,[6,13] M. Kuniyoshi,[13] A. Noutsos,[13] M. Serylak,[9,10] M. Pilia,[3] C. Sobey,[13] P. Weltevrede,[6] K. Zagkouris,[12] A. Asgekar,[3] I. M. Avruch,[1,3,15] F. Batejat,[16] M. E. Bell,[11,17] M. R. Bell,[18] M. J. Bentum,[3,19] G. Bernardi,[20] P. Best,[21] L. Bîrzan,[22] A. Bonafede,[23] F. Breitling,[24] J. Broderick,[11] M. Brüggen,[23] H. R. Butcher,[3,25] B. Ciardi,[18] S. Duscha,[3] J. Eislöffel,[26] H. Falcke,[3,13,27] R. Fender,[11] C. Ferrari,[28] W. Frieswijk,[3] M. A. Garrett,[3,22] F. de Gasperin,[23] E. de Geus,[3] A. W. Gunst,[3] G. Heald,[3] M. Hoeft,[26] A. Horneffer,[13] M. Iacobelli,[22] G. Kuper,[3] P. Maat,[3] G. Macario,[28] S. Markoff,[2] J. P. McKean,[3] M. Mevius,[3,15] J. C. A. Miller-Jones,[2,29] R. Morganti,[3,15] H. Munk,[3] E. Orrú,[3,27] H. Paas,[30] M. Pandey-Pommier,[22,31] V. N. Pandey,[32] R. Pizzo,[3] A. G. Polatidis,[3] S. Rawlings,[12] W. Reich,[13] H. Röttgering,[22] A. M. M. Scaife,[11] A. Schoenmakers,[3] A. Shulevski,[15] J. Sluman,[3] M. Steinmetz,[24] M. Tagger,[9] Y. Tang,[3] C. Tasse,[33,34,35] S. ter Veen,[27] R. Vermeulen,[3] R. H. van de Brink,[3] R. J. van Weeren,[3,20,22] R. A. M. J. Wijers,[2] M. W. Wise,[2,3] O. Wucknitz,[13,36] S. Yatawatta,[3] P. Zarka[33]

Pulsars emit from low-frequency radio waves up to high-energy gamma-rays, generated anywhere from the stellar surface out to the edge of the magnetosphere. Detecting correlated mode changes across the electromagnetic spectrum is therefore key to understanding the physical relationship among the emission sites. Through simultaneous observations, we detected synchronous switching in the radio and x-ray emission properties of PSR B0943+10. When the pulsar is in a sustained radio-"bright" mode, the x-rays show only an unpulsed, nonthermal component. Conversely, when the pulsar is in a radio-"quiet" mode, the x-ray luminosity more than doubles and a 100% pulsed thermal component is observed along with the nonthermal component. This indicates rapid, global changes to the conditions in the magnetosphere, which challenge all proposed pulsar emission theories.

Radio pulsars are powered by the energy released as the highly magnetized neutron star spins down. The radio pulses are generated in the pulsar magnetosphere, probably close to the neutron star surface (*1*, *2*). Shortly after the discovery of pulsars, it was observed that the radio pulse behavior can discretely change on time scales as short as a rotation period. These changes in emission mode can manifest as switches between ordered and disordered states or variations in intensity and pulse shape, including the complete cessation of observable radio emission (*3*, *4*).

Because the emitted radio luminosity is a negligible fraction of the available spin-down energy, usually substantially less than 10^{-5}, this phenomenology was presumed to be related solely to microphysics of the radio emission mechanism itself. This perception has recently been challenged by the identification of a relationship between the spin properties of neutron stars and their radio emission modes. PSR B1931+24 was observed to cease emitting for tens of days, during which it spins down ~50% less rapidly (*5*). PSR J1841–0500 (*6*) and PSR J1832+0029 (*7*) exhibit similar behaviors. A number of other pulsars display smaller changes in spin-down rate, which correlate with variations in their average radio pulse shapes (*8*). The implication of these results is that mode changing is due to an inherent, perhaps universal pulsar process that causes a sudden change in the rate of angular momentum loss, which is communicated along the open field lines of the magnetosphere. Whereas changes in spin-down rate can only be detected on time scales of a few days or longer, the recently identified link with the rapid switching observed in radio emission modes suggests a transformation of the global magnetospheric state in less than a rotation period. Despite the recent flurry of pulsar detections at high energies (*9*), the only causal relation between the radio pulses and emission at other wavelengths, likely emanating from different locations in the magnetosphere, has been made for optical emission and giant radio pulses from the Crab pulsar (*10*).

PSR B0943+10 is a paragon of mode-changing pulsars. Relatively old (characteristic age 5 million years), with a long spin period (1.1 s), it switches at intervals of several hours between a radio-bright, highly organized mode (B) and a quieter chaotic mode (Q) (*11*, *12*). At the B- to Q-mode transition, a subpulse drifting structure dissolves within a few seconds, the emission becomes disorganized, and an additional highly polarized radio component appears, preceding the main pulse by 52° of pulse longitude (*13*). PSR B0943+10 has also been detected in two short observations with the XMM-Newton observatory as a weak x-ray source (*14*). These observations, under the assumption that the x-rays are thermal, were used to support a model in which one system of streaming particles produces the subpulse-modulated radio emission directly, and also results in thermal x-ray emission through bombardment of the polar cap surface (*15*). Because the particle streams are thought to be determined by the magnetosphere as a whole, detection of simultaneous x-ray and radio mode switching would uniquely probe the interaction between local and global electromagnetic behavior. Moreover, this would

[1]SRON, Netherlands Institute for Space Research, Sorbonnelaan 2, 3584 CA Utrecht, Netherlands. [2]Astronomical Institute "Anton Pannekoek," University of Amsterdam, Postbus 94249, 1090 GE Amsterdam, Netherlands. [3]ASTRON, Netherlands Institute for Radio Astronomy, Postbus 2, 7990 AA Dwingeloo, Netherlands. [4]National Centre for Radio Astrophysics (NCFRA-TIFR), Post Bag 3, Ganeshkhind, Pune University Campus, Pune 411007, India. [5]Physics Department, University of Vermont, Burlington, VT 05405, USA. [6]Jodrell Bank Center for Astrophysics, School of Physics and Astronomy, University of Manchester, Manchester M13 9PL, UK. [7]Astronomy Centre, University of Sussex, Falmer, Brighton BN1 9QJ, UK. [8]Space Telescope Science Institute (STScI), 3700 San Martin Drive, Baltimore, MD 21218, USA. [9]Laboratoire de Physique et Chimie de l'Environnement et de l'Espace, LPC2E CNRS/Université d'Orléans, 45071 Orléans Cedex 02, France. [10]Station de Radioastronomie de Nançay, Observatoire de Paris, CNRS/INSU, 18330 Nançay, France. [11]School of Physics and Astronomy, University of Southampton, Southampton SO17 1BJ, UK. [12]Astrophysics, University of Oxford, Oxford OX1 3RH, UK. [13]Max-Planck-Institut für Radioastronomie, Auf dem Hügel 69, 53121 Bonn, Germany. [14]Astro Space Center of the Lebedev Physical Institute, Profsoyuznaya str. 84/32, Moscow 117997, Russia. [15]Kapteyn Astronomical Institute, P.O. Box 800, 9700 AV Groningen, Netherlands. [16]Onsala Space Observatory, Department of Earth and Space Sciences, Chalmers University of Technology, SE-43992 Onsala, Sweden. [17]ARC Centre of Excellence for All-Sky Astrophysics (CAASTRO), Sydney Institute of Astronomy, University of Sydney, Sydney, NSW 2006, Australia. [18]Max Planck Institute for Astrophysics, Karl Schwarzschild Str. 1, 85741 Garching, Germany. [19]University of Twente, P.O. Box 217, 7500 AE Enschede, Netherlands. [20]Harvard-Smithsonian Center for Astrophysics, 60 Garden Street, Cambridge, MA 02138, USA. [21]Institute of Astronomy, University of Edinburgh, Royal Observatory of Edinburgh, Blackford Hill, Edinburgh EH9 3HJ, UK. [22]Leiden Observatory, Leiden University, P.O. Box 9513, 2300 RA Leiden, Netherlands. [23]Hamburger Sternwarte, University of Hamburg, Gojenbergsweg 112, 21029 Hamburg, Germany. [24]Leibniz-Institut für Astrophysik Potsdam (AIP), An der Sternwarte 16, 14482 Potsdam, Germany. [25]Research School of Astronomy and Astrophysics, Australian National University, Mt. Stromlo Observatory, via Cotter Road, Weston, ACT 2611, Australia. [26]Thüringer Landessternwarte, Sternwarte 5, D-07778 Tautenburg, Germany. [27]Department of Astrophysics/IMAPP, Radboud University Nijmegen, P.O. Box 9010, 6500 GL Nijmegen, Netherlands. [28]Laboratoire Lagrange, UMR7293, Université de Nice Sophia-Antipolis, CNRS, Observatoire de la Côte d'Azur, 06300 Nice, France. [29]International Centre for Radio Astronomy Research, Curtin University, G.P.O. Box U1987, Perth, WA 6845, Australia. [30]Center for Information Technology (CIT), University of Groningen, 9747 AJ Groningen, Netherlands. [31]Centre de Recherche Astrophysique de Lyon, Observatoire de Lyon, 9 av. Charles André, 69561 Saint Genis Laval Cedex, France. [32]National Radio Astronomy Observatory, 520 Edgemont Road, Charlottesville, VA 22903, USA. [33]LESIA-Observatoire de Paris, CNRS, UPMC Université Paris-Diderot, 92190 Meudon, France. [34]Department of Physics and Electronics, Rhodes University, P.O. Box 94, Grahamstown 6140, South Africa. [35]SKA South Africa, 3rd Floor, The Park, Park Road, Pinelands 7405, South Africa. [36]Argelander-Institut für Astronomie, University of Bonn, Auf dem Hügel 71, 53121 Bonn, Germany.

*To whom correspondence should be addressed. E-mail: w.hermsen@sron.nl

strengthen the earlier conclusion that entire magnetospheres change, settling down within a few seconds.

To test these hypotheses, we carried out a simultaneous x-ray and radio observing campaign on PSR B0943+10 from 4 November to 4 December 2011. These observations were designed to investigate what changes, if any, occurred in the x-rays when the radio emission changed mode. The x-ray observations consisted of six 6-hour observations in the 0.2- to 10-keV energy band with ESA's XMM-Newton space observatory (*16*) (table S1), accompanied by radio observations with the Giant Metrewave Radio Telescope (GMRT) in India at 320 MHz and the international Low Frequency Array (LOFAR) at 140 MHz, both simultaneously.

To identify the radio B- and Q-mode time windows, we folded the radio pulse sequences with up-to-date ephemerides from the Jodrell Bank long-term timing program (*17*) (Fig. 1). We could determine the times of mode switches from GMRT and LOFAR data with an accuracy of a few seconds. Table S2 lists the used B- and Q-mode time windows, which completely cover our XMM-Newton observations. In the ~30 hours of usable x-ray observations, PSR B0943+10 spent roughly equal amounts of time in the B and Q modes.

PSR B0943+10 was clearly detected in each of our XMM-Newton observations with the simultaneously used charge-coupled device (CCD) detectors PN (*18*) and MOS-1+2 (*19*) of the European Photon Imaging Camera (EPIC). The derived count rates ranged from that of the previously reported value for the PN detector of 0.38 (±0.07) × 10^{-2} counts/s (0.5 to 8 keV) (*14*) up to about twice that value, providing evidence for x-ray variability in an old, rotation-powered pulsar. Dividing the 0.2- to 10-keV x-ray events into the radio-derived B- and Q-mode time windows, we found the x-ray count rate to be higher in the radio Q mode than in the B mode by more than a factor of 2 (fig. S1). In the B mode, the PN CCDs had a count rate of 0.44 (±0.07) × 10^{-2} counts/s, whereas in the Q mode this more than doubled to 1.08 (±0.08) × 10^{-2} counts/s. This finding was independently confirmed with the MOS detectors, providing evidence for simultaneous mode switching in the radio and x-ray properties.

To search for x-ray pulsations, we selected events recorded by the PN and MOS-1+2 CCDs that arrived in the Q-mode time window and within a radius of 15 arc sec from the source position. From this, we obtained a 6.6σ detection of a pulsed signal (Fig. 2B, top) at a period consistent with the rotational frequency predicted by the Jodrell Bank ephemeris (table S3). The pulse profile (energies of 0.5 to 2 keV) is broad. Surprisingly, the x-ray events detected during the radio B mode do not show any evidence for a pulsed signal (Fig. 2A, top). Figure 2 shows that the broad x-ray pulse in the Q mode covers the phases of the main radio pulse and precursor; the latter is clearly visible in the Q mode, 52° (0.14 phase) ahead of the main pulse at 320 MHz (Fig. 2B).

X-ray spectral analysis (*16*) revealed two components in the Q mode. The best spectral fit to the total (i.e., pulsed and unpulsed) spectrum is the sum of a power-law component and a thermal blackbody component (Fig. 3A; fit parameters in Table 1 and table S4). The spectrum of the pulsed component in the Q mode is best described by a single thermal blackbody model (Fig. 3B, Table 1, and table S4). It appears that the spectral fits to the thermal component in the total Q-mode spectrum and the thermal pulsed spectrum in the Q mode are statistically consistent (Δ flux = 0.1σ, ΔkT = 2.5σ). This means that the Q-mode total x-ray emission consists of an unpulsed component with a steep, nonthermal power-law spectrum, and a ~100% pulsed component with a thermal blackbody spectrum. This is also reflected in the variation of the pulsed fraction with energy (table S5). In the B mode, the spectrum can be satisfactorily described with a single power law as well as a single blackbody shape (table S4). However, the most likely shape is a nonthermal spectrum (Fig. 3C), indistinguishable from the nonthermal component in the total Q-mode spectrum (supplementary text).

PSR B0943+10 is one of only 10 old (characteristic age >1 million years), nonrecycled radio pulsars where x-ray emission has also been detected (*20*–*22*). Although the surfaces of such pulsars have cooled substantially since birth, the observed x-ray emission is argued to be thermal in

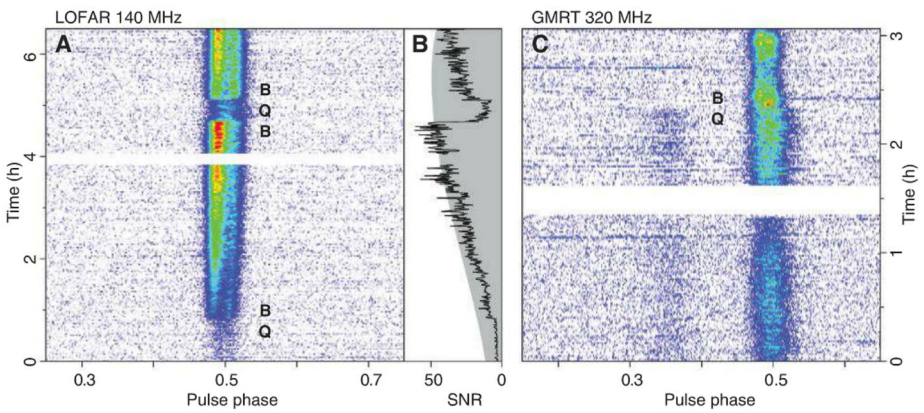

Fig. 1. (**A**) Identification of the B and Q modes with LOFAR at 140 MHz during XMM-Newton observation 1, showing pulse intensity versus rotational phase and time. A 10-min section (at the 4-hour mark) contaminated by interference is blanked out. (**B**) Comparison of the measured signal-to-noise ratio (SNR) and the nominal relative LOFAR sensitivity, changing with elevation throughout the observation (gray scale), normalized over the 4.0- to 4.5-hour range. (**C**) GMRT detection at 320 MHz of a Q- to B-mode transition in XMM-Newton observation 5. Color scale is optimized to show the simultaneous disappearance of the precursor pulse at phase ~0.35. A 15-min section (at the 1.5-hour mark) used for rephasing on a continuum source is blanked out.

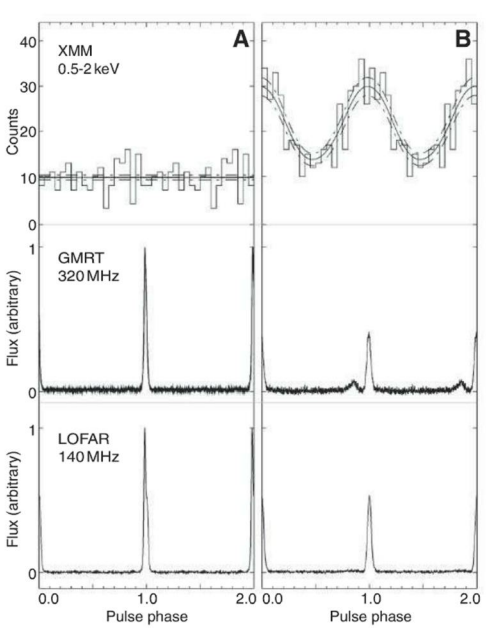

Fig. 2. Aligned x-ray and radio pulse profiles of PSR B0943+10 in its B and Q modes. (**A**) B mode: There is no evidence for a pulsed signal in the B-mode x-ray data, the flat distribution showing constant emission from the pulsar. (**B**) Q mode: The x-ray profile in the Q mode represents a 6.6σ detection on top of a flat constant level. The solid and dashed lines in the x-ray profiles are the kernel density estimator and ±1σ levels. The weak precursor, present only in the Q mode, is clearly visible in the GMRT radio profile at 320 MHz at 52° (0.14 phase) prior to the main pulse, and verified to be also weakly present in the LOFAR Q-mode profile.

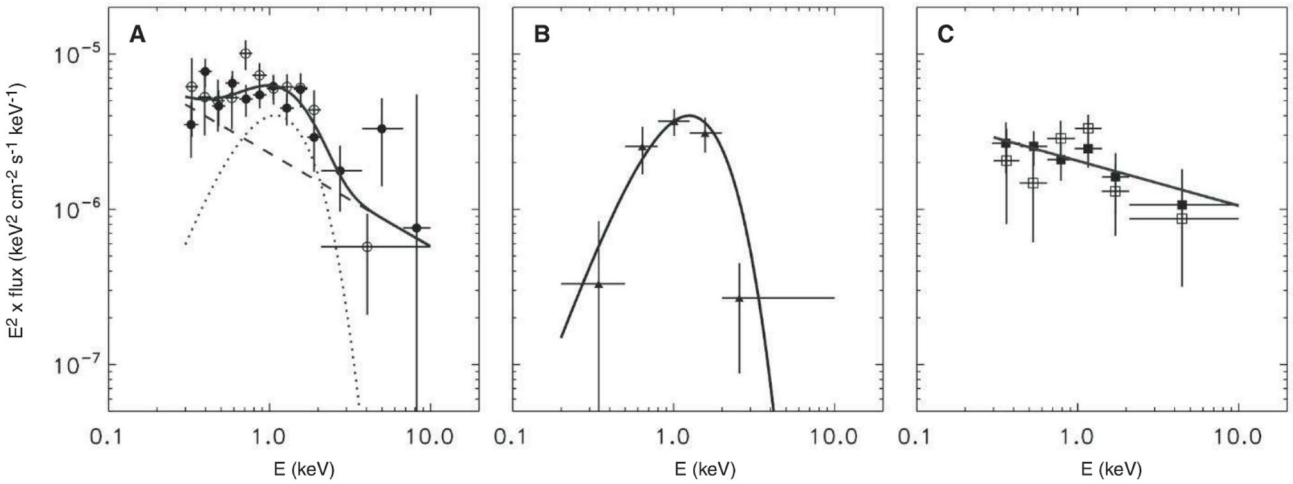

Fig. 3. Unabsorbed (i.e., corrected for absorption by interstellar gas along the line of sight) x-ray photon spectra of PSR B0943+10. (**A**) Total (i.e., pulsed and unpulsed) spectrum from spatial analyses of skymaps of Q-mode events from the XMM EPIC PN CCDs (solid symbols) and MOS1+2 CCDs (open symbols). The solid line shows the best model fit consisting of a power-law component (broken line) and a blackbody component (dotted line). (**B**) The spectrum of the pulsed emission detected only in the Q mode, analyzing the pulse profiles measured with the PN and MOS1+2 CCDs. The solid curve shows the best blackbody fit. (**C**) The total spectrum, as in (A), but here for the B-mode time windows. The solid line shows the best-fit power-law spectrum. The thermal blackbody components in (A) and (B) are statistically the same; the nonthermal power-law components in (A) and (C) are also fully consistent with being identical. All error bars are 1σ. For fit parameters, see Table 1.

Table 1. Spectral parameters for the best model fits to the x-ray spectra shown in Fig. 3. Fits are made with a blackbody (BB) shape and/or a power-law (PL) shape for the total and the pulsed emissions in the Q-mode window and the total emission in the B-mode. The column density N_H has been fixed at 4.3×10^{20} cm^{-2}. Flux values are given for energies 0.5 to 8 keV.

Mode	Model	BB (kT) (keV)	PL index Γ ($\alpha E^{-\Gamma}$)	BB flux, unabs. (10^{-15} erg cm^{-2} s^{-1})	PL flux, unabs. (10^{-15} erg cm^{-2} s^{-1})	χ^2_{red} (df)
Q total	BB + PL	0.277 ± 0.012	2.60 ± 0.34	7.52 ± 2.20	7.55 ± 1.81	0.81 (20)
Q pulsed	BB	0.319 ± 0.012	—	7.81 ± 1.64	—	0.38 (3)
B total	PL	—	2.29 ± 0.16	—	7.69 ± 1.00	0.74 (10)

some cases. This has led to the conclusion that such pulsars may have "hotspots" on their magnetic polar caps, generated by the bombardment of particles accelerated in the radio emission process. In all models, the bombarding particles result from pair creation in the pulsar magnetosphere. In polar vacuum gap models (*1*, *23*), this occurs directly above the surface. Recent adaptations of the model (*15*) predict the thermal x-ray brightness of pulsars that exhibit regular modulation of their radio subpulse drift. Such modulation is indeed observed in the B mode of PSR B0943+10 (*24*), and the original x-ray detection of this pulsar (*14*) was considered to support this prediction under the assumption that the x-rays have a thermal origin. However, the reported count rate suggests that the pulsar was in the B mode during those observations, whereas our spectral analysis shows that the x-ray emission in the B mode is actually nonthermal. Surprisingly, we detect strong thermal x-rays only in the Q mode, where the observed radio emission is weak and chaotic.

Space charge–limited flow models (*2*) also feature pair-created particles that heat the polar cap via backflow. These differ from polar gap models, however, in that charged primary particles are freely drawn from the neutron star surface. The thermal luminosities predicted for older pulsars (*25*) fall below what is observed in PSR B0943+10's Q mode and below the model's expected nonthermal cascade emission, consisting of contributions from curvature radiation, inverse Compton scattering, and synchrotron radiation (*26*). Such nonthermal emission, expected on open field lines, would almost certainly be mode-dependent, in contrast to what we observe.

Modeling of PSR B0943+10's geometry (*27*) strongly argues that the magnetic and spin axes are nearly aligned, with our line of sight passing near the pole (*24*) (Fig. 4A). This implies that the isotropically emitted x-rays of a polar hotspot should appear unmodulated throughout the rotation period, contrary to the observed Q-mode x-ray pulsations. One possible implication is that the observed x-ray pulsations result from time-dependent scattering of the emission within the closed magnetosphere (Fig. 4B)—a scenario similar to that proposed to explain magnetospheric eclipses of pulsed radio emission in the double pulsar system PSR J0737–3039 (*28*, *29*). If so, then the observed thermal emission in the Q mode is only about half the actual hotspot emission, doubling the inferred area of the hotspot.

If scattering plays an important role in the Q mode, the absence of x-ray pulsations and thermal x-rays in the B mode may be attributed to increased scattering. As suggested to explain nulling and mode switching in radio pulsars (*30*), an expansion in the volume of the closed magnetosphere might accompany the mode change, although it is unlikely to achieve the required degree of screening. It thus appears that at B-mode onset, the surface hotspot emission is reduced to undetectable levels within a few seconds, induced by a drastic reduction in the downward flow of charged particles.

In the context of the polar gap model, it has been suggested (*31*) that mode changes occur when the local surface temperature crosses a critical value, ~10^6 K, that separates dominant emission mechanisms. This would require hotspots to be detectable in both modes, in contradiction with our results. B-mode emission may represent a cooler mode where curvature radiation dominates. However, the temperature transition remains unexplained, and our results strongly suggest that a global rather than local mechanism is

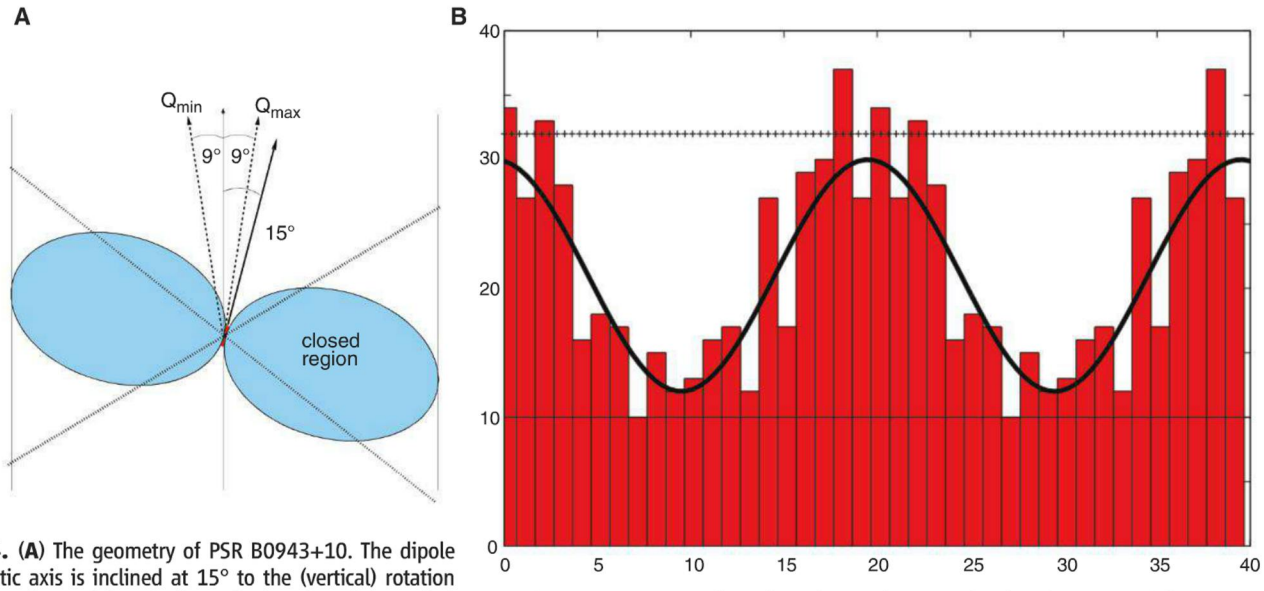

Fig. 4. (**A**) The geometry of PSR B0943+10. The dipole magnetic axis is inclined at 15° to the (vertical) rotation axis; the diagonal lines indicate the location of the null-charge surface, separating regions of positive and negative charge. As the pulsar rotates, the observer's line of sight maintains an angle of 9° to the rotation axis, with Q_{max} indicating the alignment when the radio pulse is seen (in both modes). The blue region indicates the supposed closed region, bounded by the light cylinder (at which the corotating magnetosphere reaches a rotation velocity equal to the speed of light) at 52,000 km. (**B**) If, in a toy model, extinction of thermal x-rays from the polar cap is proportional to the extent of the traversed closed region (~10,000 km at Q_{min} and ~500 km at Q_{max}), then we obtain a sinusoidal fit to the observed Q-mode x-ray pulse, so that maximum recorded emission corresponds to minimum extinction and vice versa. The lower horizontal line corresponds to the level of steady nonthermal emission and demonstrates that extinction of the thermal emission is near total at Q_{min}. The upper horizontal line then represents the level of actual unscattered x-ray emission from the polar cap.

required. Indeed, for a near-aligned pulsar such as PSR B0943+10, a range of quasi-stable magnetospheric configurations is expected (*32*, *33*), and the nonlinear system is proposed to suddenly switch between specific states, each having a specific emission beam and spin-down rate (*30*).

Whatever the true nature of the mode switch, the contrast between the Q mode's enhanced x-ray emission and reduced radio emission may well be illusory. Radio emission is only sampled on field lines instantaneously directed toward us, and our line of sight (*34*) makes only a grazing traverse of the polar cap. The core region of this polar cap, the probable site of x-ray hotspots, remains invisible to us at radio frequencies and may well change differently.

The totality of the mode transition in PSR B0943+10—changes in radio subpulse behavior and profile, the appearance of a precursor and, now, the switching on and off in x-rays of a likely hotspot—implies that we are dealing with a rapid and global magnetospheric state change. Through radio and x-ray "before" and "after" snapshots, we have shown that a magnetosphere 10 times the size of Earth completely changes personality within a few seconds; such a near-instantaneous transformation challenges our current understanding of pulsars and magnetospheres in general.

References and Notes

1. M. Ruderman, P. Sutherland, *Astrophys. J.* **196**, 51 (1975).
2. J. Arons, E. T. Scharlemann, *Astrophys. J.* **231**, 854 (1979).
3. D. C. Backer, *Nature* **228**, 42 (1970).
4. K. H. Hesse, R. Wielebinski, *Astron. Astrophys.* **31**, 409 (1974).
5. M. Kramer, A. G. Lyne, J. T. O'Brien, C. A. Jordan, D. R. Lorimer, *Science* **312**, 549 (2006).
6. F. Camilo, S. M. Ransom, S. Chatterjee, S. Johnston, P. Demorest, *Astrophys. J.* **746**, 63 (2012).
7. D. R. Lorimer *et al.*, *Astrophys. J.* **758**, 141 (2012).
8. A. Lyne, G. Hobbs, M. Kramer, I. Stairs, B. W. Stappers, *Science* **329**, 408 (2010).
9. A. A. Abdo *et al.*, *Astrophys. J. Suppl. Ser.* **187**, 460 (2010).
10. A. Shearer *et al.*, *Science* **301**, 493 (2003).
11. S. A. Suleymanova, V. A. Izvekova, *Sov. Astron.* **28**, 32 (1984).
12. J. M. Rankin, S. A. Suleymanova, *Astron. Astrophys.* **453**, 679 (2006).
13. I. Backus, D. Mitra, J. Rankin, *Mon. Not. R. Astron. Soc.* **404**, 30 (2010).
14. B. Zhang, D. Sanwal, G. G. Pavlov, *Astrophys. J.* **624**, L109 (2005).
15. J. Gil, G. Melikidze, B. Zhang, *Astrophys. J.* **650**, 1048 (2006).
16. See supplementary materials on *Science* Online.
17. G. Hobbs, A. G. Lyne, M. Kramer, C. E. Martin, C. Jordan, *Mon. Not. R. Astron. Soc.* **353**, 1311 (2004).
18. L. Strüder *et al.*, *Astron. Astrophys.* **365**, L18 (2001).
19. M. J. L. Turner *et al.*, *Astron. Astrophys.* **365**, L27 (2001).
20. W. Becker *et al.*, *Astrophys. J.* **615**, 908 (2004).
21. J. Gil *et al.*, *Astrophys. J.* **686**, 497 (2008).
22. W. W. Zhu *et al.*, *Astrophys. J.* **734**, 44 (2011).
23. J. Gil, M. Sendyk, *Astrophys. J.* **541**, 351 (2000).
24. A. A. Deshpande, J. M. Rankin, *Mon. Not. R. Astron. Soc.* **322**, 438 (2001).
25. A. K. Harding, A. G. Muslimov, *Astrophys. J.* **568**, 862 (2002).
26. B. Zhang, A. K. Harding, *Astrophys. J.* **532**, 1150 (2000).
27. J. M. Rankin, *Astrophys. J.* **405**, 285 (1993).
28. M. Lyutikov, C. Thompson, *Astrophys. J.* **634**, 1223 (2005).
29. R. P. Breton *et al.*, *Astrophys. J.* **747**, 89 (2012).
30. A. N. Timokhin, *Mon. Not. R. Astron. Soc.* **408**, L41 (2010).
31. B. Zhang, G. J. Qiao, W. P. Lin, J. L. Han, *Astrophys. J.* **478**, 313 (1997).
32. S. P. Goodwin, J. Mestel, L. Mestel, G. A. E. Wright, *Mon. Not. R. Astron. Soc.* **349**, 213 (2004).
33. A. N. Timokhin, *Mon. Not. R. Astron. Soc.* **368**, 1055 (2006).
34. J. M. Rankin, *Astrophys. J.* **301**, 901 (1986).

Acknowledgments: We thank the staff of XMM-Newton, GMRT, and LOFAR for making these observations possible. XMM-Newton is an ESA science mission with instruments and contributions directly funded by ESA member states and by NASA. GMRT is run by the National Centre for Radio Astrophysics of the Tata Institute of Fundamental Research. LOFAR, the Low Frequency Array designed and constructed by ASTRON, has facilities in several countries that are owned by various parties (each with their own funding sources) and are collectively operated by the International LOFAR Telescope (ILT) foundation under a joint scientific policy. ASTRON and SRON are supported financially by the Netherlands Organization for Scientific Research (NWO). Two of us (J.M.R., G.A.E.W.) thank NWO and ASTRON for visitor grants. C.F. was supported by Agence Nationale de la Recherche grant ANR-09-JCJC-0001-01. The used x-ray data can be retrieved from the XMM-Newton Science Archive at xmm.esac.esa.int/xsa. The applied B- and Q-mode window selections, derived from the GMRT and LOFAR observations, are listed in table S2.

Supplementary Materials

www.sciencemag.org/cgi/content/full/339/6118/436/DC1
Materials and Methods
Figs. S1 and S2
Tables S1 to S5
References (*35*–*40*)

1 October 2012; accepted 29 November 2012
10.1126/science.1230960

To Favor Survival Under Food Shortage, the Brain Disables Costly Memory

Pierre-Yves Plaçais and Thomas Preat*

The brain regulates energy homeostasis in the organism. Under resource shortage, the brain takes priority over peripheral organs for energy supply. But can the brain also down-regulate its own consumption to favor survival? We show that the brain of *Drosophila* specifically disables the costly formation of aversive long-term memory (LTM) upon starvation, a physiological state required for appetitive LTM formation. At the neural circuit level, the slow oscillations normally triggered in two pairs of dopaminergic neurons to enable aversive LTM formation were abolished in starved flies. Transient artificial activation of these neurons during training restored LTM formation in starved flies but at the price of a reduced survival. LTM formation is thus subject to adaptive plasticity that helps survival under food shortage.

Phenotypic plasticity in response to environmental changes can be adaptive or nonadaptive, depending on whether it provides the organism with higher fitness under the new conditions (*1*). Resource-mediated plasticity in general tends to be nonadaptive (*2*). For instance, because it is the central regulator of the organism's energy homeostasis, the brain enjoys primacy in the allocation of energy fluxes over supply to peripheral organs in case of resource shortage (*3*, *4*). This plasticity is nonadaptive because the brain is also the most energy-demanding of all the organs (*3*). It is much less known whether, in response to a decrease in food intake, the brain also adopts adaptive strategies and, for example, avoids excessive energy consumption by specifically inhibiting costly processes.

Because it relies on de novo protein synthesis (*5*, *6*), the formation of long-term memory (LTM) is a function that involves heavy metabolic machinery. In *Drosophila*, the substantial levy of LTM formation on the organism's metabolic resources has been directly observed (*7*). Both aversive and appetitive associative olfactory memories have been thoroughly studied over the past decades in *Drosophila*. Flies must be hungry to form (*8*–*10*) and retrieve (*11*) appetitive memory, which results from the paired delivery of sugar and odor. Typically, flies are starved for 20 to 24 hours before undergoing appetitive conditioning (*8*, *10*). These hungry flies form appetitive LTM after a single conditioning cycle (*8*, *10*). By contrast, aversive memory formation, which results from the simultaneous delivery of electric shocks and odor, does not require the flies to be hungry. Thus, studies on aversive memory have so far always been performed on fed flies. Two types of consolidated aversive memories are formed in *Drosophila*: LTM, which requires de novo protein synthesis, and anesthesia-resistant memory (ARM), which does not (*12*). Aversive LTM forms only after multiple cycles of associative training, spaced by rest intervals (spaced training) (*12*). ARM is formed after multiple massed training, without rest intervals, and after single-cycle training (*12*). LTM formation is gated by two pairs of dopaminergic neurons (DNs), named MV1 and MP1 (*13*), which project onto the mushroom body, a brain structure that plays an essential role in olfactory learning and memory (*14*). During the rest intervals of spaced training, synchronized oscillatory activity of these DNs drives the brain into the LTM consolidation pathway (*13*) by repressing the antagonist ARM pathway (*13*, *15*).

We investigated how the brain deals with the cost of aversive LTM formation in starved flies. We first studied the effect of two genetic mutations specifically affecting LTM: *crammer* (*cer*) (*16*) and *tequila* (*teq*) (*17*). As expected, when fed, these two mutants showed a strong memory deficit 24 hours after spaced training compared with wild-type *Canton-S* flies (Fig. 1, A and B). The same mutant lines showed normal performance after spaced training when deprived from food and provided with only water for 21 hours before conditioning and 24 hours after conditioning (Fig. 1, A and B). This finding suggested that after spaced training, starved flies did not form LTM but ARM, known to be insensitive to *cer* and *teq* mutations (*16*, *17*). Similar phenotypes were obtained with 18 and 24 hours of starvation before conditioning (fig. S1A), showing that turning off LTM occurred on an extended range of starvation length. To further investigate

Genes and Dynamics of Memory Systems, Neurobiology Unit, UMR 7637 École Supérieure de Physique et de Chimie Industrielles (ESPCI)/CNRS, 10 rue Vauquelin, 75005 Paris, France.

*To whom correspondence should be addressed. E-mail: thomas.preat@espci.fr

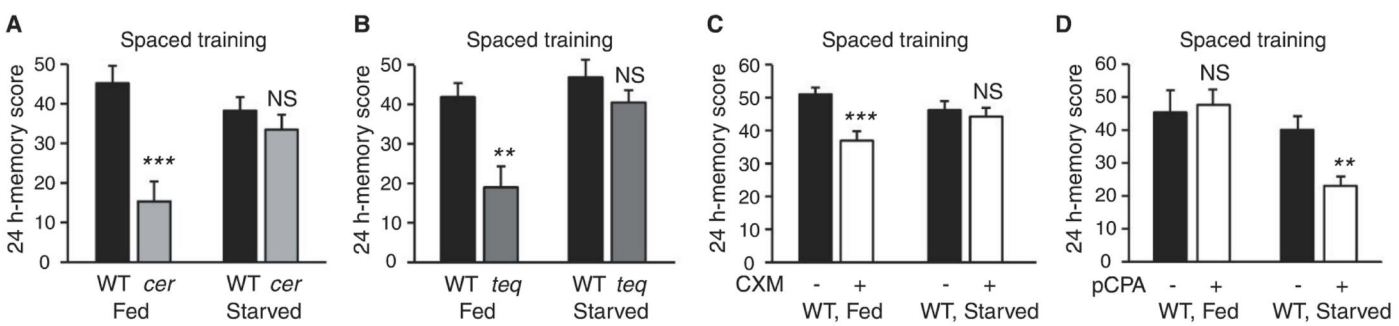

Fig. 1. Starvation prevents the formation of aversive LTM. (**A**) *cer* LTM mutant is defective for 24-hour memory after spaced training when fed (*t* test, t_{25} = 4.463, P = 0.00016, $n \geq 13$) but shows wild-type scores when starved for 21 hours before and 24 hours after conditioning (*t* test, t_{20} = 0.945, P = 0.36, n = 11). The interaction between genotype and starvation is statistically significant [two-way analysis of variance (ANOVA), $F_{(1,45)}$ = 8.230, P = 0.0063]. (**B**) *teq* LTM mutant is defective for 24-hour memory after spaced training when fed (*t* test, t_{20} = 3.573, P = 0.0019, n = 11) but performs normally when starved before and after conditioning (*t* test, t_{20} = 1.178, P = 0.25, n = 11). The interaction between genotype and starvation is statistically significant [two-way ANOVA, $F_{(1,40)}$ = 4.306, P = 0.044]. (**C**) Wild-type fed flies form CXM-sensitive LTM after spaced training (*t* test, t_{48} = 4.024, P = 0.00022, n = 25), but the memory of starved wild-type flies is unaffected by CXM treatment (*t* test, t_{48} = 0.5182, P = 0.61, n = 25). The interaction between CXM treatment and starvation is statistically significant [two-way ANOVA, $F_{(1,96)}$ = 5.47, P = 0.021]. (**D**) The LTM of wild-type fed flies is insensitive to pCPA (*t* test, t_{20} = 0.278, P = 0.78, n = 11), contrary to the memory formed by starved flies (*t* test, t_{24} = 3.404, P = 0.0023, n = 13). The interaction between pCPA treatment and starvation is statistically significant [two-way ANOVA, $F_{(1,44)}$ = 4.331, P = 0.043]. Asterisks illustrate results from two-tailed unpaired *t*-tests: $^{**}P < 0.01$; $^{***}P < 0.001$; NS, not significant, $P > 0.05$. WT, wild-type *Canton-S* flies. Error bars indicate SEM.

whether starvation prevents LTM from being formed in wild-type flies, we assessed the sensitivity to the protein synthesis inhibitor cycloheximide (CXM) of the memory formed after spaced training. The memory formed by fed flies was altered by CXM absorption, revealing LTM formation, whereas CXM treatment had no effect on the memory score of starved flies (Fig. 1C). Conversely, the ingestion of DL-p-chlorophenylalanine (pCPA), an inhibitor of serotonin synthesis that specifically affects ARM (*13*, *18*), had no effect on the memory formed by fed flies but impaired that of starved flies (Fig. 1D). Starvation thus disables aversive LTM formation and directs the brain into the ARM pathway. Refeeding flies with sucrose just before training restored LTM formation (fig. S1, B to D). Aversive ARM does not last as long as LTM (*12*), and it is less costly than LTM (*7*), suggesting that in starved flies the aversive LTM pathway is shut down to save energy.

In fed flies, MV1 and MP1 DNs (Fig. 2A) exhibit synchronized sustained activity, which on spaced training enables LTM formation (*13*).

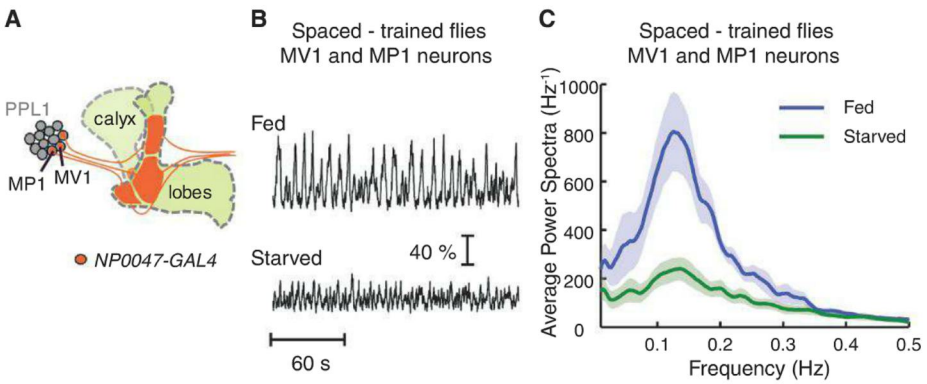

Fig. 2. Starvation silences the oscillations in MV1 and MP1 DNs that gate LTM. **(A)** Three bilateral pairs of DNs from the PPL1 cluster, among which the pairs of MV1 and MP1 neurons are included in the expression pattern of the *NP0047-GAL4* driver. These neurons symmetrically innervate the ipsi- and contralateral mushroom bodies, but each neuron type targets distinct parts of the mushroom body lobes. **(B)** Two illustrative examples of MV1 and MP1 neurons' activity after spaced training in a fed fly, featuring large, regular oscillations, and in a starved fly, where the signal amplitude is greatly reduced. **(C)** Average power spectra of MV1 and MP1 neurons' activity recorded after spaced training in fed ($n = 9$) and starved ($n = 10$) flies. Fed flies exhibit a characteristic peak, revealing an oscillatory behavior absent in starved flies.

We wondered whether these two pairs of neurons were involved in starvation-induced LTM shutdown. We performed in vivo calcium-imaging experiments to record the activity of MV1 and MP1 neurons at the level of their mushroom body projections. Calcium levels were monitored by using the genetically encoded fluorescent reporter *GCaMP3* (*19*), the expression of which was targeted to MV1 and MP1 neurons by using the *NP0047-GAL4* driver (*13*). The amplitude of the sustained activity in MV1 and MP1 neurons was lowered in naïve starved flies compared with naïve fed ones (fig. S2). Even in the absence of conditioning, starvation thus tended to reduce MV1 and MP1 neurons' activity. This is consistent with a previous study showing that blocking MP1 neurons in fed flies could mimic the starvation required to retrieve appetitive memory (*11*). In fed flies, large-amplitude oscillations are characteristically observed in MV1 and MP1 neurons after spaced training (*13*) (Fig. 2B), resulting in a peaked power spectrum (Fig. 2C). Starved flies failed to develop such large oscillations (Fig. 2B), and so the characteristic peak was dampened in the power spectrum (Fig. 2C).

We wondered whether forcing MV1 and MP1 neurons' activity during spaced training would be sufficient to restore LTM formation in starved flies. We made use of the thermosensitive cation channel *dTrpA1*, which allows artificial activation of targeted neurons at temperatures above 28°C (*11*, *13*, *20*). We performed spaced training at permissive temperature (25°C), but after each cycle of conditioning the flies underwent a 31°C air flow for the first minute of the rest interval (Fig. 3A). In flies expressing *dTrpA1* under the control of *NP0047-GAL4* driver, which drives expression in three pairs of DNs including MV1 and MP1, such brief activation is sufficient to trigger oscillatory activity of MV1 and MP1 neurons for 15 to 30 min (*13*). The activation of *NP0047-GAL4* neurons was sufficient to restore protein synthesis-dependent LTM in starved flies, as reported by CXM sensitivity (Fig. 3B). The combination with *TH-GAL80*, which specifically inhibits *dTrpA1* expression in the three pairs of DNs (*13*, *21*), prevented LTM rescue (Fig. 3B). Last, we checked that the spaced training itself, without forcing DN activity, did not induce LTM (fig. S3).

Why does the brain shut down aversive LTM formation under nutritional shortage? Because of the metabolic cost of LTM formation, fed flies that form aversive LTM die prematurely when deprived of food and water after training compared with flies that form ARM (*7*). We therefore hypothesized that LTM-gating neurons were disabled on starvation to avoid a nonvital energy expense that could compromise survival. To test this hypothesis, we sought to determine whether forcing aversive LTM formation in starved flies would shorten their survival. We subjected starved flies to spaced training, combined with DN activation after each cycle as described above, and measured their survival to food and water

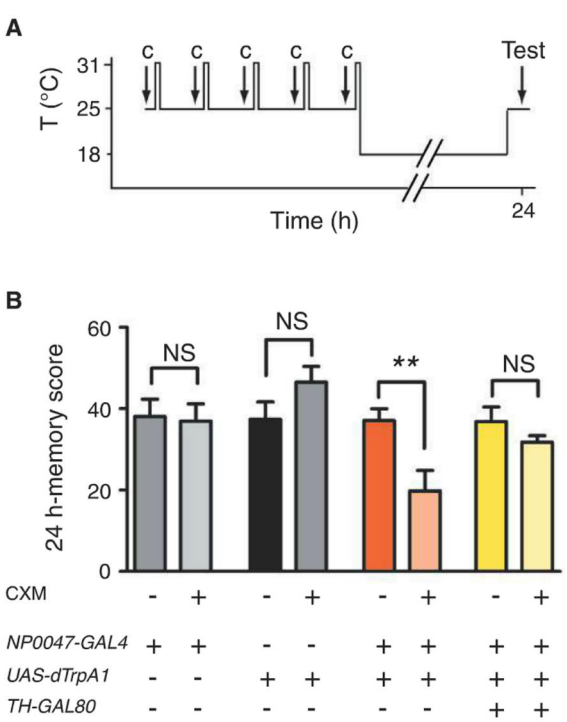

Fig. 3. Activation of oscillatory DNs during spaced training restores LTM formation in starved flies. **(A)** Experimental procedure coupling spaced training with a series of 1-min temperature shifts to 31°C immediately after each of the five cycles of conditioning (indicated by "c"). Neurons expressing *dTrpA1* are thus activated after each cycle. **(B)** Starved flies that do not express *dTrpA1* fail to form CXM-sensitive LTM. The activation of neurons labeled in *NP0047-GAL4* restores LTM formation (*t* test, $t_{25} = 3.099$, $P = 0.0048$), whereas the activation of the same set of neurons except the three pairs of DNs labeled in *NP0047-GAL4* does not (*t* test, $t_{23} = 1.265$, $P = 0.22$). The interaction between genotype and CXM treatment is statistically significant [two-way ANOVA, $F_{(3,96)} = 4.116$, $P = 0.0086$]. Asterisks report results from two-tailed unpaired *t* tests: $^{**}P < 0.01$; NS, not significant, $P > 0.05$. $n \geq 12$ for all genotypes. Error bars indicate SEM.

deprivation. Coupling activation of three pairs of DNs to spaced training shortened survival duration by about 30% (Fig. 4). Activation of the same neurons in the absence of spaced conditioning had no effect on survival duration (Fig. 4 and fig. S4, A and B). We also checked that the combination of DN activation with an unpaired protocol, where flies receive odorants and shocks separately and form no memory, did not significantly affect survival (fig. S4C). Hence, this marked reduction of survival was unequivocally attributable to the formation of aversive LTM in hungry flies.

Under food shortage, the brain will not just simply self-allocate available resources: It also trims its own metabolic expenses by turning off selected costly processes. In the present case, the shutdown of aversive LTM formation is achieved through the inhibition of a dopaminergic circuit that normally gates LTM formation (*13*), by switching memory formation from LTM to ARM. Starved flies accordingly showed enhanced ARM performance, either after a single cycle of training (fig. S5A) or after massed training (fig. S5B). This ARM increase occurred at all starvation lengths tested (fig. S5C). The mechanism of LTM gating in *Drosophila* had been previously described (*13*, *15*), but its ecological relevance remained unclear. The present work highlights a role, if not the prime one, of this LTM-gating mechanism, which is to prevent survival-threatening energy expense in a critical nutritional emergency situation. It was shown recently that the longevity of *Drosophila* males was decreased in selected lines with a higher LTM and lower ARM ability. Conversely, the longevity of males was increased in selected lines with lower LTM and improved ARM ability (*22*). This further illustrates the interplay between the cost of LTM formation and the organism's fitness. The LTM-gating mechanism we described might serve as a mechanistic basis for the modulation of LTM ability under selective pressure.

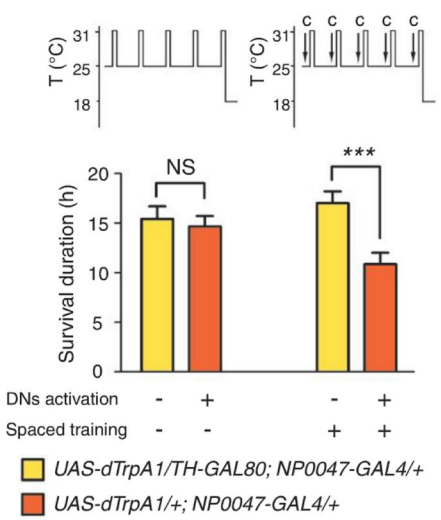

Fig. 4. Forcing aversive LTM formation in starved flies causes their premature death. Survival duration under water and food deprivation was measured for individual flies expressing *dTrpA1* under the control of *NP0047-GAL4*, either without (orange) or with (yellow) *GAL4* inhibition by *TH-GAL80*. The two conditions thus differ only by the activation of the three pairs of DNs in *NP0047-GAL4*. The various treatments are illustrated pictographically above the bar graph. A series of thermal activation alone yielded no difference between the two conditions (*t* test, $t_{52} = 0.4659$, $P = 0.64$, $n = 26$ to 28 flies for each condition). When spaced training was coupled to thermal shifts, DN activation, which forces LTM formation (Fig. 3), resulted in a ~30% decrease in survival duration (*t* test, $t_{70} = 3.696$, $P = 0.0004$, $n = 36$ flies for each condition). The interaction between DN activation and spaced training is statistically significant [two-way ANOVA, $F_{(1,122)} = 5.045$, $P = 0.0265$]. Asterisks report results from two-tailed unpaired *t* tests: ***$P < 0.001$; NS, not significant, $P > 0.05$. Error bars indicate SEM. Survival curves are shown in fig. S4.

Flies make appetitive LTM in a single conditioning cycle when they are starved. Why is the gating mechanism, and hence the starvation-induced shutdown, specific to aversive memory? Under natural conditions, reward learning occurs when a starved fly finds a food source. One can thus assume that the resulting refuelling largely exceeds the energy expense for LTM formation. In support of this argument, it has been shown that appetitive LTM forms only when flies ingest nutritious reward, whereas palatable rewards without caloric content produce only short-term memory (*23*).

How general is the mechanism evidenced here in *Drosophila*? In all species, stress may exert either positive or negative effect on memory formation depending on how stress is timed with conditioning (*24*). In particular, malnutrition (*25*) or immune response (*26*, *27*) can impair memory formation, but these impairments are consequences of stress and they do not help the animal adapting to it. On the contrary, we describe here a case of adaptive plasticity. Many of the features at play in the fly are also involved in the regulation of mammalian LTM. First, there is a growing body of evidence supporting the role of a loop between DNs of the ventrotegmental area (VTA) and the hippocampus in the control of information entry into LTM (*28*, *29*). Second, VTA DNs can exhibit a slow oscillatory firing pattern (*30*, *31*). Third, nutritional state interfere with LTM formation through cortisol receptors in the hippocampus, which among other functions, are involved in the regulation of both energy homeostasis (*3*) and long-term potentiation (*32*, *33*), a cellular basis of long-term memorization. Hence the scheme of LTM shutdown by starvation presented here may correspond, in a simplified version, to a conserved mechanism of interaction between the set point of energy homeostasis and the ability of LTM formation.

Note added in proof: In this issue of *Science*, Hirano *et al*. report that refeeding starved flies after conditioning facilitates aversive LTM formation (*34*).

References and Notes

1. C. Ghalambor, J. McKay, S. Carroll, D. N. Reznick, *Funct. Ecol.* **21**, 394 (2007).
2. L. A. Dorn, E. H. Pyle, J. Schmitt, *Evolution* **54**, 1982 (2000).
3. H. L. Fehm, W. Kern, A. Peters, *Prog. Brain Res.* **153**, 129 (2006).
4. K. M. Oltmanns *et al*., *Am. J. Physiol. Regul. Integr. Comp. Physiol.* **294**, R12 (2008).
5. H. P. Davis, L. R. Squire, *Psychol. Bull.* **96**, 518 (1984).
6. M. T. Scharf *et al*., *J. Neurophysiol.* **87**, 2770 (2002).
7. F. Mery, T. J. Kawecki, *Science* **308**, 1148 (2005).
8. M. J. Krashes, S. Waddell, *J. Neurosci.* **28**, 3103 (2008).
9. B. L. Tempel, N. Bonini, D. R. Dawson, W. G. Quinn, *Proc. Natl. Acad. Sci. U.S.A.* **80**, 1482 (1983).
10. J. Colomb, L. Kaiser, M.-A. Chabaud, T. Preat, *Genes Brain Behav.* **8**, 407 (2009).
11. M. J. Krashes *et al*., *Cell* **139**, 416 (2009).
12. T. Tully, T. Preat, S. C. Boynton, M. Del Vecchio, *Cell* **79**, 35 (1994).
13. P.-Y. Plaçais *et al*., *Nat. Neurosci.* **15**, 592 (2012).
14. M. Heisenberg, *Nat. Rev. Neurosci.* **4**, 266 (2003).
15. G. Isabel, A. Pascual, T. Preat, *Science* **304**, 1024 (2004).
16. D. Comas, F. Petit, T. Preat, *Nature* **430**, 460 (2004).
17. G. Didelot *et al*., *Science* **313**, 851 (2006).
18. P.-T. Lee *et al*., *Proc. Natl. Acad. Sci. U.S.A.* **108**, 13794 (2011).
19. L. Tian *et al*., *Nat. Methods* **6**, 875 (2009).
20. F. N. Hamada *et al*., *Nature* **454**, 217 (2008).
21. Y. Aso *et al*., *PLoS Genet.* **8**, e1002768 (2012).
22. F. Lagasse, C. Moreno, T. Preat, F. Mery, *Proc. Biol. Sci.* **279**, 4015 (2012).
23. C. J. Burke, S. Waddell, *Curr. Biol.* **21**, 746 (2011).
24. L. Schwabe, M. Joëls, B. Roozendaal, O. T. Wolf, M. S. Oitzl, *Neurosci. Biobehav. Rev.* **36**, 1740 (2012).
25. C. T. Valadares, S. de Sousa Almeida, *Nutr. Neurosci.* **8**, 39 (2005).
26. E. B. Mallon, A. Brockmann, P. Schmid-Hempel, *Proc. Biol. Sci.* **270**, 2471 (2003).
27. R. Yirmiya, I. Goshen, *Brain Behav. Immun.* **25**, 181 (2011).
28. J. E. Lisman, A. A. Grace, *Neuron* **46**, 703 (2005).
29. J. I. Rossato, L. R. M. Bevilaqua, I. Izquierdo, J. H. Medina, M. Cammarota, *Science* **325**, 1017 (2009).
30. W.-X. Shi, *J. Neurophysiol.* **94**, 3516 (2005).
31. W.-X. Shi, *J. Neural Transm. Suppl.* **73**, 103 (2009).
32. C. Pavlides, Y. Watanabe, A. M. Magariños, B. S. McEwen, *Neuroscience* **68**, 387 (1995).
33. C. Pavlides, B. S. McEwen, *Brain Res.* **851**, 204 (1999).
34. Y. Hirano *et al*., *Science* **339**, 443 (2013).

Acknowledgments: We thank G. Belliart-Guérin and V. Goguel for valuable discussion, E. Le Glou for assistance in handling the Trikinetics device, and members of the Genes and Dynamics of Memory Systems group for critical comments on the manuscript. The authors declare no conflict of interest. P.-Y.P. was supported by a postdoctoral fellowship from Région Ile-de-France. T.P. was supported by a grant from the French Agence Nationale de la Recherche.

Supplementary Materials

www.sciencemag.org/cgi/content/full/339/6118/440/DC1
Materials and Methods
Figs. S1 to S5
References (*35*–*37*)

13 June 2012; accepted 21 November 2012
10.1126/science.1226018

Fasting Launches CRTC to Facilitate Long-Term Memory Formation in *Drosophila*

Yukinori Hirano,[1,2]* Tomoko Masuda,[1] Shintaro Naganos,[1,3] Motomi Matsuno,[1] Kohei Ueno,[1] Tomoyuki Miyashita,[1] Junjiro Horiuchi,[3] Minoru Saitoe[1]*

Canonical aversive long-term memory (LTM) formation in *Drosophila* requires multiple spaced trainings, whereas appetitive LTM can be formed after a single training. Appetitive LTM requires fasting prior to training, which increases motivation for food intake. However, we found that fasting facilitated LTM formation in general; aversive LTM formation also occurred after single-cycle training when mild fasting was applied before training. Both fasting-dependent LTM (fLTM) and spaced training–dependent LTM (spLTM) required protein synthesis and cyclic adenosine monophosphate response element–binding protein (CREB) activity. However, spLTM required CREB activity in two neural populations—mushroom body and DAL neurons—whereas fLTM required CREB activity only in mushroom body neurons. fLTM uses the CREB coactivator CRTC, whereas spLTM uses the coactivator CBP. Thus, flies use distinct LTM machinery depending on their hunger state.

In *Drosophila*, canonical aversive long-term memory (LTM), which is dependent on de novo gene expression and protein synthesis, is generated after multiple rounds of spaced training (*1*, *2*). In contrast, appetitive LTM can be formed by single-cycle training (*3*). Because both aversive and appetitive LTM require protein synthesis (*1*, *3*) and activation of cyclic adenosine monophosphate (cAMP) response element–binding protein (CREB) (*3*–*5*), it is likely that both types of LTM are formed by similar mechanisms. Appetitive and aversive LTM are known to differ [i.e., octopamine is specifically involved in appetitive but not aversive memory formation (*6*)]. However, it remains unclear why single-cycle training is sufficient for appetitive but not aversive LTM formation. Appetitive LTM cannot form unless fasting precedes training (*7*). Although fasting increases motivation for food intake—a requirement for appetitive memory (*8*, *9*)—we suspected that fasting may activate a second, motivation-independent, memory mechanism that facilitates LTM formation after single-cycle training.

We deprived flies of food for various periods of time and then subjected them to aversive single-cycle training (Fig. 1A). Fasting prior to training significantly enhanced 1-day memory, with a peak at 16 hours of fasting and a return to nonfasting levels at 20 to 24 hours of fasting (Fig. 1B). In contrast, 16 hours of fasting did not increase short-term memory (STM, measured 1 hour after training) (fig. S1). In this protocol, flies were returned to food vials after training (Fig. 1A), raising a possibility that the perception of food as a reward after training may enhance the previous aversive memory. We tested this possibility by inserting refeeding periods between food deprivation and training. Although fasting followed by a 4-hour refeeding period failed to induce appetitive LTM, it significantly enhanced aversive 1-day memory (fig. S2); this finding suggests that enhancement of aversive memory occurs through a mechanism unrelated to increased motivation or perception of food as a reward. A 6-hour refeeding period was sufficient to prevent aversive memory enhancement. Continuous food deprivation after training suppressed aversive memory enhancement (fig. S3), which indicates that both fasting before training and feeding after training are required to enhance aversive memory.

Administration of the protein synthesis inhibitor cycloheximide (CHX) abolished 1-day memory enhancement (Fig. 1C) but had no effect on 1-hour memory (fig. S4), supporting the idea that memory enhancement consists of an increase of LTM. Memory remaining after CHX treatment is likely to be protein synthesis–independent, anesthesia-resistant memory (ARM) (*1*). Fasting for 16 hours neither enhanced protein synthesis–independent memory (fig. S5) nor canonical aversive LTM generated by spaced training (spLTM) (Fig. 1D). Furthermore, fasting-dependent memory decayed within 4 days, and food deprivation did not enhance 4-day spLTM (fig. S6), indicating that fasting-dependent memory is physiologically different from spLTM.

Fasting-dependent memory was blocked by acute, dose-dependent, expression of CREB2-b, a repressor isoform of CREB (*5*, *10*), in the mushroom bodies (MBs). Expression of the repressor from two copies of *UAS-CREB2-b* under control of the MB247-Switch (MBsw) GAL4 driver, which induces UAS transgene expression upon RU486 feeding (*11*), significantly suppressed fasting-dependent memory upon RU486 feeding (Fig. 1E, right panel), whereas expression from one copy of *UAS-CREB2-b* did not (Fig. 1E, center panel). Defects in LTM formation are highly correlated with CREB2-b amounts (*12*). We found significantly higher MBsw-dependent expression of CREB proteins in flies carrying two copies of *UAS-CREB2-b* relative to flies carrying one copy (fig. S7). MBsw-dependent CREB2-b expression did not affect STM in either fed or food-deprived

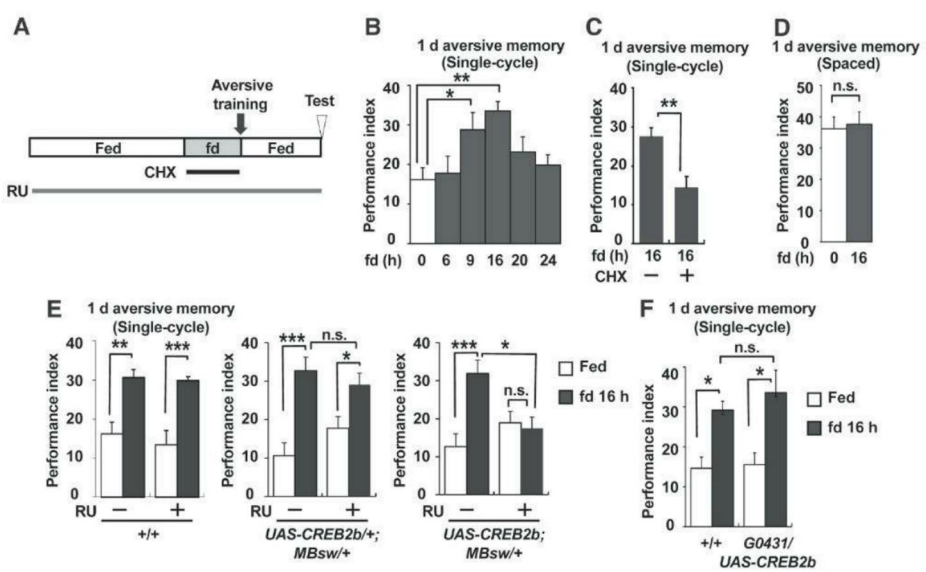

Fig. 1. Mild fasting facilitates aversive LTM formation after single-cycle training. (**A**) Schematic diagram of the experimental design; fd, food-deprived. (**B**) Fasting increases aversive 1-day memory after single-cycle training. Flies were food-deprived for the indicated times before training. (**C**) CHX treatment prevents fLTM formation. (**D**) Mild fasting does not enhance 1-day spLTM. (**E**) MB expression of CREB2-b prevents fLTM formation. (**F**) CREB2-b expression from a DAL GAL4 driver, *G0431*, does not affect fLTM. $n = 8$ to 14 for all data; n.s., not significant ($P > 0.05$); *$P < 0.05$, **$P < 0.01$, ***$P < 0.001$.

[1]Department of Sensory and Motor Systems, Tokyo Metropolitan Institute of Medical Science, 2-1-6 Kamikitazawa, Setagaya, Tokyo 156-0057, Japan. [2]Japan Science and Technology Agency, PRESTO, 4-4-8 Honcho Kawaguchi, Saitama 332-0012, Japan. [3]Department of Biological Science, Tokyo Metropolitan University, 1-1 Minami-osawa, Hachioji, Tokyo 192-0397, Japan.

*To whom correspondence should be addressed. E-mail: saito-mn@igakuken.or.jp (M.S.); hirano-yk@igakuken.or.jp (Y.H.)

conditions (fig. S8). Because the aversive memory enhanced by fasting is mediated by protein synthesis and CREB, we refer to this memory as fasting-dependent LTM (fLTM). Similar to the results in aversive fLTM, MBsw-dependent CREB2-b expression also decreased appetitive LTM but not appetitive STM (fig. S9).

A recent study (*13*) concluded that CREB activity in MB neurons is not required for spLTM. In that study, CREB2-b was expressed using the OK107 MB driver and GAL80ts was used to restrict *CREB2-b* expression to 30°C. However, we found that the GAL80ts construct still inhibited expression of CREB considerably at 30°C (fig. S7). When we acutely expressed higher amounts of CREB2-b in MBs using MBsw, we observed a significant decrease in 1-day spLTM (fig. S10), indicating that CREB activity in the MBs is likely to be required for spLTM.

Consistent with the results of (*13*), expression of CREB2-b in two dorsal-anterior-lateral (DAL) neurons impaired aversive spLTM (fig. S11). In contrast, expression of CREB2-b in DAL neurons did not affect aversive fLTM (Fig. 1F). Moreover, appetitive LTM was also not affected by expression of CREB2-b in DAL neurons (fig. S12). MBsw did not express GAL4 in DAL neurons (fig. S13).

CREB requires coactivators, including CBP (CREB-binding protein), to activate transcription needed for LTM formation (*14*–*16*). Acute expression of an inverted repeat of *CBP* (*CBP-IR*) (fig. S14A) in MBs significantly impaired spLTM (Fig. 2A) without affecting either STM or 1-day memory after multiple massed trainings, which do not lead to LTM formation (*1*) (fig. S14, B and C). However, neither aversive fLTM nor appetitive LTM was impaired by *CBP-IR* expression (Fig. 2B and fig. S14D), indicating that an alternative coactivator may be required for fasting-dependent memory.

Recent studies demonstrate the involvement of a cAMP-regulated transcriptional coactivator (CRTC) in hippocampal plasticity (*17*, *18*). In metabolic tissues, phosphorylated CRTC is sequestered in the cytoplasm while dephosphorylated CRTC translocates to the nucleus (*19*, *20*) to promote CREB-dependent gene expression (*21*–*23*). Fasting causes CRTC dephosphorylation and activation (*24*). In line with this, we found significant accumulation of hemagglutinin (HA)–tagged CRTC (CRTC-HA) within MB nuclei after 16 hours of food deprivation (Fig. 2, C and D, and fig. S15A). Subcellular fractionation indicated that food deprivation causes CRTC-HA nuclear translocation without affecting total CRTC-HA amounts (fig. S15C).

To examine the role of CRTC in fLTM and spLTM, we acutely expressed a *CRTC* inverted repeat (*CRTC-IR*) (fig. S16A) using MBsw, and observed suppression of aversive fLTM (Fig. 2E) but no effect on STM (fig. S16B). CHX treatment did not further decrease 1-day aversive memory (fig. S16C), and *CRTC-IR* expression from a second MB driver, OK107, also impaired fLTM formation (fig. S16D). *CRTC-IR* expression from MBsw also impaired appetitive LTM (Fig. 2F) without affecting appetitive STM (fig. S16E). In contrast, *CRTC-IR* expression from MBsw did not impair spLTM (Fig. 2G). *CRTC-IR* expression in DAL neurons had no effect on either aversive fLTM or appetitive LTM (fig. S17). Consistent with our results showing lack of fLTM after 24-hour fasting (Fig. 1B), 1-day aversive memory after 24-hour fasting did not decrease upon *CRTC-IR* expression in MBs (fig. S16F).

To examine the effects of spaced training on fLTM and the effects of fasting on spLTM, we space-trained fed or fasted flies expressing either *CBP-IR* or *CRTC-IR*. When *CBP-IR* was expressed to impair spLTM, 1-day memory after spaced training was impaired in fed conditions but not in fasting conditions (fig. S18), which suggested that spaced training protocols do not block fLTM. When *CRTC-IR* was expressed to impair fLTM formation, 1-day memory after spaced training was not affected by fasting (fig. S18), which suggested that mild fasting does not impair spLTM formation.

Is activation of CRTC sufficient to generate fLTM in the absence of fasting? We expressed HA-tagged constitutively active CRTC (CRTC-SA-HA) (*24*) from MBsw and observed its nuclear accumulation in the absence of fasting (Fig. 3, A and B, and fig. S19). Acute expression of CRTC-SA-HA from MBsw increased 1-day aversive memory after single-cycle training in fed flies, and this increase was not further enhanced by fasting (Fig. 3C). In contrast, expression of control CRTC-HA did not alter the fasting requirement for memory enhancement (Fig. 3D). CRTC-SA-HA expression did not affect feeding itself (fig. S20), which suggested that the memory enhancement is not due to impaired feeding. Taken together, CRTC activity in MBs is necessary and sufficient to form fLTM. Similar to the effects of fasting, CRTC-SA-HA expression did not affect STM (fig. S21) or 4-day spLTM (Fig. 3E).

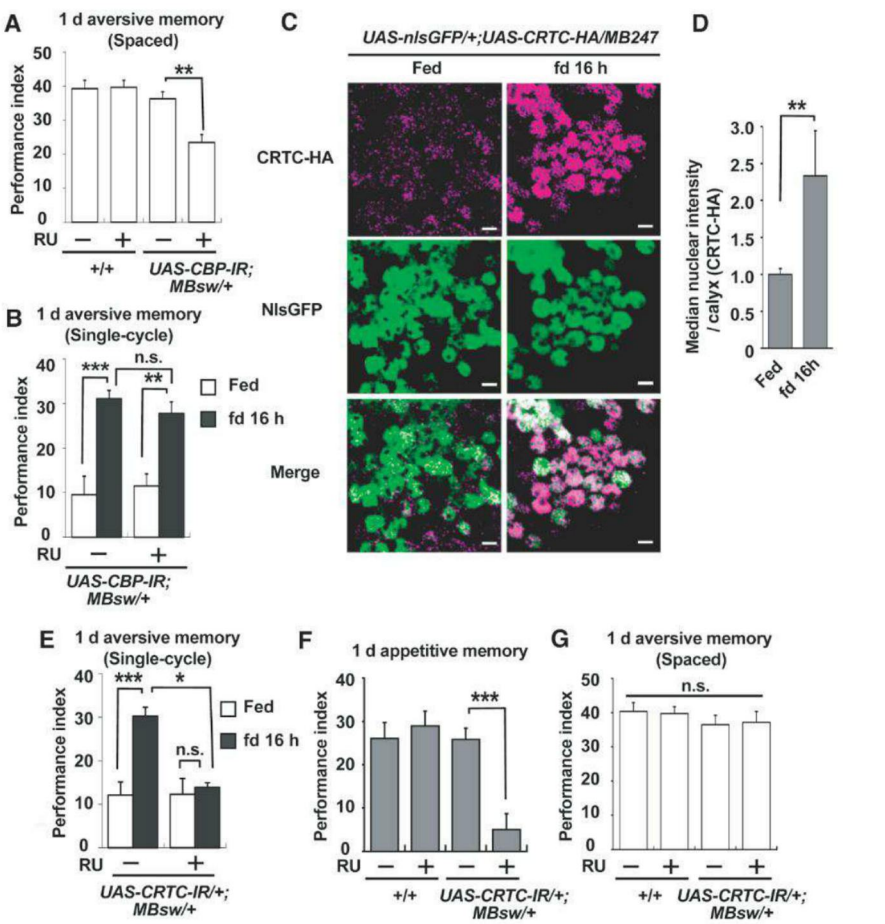

Fig. 2. Exclusive role of CBP in spLTM and of CRTC in fLTM. (**A** and **B**) Acute expression of *CBP-IR* in MBs inhibits aversive spLTM (A) but not fLTM (B) formation. (**C**) Nuclear accumulation of CRTC in MBs after 16 hours of food deprivation. CRTC-HA was coexpressed with nlsGFP [green fluorescent protein (GFP) fused to nuclear localization signal] from a MB GAL driver, *MB247*. Scale bars, 2 μm. (**D**) Nuclear intensity of CRTC relative to the dendritic region of MBs; calyx is increased after food deprivation for 16 hours (see fig. S15A). (**E** and **F**) Acute *CRTC-IR* expression in MBs suppresses both aversive (E) and appetitive (F) fLTM formation. (**G**) Acute *CRTC-IR* expression in MBs does not affect spLTM formation. $n = 8$ to 12 for all data; n.s., not significant ($P > 0.05$); $^*P < 0.05$, $^{**}P < 0.01$, $^{***}P < 0.001$.

In mammalian metabolic tissues, CRTC is phosphorylated by insulin signaling, which is suppressed by fasting (*21*, *24*, *25*). CRTC phosphorylation is also regulated by insulin signaling in flies (*24*). To determine whether reduced insulin signaling activates CRTC and promotes fLTM formation, we tested heterozygous mutants for *chico*, which encodes an adaptor protein required for insulin signaling (*26*). Although *chico*^{1} null mutants are semilethal and defective for olfactory learning, heterozygous *chico*^{1}/+ mutants are viable and display normal learning (*27*).

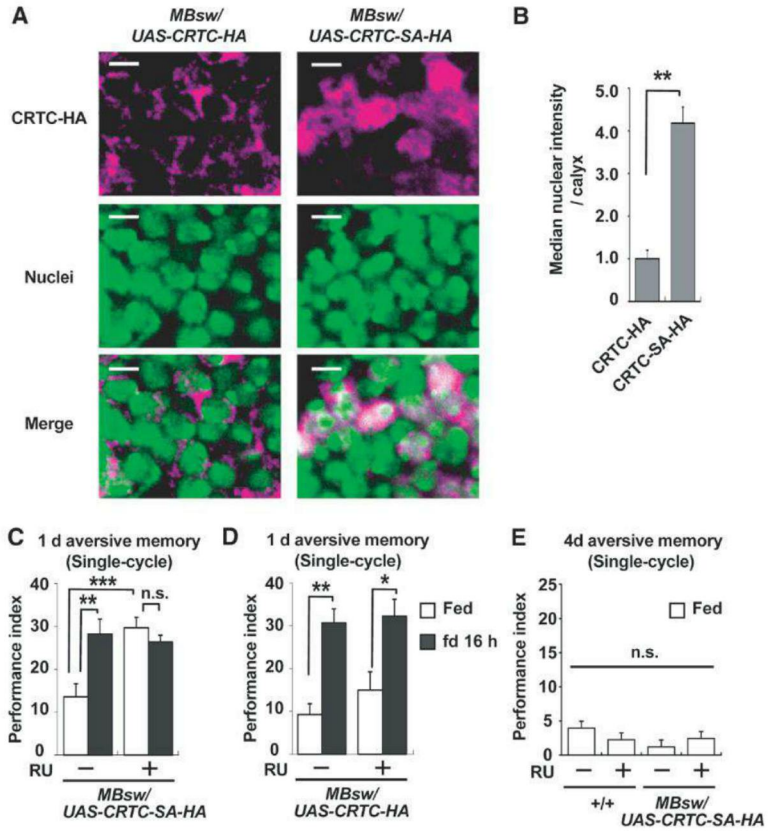

Fig. 3. Expression of constitutive active CRTC induces aversive fLTM formation in the absence of fasting. (**A**) CRTC-SA accumulates in MB nuclei, without fasting. Scale bars, 2 μm. (**B**) Nuclear localization of CRTC-SA, relative to calyx, is increased relative to wild-type CRTC (see fig. S19). (**C** and **D**) Acute expression of CRTC-SA-HA (C) but not CRTC-HA (D) in MBs increases 1-day memory after single-cycle training without fasting. (**E**) Memory enhanced by CRTC-SA-HA decays within 4 days. $n = 8$ to 10 for all data; n.s., not significant ($P > 0.05$); *$P < 0.05$, **$P < 0.01$, ***$P < 0.001$.

CRTC accumulated in MB nuclei in *chico*^{1}/+ mutants in the absence of food deprivation (Fig. 4, A and B, and fig. S22). Under conditions where flies were fed, *chico*^{1}/+ flies had significantly greater 1-day memory after single-cycle training relative to control flies (Fig. 4C), whereas 1-hour memory was unaffected (fig. S23). Enhanced 1-day memory in *chico*^{1}/+ flies was not further enhanced by fasting (Fig. 4C). Because the *chico*^{1}/+ mutation does not affect feeding itself (*28*), the memory enhancement would not seem to be attributable to impaired feeding. The increased 1-day memory in *chico*^{1}/+ mutants was suppressed by CHX treatment (fig. S24) and *CRTC-IR* expression using MBsw (Fig. 4D), which suggests that reduced insulin signaling mimics fLTM through activation of CRTC in MBs.

Single-cycle training after mild fasting generates both appetitive and aversive LTM, and CRTC in the MBs plays a key role in both types of LTM. A CRTC-dependent LTM pathway is unlikely to be involved in increasing motivation required to form appetitive memory, because CRTC knockdown did not affect appetitive STM (fig. S16E) and because CRTC-SA expression was not sufficient to form appetitive LTM without prior fasting (fig. S25). Although mild 16-hour fasting induced aversive fLTM, longer 24-hour fasting impaired aversive fLTM (Fig. 1B) but not appetitive LTM (fig. S26). Thus, although aversive and appetitive fLTM share mechanistic similarities, they may be regulated by different inputs controlling motivation and fasting time courses. Because nuclear translocation of CRTC was sustained even after 24 hours of food deprivation (fig. S15, A, B, and E), prolonged fasting may suppress a CRTC-independent step in aversive fLTM formation. spLTM was not affected by 24-hour fasting prior to training (fig. S27), which suggests that the unknown inhibitory effect of 24-hour fasting does not occur after spaced training. Continuous food deprivation after training suppressed aversive fLTM (fig. S3). Elsewhere in this issue, Plaçais and Preat (*29*) report that

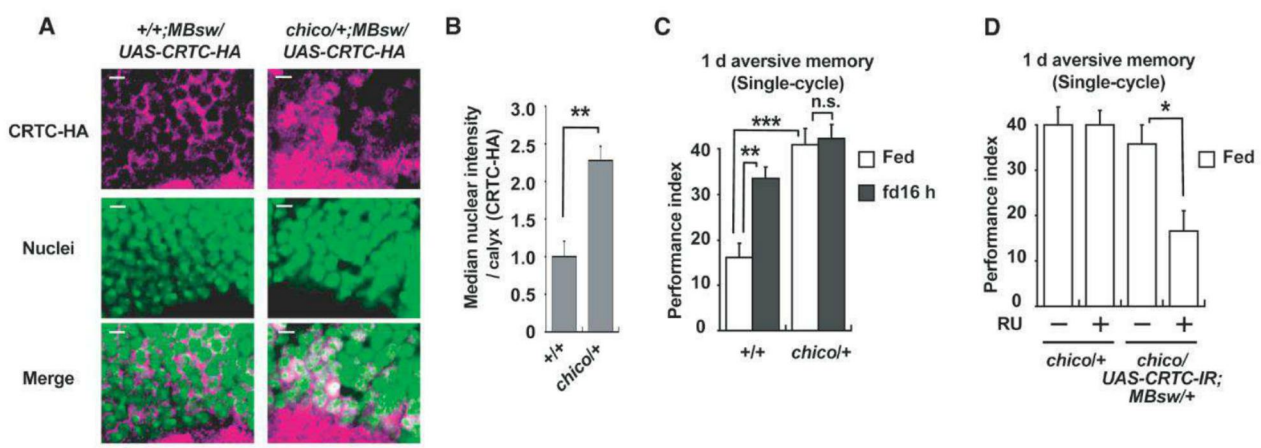

Fig. 4. Reduced insulin signaling induces fLTM formation in the absence of fasting. (**A**) CRTC-HA accumulates in MB nuclei in *chico*^{1}/+ mutants. Scale bars, 2 μm. (**B**) The nuclear localization of CRTC, relative to calyx, is increased in *chico*^{1}/+ mutants (see fig. S22). (**C**) The *chico*^{1}/+ mutation increases aversive 1-day memory after single-cycle training in the absence of food deprivation. (**D**) Acute *CRTC-IR* expression in the MBs suppresses the increased aversive 1-day memory of *chico*^{1}/+ mutants. $n = 8$ for all data; n.s., not significant ($P > 0.05$); *$P < 0.05$, **$P < 0.01$, ***$P < 0.001$.

continuous food-deprivation after spaced training suppresses spLTM as well.

Suppression of aversive LTM by prolonged fasting may ensure that starving flies pursue available food, with less concern for safety. Although the biological importance of aversive fLTM in natural environments is currently unclear, our results indicate that different physiological states may induce different types of LTM in flies.

References and Notes

1. T. Tully, T. Preat, S. C. Boynton, M. Del Vecchio, *Cell* **79**, 35 (1994).
2. M. R. Pagani, K. Oishi, B. D. Gelb, Y. Zhong, *Cell* **139**, 186 (2009).
3. M. J. Krashes, S. Waddell, *J. Neurosci.* **28**, 3103 (2008).
4. D. Yu, D. B. Akalal, R. L. Davis, *Neuron* **52**, 845 (2006).
5. J. C. Yin *et al.*, *Cell* **79**, 49 (1994).
6. M. Schwaerzel *et al.*, *J. Neurosci.* **23**, 10495 (2003).
7. B. L. Tempel, N. Bonini, D. R. Dawson, W. G. Quinn, *Proc. Natl. Acad. Sci. U.S.A.* **80**, 1482 (1983).
8. C. B. Saper, T. C. Chou, J. K. Elmquist, *Neuron* **36**, 199 (2002).
9. M. J. Krashes *et al.*, *Cell* **139**, 416 (2009).
10. B. Perazzona, G. Isabel, T. Preat, R. L. Davis, *J. Neurosci.* **24**, 8823 (2004).
11. Z. Mao, G. Roman, L. Zong, R. L. Davis, *Proc. Natl. Acad. Sci. U.S.A.* **101**, 198 (2004).
12. T. Miyashita *et al.*, *Neuron* **74**, 887 (2012).
13. C. C. Chen *et al.*, *Science* **335**, 678 (2012).
14. J. M. Alarcón *et al.*, *Neuron* **42**, 947 (2004).
15. E. Korzus, M. G. Rosenfeld, M. Mayford, *Neuron* **42**, 961 (2004).
16. Y. Oike *et al.*, *Hum. Mol. Genet.* **8**, 387 (1999).
17. K. A. Kovács *et al.*, *Proc. Natl. Acad. Sci. U.S.A.* **104**, 4700 (2007).
18. Y. Zhou *et al.*, *PLoS ONE* **1**, e16 (2006).
19. M. A. Bittinger *et al.*, *Curr. Biol.* **14**, 2156 (2004).
20. R. A. Screaton *et al.*, *Cell* **119**, 61 (2004).
21. J. Y. Altarejos, M. Montminy, *Nat. Rev. Mol. Cell Biol.* **12**, 141 (2011).
22. M. D. Conkright *et al.*, *Mol. Cell* **12**, 413 (2003).
23. V. Iourgenko *et al.*, *Proc. Natl. Acad. Sci. U.S.A.* **100**, 12147 (2003).
24. B. Wang *et al.*, *Cell Metab.* **7**, 434 (2008).
25. R. Dentin *et al.*, *Nature* **449**, 366 (2007).
26. A. A. Teleman, *Biochem. J.* **425**, 13 (2010).
27. S. Naganos, J. Horiuchi, M. Saitoe, *Neurosci. Res.* **73**, 49 (2012).
28. R. Wong, M. D. Piper, B. Wertheim, L. Partridge, *PLoS ONE* **4**, e6063 (2009).
29. P.-Y. Plaçais, T. Preat, *Science* **339**, 440 (2013).

Acknowledgments: We thank M. Montminy, J.Yin, R. Davis, and T. Tabata for materials, and H. Tanimoto and H. Takemori for suggestions. Supported by the Ministry of Education, Culture, Sports, Science, and Technology (MEXT), Japan (grant-in-aid in innovative areas "Systems Molecular Ethology" and KAKENHI grant 21300144) (M.S.); the Japan Science and Technology Agency and PRESTO (Y.H.); and MEXT/Japan Society for the Promotion of Science KAKENHI grants 24700415 and 23700405 (M.M. and K.U.).

Supplementary Materials

www.sciencemag.org/cgi/content/full/339/6118/443/DC1
Materials and Methods
Figs. S1 to S27
References (*30*–*36*)

9 July 2012; accepted 2 November 2012
10.1126/science.1227170

The Human THAP9 Gene Encodes an Active *P*-Element DNA Transposase

Sharmistha Majumdar,[1] Anita Singh,[1] Donald C. Rio[1,2,3]*

The human genome contains ~50 genes that were derived from transposable elements or transposons, and many are now integral components of cellular gene expression programs. The human THAP9 gene is related to the *Drosophila P*-element transposase. Here, we show that human THAP9 can mobilize *Drosophila P*-elements in both *Drosophila* and human cells. Chimeric proteins formed between the *Drosophila P*-element transposase N-terminal THAP DNA binding domain and the C-terminal regions of human THAP9 can also mobilize *Drosophila P* elements. Our results indicate that human THAP9 is an active DNA transposase that, although "domesticated," still retains the catalytic activity to mobilize *P* transposable elements across species.

Transposable elements or transposons are mobile segments of DNA found in both prokaryotic and eukaryotic genomes (*1*). Large portions of eukaryotic genomes (up to 50% of the human genome) are made up of transposable elements (*1*–*3*), and these elements are thought to facilitate genome evolution (*1*, *4*). Mobile elements can undergo "molecular domestication," where the transposon genes are incorporated into cellular gene expression programs, but are no longer mobile (*1*, *3*, *5*–*9*). They can also evolve cellular DNA recombination functions, such as the V(D)J antigen receptor–recombination system (*10*, *11*).

The THAP domain is a C_2CH zinc-coordinating DNA binding domain (*12*). The human genome has 12 THAP domain–containing genes (*12*). Human THAP9 (hTh9) is homologous with (25% identical with and 40% similar to) (fig. S1) the *Drosophila P*-element transposase (DmTNP), the founding member of the THAP domain family of DNA binding proteins (fig. S1A) (*7*, *12*, *13*). Given the homology and similarities in the DNA binding sites between hTh9 and DmTNP (*14*), we tested the human THAP9 protein to see if it might be able to mobilize *Drosophila P* elements in *Drosophila* cells and human embryonic kidney–293 (HEK293) cells. We used a plasmid-based assay for *P*-element excision (fig. S3), which relies on scoring *P*-element–transposase–induced transposon excision events in bacteria (*15*). When either hTh9 or two different chimeric fusion proteins in which the *Drosophila P*-element transposase N-terminal THAP DNA binding domain was fused to C-terminal portions of human THAP9 (fig. S1B), full-length human THAP9, as well as these chimeras (chimera 1 and chimera 2), gave ~60 to 80% of the *P*-element excision activity observed with wild-type *Drosophila P*-element transposase in *Drosophila* and human cells (Fig. 1 and fig. S4E). Immunoblot analysis indicated that DmTNP, hTh9, and the fusion proteins were expressed at similar levels upon transfection of *Drosophila* L2 cells with the use of an epitope tag antibody (fig. S2, A and B). No *P*-element activity was observed in negative-control experiments in which DmTNP or hTh9 expression was lacking (Fig. 1 and fig. S4E). Analysis of plasmid DNA excision products recovered from bacteria indicated that *P*-element excision had occurred with both human THAP9 and the *Drosophila* transposase-THAP9 fusion proteins (figs. S4 and S5).

Next, we tested whether human THAP9 could carry out transposition of a genetically marked *Drosophila P* element from a plasmid into the human genome in HEK293 cells. We used an assay for integration in which the Cg4 *P*-element vector carried an SV40 promoter–neomycin phosphotransferase fusion (Cg4-neo) that can confer G418 resistance in mammalian cells upon transposition into human chromosomes (fig. S6) (*16*). Upon transfection of the DmTNP or hTh9 expression vectors into human HEK293 cells along with Cg4-neo and subsequent G418 selection, many colonies were obtained (Fig. 2, A and C).

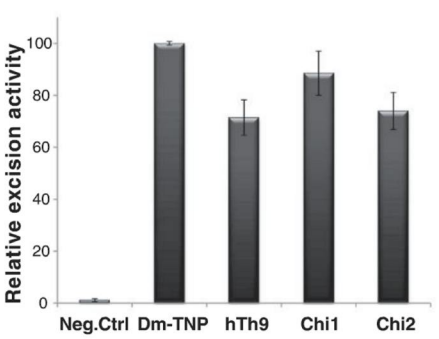

Fig. 1. Human THAP9 can excise *P* elements. *P*-element excision activities generated from a negative-control plasmid (pBluescript empty vector) versus the wild-type *P*-element transposase, human THAP9, or chimera 1 or chimera 2 expression vectors in *Drosophila* L2 cells. Values are the average (± SEM) of three independent experiments ($n = 3$), each done in duplicate, $P < 0.05$.

[1]Department of Molecular and Cell Biology, University of California, Berkeley, CA 94720–3204, USA. [2]Center for Integrative Genomics, University of California, Berkeley, CA 94720–3204, USA. [3]California Institute for Quantitative Biosciences, University of California, Berkeley, CA 94720–3204, USA.

*To whom correspondence should be addressed. E-mail: don_rio@berkeley.edu

[On average, ~50 to 75 colonies were obtained per 10-cm plate with hTh9 or DmTNP) (details in fig. S7).] To examine the levels of random integration, independent of *P* element–mediated transposition, the integration assay was also carried out with the pSV2-neo reporter plasmid, which contains an SV40 promoter–neomycin phosphotransferase fusion gene but lacks the *P*-element transposon termini. Transfection of pSV2-neo along with the DmTNP or hTh9 expression vectors gave rise to fewer G418-resistant colonies, by a factor of 3 to 5, than those obtained in the experiments

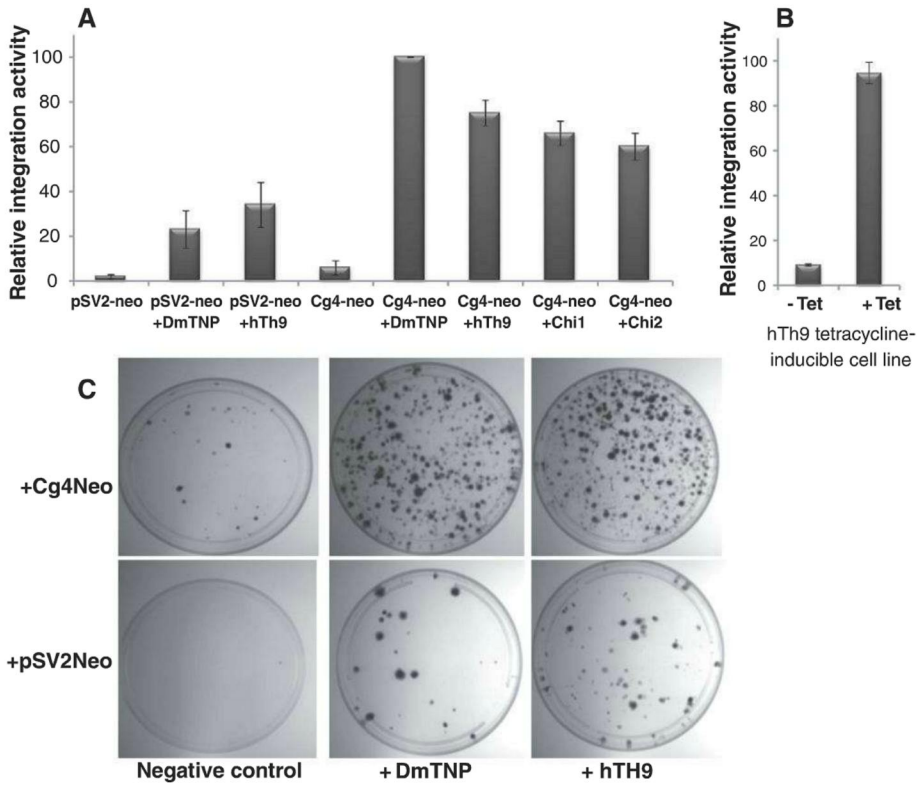

Fig. 2. Human THAP9 can transpose *P* elements. (**A**) A comparison of the *P*-element transposition activities of a negative control plasmid (pBluescript empty vector) versus the *P*-element transposase, human THAP9, chimera 1 or chimera 2 expression vectors cotransfected with Cg4-neo or pSV2-neo in HEK293 cells. (**B**) A comparison of *P*-element transposition activity after Cg4-neo was transfected into a tetracycline-inducible, stable HEK293 cell line expressing human THAP9. Values are the average (±SEM) of five independent experiments ($n = 5$), each done in duplicate, $P < 0.05$. (**C**) Crystal-violet staining of colonies obtained after G418 selection of HEK293 cells cotransfected with the Cg4-neo reporter plasmid or pSV2-neo along with a negative-control plasmid (pBluescript empty vector), *P*-element transposase, or human THAP9 expression vectors.

Table 1. DNA sequence analysis of *P*-element integration sites and identification of unique TSDs. Sequencing was performed from both the 5′ and 3′ ends of a *P*-element integration site. The exact locations of the integrations into a specific human chromosome, as well as nearby genes, are indicated.

Unique 8-bp TSD	Human chromosome integrated into	Coordinates of integration	Nearby features
Cg4 TSD (*20*)			
GTCTGGCC			
		Drosophila P-*element transposase*	
GTGGCCAT	17	4627461	Zinc finger protein 232 and ubiquitin carboxyl-terminal hydrolase 6
GTCTGCCA	20	16559372	Kinesin-like protein KIF16B isoform 1 and U2 small nuclear ribonucleoprotein B
GTGTTCGA	21	3044319	Ubiquitin carboxyl-terminal hydrolase 25 and coxsackievirus and adenovirus receptor isoform 5 precursor
TCTGCCTT	11	25665157	BH3-like motif-containing cell death inducer and ubiquitin-associated and Src homology 3 (SH3) domain–containing protein B
GTCGGCCT	3	61490435	Receptor-type tyrosine-protein phosphatase gamma
GGATCTCG	9	25168146	Izumo sperm-egg fusion protein 3 and tumor suppressor candidate gene 1 protein
		Human THAP9	
TCGGCCTG	14	68818627	Leucine-rich repeat transmembrane protein FLRT2 precursor and galactocerebrosidase isoform d
GTCTCTCT	11	18181696	FCH and double SH3 domains protein 2 and P2Y purinoceptor 2
GTCTGCCT	X	6771218	Glutamate receptor 3 isoform 1 precursor, glutamate receptor 3 isoform 2 precursor
GTGTCTGC	11	24531338	Teneurin-4 and protein FAM181B

performed with *P*-element–transposon–containing Cg4-neo and DmTNP or hTh9 (Fig. 2, B and C, and fig. S7). These observations imply that the DmTNP and hTh9 proteins can nick DNA, independent of having *P*-element termini, which would lead to elevated gene transfer via DNA linearization. A similar observation was made for the SET domain and mariner transposase fusion gene–containing protein (SETMAR or Metnase protein), but this protein is inactive for transposition of HsMAR transposons (*8*, *9*). However, most important, the presence of *P*-element termini on Cg4-neo enhanced the DNA integration activity of both DmTNP and hTh9 3 to 5 times above background, which suggested transpositional DNA integration. Many G418-resistant colonies were also obtained (fig. S7) when Cg4-neo was transfected into a stable HEK293 cell line induced to express a tetracycline-inducible human THAP9 gene (Fig. 2B).

To analyze the nature of the DNA integration events in the G418-resistant colonies, genomic DNA was isolated from individual colonies obtained from DmTNP or hTh9 cotransfections with Cg4-neo, and the sites of *P*-element insertion were characterized by splinkerette polymerase chain reaction (PCR) (*17*, *18*) followed by DNA sequencing. DNA sequence analysis of PCR integration sites identified distinct integration sites with novel 8–base pair (bp) target-site duplications (TSDs) for individual integration events into the human genome that had occurred with both DmTNP and hTh9 (Table 1 and tables S1 and S2). Taken together, these data indicate that human THAP9 actively integrates genetically marked *Drosophila P*-element vectors into human cells by transposition.

The studies reported here indicate that the human THAP9 gene encodes an active DNA transposase that can mobilize *Drosophila P*-element transposons in *Drosophila* and human cells. It will be interesting to investigate the physiological relevance of THAP9's transposition function and to find out if any THAP9 recombination signal DNA elements can be found in the human genome. This is the first report, beyond the V(D)J recombination system, of an active DNA transposase in the human genome. *P* element–like transposons and THAP9-related genes are not restricted to *Drosophila* or related insect species but are widely distributed in eukaryotic genomes like *Ciona* (sea squirt), zebrafish, chicken, and *Trichomonas vaginalis* (a parasitic protozoan) (*7*, *19*). The THAP9 gene is absent and has apparently been lost from sequenced rodent genomes (*6*). Although many of the human transposase–related genes are derived from DNA transposons (43 of 47) (*2*), most have not been characterized, with the exception of the V(D)J recombinase RAG1 and RAG2 (*10*, *11*) and the SETMAR (Metnase) protein (*8*). It is possible that other human genes of this class, besides THAP9, may also encode active DNA transposases.

References and Notes

1. C. Feschotte, E. J. Pritham, *Annu. Rev. Genet.* **41**, 331 (2007).
2. E. S. Lander *et al.*, *Nature* **409**, 860 (2001).
3. S. Schaack, C. Gilbert, C. Feschotte, *Trends Ecol. Evol.* **25**, 537 (2010).
4. H. H. Kazazian Jr., *Science* **303**, 1626 (2004).
5. C. Feschotte, *Nat. Rev. Genet.* **9**, 397 (2008).
6. S. E. Hammer, S. Strehl, S. Hagemann, *Mol. Biol. Evol.* **22**, 833 (2005).
7. H. Quesneville, D. Nouaud, D. Anxolabehere, *Mol. Biol. Evol.* **22**, 741 (2005).
8. M. Shaheen, E. Williamson, J. Nickoloff, S.-H. Lee, R. Hromas, *Genetica* **138**, 559 (2010).
9. S.-H. Lee *et al.*, *Proc. Natl. Acad. Sci. U.S.A.* **102**, 18075 (2005).
10. S. D. Fugmann, A. I. Lee, P. E. Shockett, I. J. Villey, D. G. Schatz, *Annu. Rev. Immunol.* **18**, 495 (2000).
11. M. Gellert, *Annu. Rev. Biochem.* **71**, 101 (2002).
12. M. Roussigne *et al.*, *Trends Biochem. Sci.* **28**, 66 (2003).
13. S. Hagemann, W. Pinsker, *Mol. Biol. Evol.* **18**, 1979 (2001).
14. A. Sabogal, A. Y. Lyubimov, J. E. Corn, J. M. Berger, D. C. Rio, *Nat. Struct. Mol. Biol.* **17**, 117 (2010).
15. Y. M. Mul, D. C. Rio, *EMBO J.* **16**, 4441 (1997).
16. P. J. Southern, P. Berg, *J. Mol. Appl. Genet.* **1**, 327 (1982).
17. C. Horn *et al.*, *Nat. Genet.* **39**, 933 (2007).
18. C. J. Potter, L. Luo, *PLoS ONE* **5**, e10168 (2010).
19. J. M. Carlton *et al.*, *Science* **315**, 207 (2007).
20. E. L. Beall, D. C. Rio, *Genes Dev.* **10**, 921 (1996).

Acknowledgments: We thank J. M. Taliaferro, J. Aspden, and M. Francis for comments and discussion; R. Rawat for technical assistance; and C. J. Potter (Johns Hopkins Medical School) for helpful suggestions about the splinkerette PCR experiments. This work was supported by NIH grants R01GM48862, R01GM61987, R01 GM097352, R01GM104385, and R01GM094890. S.M. and D.C.R. conceived the experiments. S.M., A.S., and D.C.R. performed cell culture and molecular biological experiments and analyzed data. S.M. and D.C.R. wrote the paper. The authors declare no competing financial interests. Requests for materials should be addressed to the corresponding author.

Supplementary Materials

www.sciencemag.org/cgi/content/full/339/6118/446/DC1
Materials and Methods
Figs. S1 to S7
Tables S1 and S2
References (*21*, *22*)

19 October 2012; accepted 27 November 2012
10.1126/science.1231789

Germline DNA Demethylation Dynamics and Imprint Erasure Through 5-Hydroxymethylcytosine

Jamie A. Hackett,[1,2] Roopsha Sengupta,[1,2]* Jan J. Zylicz,[1,2,3]* Kazuhiro Murakami,[1,2]* Caroline Lee,[1,2] Thomas A. Down,[1] M. Azim Surani[1,2,3]†

Mouse primordial germ cells (PGCs) undergo sequential epigenetic changes and genome-wide DNA demethylation to reset the epigenome for totipotency. Here, we demonstrate that erasure of CpG methylation (5mC) in PGCs occurs via conversion to 5-hydroxymethylcytosine (5hmC), driven by high levels of TET1 and TET2. Global conversion to 5hmC initiates asynchronously among PGCs at embryonic day (E) 9.5 to E10.5 and accounts for the unique process of imprint erasure. Mechanistically, 5hmC enrichment is followed by its protracted decline thereafter at a rate consistent with replication-coupled dilution. The conversion to 5hmC is an important component of parallel redundant systems that drive comprehensive reprogramming in PGCs. Nonetheless, we identify rare regulatory elements that escape systematic DNA demethylation in PGCs, providing a potential mechanistic basis for transgenerational epigenetic inheritance.

Specification of primordial germ cells (PGCs) from epiblast cells at ~embryonic day (E) 6.25 is linked with extensive epigenetic reprogramming—including global DNA demethylation, chromatin reorganization, and imprint erasure—that is vital for generating totipotency (*1*, *2*). The erasure of CpG methylation (5mC) is a key component of this program, but the dynamics and underlying mechanisms of the process remain unclear (*3*). Here, we report a comprehensive analysis of PGCs by combining immunofluorescence, genome-wide 5-(hydroxy)methylcytosine DNA immunoprecipitation sequencing [(h)meDIP-seq], single-cell RNA sequencing (RNA-seq), bisulfite sequencing, and functional analyses to address the mechanistic basis of epigenetic reprogramming in PGCs.

We investigated *Tet* expression by using single-cell RNA-seq, which revealed that *Tet1* and *Tet2* are expressed in PGCs and peak between E10.5 and E11.5 but that *Tet3* is undetectable (Fig. 1A). Immunofluorescence (IF) showed that TET1 and TET2 are nuclear and expressed at significantly higher levels in PGCs than in neighboring somatic cells between E9.5 and E11.5 (Fig. 1B and figs.

[1]Wellcome Trust/Cancer Research UK Gurdon Institute, University of Cambridge, Cambridge CB2 1QN, UK. [2]Wellcome Trust/Medical Research Council Stem Cell Institute, University of Cambridge, Cambridge, UK. [3]Department of Physiology, Development and Neuroscience, University of Cambridge, Cambridge, UK.

*These authors contributed equally to this work.
†To whom correspondence should be addressed. E-mail: a.surani@gurdon.cam.ac.uk

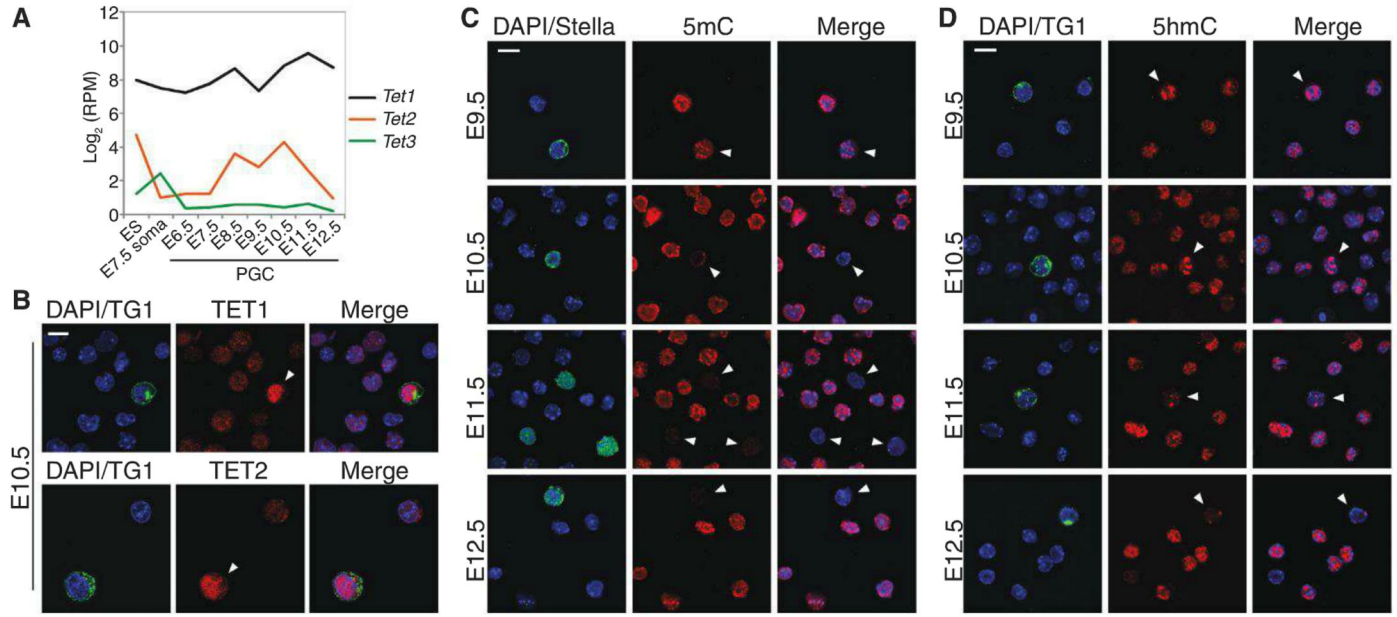

Fig. 1. Global dynamics of 5mC, 5hmC, and TETs in PGCs. (**A**) Single-cell RNA-seq analysis of *Tet1*, *Tet2*, and *Tet3* expression. Shown is $\log_2$ reads per million (RPM). (**B**) Expression of TET1 and TET2 in E10.5 PGCs (arrowheads) and soma. (**C**) Dynamics of DNA methylation (5mC) in PGCs shows 5mC erasure between E9.5 and E11.5. (**D**) Kinetics of 5hmC in PGCs. TG1/STELLA mark PGCs. Scale bars indicate 10 μm.

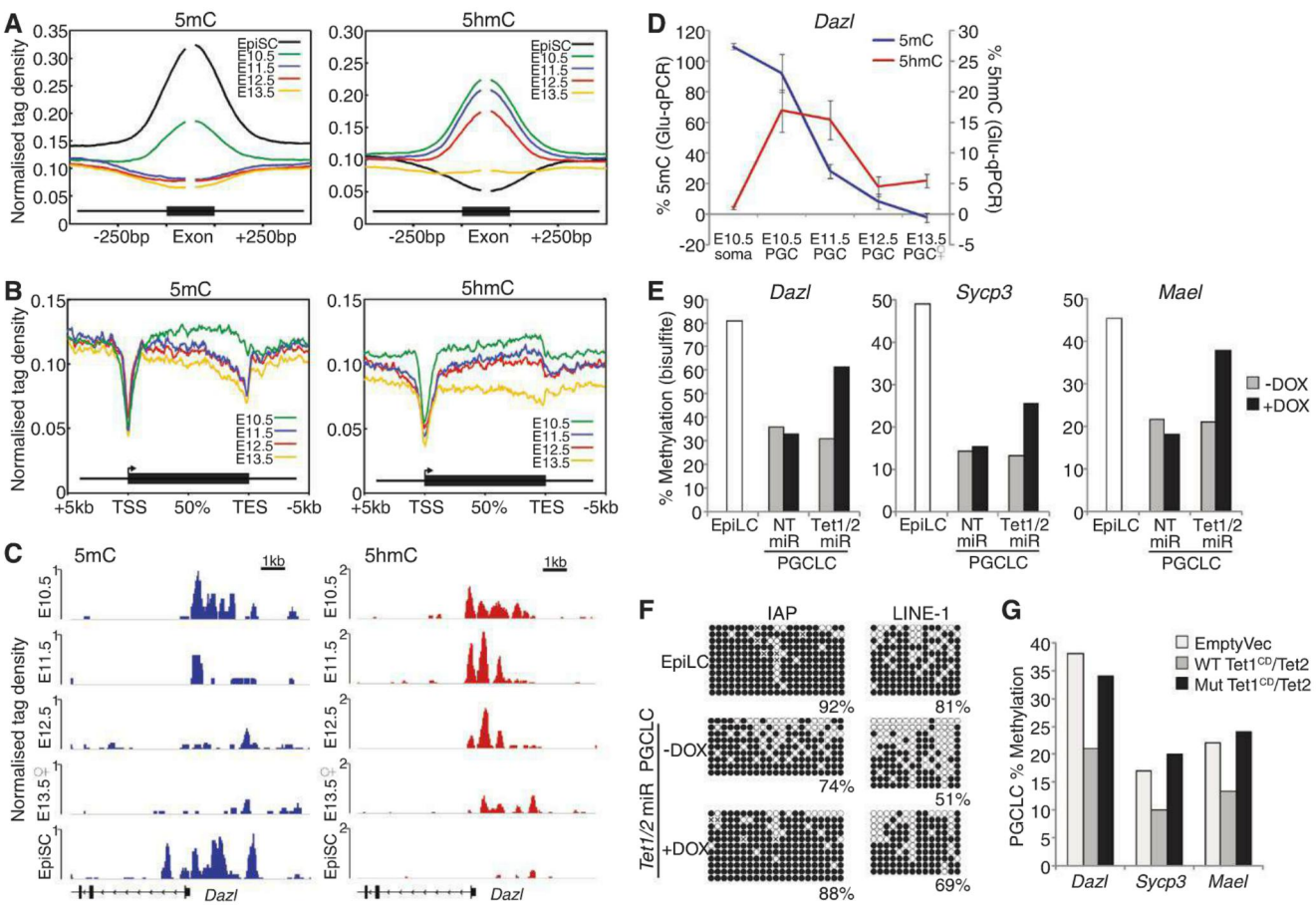

Fig. 2. Erasure of 5mC is coupled to 5hmC conversion. (**A**) Enrichment of 5mC and 5hmC in E10.5 to E13.5 PGCs and EpiSCs over internal exons. (**B**) Distributions of 5mC and 5hmC relative to a metagene. TSS, transcription start site; TES, transcription end site. (**C**) Profiles of 5mC (blue) and 5hmC (red) at the *Dazl* promoter. (**D**) Glu-qPCR showing quantitative levels of 5mC and 5hmC at a CCGG site in the *Dazl* promoter. Error bars represent SEM. (**E** and **F**) DNA methylation (%) by bisulfite sequencing of –DOX or +DOX *Tet1/Tet2* miR or NT miR PGCLCs at (E) gene promoters and (F) repeat elements. Open and solid circles represent unmethylated and methylated CpGs, respectively. (**G**) DNA methylation in PGCLCs stably expressing catalytically active (WT) or mutant (Mut) TET1 and TET2.

S1 and S2). This suggests that erasure of 5mC in PGCs could occur through conversion to 5hmC by TET1 and TET2 together (*4*, *5*).

We pursued this possibility by IF and found a progressive reduction of 5mC in PGCs between E9.5 and E10.5, until it became undetectable by E11.5 (Fig. 1C). The loss of 5mC occurs concurrently with a global enrichment of 5-hydroxymethylcytosine (5hmC) in PGCs between E9.5 and E10.5, suggesting a genome-scale conversion of 5mC to 5hmC (Fig. 1D). The global conversion to 5hmC initiates asynchronously among PGCs from E9.5, perhaps reflecting developmental heterogeneity (figs. S3 to S5). Indeed, TET1 up-regulation also initially occurs in a subset of PGCs from E9.5, which apparently also exhibit lower 5mC signal (fig. S6). In contrast to soma and embryonic stem (ES) cells (*6*), we observed that 5hmC exhibited a distinct localization in PGCs that coincided with 4′,6-diamidino-2-phenylindole (DAPI)–dense chromocenters, indicating that the conversion of 5mC to 5hmC includes heterochromatic satellite regions (fig. S7). The enrichment of 5hmC in PGCs at E10.5 is followed by its progressive reduction, suggesting that 5hmC is an intermediate toward demethylation to unmodified cytosine (C) (Fig. 1D). We checked whether 5hmC is subsequently converted to 5-formylcytosine or 5-carboxycytosine but found no detectable enrichment of these derivatives in PGCs (fig. S8) (*7*).

To gain further insight into the dynamics of 5mC to 5hmC conversion, we performed meDIP-seq and hmeDIP-seq in E10.5 to E13.5 PGCs (fig. S9). Because before E10.5 PGCs were highly limiting, we also profiled epiblast stem cells (EpiSCs), which are derived from the same post-implantation epiblast as nascent PGCs, and embryonic soma (E10.5) as references (fig. S10). Unlike bisulfite sequencing, our approach distinguishes between 5mC and 5hmC but generates a relative rather than a quantitative measure of modifications (*6*). We therefore initially examined exonic sequences, which are highly methylated and thus exhibit an informative dynamic range of relative (h)meDIP signal when they become demethylated. We found significantly reduced 5mC in E10.5 PGCs relative to EpiSC and soma and erasure by E11.5 (Fig. 2A and figs. S11 to S13). The loss of 5mC in PGCs is paralleled by a strong exonic enrichment of 5hmC, indicating 5mC-to-5hmC conversion (Fig. 2A and fig. S11). Once 5mC is converted to 5hmC, it is set on a pathway toward demethylation, because there are no 5hmC maintenance mechanisms (*6*). Consistent with this, 5hmC undergoes a progressive depletion during PGC development, which is delayed relative to loss of 5mC (Fig. 2, A and B).

Next, we examined methylation-dependent genes such as *Dazl*, which are activated by promoter demethylation in PGCs (*8*, *9*), and observed strong 5hmC enrichment coincident with loss of 5mC at their promoters (Fig. 2C and fig. S14). We confirmed that 5mC erasure is coupled to 5hmC enrichment at the *Dazl* promoter quantitatively, by using the glucosyltransferase–quantitative polymerase chain reaction (Glu-qPCR) assay (Fig. 2D). RNA-seq revealed that transcriptional activation of *Dazl* and other methylation-dependent germline genes initiates at E9.5 and increases progressively until ~E11.5 (fig. S15). This represents an important functional readout of the timing of DNA demethylation in PGCs.

To functionally link 5hmC to DNA demethylation, we used in vitro PGC-like cells (PGCLC). PGCLCs are specified from epiblast-like cells (EpiLCs) and exhibit the fundamental properties of migratory PGCs in vivo, including global DNA demethylation and chromatin reorganization (fig. S10) (*10*). TET1 and TET2 are both active in PGCs, so we generated PGCLCs carrying a doxycycline (DOX)–inducible compound microRNA (miR) knockdown of *Tet1* and *Tet2* (T-KD). We

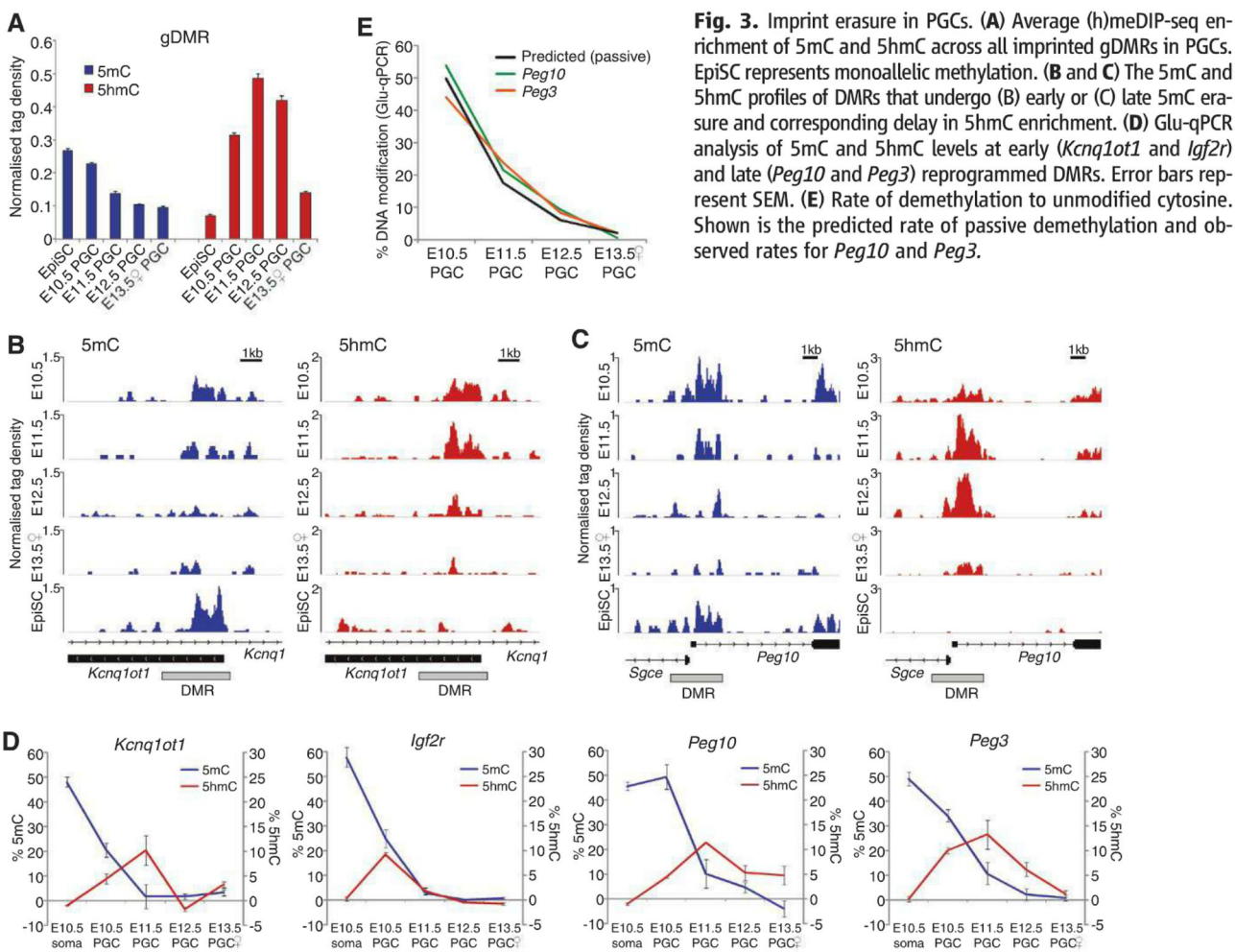

Fig. 3. Imprint erasure in PGCs. (**A**) Average (h)meDIP-seq enrichment of 5mC and 5hmC across all imprinted gDMRs in PGCs. EpiSC represents monoallelic methylation. (**B** and **C**) The 5mC and 5hmC profiles of DMRs that undergo (B) early or (C) late 5mC erasure and corresponding delay in 5hmC enrichment. (**D**) Glu-qPCR analysis of 5mC and 5hmC levels at early (*Kcnq1ot1* and *Igf2r*) and late (*Peg10* and *Peg3*) reprogrammed DMRs. Error bars represent SEM. (**E**) Rate of demethylation to unmodified cytosine. Shown is the predicted rate of passive demethylation and observed rates for *Peg10* and *Peg3*.

found that genes known to be demethylated in PGCs in vivo (*8*) also underwent DNA demethylation upon specification of control uninduced (–DOX) T-KD PGCLCs and in nontargeting (NT) miR PGCLCs (+/–DOX). In contrast, induction of *Tet1/Tet2* miR (+DOX) resulted in a substantial inhibition of DNA demethylation in PGCLCs but did not reduce the efficiency of their specification (Fig. 2E and fig. S16). Knockdown of *Tet1/Tet2* also inhibited DNA demethylation at long interspersed nuclear element 1 (LINE-1) sites and prevented the limited erasure of 5mC that occurs at intracisternal-A-particles (IAP) (Fig. 2F). These findings are important considering that both the maintenance and de novo DNA methylation systems are repressed in PGCs and PGCLCs (*10*), which likely accounts for some direct passive demethylation. Moreover, constitutive overexpression of catalytically active, but not catalytic mutant, TET1 and TET2 in PGCLCs promoted 5mC erasure to a greater extent (Fig. 2G). Thus, TET-mediated 5hmC conversion is a key event toward DNA demethylation in PGCs.

The reprogramming of gonadal PGCs in vivo uniquely entails the complete erasure of genomic imprints (*11*). Analysis of imprinted gametic differentially methylated regions (gDMRs) ($n = 21$) in PGCs revealed that erasure of 5mC is coupled to a significant increase of 5hmC enrichment (Fig. 3A). However, the precise timing of 5mC erasure is imprinted locus-specific. For example, the DMRs at *Kcnq1ot1* and *Igf2r* exhibit loss of 5mC by E10.5 relative to EpiSC (which represent ~50% allelic 5mC) and erasure by E11.5 (Fig. 3B), whereas *Peg10* and *Peg3* remain methylated until E11.5 (Fig. 3C and fig. S17). Moreover, *Kcnq1ot1* and *Igf2r* are enriched in 5hmC by E10.5, whereas 5hmC enrichment at *Peg10* and *Peg3* is delayed until E11.5, suggesting that conversion to 5hmC follows a defined temporal order at imprinted DMRs, which dictates the timing of demethylation in PGCs. Indeed, we observed that other genomic regions also exhibited differential onset of 5mC erasure (compare *Peg10* DMR versus exon, Fig. 3C). Glu-qPCR analysis confirmed that the *Peg10* and *Peg3* DMRs maintained 5mC levels of 50% and 34%, respectively, in E10.5 PGCs, whereas *Kcnq1ot1* and *Igf2r* DMRs were already reduced to 21% and 25%, respectively (Fig. 3D). Glu-qPCR also established the quantitative enrichment of 5hmC at imprinted DMRs in PGCs. The cumulative data suggest that conversion of 5mC to 5hmC by TET1 and TET2 is a general mechanism for the erasure of imprints in PGCs.

Conversion of 5mC to 5hmC at exons, promoters, and gDMRs in PGCs was followed by a protracted period of progressive 5hmC depletion between E11.5 and E13.5 (Figs. 2, A to D, and 3), suggesting a replication-coupled process (*12*). This prompted us to examine the rate of DNA demethylation between E10.5 and E13.5 quantitatively by using Glu-qPCR. Because demethylation commences asynchronously in PGCs, it is necessary to examine loci that have not initiated substantial 5mC erasure by E10.5, such as *Peg10* and *Peg3*. Because PGCs have an estimated cell cycle of ~16 hours between E10.5 and E13.5 (*13*), we would predict a reduction of DNA modification of ~threefold per 24 hours (1.5 population doublings) if the process is coupled to DNA replication. We observed that the rate of demethylation at *Peg10* ($P = 0.0022$) and *Peg3* ($P = 0.0019$) fits highly significantly with the predicted rate (Fig. 3E), suggesting that 5hmC may be removed from these loci by replication-coupled dilution. We obtained similar results for the *Dazl* promoter ($P = 0.0014$).

We next asked whether any promoters or regulatory elements can escape the comprehensive 5mC reprogramming in PGCs. We screened for CpG islands (CGI) that remain methylated in female PGCs at E13.5, because these cells represent the lowest point of global demethylation (fig. S18) (*14*). We identified 11 CGIs with significant 5mC enrichment in E13.5 PGCs (figs. S19 and S20). Validation by bisulfite sequencing showed that the promoter CGIs of *Vmn2r29* and *Sfi1* and the exonic CGI of *Srrm2* were all methylated in PGCs at E10.5 and maintained CpG methylation throughout reprogramming (Fig. 4A).

To define the extent of 5mC erasure at single-base resolution, we performed whole-genome bisulfite sequencing (WGBS), which revealed that global CpG methylation is reduced to 2.2% in female E13.5 PGCs (fig. S21). However, we identified 4730 loci that escape demethylation (>40% 5mC) in PGCs, which are predominately repeat associated (>95%). Resistant loci predominantly correspond to IAP elements, but the IAPLTR1 subclass is significantly more methylated than any other (fig. S22). IAPLTR1 is the most active and hence hazardous IAP subclass to genomic integrity, suggesting specific systems are mobilized to maintain 5mC at IAPLTR1 during reprogramming to protect genome stability (*15*). We were unable to determine any unique sequence characteristics of the 233 single-copy loci with >40% 5mC, suggesting that positional context or chromatin structure may contribute to their escape from reprogramming. Indeed, "escapees" were often adjacent to IAP elements or telomeric regions. Considered with the recent observations that many regulatory elements can evade zygotic 5mC erasure (*16*, *17*), our data suggest that rare but potentially functionally relevant 5mC epialleles could be inherited over multiple generations by evading erasure during both zygotic and PGC reprogramming.

We demonstrate here that comprehensive DNA demethylation in PGCs, including imprint erasure, entails conversion of 5mC to 5hmC, likely redundantly by TET1 and TET2. In vivo 5hmC conversion initiates asynchronously in PGCs between E9.5 and E10.5 and is largely complete by E11.5. The rate of progressive decline of 5hmC thereafter, both globally and at single-copy loci, is consistent with a replication-dependent mechanism of demethylation toward unmodified cytosines (Fig. 4B). In parallel to 5hmC conversion, repression of the de novo (*Dnmt3a/b*) and maintenance (*Uhrf1*) DNA methylation systems in PGCs prevents cyclical remethylation and simultaneously renders PGCs permissive for direct

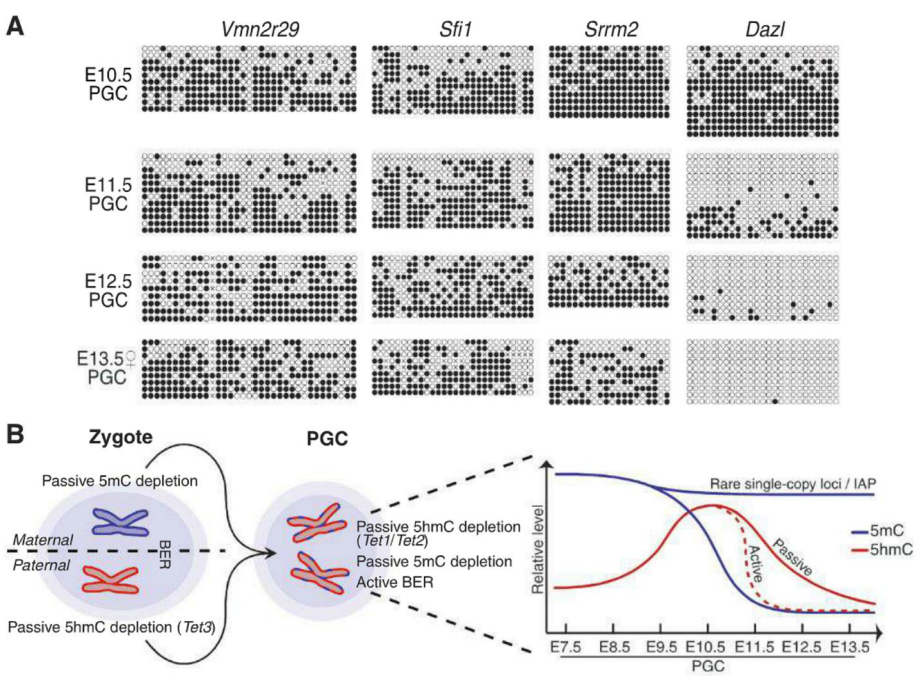

Fig. 4. Inheritance of 5mC through reprogramming. (**A**) The *Vmn2r29*, *Sfi1*, and *Srrm2* CGIs escape reprogramming in PGCs. Open and solid circles represent unmethylated and methylated CpGs, respectively. *Dazl* is representative of demethylation at most loci. (**B**) Model for the mechanisms and dynamics of DNA demethylation in PGCs.

passive 5mC depletion (fig. S23) (*18*), which may contribute to the partial demethylation observed in *Tet1* and *Tet2* knockdown PGCLCs. Thus, whereas in zygotes 5mC reprogramming is mechanistically compartmentalized into TET3-mediated 5hmC conversion of the paternal genome and direct passive 5mC depletion on the maternal genome (*12*, *19*–*21*), both of these mechanisms operate together in PGCs (Fig. 4B). In addition, up-regulation of the base excision repair (BER) pathway in PGCs may both protect against cumulative genetic damage and act as an auxiliary active demethylation mechanism, perhaps for specific loci (*22*, *23*). Reprogramming in PGCs therefore involves multiple redundant mechanisms to reset the epigenome for totipotency, which accounts for the apparent fertility (albeit subfertile) of mice lacking individual components, such as *Tet1* (*24*). The existence of multiple mechanisms may also underpin the comprehensive nature of DNA demethylation in PGCs (*3*). Nonetheless, some rare single-copy sites of CpG methylation escape from 5mC erasure (*25*), which may provide mechanistic avenues for investigations into transgenerational epigenetic inheritance.

References and Notes

1. M. A. Surani, K. Hayashi, P. Hajkova, *Cell* **128**, 747 (2007).
2. P. Hajkova *et al.*, *Nature* **452**, 877 (2008).
3. J. A. Hackett, J. J. Zylicz, M. A. Surani, *Trends Genet.* **28**, 164 (2012).
4. M. Tahiliani *et al.*, *Science* **324**, 930 (2009).
5. S. Ito *et al.*, *Nature* **466**, 1129 (2010).
6. G. Ficz *et al.*, *Nature* **473**, 398 (2011).
7. S. Ito *et al.*, *Science* **333**, 1300 (2011); 10.1126/science.1210597.
8. D. M. Maatouk *et al.*, *Development* **133**, 3411 (2006).
9. J. A. Hackett *et al.*, *Development* **139**, 3623 (2012).
10. K. Hayashi, H. Ohta, K. Kurimoto, S. Aramaki, M. Saitou, *Cell* **146**, 519 (2011).
11. P. Hajkova *et al.*, *Mech. Dev.* **117**, 15 (2002).
12. A. Inoue, Y. Zhang, *Science* **334**, 194 (2011); 10.1126/science.1212483.
13. P. P. Tam, M. H. Snow, *J. Embryol. Exp. Morphol.* **64**, 133 (1981).
14. C. Popp *et al.*, *Nature* **463**, 1101 (2010).
15. C. Qin *et al.*, *Mol. Carcinog.* **49**, 54 (2010).
16. S. A. Smallwood *et al.*, *Nat. Genet.* **43**, 811 (2011).
17. J. Borgel *et al.*, *Nat. Genet.* **42**, 1093 (2010).
18. K. Kurimoto *et al.*, *Genes Dev.* **22**, 1617 (2008).
19. T. P. Gu *et al.*, *Nature* **477**, 606 (2011).
20. M. Wossidlo *et al.*, *Nat. Commun.* **2**, 241 (2011).
21. K. Iqbal, S. G. Jin, G. P. Pfeifer, P. E. Szabó, *Proc. Natl. Acad. Sci. U.S.A.* **108**, 3642 (2011).
22. P. Hajkova *et al.*, *Science* **329**, 78 (2010).
23. S. Cortellino *et al.*, *Cell* **146**, 67 (2011).
24. M. M. Dawlaty *et al.*, *Cell Stem Cell* **9**, 166 (2011).
25. S. Guibert, T. Forné, M. Weber, *Genome Res.* **22**, 633 (2012).

Acknowledgments: We thank N. Miller for fluorescence-activated cell sorting analysis, F. Tang and W. Tang for experimental support, and G-L. Xu for reagents. This work was funded by the Wellcome Trust (RG49135, RG44593, and 083563) and the Human Frontier Science Program. Sequencing data have been deposited in the Sequence Read Archive (SRA060914).

Supplementary Materials

www.sciencemag.org/cgi/content/full/science.1229277/DC1
Materials and Methods
Figs. S1 to S24
References (*25*, *26*)

24 August 2012; accepted 16 November 2012
Published online 6 December 2012;
10.1126/science.1229277

Actin, Spectrin, and Associated Proteins Form a Periodic Cytoskeletal Structure in Axons

Ke Xu,[1]* Guisheng Zhong,[1]* Xiaowei Zhuang[1,2]†

Actin and spectrin play important roles in neurons, but their organization in axons and dendrites remains unclear. We used stochastic optical reconstruction microscopy to study the organization of actin, spectrin, and associated proteins in neurons. Actin formed ringlike structures that wrapped around the circumference of axons and were evenly spaced along axonal shafts with a periodicity of ~180 to 190 nanometers. This periodic structure was not observed in dendrites, which instead contained long actin filaments running along dendritic shafts. Adducin, an actin-capping protein, colocalized with the actin rings. Spectrin exhibited periodic structures alternating with those of actin and adducin, and the distance between adjacent actin-adducin rings was comparable to the length of a spectrin tetramer. Sodium channels in axons were distributed in a periodic pattern coordinated with the underlying actin-spectrin–based cytoskeleton.

Actin plays critical roles in shaping and maintaining cell morphology, as well as in supporting various cellular functions, including cell motility, cell division, and intracellular transport (*1*). In neurons, actin is essential for the establishment of neuronal polarity, cargo transport, neurite growth, and stabilization of synaptic structures (*2*–*4*). Despite its importance, our understanding of actin structures in neurons remains incomplete. Electron microscopy has shown detailed actin ultrastructure in growth cones and dendritic spines (*5*, *6*), in which actin is the dominant cytoskeletal protein, but little is known about the organization of actin in the axonal and dendritic shafts (*4*). These neurites contain a high density of different types of cytoskeletal filaments, such as microtubules and neurofilaments (*6*–*8*). Hence, the challenge of resolving the organization of actin in axons and dendrites requires imaging tools with both high spatial resolution and molecular specificity.

A prototypical actin-spectrin–based cytoskeleton structure is found in red blood cells (erythrocytes) (*9*, *10*), where actin, spectrin, and associated proteins form a two-dimensional (2D) polygonal network (mostly composed of hexagons and pentagons) underneath the erythrocyte membrane (*11*, *12*). Spectrin analogs have been found in many other animal cells (*9*, *10*), including neurons (*13*, *14*). These analogs play important roles, ranging from regulation of the heartbeat to stabilization of axons, formation of axon initial segments and nodes of Ranvier, and stabilization of synapses in neurons (*9*, *10*, *15*). An erythrocyte-like, polygonal lattice structure has been observed for spectrin in the *Drosophila* neuromuscular junction (*16*), and models similar to the erythrocyte cytoskeleton have also been proposed for other systems (*10*). However, the ultrastructural organization of spectrin in nonerythrocyte cells is largely unknown due to similar challenges in imaging.

Recent advances in superresolution fluorescence microscopy (*17*, *18*) allow resolutions down to ~10 nm to be achieved with molecular specificity, providing a promising solution to the above challenges. In particular, superresolution studies of neurons have provided valuable structural and dynamic information of actin in dendritic spines (*19*–*22*). In this work, we used a superresolution fluorescence imaging method, stochastic optical reconstruction microscopy (STORM) (*23*–*27*), to study the 3D ultrastructural organization of actin and spectrin in neurons.

To image actin in neurons, we fixed cultured rat hippocampal neurons at various days in vitro (DIV) and labeled actin filaments with phalloidin conjugated to a photoswitchable dye, Alexa Fluor 647 (Invitrogen, Carlsbad, CA) (Fig. 1) (*28*). To identify axons and dendrites, we immunolabeled MAP2, a microtubule-associated protein enriched in dendrites, or NrCAM, a cell adhesion molecule found in the initial segments of axons (*15*), using a dye of a different color (Fig. 1) (*28*). In the conventional fluorescence images (Fig. 1, A, D, and F), MAP2 specifically stained dendrites, and NrCAM specifically labeled the initial segments of axons, whereas actin was found in both dendrites and axons.

Next, we used 3D STORM (*27*) with a dual-objective astigmatism-imaging scheme (*28*, *29*)

[1]Howard Hughes Medical Institute (HHMI), Department of Chemistry and Chemical Biology, Harvard University, Cambridge, MA 02138, USA. [2]Department of Physics, Harvard University, Cambridge, MA 02138, USA.

*These authors contributed equally to this work.
†To whom correspondence should be addressed. E-mail: zhuang@chemistry.harvard.edu

to image the ultrastructure of actin. Only a sparse subset of the labeled Alexa 647 molecules were activated with 405-nm light at any instant and imaged with 647-nm light using a continuous illumination and detection mode (*30*). The *xy* and *z* coordinates of the activated molecules were determined from the centroid positions and ellipticity values of their images, respectively (*27*, *29*). Iterating this procedure allowed numerous molecules to be localized and a 3D superresolution image to be constructed from the coordinates of these molecules.

In contrast to the conventional images, individual actin filaments were resolved in the STORM images (Fig. 1, B, C, E, and G, and fig. S1B) (*28*). We observed long actin filaments in dendrites (Fig. 1, B and C, and fig. S1B). These filaments were primarily distributed within a cortical layer beneath the plasma membrane and largely ran along the long axes of dendrites, though crossing filaments were also observed (Fig. 1, B and C). Our findings here were focused on dendritic shafts and do not exclude the possibility of different actin organizations in dendritic spines (*3*, *6*).

In contrast, we observed a drastically different organization of actin in axons. Actin filaments appeared to be arranged into isolated rings that wrapped around the circumference of the axons (Fig. 1, E and G). These rings were periodically distributed along the axonal shafts, forming a ladderlike, quasi-1D lattice with a long-range order (Fig. 1, E and G). Examination of neurons at different developmental stages showed that the periodic actin pattern started to appear at ~5 DIV, became clearly visible at ~7 DIV (fig. S2) (*28*), and was maintained in older mature neurons (e.g., 28 DIV) (fig. S3) (*28*). In mature neurons, more than 80% of the neuronal processes that could be identified as axon shafts (that is, neurites positive for NrCAM or those devoid of MAP2 and wider than 50 nm) exhibited the periodic, ladderlike actin pattern, whereas some filopodia-like processes branching from axon shafts did not (fig. S3). Although long actin filaments were also observed along some axons, especially in thicker axons (Fig. 1, E and G, and figs. S2E and S3B), the periodic, ringlike pattern was the most pronounced actin feature in the axon shafts. We found similar periodic patterns in both the initial segments of axons (Fig. 1G) and distal axons that were not close to the cell body (figs. S1B and S3).

The periodicity of the actin pattern in axons appeared highly regular (Fig. 2). Projection of the 3D images of actin to the long axis of the axon led to well-separated peaks with nearly identical spacing (Fig. 2A). A Fourier transform of the 1D projection yielded fundamental frequencies and overtones corresponding to a spatial period of ~190 nm (Fig. 2B). Statistical analysis of the spacings showed a narrow distribution with a mean value of 182 nm and a SD of 16 nm (Fig. 2C).

The quasi-1D, periodic actin structure prompted us to search for a molecular mechanism underlying this organization. In particular, the isolated actin ringlike structures with ~180- to 190-nm spacing did not appear to form a cohesive network by themselves. Thus, we reasoned that a linker component may be present to connect the actin structures into a network, thereby giving mechanical support to the membrane, and to provide a mechanism for the regular spacing between the actin rings. We hypothesized that spectrin could be a good candidate for this linker component. The rod-shaped spectrin tetramers, typically 150 to 250 nm in length, cross-link short actin filaments in the erythrocyte membrane cytoskeleton to form a 2D, polygonal network (*9*–*12*). Spectrin analogs, in particular αII-βII spectrin, are present in the mammalian brain (*10*, *13*, *14*). Moreover, brain spectrin interacts with actin, and spectrin tetramers isolated from the brain exhibit a rodlike shape, with an average length of 195 nm (*14*), comparable to the spatial periodicity we observed for the actin rings.

To test this hypothesis, we performed 3D STORM imaging of βII-spectrin, which is enriched in distal axons (*31*). We immunolabeled βII-spectrin with the use of an antibody (*28*) that specifically targeted the C terminus of βII-spectrin, which should label the center of the rodlike αII-βII spectrin tetramer (*9*, *10*). If the adjacent actin rings are connected by spectrin tetramers, we expect the centers of the spectrin tetramers to also form a periodic pattern of ringlike structures with a quantitatively similar periodicity. We observed highly periodic, ringlike structures for the C terminus of βII-spectrin in axons (Fig. 3A and

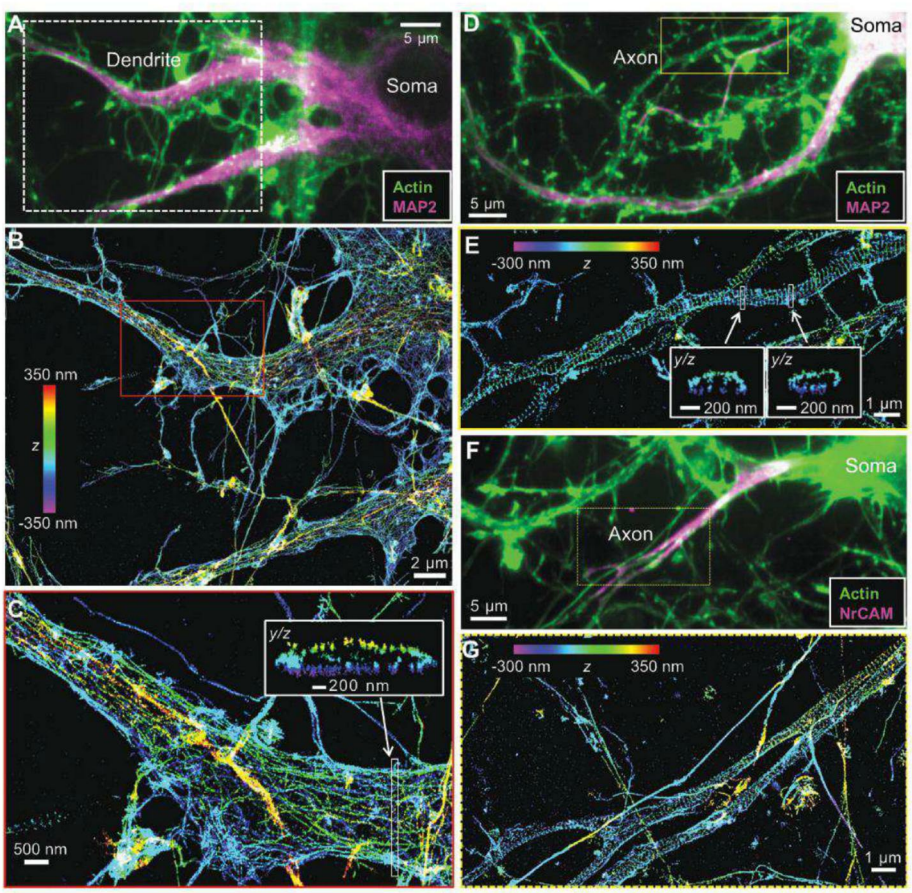

Fig. 1. STORM imaging reveals distinct organization of actin filaments in the axons and dendrites of neurons. (**A**) Conventional fluorescence image of actin (green) and a dendritic marker, MAP2 (magenta), in a cultured hippocampal neuron fixed at 7 DIV. (**B**) Three-dimensional STORM image of actin in a dendritic region corresponding to the white box in (A). The *z* positions in the STORM image are color-coded according to the color scale, with violet and red indicating the positions closest to and farthest from the substratum, respectively. (**C**) Magnification of the region inside the red box in (B). The *yz* cross section corresponding to the white-boxed region is shown in the inset. (**D**) Conventional fluorescence image of actin (green) and MAP2 (magenta) in a neuron fixed at 12 DIV. (**E**) Three-dimensional STORM image of actin in a region containing axons (devoid of the dendritic marker MAP2), corresponding to the yellow box in (D). The *yz* cross sections corresponding to the white-boxed regions are shown in the insets. The 3D STORM image of a region containing a dendrite of this neuron is shown in fig. S1B (*28*). (**F**) Conventional fluorescence image of actin (green) and an axon initial segment marker, NrCAM (magenta), in a neuron fixed at 9 DIV. (**G**) Three-dimensional STORM image of actin in a region containing the axon initial segments, corresponding to the yellow box in (F).

figs. S4 and S5) but not in dendrites (fig. S5) (*28*). Statistics of the spacings between adjacent rings gave a mean value of 182 nm and a SD of 18 nm (Fig. 3B), which are nearly identical to the values measured for the actin rings (Fig. 2C), suggesting that spectrin and actin may form a coordinated periodic network. βIV-spectrin, a spectrin subtype specifically located in the axon initial segment (fig. S6) (*15*, *28*, *32*), also exhibited a quasi-1D, periodic pattern (Fig. 3, C and D) similar to those of actin and βII-spectrin, consistent with the observation that the periodic actin structure was detected in both axon initial segments (Fig. 1G) and distal axons (figs. S1B and S3).

In the erythrocyte cytoskeleton, the network formed by short actin filaments (12 to 16 monomers) and spectrin tetramers contains other proteins, such as adducin (a protein that caps the growing end of actin filaments and promotes the binding of spectrin to actin) and ankyrin (a protein that helps to anchor spectrin to the membrane) (*9*, *10*). Thus, we also probed the distributions of these molecules in axons. Immunolabeled adducin formed periodic, ladderlike structures in axons (Fig. 3E), with a periodicity quantitatively similar to those of the actin and spectrin structures (Fig. 3F). Immunolabeled ankyrin-B exhibited a semiperiodic pattern with a similar periodicity but a less regular distribution compared with those observed for actin, spectrin, and adducin (fig. S7) (*28*). The less regular distribution is expected for ankyrin-B because each spectrin tetramer contains two separate ankyrin-binding sites that are both away from the center of the spectrin tetramer, neither of which is necessarily occupied by ankyrin (*9*, *10*).

To confirm that the periodic actin-spectrin structure exists in the brain, we performed STORM imaging of hippocampal tissue slices of adult mice (fig. S8) (*28*). Because axons, dendrites, and cell bodies are densely packed in all three dimensions in brain tissues, we needed a positive marker to unambiguously identify axons in these experiments. We used βIV-spectrin, which is specifically localized to the initial segments of axons (fig. S6) (*15*, *28*, *32*), as such a marker. We performed STORM imaging on either immunolabeled βIV-spectrin or phalloidin-labeled actin. We observed quasi-1D, periodic structures for both βIV-spectrin (fig. S8, A and B) and actin (fig. S8, G and I) in axon segments stained by βIV-spectrin, with periodicities quantitatively similar to those observed in cultured neurons (fig. S8, C to E and J to L).

Next, we performed two-color STORM imaging of cultured neurons to determine the relative positions of the molecular components observed in the quasi-1D, periodic axonal cytoskeleton (Fig. 4). To this end, we labeled actin and spectrin (or adducin) with spectrally distinct photoswitchable dyes (*28*). We detected highly regular, alternating patterns of actin and spectrin in axons with the spectrin stripes falling midway between adjacent actin stripes (Fig. 4A and fig. S9A) (*28*).

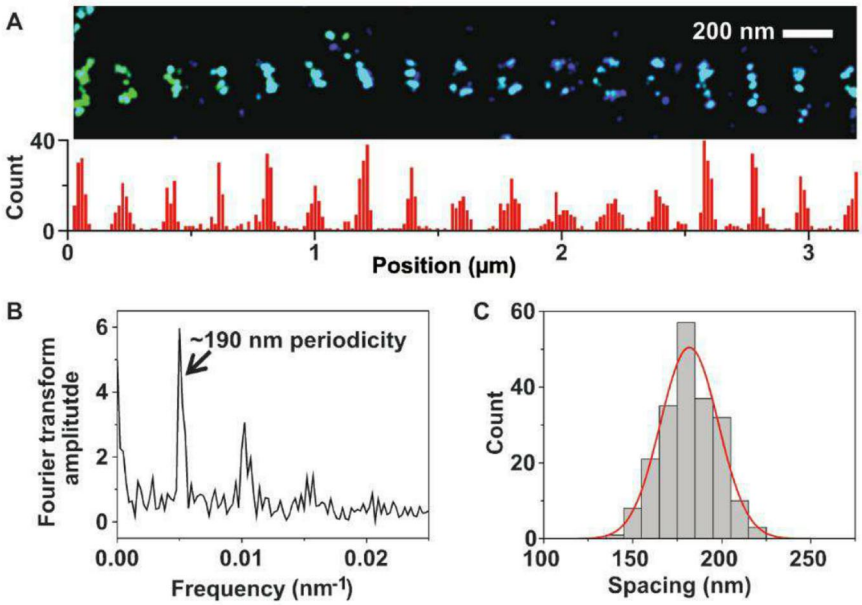

Fig. 2. Actin filaments in axons form a quasi-1D, periodic structure with a uniform spacing of ~180 to 190 nm. (**A**) Three-dimensional STORM image of a segment of axon (top) and the distribution of localized molecules after the 3D image was projected to one dimension along the axon long axis (bottom). (**B**) Fourier transform of the 1D localization distribution shown in (A). The Fourier transform shows a fundamental frequency of $(190\ nm)^{-1}$ and an overtone. (**C**) Histogram of the spacings between adjacent actin ringlike structures (N = 204 spacings). The red line is a Gaussian fit with a mean of 182 nm and a SD of 16 nm.

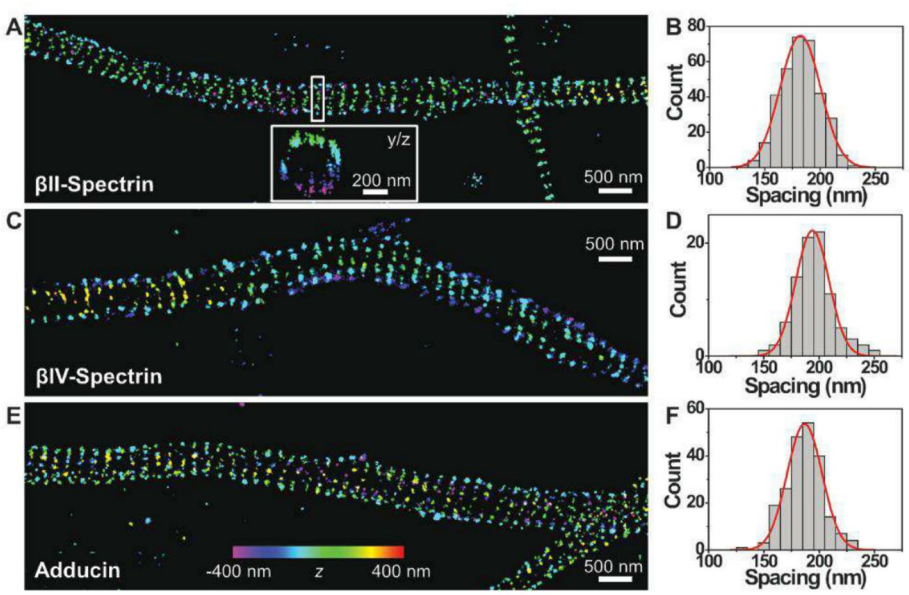

Fig. 3. Spectrin and adducin exhibit quasi-1D, periodic patterns in axons, quantitatively similar to that observed for actin. (**A**) Three-dimensional STORM image of βII-spectrin in axons. βII-spectrin is immunostained against its C-terminal region, which is situated at the center of the rodlike αII-βII spectrin tetramer. (Inset) The *yz* cross section of the boxed region showing the ringlike structure. The smaller white box denotes the position of the inset image. (**B**) Histogram of the spacings between adjacent spectrin rings (N = 340 spacings). The red line is a Gaussian fit with a mean of 182 nm and a SD of 18 nm. (**C** and **D**) Same as (A) and (B) but for βIV-spectrin, which is specifically located in the initial segments of axons. βIV-spectrin is immunostained against its N-terminal region, which corresponds to the ends of the spectrin tetramer. The red line superimposed on the histogram is a Gaussian fit with a mean of 194 nm and a SD of 15 nm (N = 88 spacings). (**E** and **F**) Same as (A) and (B) but for adducin, an actin-capping protein. The red line superimposed on the histogram is a Gaussian fit with a mean of 187 nm and a SD of 16 nm (N = 216 spacings).

Given that the antibody specifically labeled the C-terminal region of the βII-spectrin, which is at the center of the αII-βII spectrin tetramer, and that the spacing between adjacent actin stripes was comparable to the length of the spectrin tetramer, our observations suggest that spectrin tetramers are aligned longitudinally along the axonal shaft and connect the adjacent actin ringlike structures. Treatment with an actin-depolymerizing drug, latrunculin A, not only eliminated the periodic actin structures, but also disrupted the periodic structures of spectrin (fig. S10) (*28*), suggesting that the actin and spectrin structures are interconnected.

The adducin stripes, on the other hand, appeared to colocalize with the actin stripes (Fig. 4B and fig. S9B) (*28*). Given that adducin caps one end of actin filaments, this result suggests that the ringlike actin structures probably do not represent long, continuous filaments spanning the entire ring, but rather are made of capped, short filaments aligned along the circumferential direction of the axon, probably facilitated by actin-binding or –cross-linking proteins (*2*, *3*). As described earlier, long actin filaments running along axons were sometimes observed, but the filaments did not appear to have a well-defined spatial relation with either spectrin or adducin (fig. S9A and B). Consistent with the above results, βII-spectrin (C terminus) and adducin stripes also alternated with each other along the axon (Fig. 4C and fig. S9C) (*28*).

To further analyze the data quantitatively, we calculated the cross-correlation between the two color channels for each of the three combinations: actin/spectrin, actin/adducin, and spectrin/adducin (Fig. 4E). The cross-correlation was determined for the 1D localization distributions, as shown in fig. S9 (*28*). The ~180- to 190-nm periodicities were apparent for all three correlation functions (Fig. 4E). The actin-adducin pair appeared to be correlated, exhibiting a maximum near zero shift, indicating that actin and adducin colocalize with each other. The actin-spectrin (C terminus of βII-spectrin) and adducin-spectrin (C terminus of βII-spectrin) pairs were both anticorrelated, exhibiting a minimum at zero shift and maxima at ~90- to 100-nm shifts, indicating that the centers of the spectrin tetramers lie halfway between the adjacent actin-adducin rings.

Finally, to assess the possible functional implication of this quasi-1D, periodic cytoskeletal structure, we performed two-color imaging of βIV-spectrin and sodium channels (Na_v) in the axon initial segments (*28*). Sodium channels are enriched in the axon initial segments and are important for the generation of action potentials (*15*, *33*). We immunostained the N-terminal region of βIV-spectrin, which is at the two ends of the spectrin tetramer. Interestingly, Na_v and the N terminus of βIV-spectrin exhibited alternating periodic patterns, with Na_v being most abundant approximately halfway between the ends of the spectrin tetramers (Fig. 4, D and E, and fig. S9D) (*28*). Thus, the periodic distribution of Na_v is most likely coordinated by the underlying periodic cytoskeleton structure, presumably through ankyrin-G (*34*), which interacts with both sodium channels and βIV-spectrin (*9*, *15*, *35*, *36*). The periodic pattern of Na_v appeared less regular than that of βIV-spectrin, potentially because each spectrin tetramer contains two separate Na_v binding sites (through ankyrin-G) that are not fully occupied, or because not every Na_v molecule is anchored to the underlying cytoskeleton. It is also possible that the antibody against Na_v was less specific.

The above results suggest that the cortical cytoskeleton of axons is composed of short actin filaments that are capped by adducin at one end and arranged into ringlike structures, which wrap around the circumference of the axon (Fig. 4F). Spectrin tetramers connect the neighboring actin/adducin rings along the long axis of the axon, tightly regulating the periodicity of the cytoskeleton structure to ~180 to 190 nm and

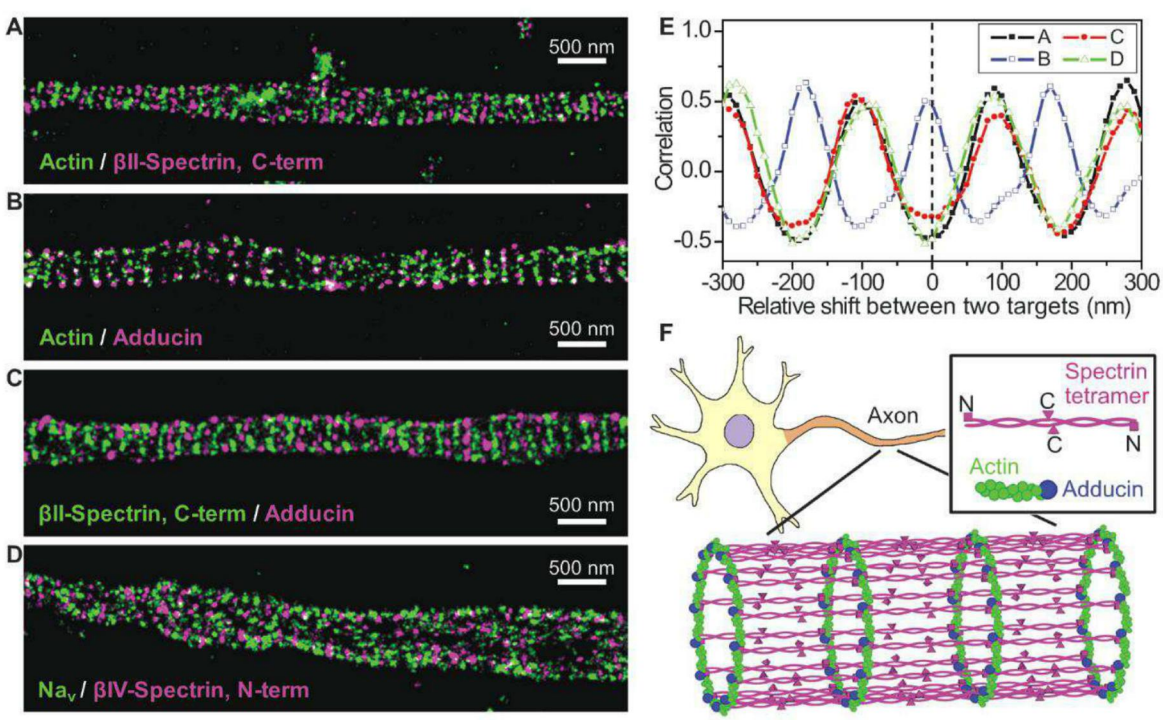

Fig. 4. Actin, spectrin, and adducin form a coordinated, quasi-1D lattice structure in axons, and sodium channels are distributed in a periodic pattern in coordination with the actin-spectrin–based submembrane cytoskeleton. (**A**) Two-color STORM image of actin (green) and βII-spectrin (magenta). βII-spectrin is immunostained against its C-terminal region, which is situated at the center of the spectrin tetramer. (**B**) Two-color STORM image of actin (green) and adducin (magenta). (**C**) Two-color STORM image of βII-spectrin (green) and adducin (magenta). (**D**) Two-color STORM image of sodium channels (Na_v, green) and βIV-spectrin (magenta). βIV-spectrin is immunostained against its N-terminal region, which is situated at the two ends of the spectrin tetramer. The distributions of the localized molecules along the axon shafts are shown in fig. S9 (*28*). (**E**) Spatial correlations between actin and the βII-spectrin C terminus [(A), black], between actin and adducin [(B), blue], between adducin and the βII-spectrin C terminus [(C), red], and between sodium channels and the βIV-spectrin N terminus [(D), green]. The correlation function is calculated for varying relative shifts between the two color channels along the axons. (**F**) A model for the cortical cytoskeleton in axons. Short actin filaments (green), capped by adducin (blue) at one end, form ringlike structures wrapping around the circumference of the axon. Spectrin tetramers (magenta) connect the adjacent actin/adducin rings along the axon, creating a quasi-1D lattice structure with a periodicity of ~180 to 190 nm. The letters "C" and "N" denote the C terminus (magenta triangles) and N terminus (magenta squares) of β-spectrin, respectively. Ankyrin and sodium channels, not shown in the model, also form semiperiodic patterns in coordination with the periodic cytoskeletal structure.

giving the axonal cytoskeleton a long-range order. Despite the molecular composition differences between the axon initial segments and distal axons [for example, ankyrin-G and βIV-spectrin are confined in the axon initial segment by an exclusion effect of the distal axon proteins ankyrin-B and βII-spectrin (*31*)], the cytoskeletal organization is similar between the initial and distal segments of the axons, both adopting a quasi-1D, periodic structure. Interestingly, we found this periodic cytoskeleton structure to be present only in axons, not in dendrites, which instead primarily contained long actin filaments running along the dendritic axis. Although the microscopic interactions between the molecular components of the axon cytoskeleton are probably similar to those between the erythrocyte analogs (*9*, *10*), the overall structure of this quasi-1D, periodic cytoskeleton in axons is distinct from the 2D, pentagonal or hexagonal structure observed for the erythrocyte membrane cytoskeleton (*11*, *12*). In *Drosophila* motoneuron axons near the neuromuscular junctions, spectrin and ankyrin appear to organize into an erythrocyte-like, pentagonal or hexagonal lattice structure (*16*), which is distinct from the quasi-1D, periodic, ladderlike structure that we observed in the axons of vertebrate brains. Whether the difference is due to invertebrate versus vertebrate animals or peripheral versus central nervous systems is a topic for future investigations.

The periodic, actin-spectrin–based cytoskeleton observed here may not be involved in myosin-dependent axonal transport. If the analogy to the erythrocyte membrane cytoskeleton holds, the capped short actin filaments in the ringlike actin structures in axons are probably bound by tropomyosin (*9*, *10*), which could potentially prevent the binding of myosins. Myosin-dependent axonal transport could, however, be mediated by the long actin filaments that run along the axon shaft. The quasi-1D, periodic, actin-spectrin cytoskeleton may instead provide elastic and stable mechanical support for the axon membrane, given the flexibility of spectrin. Elastic and stable support is particularly important for axons, because they can be extremely long and thin and have to withstand mechanical strains as animals move (*37*). Indeed, the loss of β-spectrin in *Caenorhabditis elegans* leads to spontaneous breaking of axons, which is caused by mechanical strains generated by animal movement and can be prevented by paralyzing the animal (*37*). The highly periodical submembrane cytoskeleton can also influence the molecular organization of the plasma membrane by organizing important membrane proteins along the axon. We found that sodium channels were distributed periodically along the axon initial segment in a coordinated manner with the underlying actin-spectrin cytoskeleton. An axonal plasma membrane with periodically varying biochemical and mechanical properties may not only influence how an action potential is generated and propagated, but might also affect how axons interact with other cells.

References and Notes

1. T. D. Pollard, J. A. Cooper, *Science* **326**, 1208 (2009).
2. E. W. Dent, F. B. Gertler, *Neuron* **40**, 209 (2003).
3. L. A. Cingolani, Y. Goda, *Nat. Rev. Neurosci.* **9**, 344 (2008).
4. L. C. Kapitein, C. C. Hoogenraad, *Mol. Cell. Neurosci.* **46**, 9 (2011).
5. A. K. Lewis, P. C. Bridgman, *J. Cell Biol.* **119**, 1219 (1992).
6. F. Korobova, T. Svitkina, *Mol. Biol. Cell* **21**, 165 (2010).
7. N. Hirokawa, *J. Cell Biol.* **94**, 129 (1982).
8. B. J. Schnapp, T. S. Reese, *J. Cell Biol.* **94**, 667 (1982).
9. V. Bennett, A. J. Baines, *Physiol. Rev.* **81**, 1353 (2001).
10. A. J. Baines, *Protoplasma* **244**, 99 (2010).
11. T. J. Byers, D. Branton, *Proc. Natl. Acad. Sci. U.S.A.* **82**, 6153 (1985).
12. S. C. Liu, L. H. Derick, J. Palek, *J. Cell Biol.* **104**, 527 (1987).
13. J. Levine, M. Willard, *J. Cell Biol.* **90**, 631 (1981).
14. V. Bennett, J. Davis, W. E. Fowler, *Nature* **299**, 126 (1982).
15. M. N. Rasband, *Nat. Rev. Neurosci.* **11**, 552 (2010).
16. J. Pielage *et al.*, *Neuron* **58**, 195 (2008).
17. S. W. Hell, *Nat. Methods* **6**, 24 (2009).
18. B. Huang, H. Babcock, X. Zhuang, *Cell* **143**, 1047 (2010).
19. V. Tatavarty, E. J. Kim, V. Rodionov, J. Yu, *PLoS ONE* **4**, e7724 (2009).
20. N. A. Frost, H. Shroff, H. H. Kong, E. Betzig, T. A. Blanpied, *Neuron* **67**, 86 (2010).
21. N. T. Urban, K. I. Willig, S. W. Hell, U. V. Nägerl, *Biophys. J.* **101**, 1277 (2011).
22. I. Izeddin *et al.*, *PLoS ONE* **6**, e15611 (2011).
23. M. J. Rust, M. Bates, X. Zhuang, *Nat. Methods* **3**, 793 (2006).
24. E. Betzig *et al.*, *Science* **313**, 1642 (2006).
25. S. T. Hess, T. P. K. Girirajan, M. D. Mason, *Biophys. J.* **91**, 4258 (2006).
26. M. Bates, B. Huang, G. T. Dempsey, X. Zhuang, *Science* **317**, 1749 (2007).
27. B. Huang, W. Wang, M. Bates, X. Zhuang, *Science* **319**, 810 (2008).
28. Supplementary materials, including materials and methods, are available on *Science* Online.
29. K. Xu, H. P. Babcock, X. Zhuang, *Nat. Methods* **9**, 185 (2012).
30. A. Egner *et al.*, *Biophys. J.* **93**, 3285 (2007).
31. M. R. Galiano *et al.*, *Cell* **149**, 1125 (2012).
32. S. Berghs *et al.*, *J. Cell Biol.* **151**, 985 (2000).
33. M. H. Kole, G. J. Stuart, *Neuron* **73**, 235 (2012).
34. E. Kordeli, S. Lambert, V. Bennett, *J. Biol. Chem.* **270**, 2352 (1995).
35. D. X. Zhou *et al.*, *J. Cell Biol.* **143**, 1295 (1998).
36. A. Brachet *et al.*, *J. Cell Biol.* **191**, 383 (2010).
37. M. Hammarlund, E. M. Jorgensen, M. J. Bastiani, *J. Cell Biol.* **176**, 269 (2007).

Acknowledgments: We thank M. Rasband for providing the βIV-spectrin and sodium channel antibodies and M. Ericsson, B. Kasthuri, R. Schalek, G. Hao, and C. Speer for help in the preparation of hippocampal tissue slices. This work is supported in part by the NIH and the Collaborative Innovation Award from the HHMI. X.Z. is a HHMI investigator.

Supplementary Materials

www.sciencemag.org/cgi/content/full/science.1232251/DC1
Materials and Methods
Figs. S1 to S10
References (*38*–*42*)

1 November 2012; accepted 5 December 2012
Published online 13 December 2012;
10.1126/science.1232251

Comparative Analysis of Bat Genomes Provides Insight into the Evolution of Flight and Immunity

Guojie Zhang,[1,2]*† Christopher Cowled,[3]* Zhengli Shi,[4]* Zhiyong Huang,[1]* Kimberly A. Bishop-Lilly,[5]* Xiaodong Fang,[1] James W. Wynne,[3] Zhiqiang Xiong,[1] Michelle L. Baker,[3] Wei Zhao,[1] Mary Tachedjian,[3] Yabing Zhu,[1] Peng Zhou,[3,4] Xuanting Jiang,[1] Justin Ng,[3] Lan Yang,[1] Lijun Wu,[4] Jin Xiao,[1] Yue Feng,[1] Yuanxin Chen,[1] Xiaoqing Sun,[1] Yong Zhang,[1] Glenn A. Marsh,[3] Gary Crameri,[3] Christopher C. Broder,[6] Kenneth G. Frey,[5] Lin-Fa Wang,[3,7]† Jun Wang[1,8,9]†

Bats are the only mammals capable of sustained flight and are notorious reservoir hosts for some of the world's most highly pathogenic viruses, including Nipah, Hendra, Ebola, and severe acute respiratory syndrome (SARS). To identify genetic changes associated with the development of bat-specific traits, we performed whole-genome sequencing and comparative analyses of two distantly related species, fruit bat *Pteropus alecto* and insectivorous bat *Myotis davidii*. We discovered an unexpected concentration of positively selected genes in the DNA damage checkpoint and nuclear factor κB pathways that may be related to the origin of flight, as well as expansion and contraction of important gene families. Comparison of bat genomes with other mammalian species has provided new insights into bat biology and evolution.

Bats belong to the order Chiroptera within the mammalian clade Laurasiatheria (*1*). Although consensus has not been reached on the exact arrangement of groups within Laurasiatheria, a recent study placed Chiroptera as a sister taxon to Cetartiodactyla (whales + even-toed ungulates such as cattle, sheep, and pigs) (*2*). The Black flying fox (*Pteropus alecto*) and David's Myotis (*Myotis davidii*) represent the Yinpterochiroptera and Yangochiroptera suborders, respectively, and display a diverse range of phenotypes (Fig. 1). Captive colonies, immortalized cell lines, and bat-specific reagents have been developed for these two species; however, genomic data are currently unavailable.

The most conspicuous feature of bats, distinguishing them from all other mammalian species, is the capacity for sustained flight. Positive selection in the oxidative phosphorylation (OXPHOS) pathway suggests that increased metabolic capac-

ity played a key role in its evolution (*3*), yet the by-products of oxidative metabolism [such as reactive oxygen species (ROS)] can produce harmful side effects including DNA damage (*4*). We hypothesize that genetic changes during the evolution of flight in bats likely included adaptations to limit collateral damage caused by by-products of elevated metabolic rate. Another phenomenon that has sparked intense interest in recent years is the discovery that bats maintain and disseminate numerous deadly viruses (*5*). In this context, we further hypothesize that the long-term coexistence of bats and viruses must have imposed strong selective pressures on the bat genome, and the genes most likely to reflect this are those directly related to the first line of antiviral defense—the innate immune system.

We performed high-throughput whole-genome sequencing of individual wild-caught specimens of *P. alecto* and *M. davidii* using the Illumina HiSeq platform (*6*). More than 100 × coverage high-quality reads were obtained for *P. alecto* and *M. davidii*, which resulted in high-quality assemblies (tables S1 to S3 and fig. S1). The two bat genomes, at ~2 Gb, were smaller in size than other mammals (*7*) (fig. S2), whereas the number of genes we identified was similar to those of other mammals (21,392 and 21,705 in *P. alecto* and *M. davidii*, respectively) (fig. S3). Both species displayed a high degree of heterozygosity at the whole-genome level (0.45% and 0.28% in *P. alecto* and *M. davidii*, respectively) (tables S4 and S5), whereas repetitive content accounted for slightly less than one-third of each genome (tables S6 and S7). We identified a novel endogenous viral element derived from *Saimiriine herpesvirus 2* that has expanded to 126 copies in *P. alecto* (table S8 and fig. S4). Gene family expansion and contraction analysis (tables S9 to S12) revealed significant expansion ($P < 0.05$) of 71 gene families in *M. davidii* compared with only 13 in *P. alecto*, which may be related to a recent wave of DNA transposon activity (*8*).

We screened all nuclear-encoded bat genes to identify those for which a single orthologous copy was unambiguously present in both bat species

Trait	*Myotis davidii*	*Pteropus alecto*
Common name	David's Myotis	Black flying fox
Suborder	Yangochiroptera	Yinpterochiroptera
Distribution	China	Australia, PNG, Indonesia
Habitat	Rock cavities	Trees, mangroves, rainforest
Diet	Insectivorous	Frugivorous, nectarivorous
Hibernation	Hibernates Nov-May	No
Echolocation	Yes	No
Viral reservoir	Potential	Yes

Fig. 1. Comparison of bat biological traits. *P. alecto* and *M. davidii* represent two distinct Chiropteran suborders and demonstrate diverse evolutionary adaptations. PNG, Papua New Guinea.

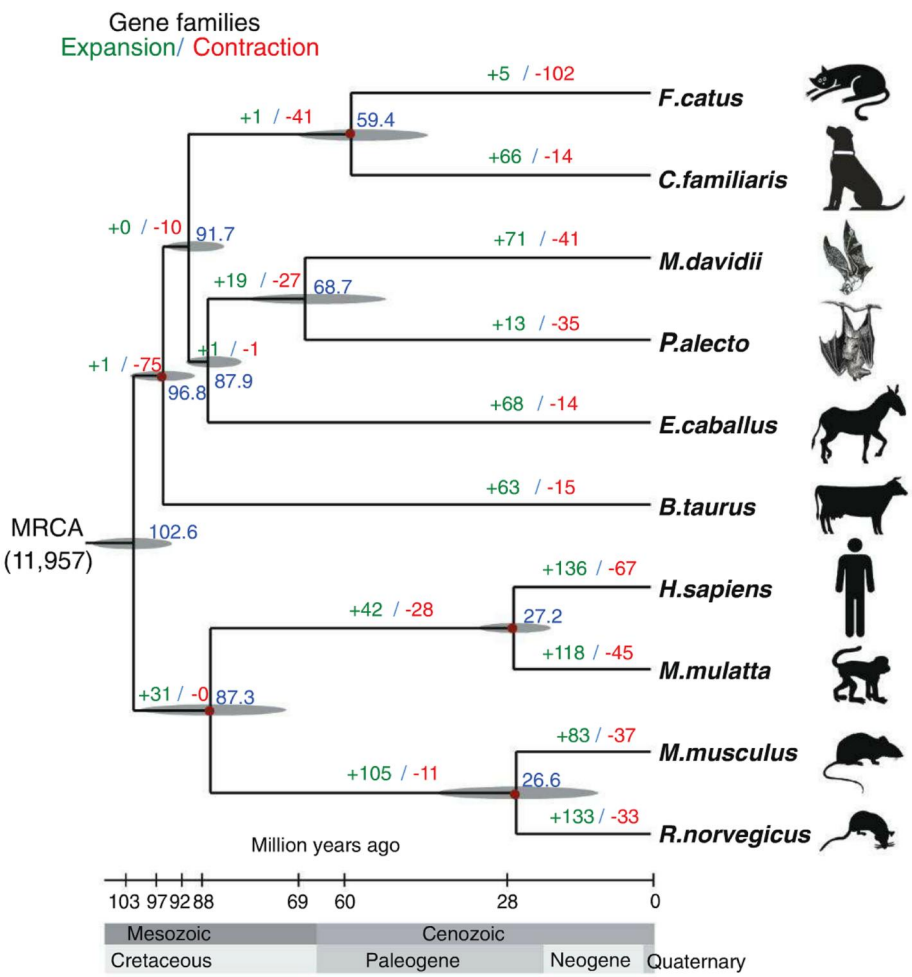

Fig. 2. Phylogenomic analysis. Maximum-likelihood phylogenomic analysis of 2492 genes from *M. davidii*, *P. alecto*, and eight mammalian species. Divergence time estimates in blue, gene family expansion events in green, and gene family contraction events in red. MRCA, most recent common ancestor.

[1]BGI-Shenzhen, Shenzhen, 518083, China. [2]Centre for Social Evolution, Department of Biology, University of Copenhagen, Universitetsparken 15, DK-2100 Copenhagen, Denmark. [3]Commonwealth Scientific and Industrial Research Organization (CSIRO) Australian Animal Health Laboratory, Geelong, Victoria 3220, Australia. [4]State Key Laboratory of Virology, Wuhan Institute of Virology, Chinese Academy of Sciences, Wuhan 430071, China. [5]Naval Medical Research Center and Henry M. Jackson Foundation, Fort Detrick, Frederick, MD 21702, USA. [6]Department of Microbiology and Immunology, Uniformed Services University of the Health Sciences, Bethesda, MD 20814, USA. [7]Program in Emerging Infectious Diseases, Duke–National University of Singapore Graduate Medical School, Singapore 169857. [8]Novo Nordisk Foundation Center for Basic Metabolic Research, University of Copenhagen, DK-2200 Copenhagen, Denmark. [9]Department of Biology, University of Copenhagen, DK-2200 Copenhagen, Denmark.

*These authors contributed equally to this work.
†To whom correspondence should be addressed. E-mail: zhanggj@genomics.org.cn (G.Z.); linfa.wang@csiro.au (L.-F.W.); wangj@genomics.org.cn (J.W.)

as well as in human, rhesus macaque, mouse, rat, dog, cat, cattle, and horse. From this, 2492 genes were used to perform maximum-likelihood and Bayesian phylogenomic analysis (Fig. 2 and figs. S5 to S7). All phylogenetically informative signals, including concatenated nucleotides and amino acids, vigorously supported bats as a member of Pegasoferae (Chiroptera + Perissodactyla + Carnivora) (*9*), with the bat lineage diverging from the *Equus* (horse) lineage ~88 million years ago, buttressed by findings at the transcript level (*10*). However, phylogenetic reconstruction with mitochondrial DNA sequences resulted in bats occupying an outlying position in Laurasiatheria (fig. S8). The incongruence between nuclear and mitochondrial trees likely reflects rapid evolution of the mitochondrial genome of the bat ancestor during the evolution of flight (*3*).

To identify mechanisms that facilitated the origin of flight in bats, we surveyed genes involved in detection and repair of genetic damage. A high proportion of genes in the DNA damage checkpoint–DNA repair pathway were found to be under positive selection in the bat ancestor, including *ATM*, the catalytic subunit of DNA-dependent protein kinase (DNA-PKc), *RAD50*, *KU80*, and *MDM2* (Fig. 3A and Table 1). We propose that these changes may be directly related to minimizing and/or repairing the negative effects of ROS generated as a consequence of flight. Additionally in this pathway, *TP53* (*p53*) and *BRCA2* were shown to be under positive selection in *M. davidii*, whereas *LIG4* was under positive selection in *P. alecto* (Table 1). Bat-specific mutations in a nuclear localization signal in *p53* and a nuclear export signal in *MDM2* (Fig. 3B and fig. S9) may affect subcellular localization and function in both species (*11*, *12*). Other candidate flight-related genes under positive selection in the bat ancestor included *COL3A1*, involved in skin elasticity, and *CACNA2D1*, which has a role in muscle contraction (table S13).

We next examined genes of the innate immune system (Table 1). Positively selected genes in the bat ancestor included c-*REL*, a member of the nuclear factor κB (NF-κB) family of transcription factors, which also contained amino acid changes potentially affecting inhibitor of NF-κB (IκB) binding (fig. S10). In addition to diverse roles in innate and adaptive immunity (*13*), c-*REL* plays a role in the DNA damage response by activating *ATM* (*14*) and *CLSPN* (*15*), whereas *ATM* is also an upstream regulator of *NF-κB* (*16*). The DNA damage response plays an important role in host defense and is a known target for virus interaction (*17*), which raises the possibility that changes in DNA damage response mechanisms during selection for flight could have influenced the bat immune system.

It is intriguing that both *P. alecto* and *M. davidii* have lost the entire locus containing the PYHIN gene family, including *AIM2* and *IFI16*, both of which are involved in sensing microbial DNA and the formation of inflammasomes (fig. S11). The association between PYHIN genes and cell cycle regulation in other species (*18*) hints that loss of the PYHIN family in bats may be connected to changes in the DNA damage pathway, because at least one PYHIN gene is present in all other major groups of eutherian mammals (*19*). *NLRP3*, triggered by both viral infection and ROS in other mammals (*20*), plays an analogous role to *AIM2* in inflammasome assembly and was also under positive selection in the bat ancestor (Table 1).

Natural killer (NK) cells provide a first line of defense against viruses and tumors and include two families of NK cell receptors; killer-cell immunoglobulin like receptors (KIRs), encoded by genes in the leukocyte receptor complex (LRC), and killer cell lectin-like receptors (KLRs, also known as Ly49 receptors), encoded within the natural killer gene complex (NKC). KLRs and KIRs were entirely absent in *P. alecto* and reduced to a single *Ly49* pseudogene in *M. davidii* (table S14). KIR-like receptors identified in other species (*21*) were also absent from both *P. alecto* and *M. davidii* genomes, which was supported by transcript analysis in *P. alecto* (*10*). This likely indicates that bat NK cells use a novel class of receptors to recognize classical major histocompatibility complex class I molecules. Furthermore, additional LRC members of the immunoglobulin superfamily [including sialic acid–binding immunoglobulin-like lectins (SIGLECs), leukocyte

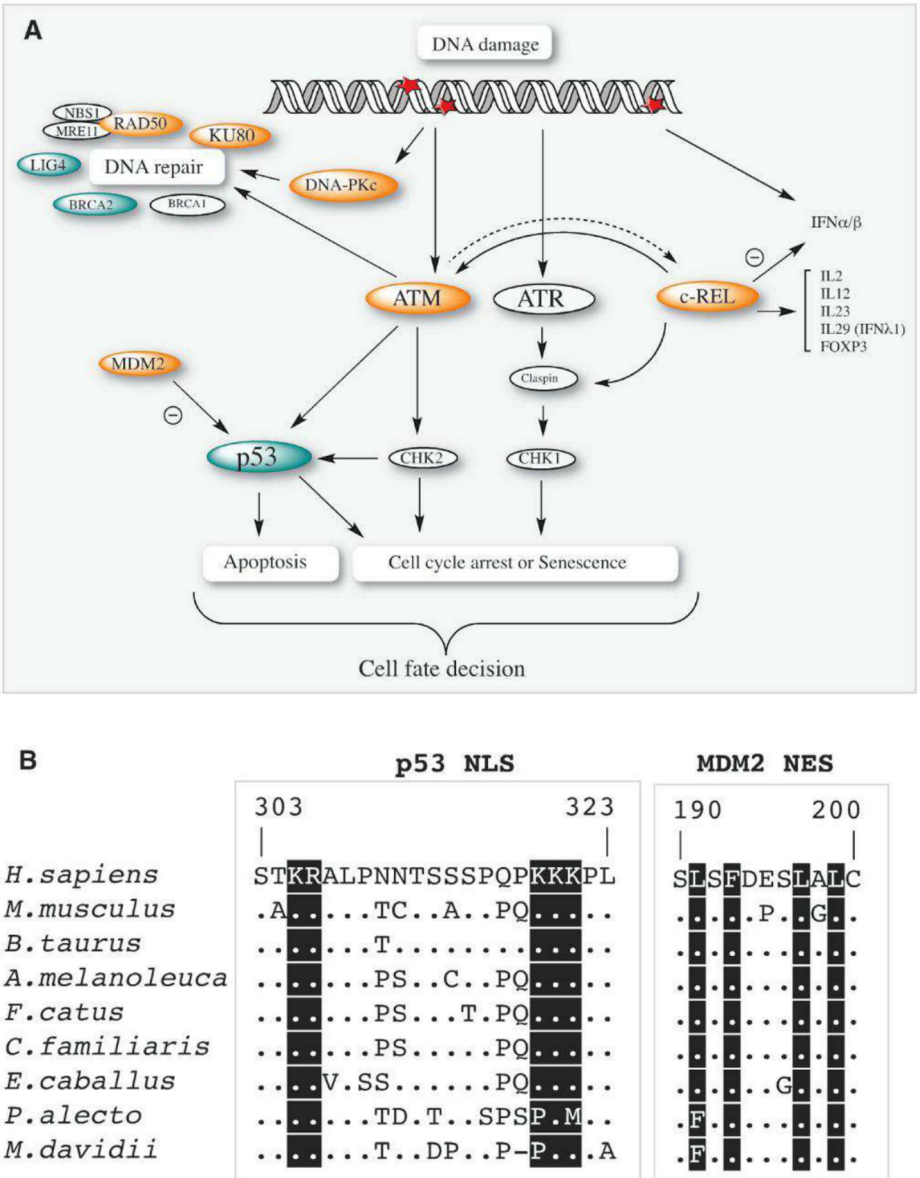

Fig. 3. Accelerated evolution in the DNA damage checkpoint in bats. (**A**) Positive selection in the DNA damage checkpoint–DNA repair pathway. Genes under positive selection in the bat ancestor are highlighted in orange. Genes under positive selection in *M. davidii* only (*p53*, *BRCA2*) or *P. alecto* only (*LIG4*) are highlighted in blue. IFN, interferon; IL, interleukin. (**B**) Mutations unique to bats were detected in the functionally relevant regions of the *p53* nuclear localization signal (NLS) and *MDM2* nuclear export signal (NES) (black shading).

Table 1. DNA damage checkpoint and innate immune genes under positive selection in the bat lineages. The rate ratio ω of dN/dS was calculated using multiprotein alignments of *P. alecto* and *M. davidii* sequences with orthologous sequences from human, rhesus macaque, mouse, rat, dog, cattle, and horse. ω0 is the average ratio in all branches, ω1 is the average ratio in nonbat branches, and ω2 is the ratio in the bat branch. A low *P* value indicates that the ω2 model fits the data better than the ω1 model.

Lineage	Symbol	Gene	ω0 (average)	ω1 (other)	ω2 (target)	*P* value
Ancestor	*TLR7*	Toll-like receptor 7	0.2821	0.2670	2.7778	3.54E-07
	ATM	Ataxia telangiectasia mutated	0.20096	0.19595	0.7163	1.34E-05
	MDM2	Mdm2 p53 binding protein homolog (mouse)	0.13358	0.12615	0.81085	4.05E-04
	NLRP3	NLR family, pyrin domain–containing 3	0.1788	0.1714	1.1884	1.93E-04
	MAP3K7	Mitogen-activated protein kinase kinase kinase 7	0.0216	0.0194	0.4786	8.93E-03
	RAD50	RAD50 homolog	0.09657	0.09343	0.28882	7.95E-03
	PRKDC	Protein kinase, DNA-activated, catalytic polypeptide	0.23036	0.22768	0.45155	6.80E-03
	KU80	X-ray repair complementing defective repair in Chinese hamster cells 5	0.31145	0.30436	0.91747	3.75E-02
	c-*REL*	v-*rel* reticuloendotheliosis viral oncogene homolog (avian)	0.2495	0.2403	1.5717	1.11E-02
P. alecto	*TBK1*	TANK-binding kinase 1	0.0643	0.0522	0.2930	1.29E-09
	LIG4	Ligase IV, DNA, ATP-dependent	0.12033	0.11376	0.24797	8.91E-04
	IL18	Interleukin 18 (interferon-γ–inducing factor)	0.5298	0.4532	1.7647	2.66E-04
	IFNG	Interferon-γ	0.5010	0.4527	1.3282	4.89E-03
	ISG15	ISG15 ubiquitin-like modifier	0.2069	0.1909	0.4387	2.63E-02
	DDX58	DEAD (Asp-Glu-Ala-Asp) box polypeptide 58	0.3040	0.2923	0.4661	1.23E-02
M. davidii	*IFNAR1*	Interferon (α, β, and ω) receptor 1	0.4954	0.4723	31.0924	7.00E-03
	TP53	Tumor protein p53	0.25623	0.23933	0.48123	7.00E-03
	BRCA2	Breast cancer 2, early onset	0.49002	0.47732	0.64213	1.31E-03
	IRAK4	Interleukin-1 receptor–associated kinase 4	0.1670	0.1583	0.3531	1.96E-02

immunoglobulin-like receptors (LILRs), carcinoembryonic antigen-related cell adhesion molecules (CEACAMs), and leukocyte-associated immunoglobulin-like receptors (LAIRs)] have undergone considerable gene duplication in *M. davidii* and other mammals yet have almost completely failed to expand in *P. alecto* (fig. S12). As the genes encoded within the LRC bind a variety of ligands and play multiple roles in immune regulation, these observations have diverse implications for differences in immune function between *P. alecto* and *M. davidii* and between bats and other mammals.

We identified seven complete and two partial copies of the digestive enzyme *RNASE4* in *M. davidii* (table S15), whereas *P. alecto RNASE4* has acquired a frameshift mutation resulting in loss of catalytic residues (fig. S13). We also identified critical amino acid changes in *M. davidii RNASE4* genes (relative to the mammalian consensus) that suggest diversification of substrate specificity (fig. S13). With a proven role in host defense against RNA viruses (*22*), *RNASE4* expansion in *M. davidii* may have implications for virus resistance but may also reflect the insectivorous diet of *M. davidii*, in contrast with that of *P. alecto*, which consumes predominantly fruit, flowers, and nectar.

M. davidii also differs from *P. alecto* in aspects including hibernation and echolocation (Fig. 1). Bile salt–stimulated lipase (BSSL), capable of hydrolyzing triglycerides into monoglycerides and subsequently releasing digestible free fatty acids, has been specifically expanded in *M. davidii* compared with *P. alecto* and other mammals (fig. S14). In addition, we observed six candidate genes related to hibernation, which showed positive selection in *M. davidii* and three other hibernating species relative to nonhibernators (table S16). Seven echolocation-related genes, including new candidates *WNT8A* and *FOS* (a subunit of the AP-1 transcription factor), had significantly higher ratio of nonsynonymous to synonymous substitutions (dN/dS) in the echolocating *M. davidii* branch relative to non-echolocating branches (table S17). Of note, the third exon in *M. davidii FOXP2* had even greater variation from the mammalian consensus than two previously identified variable sites (fig. S15), which suggests a specific transcript variant is involved in echolocation (*23*).

In summary, comparative analysis of *P. alecto* and *M. davidii* genomes has provided insight into the phylogenetic placement of bats and has revealed evidence of genetic changes that may have contributed to their evolution. Gene duplication events played a particularly prominent role in the evolution of *Myotis* bats and may have helped contribute to their speciation. Concentration of positively selected genes in the DNA damage checkpoint pathway in bats may indicate an important step in the evolution of flight, whereas evidence of change in components shared by the DNA damage pathway and the innate immune system raises the interesting possibility that flight-induced adaptations have had inadvertent effects on bat immune function and possibly also life expectancy (*24*). The data generated by this study will help to address major gaps in our understanding of bat biology and to provide new directions for future research.

References and Notes

1. E. C. Teeling *et al.*, *Science* **307**, 580 (2005).
2. M. F. Nery, D. J. González, F. G. Hoffmann, J. C. Opazo, *Mol. Phylogenet. Evol.* **64**, 685 (2012).
3. Y. Y. Shen *et al.*, *Proc. Natl. Acad. Sci. U.S.A.* **107**, 8666 (2010).
4. A. Barzilai, G. Rotman, Y. Shiloh, *DNA Repair (Amsterdam)* **1**, 3 (2002).
5. L. F. Wang, P. J. Walker, L. L. Poon, *Curr. Opin. Virol.* **1**, 649 (2011).
6. Materials and methods are available as supplementary materials on *Science* Online.
7. J. D. L. Smith, T. R. Gregory, *Biol. Lett.* **5**, 347 (2009).
8. E. J. Pritham, C. Feschotte, *Proc. Natl. Acad. Sci. U.S.A.* **104**, 1895 (2007).
9. H. Nishihara, M. Hasegawa, N. Okada, *Proc. Natl. Acad. Sci. U.S.A.* **103**, 9929 (2006).
10. A. T. Papenfuss *et al.*, *BMC Genomics* **13**, 261 (2012).
11. K. O'Keefe, H. P. Li, Y. P. Zhang, *Mol. Cell. Biol.* **23**, 6396 (2003).
12. J. Roth, M. Dobbelstein, D. A. Freedman, T. Shenk, A. J. Levine, *EMBO J.* **17**, 554 (1998).
13. T. D. Gilmore, S. Gerondakis, *Genes Cancer* **2**, 695 (2011).
14. A. De Siervi *et al.*, *Cell Cycle* **8**, 2093 (2009).
15. N. S. Kenneth, S. Mudie, S. Rocha, *EMBO J.* **29**, 2966 (2010).
16. K. Brzóska, I. Szumiel, *Mutagenesis* **24**, 1 (2009).
17. A. S. Turnell, R. J. Grand, *J. Gen. Virol.* **93**, 2076 (2012).
18. S. A. Schattgen, K. A. Fitzgerald, *Immunol. Rev.* **243**, 109 (2011).
19. J. A. Cridland *et al.*, *BMC Evol. Biol.* **12**, 140 (2012).
20. J. Tschopp, K. Schroder, *Nat. Rev. Immunol.* **10**, 210 (2010).
21. J. G. Sambrook, S. Beck, *Curr. Opin. Immunol.* **19**, 553 (2007).
22. F. Cocchi *et al.*, *Proc. Natl. Acad. Sci. U.S.A.* **109**, 5411 (2012).
23. G. Li, J. H. Wang, S. J. Rossiter, G. Jones, S. Y. Zhang, *PLoS ONE* **2**, e900 (2007).
24. A. K. Brunet-Rossinni, S. N. Austad, *Biogerontology* **5**, 211 (2004).

Acknowledgments: We thank H. Field, C. Smith, and M. Yu for helping source genomic DNA; K. Itahana and J. J. Boomsma for constructive discussion; and M. Cowled for graphics assistance. We acknowledge financial support from the China National Genebank at Shenzhen, CSIRO (Office of the Chief Executive Science Leaders Award, Julius Award), The Australian

Research Council (FT110100234), State Key Program for Basic Research (2011CB504701), National Natural Science Foundation of China (81290341), and the Defense Threat Reduction Agency of the USA. The views expressed in this article are those of the authors and do not necessarily reflect the official policy or position of the Department of the Navy, Department of Defense, or the U.S. government. K.A.B.-L. and K.G.F. are contractors for the U.S. government. This work was prepared as part of their official duties. Title 17 U.S.C. §105 provides that "Copyright protection under this title is not available for any work of the United States Government." Title 17 U.S.C. §101 defines a U.S. government work as a work prepared by a military service member or employee of the U.S. government as part of that person's official duties. *P. alecto* and *M. davidii* genomes have been deposited at DNA Data Bank of Japan/European Molecular Biology Laboratory/GenBank under the accession nos. ALWS01000000 and ALWT01000000. Short-read data have been deposited into the Short Read Archive under accession nos. SRA056924 and SRA056925. Raw transcriptome data have been deposited in Gene Expression Omnibus as GSE39933. Tree files and alignments have been submitted to TreeBASE under Study Accession URL: http://purl.org/phylo/treebase/phylows/study/TB2:S13654. We also thank the editor and two anonymous reviewers for their helpful comments and suggestions.
Author contributions: J.W., L.-F.W., G.Z., C.C.B., and K.A.B.-L. conceived the study. M.T., M.L.B., G.A.M., G.C., L.W., and Z.S. prepared the samples. G.Z., Z.H., X.F., Z.X., W.Z., Y. Zhu, X.J., L.Y., J.X., Y.F., Y.C., X.S., Y. Zhang, K.G.F., K.A.B.-L., and J.W. performed genome sequencing, assembly, and annotation. G.Z. and J.W. supervised genome sequencing, assembly, and annotation. G.Z., C.C., Z.H., X.F., J.W.W., Z.X., J.N., W.Z., P.Z., Y. Zhu, M.T., and M.L.B. performed genome analyses. G.Z., Z.H., C.C., and J.W.W. carried out genetic analyses. G.Z., C.C., Z.H., X.F., P.Z., J.N., M.T., J.W.W., M.L.B., and L.-F.W. discussed the data. All authors contributed to data interpretation. C.C. and J.W.W. wrote the paper with significant contributions from G.Z., Z.H., P.Z., J.N., M.T., M.L.B., and L.-F.W. and input from all authors. The authors declare no competing financial interests. Requests for materials should be addressed to the authors for correspondence.

Supplementary Materials
www.sciencemag.org/cgi/content/full/science.1230835/DC1
Materials and Methods
Figs. S1 to S15
Tables S1 to S17
References (*25*–*52*)

28 September 2012; accepted 10 December 2012
Published online 20 December 2012;
10.1126/science.1230835

Tunable Signal Processing Through Modular Control of Transcription Factor Translocation

Nan Hao,[1,2] Bogdan A. Budnik,[1] Jeremy Gunawardena,[3] Erin K. O'Shea[1,2]*

Signaling pathways can induce different dynamics of transcription factor (TF) activation. We explored how TFs process signaling inputs to generate diverse dynamic responses. The budding yeast general stress–responsive TF Msn2 acted as a tunable signal processor that could track, filter, or integrate signals in an input-dependent manner. This tunable signal processing appears to originate from dual regulation of both nuclear import and export by phosphorylation, as mutants with one form of regulation sustained only one signal-processing function. Versatile signal processing by Msn2 is crucial for generating distinct dynamic responses to different natural stresses. Our findings reveal how complex signal-processing functions are integrated into a single molecule and provide a guide for the design of TFs with "programmable" signal-processing functions.

Many transcription factors (TFs) display diverse activation dynamics in response to various external stimuli (*1*–*4*). To investigate how TFs process upstream signals, we studied the *Saccharomyces cerevisiae* general stress–responsive TF Msn2 (*5*). In the absence of stress, Msn2 is phosphorylated by protein kinase A (PKA) and localized to the cytoplasm; in response to stress, Msn2 is dephosphorylated and translocates to the nucleus, where it induces gene expression (*5*).

Natural stresses elicit highly variable dynamics of Msn2 nuclear translocation (Fig. 1A) (*6*, *7*), which are thought to result from oscillatory signaling inputs (presumably PKA activity) (*8*). To study how Msn2 processes oscillatory PKA inputs, we used an engineered yeast strain (*6*) carrying mutations in all three PKA isoforms that enable selective inhibition of PKA activity by a cell-permeable inhibitor, 1-NM-PP1 (*9*). We used this synthetic system and a microfluidics platform (*10*) mounted on a microscope to produce oscillatory inputs of PKA inhibition and monitored translocation of Msn2 to the nucleus. The input amplitude was chosen on the basis of the steady-state amount of Msn2 nuclear localization in response to sustained inputs: high-amplitude input (3 μM 1-NM-PP1) led to maximal nuclear localization of Msn2, whereas low-amplitude input (0.2 μM 1-NM-PP1) induced an intermediate amount of nuclear localization (Fig. 1B, black circles). The pulse duration of oscillatory input was selected on the basis of duration of pulsatile Msn2 nuclear bursts in the physiological response to glucose limitation (*6*). With high-amplitude oscillatory input, each input pulse induced a large amount of nuclear localization (Fig. 1C, left). In contrast, oscillatory input with low amplitude barely elicited any localization responses, although sustained input with the same amplitude led to a half-maximal amount of nuclear localization (Fig. 1C, right). Therefore, Msn2 filters temporal fluctuations of the input in an amplitude-dependent manner such that it tracks high-amplitude inputs, but responds in a limited manner to low-amplitude signals.

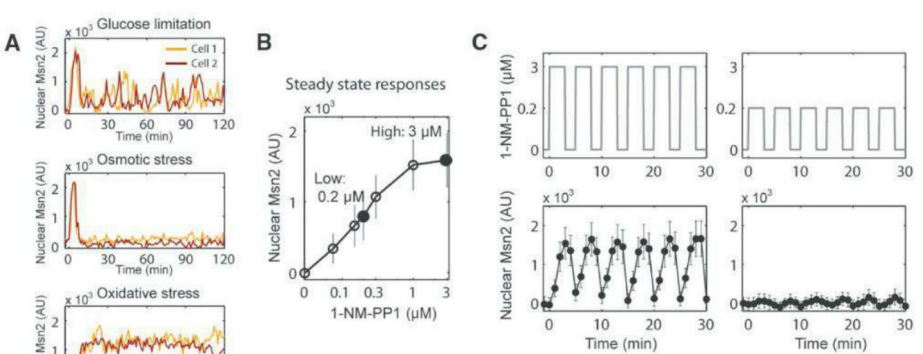

Fig. 1. Tunable signal-processing behaviors of Msn2. (**A**) Illustration of the distinct single-cell dynamic responses of Msn2 to various stresses. (**B**) Steady-state abundance of Msn2 in the nucleus in response to various concentrations of 1-NM-PP1. In response to each concentration of 1-NM-PP1, Msn2 exhibited uniform and stable nuclear localization in single cells and did not exhibit stochastic fluctuations as observed in natural stress responses. Open circles: responses to different concentrations of 1-NM-PP1; closed circles: responses to 3 μM and 0.2 μM 1-NM-PP1, which are used as high- and low-amplitude inputs, respectively, for the following analyses. AU, arbitrary unit. (**C**) Averaged single-cell time traces of Msn2 nuclear translocation (bottom: $n \approx 50$ cells; error bar: single-cell variances) in response to oscillatory inputs with high and low amplitudes (top). (Left) High-amplitude input produced by 3 μM 1-NM-PP1; (right) low-amplitude input produced by 0.2 μM 1-NM-PP1. Pulse duration of 3 min; pulse interval of 2 min. To emphasize the fact that 3 μM 1-NM-PP1 elicits a steady-state response that is about twice the response elicited by 0.2 μM 1-NM-PP1, the top *y* axes are not presented on a linear scale.

[1]Harvard University Faculty of Arts and Sciences Center for Systems Biology, Cambridge, MA 02138, USA. [2]Howard Hughes Medical Institute, Department of Molecular and Cellular Biology, and Department of Chemistry and Chemical Biology, Harvard University, Cambridge, MA 02138, USA. [3]Department of Systems Biology, Harvard Medical School, Boston, MA 02115, USA.

*To whom correspondence should be addressed. E-mail: erin_oshea@harvard.edu

To understand how Msn2 translates signaling inputs into different translocation responses, we characterized Msn2 phosphorylation, which controls nuclear translocation (*5*, *11*). We detected phosphorylation of eight PKA consensus sites, primarily located within the nuclear export signal (NES) and nuclear localization signal (NLS) domains (*11*) (fig. S1). Two sites in the NES (serine at positions S288 and S304) and four sites in the NLS (S582, S620, S625, S633) were functionally important for regulation of nuclear transport (fig. S2).

To intuitively understand the behaviors of the translocation system, we conducted a steady-state analysis that incorporated the separation of time scales for nuclear transport and phosphorylation. For simplicity, we represented regulation of nuclear export and import by phosphorylation of one site in the NES and a second site in the NLS, that act independently of each other (Fig. 2A). We assumed that the slowest time scales occur for nuclear import when the NLS is phosphorylated (k_{in}) and for nuclear export when the NES is unphosphorylated (k_{out}). In contrast, when the NLS is unphosphorylated or when the NES is phosphorylated, nuclear import and export, respectively, both were assumed to occur on faster time scales ($\boldsymbol{k_{in}'}$, $\boldsymbol{k_{out}'}$) (*12*). This scheme gives four phosphoforms with distinct combinations of transport rates (Fig. 2B). Finally, we assumed that phosphorylation and dephosphorylation are fast relative to the translocation time scales (*13*, *14*), so that we could treat transitions between the four phosphoforms, which are triggered by input of PKA inhibition, as effectively instantaneous. PKA and Msn2 phosphatases localize to both the cytoplasm and the nucleus in yeast (*15*–*17*), so Msn2 can be phosphorylated and dephosphorylated in both compartments.

For purposes of illustration, we used a weak and a strong input to represent the amplitude of PKA inhibition (Fig. 2C). Because sites in the

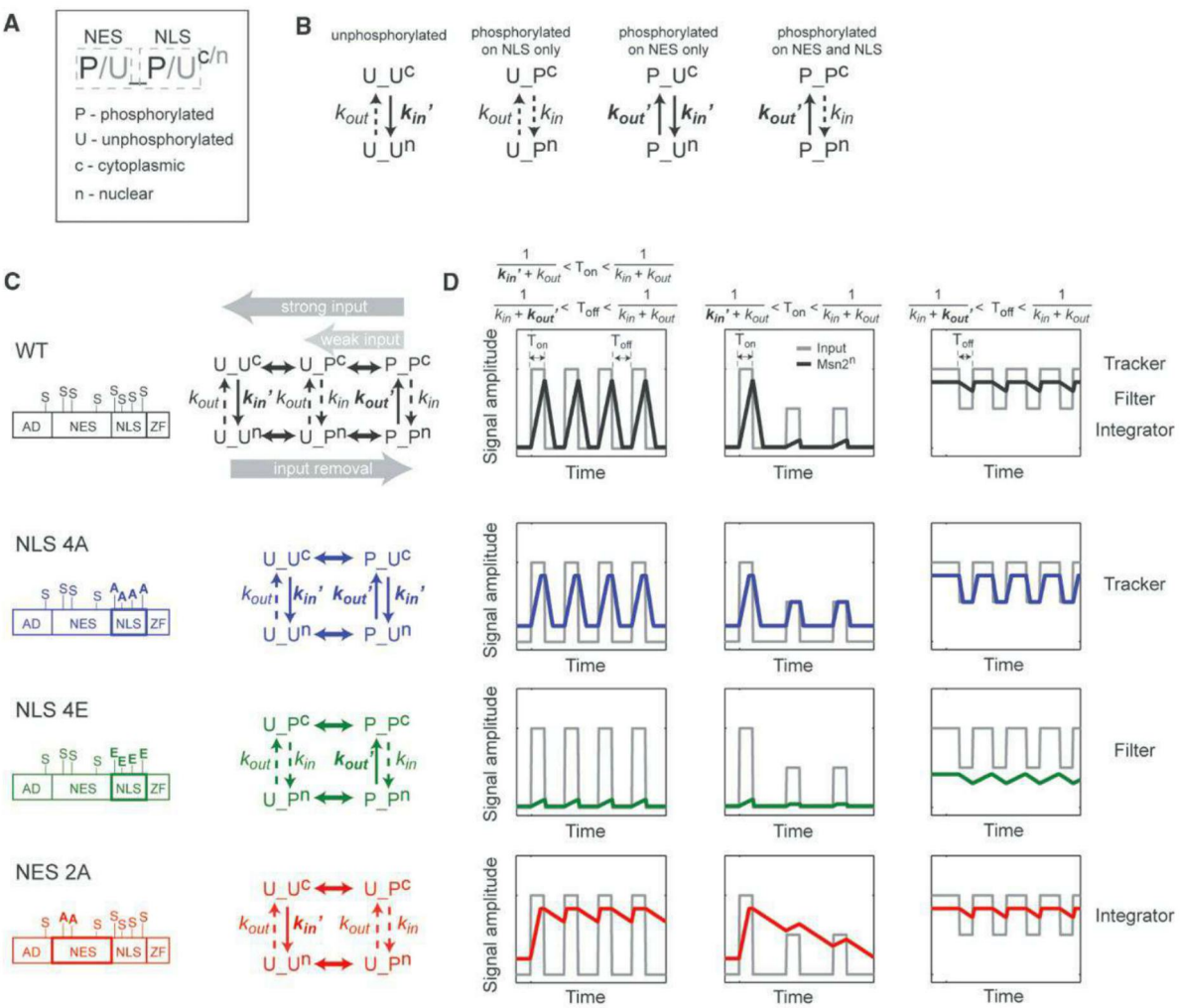

Fig. 2. A theoretical analysis of TF translocation. (**A**) Nomenclature used to define the status of phosphorylation and localization of the TF: for example, the first "P/U": the NES is phosphorylated (P) or unphosphorylated (U); "c/n": superscript shows location in the cytoplasm (c) or nucleus (n). (**B**) Phosphorylation states determine the rate constants of nucleocytoplasmic transport. Unphosphorylated or phosphorylated NES has slow (dashed line) or fast (solid line) nuclear export rates (k_{out}, $\boldsymbol{k_{out}'}$), respectively; unphosphorylated or phosphorylated NLS has fast (solid line) or slow (dashed line) nuclear import rates ($\boldsymbol{k_{in}'}$, k_{in}), respectively. Thus, each phosphoform has a specific combination of nuclear import and export rates. (**C**) The translocation model. (Left) Schematic of WT and phosphosite mutants; (right) model structures and reaction flows (gray arrows) in response to strong or weak inputs and input removal. First row: WT; second row: NLS 4A at S582A, S620A, S625A, and S633A; third row: NLS 4E at S582E, S620E, S625E, and S633E; fourth row: NES 2A at S288A and S304A. We did not specifically study the case in which the NES sites are constitutively phosphorylated because Ser-to-Glu mutants of the NES sites behaved similarly to Ser-to-Ala mutants, which suggests that Glu cannot mimic phosphorylation on NES sites (fig. S2A). (**D**) Predicted responses to various dynamic inputs—first column: oscillatory high-amplitude input, second column: oscillatory input with varied amplitudes, third column: input fluctuating between high and low amplitudes. Color key—black: responses of WT, blue: NLS 4A, green: NLS 4E, red: NES 2A. The ranges of input time scales necessary to generate the predicted responses are determined by the fast and slow time scales of transport rates and are listed above each column. Model output was generated by a steady-state analysis of the translocation system (supplementary materials).

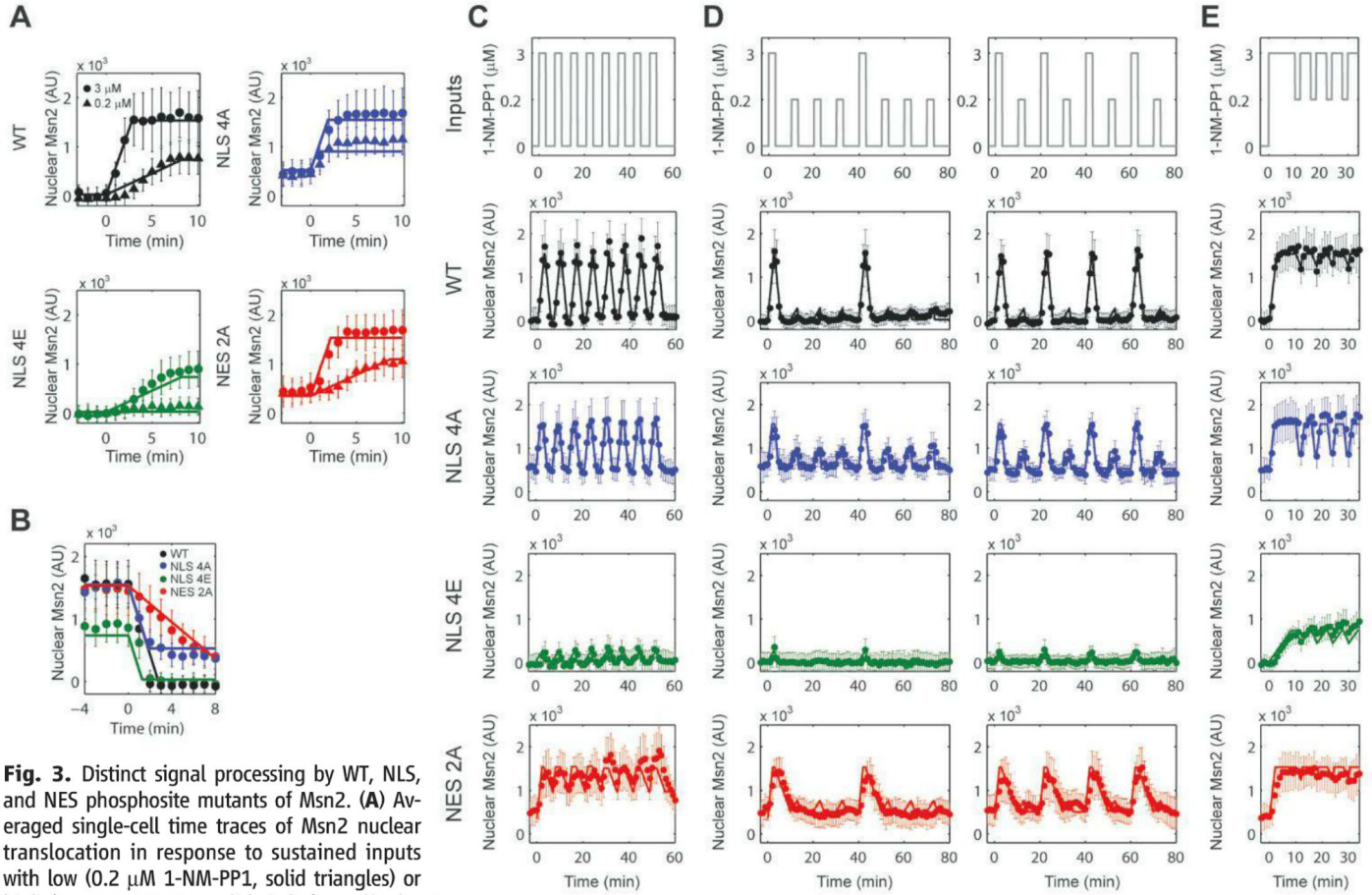

Fig. 3. Distinct signal processing by WT, NLS, and NES phosphosite mutants of Msn2. (**A**) Averaged single-cell time traces of Msn2 nuclear translocation in response to sustained inputs with low (0.2 μM 1-NM-PP1, solid triangles) or high (3 μM 1-NM-PP1, solid circles) amplitudes. Inputs were applied at time point zero. (**B**) Averaged single-cell time traces of Msn2 nuclear translocation in response to removal of high-amplitude input (3 μM 1-NM-PP1). (**C**) Averaged single-cell time traces of Msn2 nuclear translocation in response to oscillatory high-amplitude (3 μM 1-NM-PP1) inputs. Pulse duration of 3 min; pulse interval of 4 min. (**D**) Time traces of Msn2 nuclear translocation in response to oscillatory inputs with a mixture of low- and high-amplitude pulses (0.2 μM 1-NM-PP1 and 3 μM 1-NM-PP1, respectively). (**E**) Time traces of Msn2 nuclear translocation in response to input fluctuating between high (3 μM 1-NM-PP1) and low (0.2 μM 1-NM-PP1) amplitudes. For (A) to (E), data points are averaged single-cell time traces ($n \approx 50$ cells; error bar: single-cell variances). The simple model in Fig. 2 has been fitted to the time trace data in this figure, and the solid lines in (A) to (E) are model fitting results (see supplementary materials, "Model parameters are constrained by experimental data" for details). The dependence of the responses on the time scales of input and transport rates is presented in the supplementary materials, "The relation between time scales of input and time scales of transport rates."

NLS are preferred for PKA phosphorylation over those in the NES (*11*, *18*) (fig. S3), we assumed that weak input (partial inhibition of PKA) would lead to dephosphorylation of only the NES, and the NLS phosphorylated form (U_P^c) would then go to the nucleus with a slow import rate (k_{in}). In contrast, strong input would lead to dephosphorylation of both the NES and NLS, and the fully unphosphorylated form (U_U^n) would be transported into the nucleus with a fast rate ($\boldsymbol{k_{in}'}$). Upon input removal, the NES and NLS are rephosphorylated and the doubly phosphorylated form (P_P^n) is expected to be exported with a fast export rate ($\boldsymbol{k_{out}'}$) (Fig. 2C, first row). In accordance with this analysis, strong input (3 μM 1-NM-PP1) led to rapid Msn2 translocation, whereas weak input (0.2 μM 1-NM-PP1) resulted in slower translocation, and export is rapid when PKA inhibition is removed [Fig. 3, A and B, wild type (WT)].

We then analyzed how Msn2 might respond to oscillatory inputs. In response to a strong oscillatory input, Msn2 would go in and out of the nucleus with import and export rates ($\boldsymbol{k_{in}'}$, $\boldsymbol{k_{out}'}$) that are fast relative to the input pulse duration and interpulse interval. Hence, Msn2 responded fully to each pulse and tracked the input dynamics (model: Fig. 2D, first row, left; data: Fig. 3C, WT). In response to a weak oscillatory input, Msn2 would enter the nucleus with a slow import rate (k_{in}) relative to the time scale of the input pulse, and therefore, only a small amount of Msn2 entered the nucleus, effectively filtering out low-amplitude signals (model: Fig. 2D, first row, middle; data: Fig. 3D, WT). In response to an input fluctuating between high and low amplitudes, because Msn2 would go out of the nucleus with a slow export rate (k_{out}) relative to the time scale of the interpulse intervals, Msn2 was not fully exported during the interval and integrated the input fluctuations (model: Fig. 2D, first row, right; data: Fig. 3E, WT).

To further test the model and explore the influence of regulation of both import and export on signal processing, we studied cases in which only nuclear import or export, but not both, was regulated by phosphorylation because the functional phosphosites within the NES or NLS were mutated (Figs. 2, C and D, and 3).

In the case in which the NLS sites could not be phosphorylated (NLS 4A), Msn2 would enter the nucleus with a constitutively fast import rate ($\boldsymbol{k_{in}'}$) and go out of the nucleus with a fast export rate ($\boldsymbol{k_{out}'}$) upon input removal (Fig. 2C, second row; data: Fig. 3, A and B, NLS 4A). Hence, in response to oscillatory inputs with high amplitude, low amplitude, or fluctuating between high and low amplitudes, Msn2 would have fast import and export rates; it fully entered the nucleus during a pulse and exited the nucleus during interpulse intervals (model: Fig. 2D, second row; data: Fig. 3, C to E, NLS 4A).

If NLS sites were mutated to mimic constitutive phosphorylation (NLS 4E), Msn2 would enter the nucleus with a constitutively slow im-

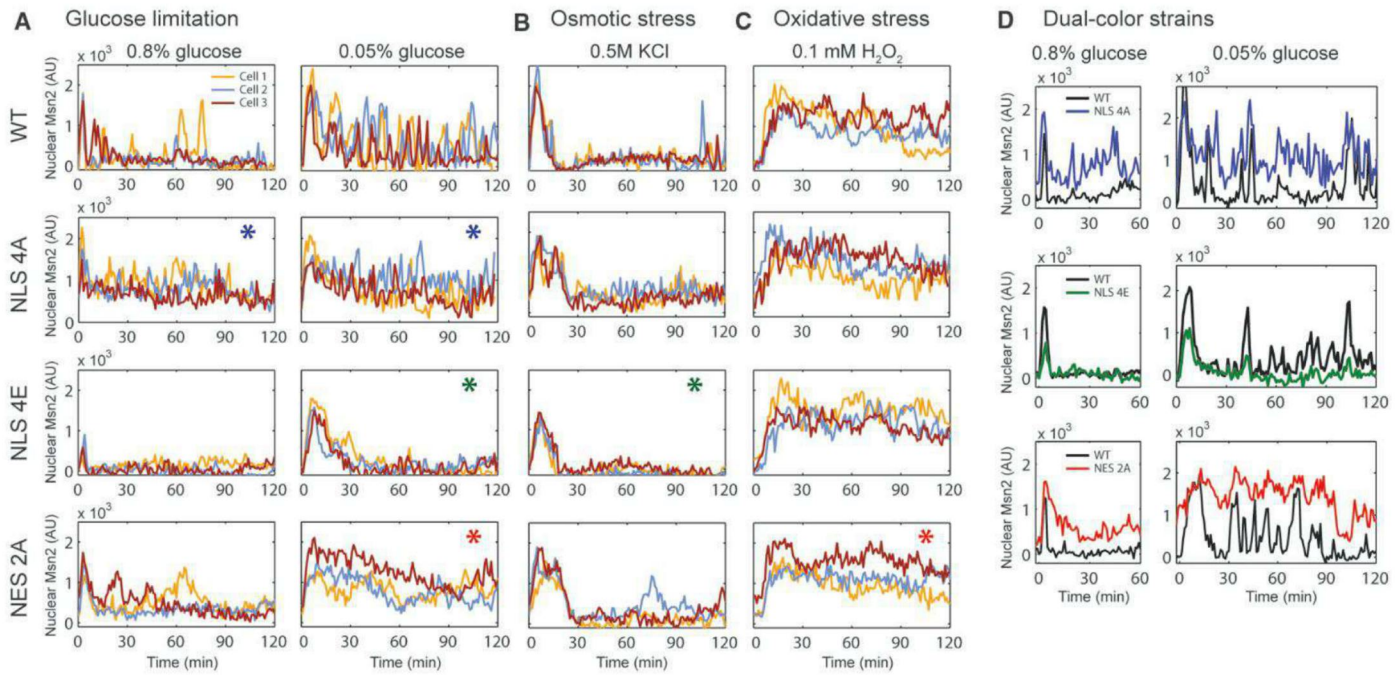

Fig. 4. Distinct responses of WT, NLS, and NES phosphosite mutants of Msn2 to natural stresses. Single-cell responses of WT, NLS 4A, NLS 4E, and NES 2A to glucose limitation (**A**), osmotic stress (**B**), and oxidative stress (**C**) ($n \approx 50$ cells, each stress condition). Representative single-cell time traces of Msn2 nuclear translocation are shown. Asterisks emphasize the conditions under which the mutants fail to distinguish two different stresses. Quantification of the time traces is presented in fig. S4. (**D**) Time traces of WT Msn2-mCherry and mutant Msn2-YFP, monitored in the same cells, in response to glucose limitation (black, WT; blue, NLS 4A; green, NLS 4E; red, NES 2A). More single-cell traces are shown in fig. S5.

port rate (k_{in}) (Fig. 2C, third row; data: Fig. 3A, NLS 4E). In response to oscillatory inputs, when the input duration is short relative to the time scale of the slow import rate, Msn2 went into the nucleus slowly and reached low concentrations (model: Fig. 2D, third row; data: Fig. 3, C to E, NLS 4E).

If NES sites cannot be phosphorylated (NES 2A), Msn2 would exit the nucleus with a constitutively slow export rate (k_{out}) (Fig. 2C, fourth row; data: Fig. 3B, NES 2A). In response to oscillatory inputs with high amplitude, low amplitude or fluctuating between high and low amplitudes, when the interval is short relative to the time scale of the slow export rate, Msn2 would have a slow export rate, could not fully exit the nucleus during intervals, and, therefore, it integrated responses to rapidly changing inputs (model: Fig. 2D, fourth row; data: Fig. 3, C to E, NES 2A). In summary, NLS 4A, NLS 4E, or NES 2A "tracks," "filters," or "integrates" the oscillatory inputs, respectively, whereas WT Msn2 exhibits a combination of all these processing behaviors.

To study the processing of natural stress signals, we monitored WT and mutant Msn2 translocation in response to different stresses (Fig. 4, A to C, and fig. S4). We also monitored the dynamics of WT Msn2-mCherry and mutant Msn2-YFP (fused to yellow fluorescent protein) expressed together in the same cells—this allowed us to directly compare the responses of WT and mutant Msn2 to the same stochastic input signals triggered by natural stress (Fig. 4D and fig. S5). Glucose limitation induced sporadic pulses of rapid nuclear localization of WT Msn2 with frequency regulated by stress intensity; osmotic stress elicited a single pulse of nuclear accumulation; and oxidative stress led to sustained nuclear localization (Fig. 4, A to C, and fig. S4, WT). NLS 4A, which tracks the inputs, was more responsive to inputs and exhibited a high frequency of small rapid bursts of nuclear translocation (Fig. 4D, first row), and thus produced similar response frequencies to low and high levels of glucose limitation (Fig. 4, A to C, second row, marked with blue asterisks; fig. S4D, left, blue circles). By contrast, NLS 4E filtered out the sporadic translocation bursts in response to glucose limitation (Fig. 4D, second row), and therefore, NLS 4E exhibits similar dynamics in response to glucose limitation and osmotic stress (Fig. 4, A to C, third row, marked with green asterisks). NES 2A integrated the sporadic bursts in response to strong glucose limitation (Fig. 4D, third row) and exhibited prolonged nuclear accumulation, similar to that of oxidative stress responses (Fig. 4, A to C, fourth row, marked with red asterisks). Consistent with the analysis of artificial inputs, WT Msn2 and the mutants differed in how they processed signaling inputs triggered by natural stresses and, therefore, generated different responses. WT Msn2 with dual regulation of nuclear import and export generates distinct translocation responses to different stress conditions, whereas the mutants that have only one mode of nuclear transport regulation fail to fully differentiate the different stresses into distinct translocation outputs. Cells may use these diverse TF translocation patterns to induce distinct gene expression programs (*6*) or to elicit different levels of noise in single-cell responses, both of which might be beneficial for survival under stressful conditions.

Nucleocytoplasmic translocation of many mammalian TFs—such as nuclear factors of activated T cells, signal transducers and activators of transcription, and Smads (*19*–*21*)—is controlled by regulation of both their nuclear localization and nuclear export signals. Hence, the proposed dual regulation mechanism may represent a general mechanism for shaping the dynamic behaviors of these TFs. Complex signal-processing behaviors can be achieved by signaling circuits composed of multiple molecules (*22*–*29*). We reveal that a single TF molecule can also mediate sophisticated signal-processing functions by assembling independent functional modules. These functions are "tunable" by phosphorylation at multiple sites in each module and "programmable" by mutating or reassembling functional modules.

References and Notes

1. S. L. Werner, D. Barken, A. Hoffmann, *Science* **309**, 1857 (2005).
2. E. Batchelor, A. Loewer, C. Mock, G. Lahav, *Mol. Syst. Biol.* **7**, 488 (2011).
3. T. K. Lee *et al.*, *Sci. Signal.* **2**, ra65 (2009).
4. J. E. Purvis *et al.*, *Science* **336**, 1440 (2012).
5. W. Görner *et al.*, *Genes Dev.* **12**, 586 (1998).
6. N. Hao, E. K. O'Shea, *Nat. Struct. Mol. Biol.* **19**, 31 (2012).
7. L. Cai, C. K. Dalal, M. B. Elowitz, *Nature* **455**, 485 (2008).

8. C. Garmendia-Torres, A. Goldbeter, M. Jacquet, *Curr. Biol.* **17**, 1044 (2007).
9. A. C. Bishop *et al.*, *Nature* **407**, 395 (2000).
10. P. Hersen, M. N. McClean, L. Mahadevan, S. Ramanathan, *Proc. Natl. Acad. Sci. U.S.A.* **105**, 7165 (2008).
11. W. Görner *et al.*, *EMBO J.* **21**, 135 (2002).
12. A. Komeili, E. K. O'Shea, *Science* **284**, 977 (1999).
13. N. Shulga *et al.*, *J. Cell Biol.* **135**, 329 (1996).
14. J. A. Adams, S. S. Taylor, *J. Biol. Chem.* **268**, 7747 (1993).
15. W. K. Huh *et al.*, *Nature* **425**, 686 (2003).
16. V. Tudisca *et al.*, *Eur. J. Cell Biol.* **89**, 339 (2010).
17. J. M. Tkach *et al.*, *Nat. Cell Biol.* **14**, 966 (2012).
18. G. Neuberger, G. Schneider, F. Eisenhaber, *Biol. Direct* **2**, 1 (2007).
19. H. Okamura *et al.*, *Mol. Cell* **6**, 539 (2000).
20. N. C. Reich, L. Liu, *Nat. Rev. Immunol.* **6**, 602 (2006).
21. X. Chen, L. Xu, *Cell Biosci.* **1**, 40 (2011).
22. S. Levy, M. Kafri, M. Carmi, N. Barkai, *Science* **334**, 1408 (2011).
23. D. M. Longo, A. Hoffmann, L. S. Tsimring, J. Hasty, *Syst. Synth. Biol.* **4**, 15 (2010).
24. W. A. Lim, *Nat. Rev. Mol. Cell Biol.* **11**, 393 (2010).
25. J. C. W. Locke, J. W. Young, M. Fontes, M. J. Hernández Jiménez, M. B. Elowitz, *Science* **334**, 366 (2011).
26. E. C. O'Shaughnessy, S. Palani, J. J. Collins, C. A. Sarkar, *Cell* **144**, 119 (2011).
27. M. Behar, A. Hoffmann, *Curr. Opin. Genet. Dev.* **20**, 684 (2010).
28. M. R. Bennett *et al.*, *Nature* **454**, 1119 (2008).
29. C. J. Bashor, N. C. Helman, S. Yan, W. A. Lim, *Science* **319**, 1539 (2008).

Acknowledgments: We thank A. Murray, P. Cluzel, S. Ramanathan, B. Stern, and M. Rust for comments on the manuscript and S. Mukherji, X. Zhou, A. S. Hansen, and other members of the O'Shea lab for helpful discussions. J.G. is supported by NIH R01 GM081578. E.K.O. is an Investigator of the Howard Hughes Medical Institute.

Supplementary Materials

www.sciencemag.org/cgi/content/full/339/6118/460/DC1
Materials and Methods
Supplementary Text
Figs. S1 to S5
References (*30*–*33*)

11 July 2012; accepted 7 December 2012
10.1126/science.1227299

An Actin-Dependent Step in Mitochondrial Fission Mediated by the ER-Associated Formin INF2

Farida Korobova,[1] Vinay Ramabhadran,[2] Henry N. Higgs[1]*

Mitochondrial fission is fundamentally important to cellular physiology. The dynamin-related protein Drp1 mediates fission, and interaction between mitochondrion and endoplasmic reticulum (ER) enhances fission. However, the mechanism for Drp1 recruitment to mitochondria is unclear, although previous results implicate actin involvement. Here, we found that actin polymerization through ER-localized inverted formin 2 (INF2) was required for efficient mitochondrial fission in mammalian cells. INF2 functioned upstream of Drp1. Actin filaments appeared to accumulate between mitochondria and INF2-enriched ER membranes at constriction sites. Thus, INF2-induced actin filaments may drive initial mitochondrial constriction, which allows Drp1-driven secondary constriction. Because INF2 mutations can lead to Charcot-Marie-Tooth disease, our results provide a potential cellular mechanism for this disease state.

Mitochondrial function extends far beyond that of energy generation, because mitochondria act as sensors of metabolic homeostasis and are key players in cell death pathways (*1*–*4*). The dynamic ability of mitochondria to undergo fission and fusion and to move in cells is important for mitochondrial function, and defects in mitochondrial dynamics are implicated in many neurodegenerative diseases (*5*, *6*). Fission involves oligomerization of dynamin-related protein 1 (Drp1, called Dnm1 in yeast) into a helical ring around the outer mitochondrial membrane, followed by ring constriction. The mechanism for Drp1 recruitment to fission sites, however, is unclear. The diameter of the Drp1 ring is narrower (100 to 130 nm for Dnm1) than an unconstricted mitochondrion (*7*), which suggests that prior constriction may be required. Mitochondrial fission occurs preferentially at endoplasmic reticulum (ER) contact sites, with ER circumscribing mitochondria (*8*). Mitochondria are constricted at these ER contact sites even when Drp1 activity is compromised (*8*). Drp1- and Dnm1-independent constriction is also observed in *Caenorhabditis elegans* (*9*) and budding yeast (*10*), respectively. The mechanism of Drp1-independent mitochondrial constriction is unknown, although actin filaments are implicated in the process (*11*).

Inverted formin 2 (INF2) is a vertebrate formin protein that accelerates both actin polymerization and depolymerization (*12*). In mammalian cells, INF2 exists as two isoforms differing in C-terminal sequence (fig. S1): the prenylated (CAAX) isoform, which is tightly bound to ER (*13*), and the nonCAAX isoform, which is cytoplasmic (*14*). Suppression of INF2-nonCAAX in tissue culture cells causes Golgi dispersal (*14*). In contrast, the cellular function of INF2-CAAX is unclear because its suppression has no apparent effect on ER structure or dynamics (*13*). Physiologically, mutations in INF2 are linked to two human diseases: focal and segmental glomerulosclerosis, a degenerative kidney disease (*15*), and Charcot-Marie-Tooth disease (CMTD), a peripheral neuropathy (*16*).

We decided to test a role for INF2 in controlling mitochondrial size, on the basis of two factors. First, mitochondrial fission takes place at ER contact sites (*8*). Second, other proteins mutated in CMTD affect mitochondrial dynamics (*17*–*19*). INF2 suppression by small interfering RNAs (siRNAs) in either a human osteosarcoma cell line (U2OS) (Fig. 1, A and B, and fig. S2C) or a mouse fibroblast line (NIH 3T3) (fig. S2, A and B) resulted in significant increases in mitochondrial average length and in the percentage of mitochondria over 5 μm. We then tested whether specific suppression of INF2-CAAX in U2OS cells would result in similar mitochondrial elongation. When we treated U2OS cells with two distinct siRNAs that specifically suppressed INF2-CAAX (fig. S3), mitochondrial length increased 2.5 times (Fig. 1, A and B). However, INF2-CAAX depletion did not cause Golgi expansion (fig. S4), an effect attributable to INF2-nonCAAX (*14*). U2OS cells express considerably less INF2-CAAX than NIH 3T3 cells (*14*) but did express detectable levels of INF2-CAAX protein (fig. S3B). Thus, suppression of INF2-CAAX, which localizes to ER, causes an increase in mitochondrial length.

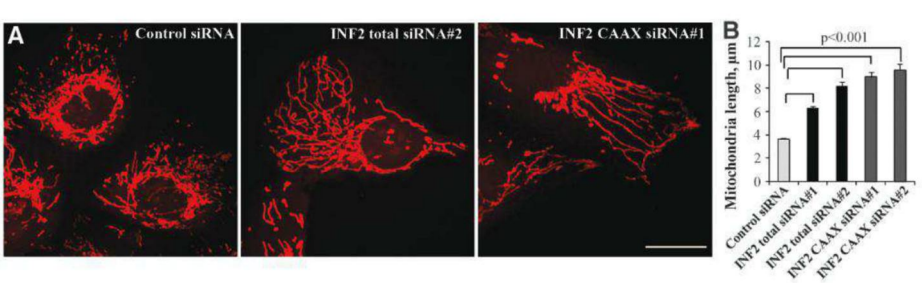

Fig. 1. INF2 suppression increases mitochondrial length. (**A**) Maximum intensity projections of confocal images of MitoTracker-labeled U2OS cells treated with the indicated siRNAs. Scale bar, 20 μm. (**B**) Quantification of mitochondrial lengths. n = 157 to 531 mitochondria. Error bars, SEM.

[1]Department of Biochemistry, Geisel School of Medicine at Dartmouth, Hanover, NH 03755, USA. [2]Howard Hughes Medical Institute, Sackler School of Graduate Biomedical Sciences, Tufts University, Boston, MA 02111, USA.

*To whom correspondence should be addressed. E-mail: henry.higgs@dartmouth.edu

We then tested whether INF2-CAAX overexpression would induce an effect on mitochondria opposite to INF2-CAAX suppression. A green fluorescent protein (GFP)–fusion construct of INF2-CAAX wild type (INF2-WT) localized to ER in U2OS cells (*14*). However, this construct did not cause a significant change in mitochondrial length (Fig. 2, A and B). We reasoned that INF2-WT might be autoinhibited, because INF2 has autoinhibitory sequences similar to other formins (*13*). To test this hypothesis, we changed Ala^{149} to aspartic acid (D), because a similar mutation in the formin mDia1 causes constitutive activation (*20*). INF2-A149D decreased mitochondrial length by a factor of 2.2 (Fig. 2, A and B). In addition, INF2-A149D cells displayed a higher frequency of constricted ER-mitochondrial contact sites than control cells (Fig. 2C and fig. S5D). Thus, constitutively active INF2-CAAX causes a decrease in mitochondrial length and an increase in mitochondrial constriction frequency.

We examined INF2-A149D effects in more detail by live-cell microscopy, using ER-green [ER-targeting sequence of ubiquitin-conjugating enzyme E2 6 (UBC6) fused to GFP (*21*)] as a negative control. In ER-green cells, infrequent fission events occurred (fig. S5A and movie S1). In contrast, fission events were about three times as frequent in INF2-A149D cells (fig. S5, B and C). These fission events always corresponded to regions where INF2 circumscribed the mitochondrion (Fig. 2D and movie S2). In addition, mitochondria were less mobile in INF2-A149D cells than in ER-green or INF2-WT cells (Fig. 2E, fig. S6, and movies S3 to S6).

The decrease in mitochondrial mobility raised the possibility that INF2's effect on mitochondrial size was due to an indirect effect on fusion, because it prevented mitochondria from interacting. Indeed, quantification of live-cell images indicated a decrease by a factor of 2.3 in mitochondrial fusion in INF2-A149D cells (fig. S5, B and C). Thus, INF2-A149D results in both an increase in fission and a decrease in fusion. However, analysis of live-cell images of INF2-suppressed cells revealed a drop by a factor of 2.2 in fission events with only a minor decrease in fusion (fig. S5, B and C). Thus, we conclude that INF2 has a direct effect on mitochondrial fission, whereas the effect of INF2-A149D on fusion is indirect, owing to a decrease in mitochondrial mobility.

Because Drp1 acts in mitochondrial fission, we examined a potential connection between INF2 and Drp1. Drp1 localized to cytoplasm and to mitochondrially associated puncta in U2OS cells (Fig. 3, A and C). Suppression of Drp1 reduced mitochondrially associated puncta, in addition to causing mitochondrial elongation (Fig. 3A and fig. S7, A and B). Drp1 puncta also decreased upon INF2 suppression (Fig. 3, A and B), without a reduction in total cellular Drp1 (fig. S7A). In contrast, INF2-A149D expression caused dense Drp1 puncta associated with mitochondria (Fig. 3D). Thus, INF2 facilitates interaction of Drp1 with mitochondria. If Drp1 acts downstream of INF2, alterations in Drp1 activity should inhibit INF2-A149D–induced mitochondrial fission. Both Drp1 suppression by siRNA and the dominant-negative (guanosine triphosphatase–deficient) K38E Drp1 construct (in which Glu replaces Lys^{38}) reversed the effect of INF2-A149D on mitochondria size, with the K38E mutant producing a stronger effect (Fig. 3. E and F). Thus, INF2-mediated mitochondrial fission occurs through Drp1.

The fact that Drp1 suppression resulted in longer average mitochondria than did INF2 suppression (fig. S7B and Fig. 1B) might be due to several factors that are not mutually exclusive. First, INF2 may only participate in a subset of fission reactions. Second, INF2 activity may not be essential for fission but may facilitate the process. Third, low levels of INF2-CAAX may be sufficient to mediate fission, such that RNA interference–mediated suppression is insufficient for full inhibition.

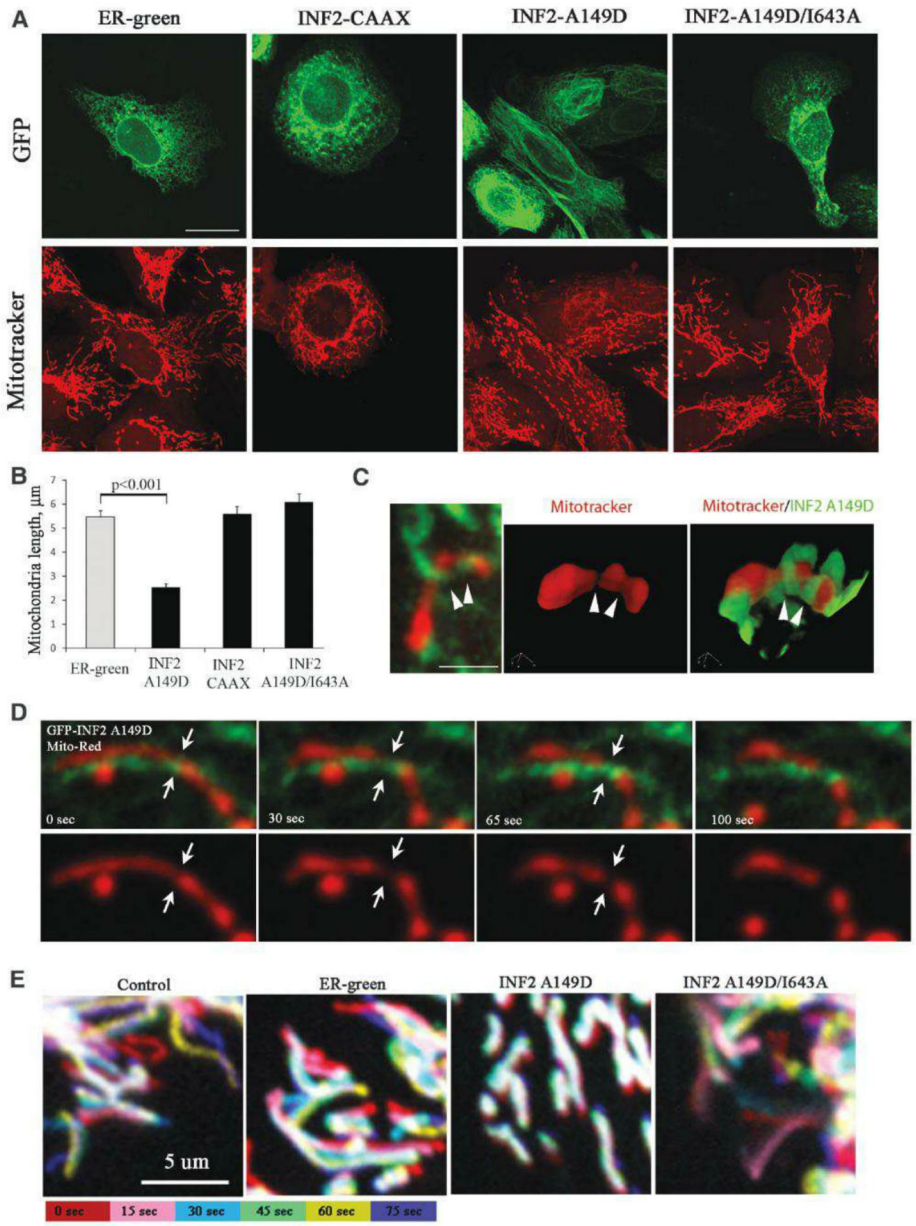

Fig. 2. Constitutively active INF2-CAAX decreases mitochondrial length and dynamics. (**A**) Micrographs of U2OS cells transfected with GFP-fusions and labeled with MitoTracker. INF2 constructs are CAAX. Scale bar, 20 μm. (**B**) Quantifications of mitochondrial length. n = 158 to 537 mitochondria. Error bars, SEM. (**C**) Confocal micrographs of mitochondrion in close association with INF2-A149D. (Left) Maximum intensity projection of z stack. (Right) 3D reconstruction of MitoTracker alone or MitoTracker with GFP overlay. Arrowheads indicate constriction and/or fission sites. Scale bar, 2 μm. (**D**) Mitochondrial dynamics (mitochondria labeled using Mito Red) in U2OS transfected with GFP–INF2-A149D. Arrows indicate the fission event. Scale bar, 5 μm. (**E**) Overlays of mitochondrial dynamics time course in cells transfected with indicated constructs. Colors depict time points in the sequence, with white color indicating relative immobility.

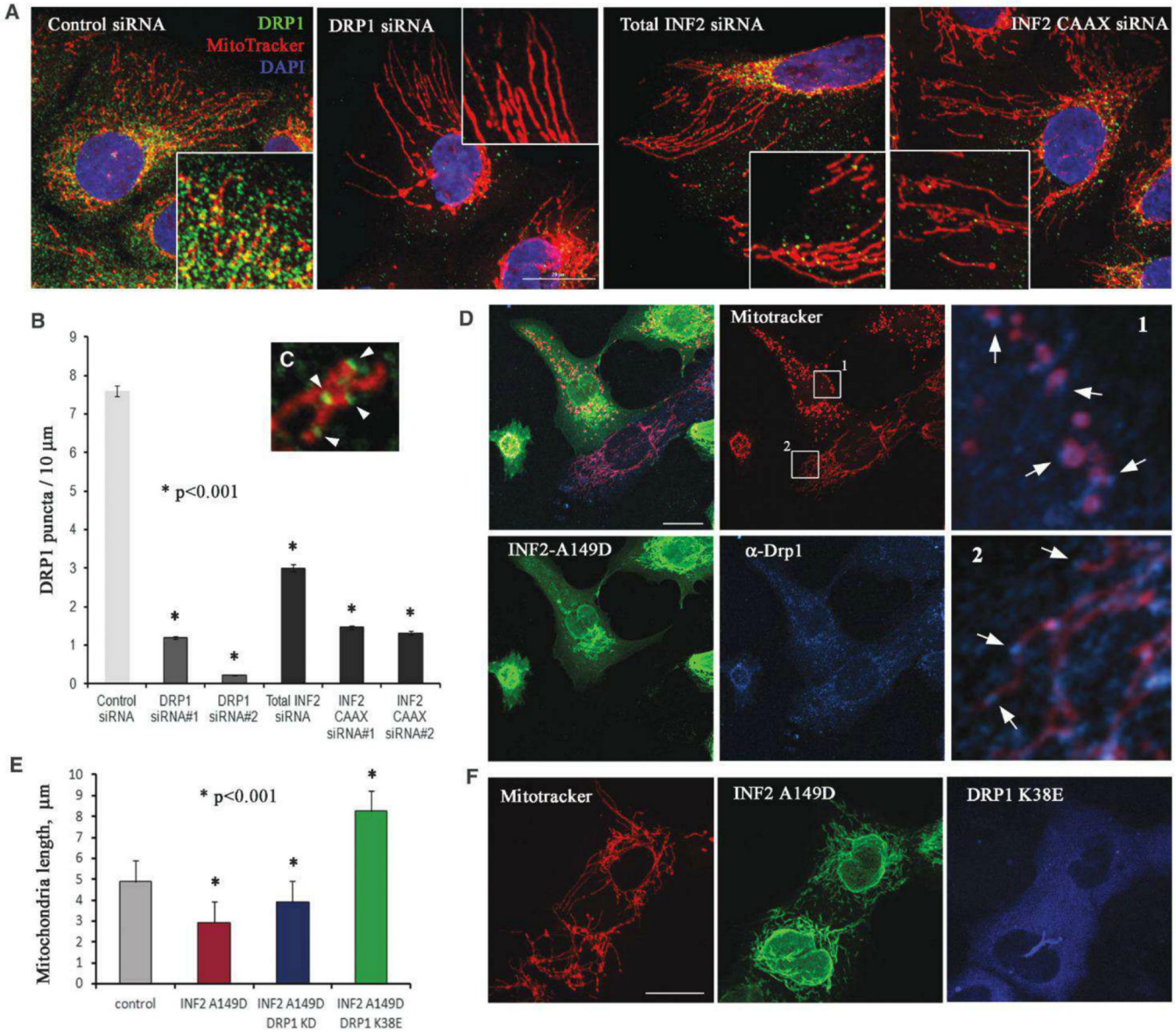

Fig. 3. INF2 enhances Drp1-mitochondria association. **(A)** Confocal micrographs of U2OS cells labeled with an antibody against Drp1 (green) after indicated siRNA treatment. MitoTracker staining (red), and 4′,6-diamidino-2-phenylindole (DAPI) staining (blue). (Insets) Close-ups of peripheral cellular regions. Scale bar, 20 μm. **(B)** Quantification of Drp1 puncta per mitochondrial length, $n = 40$ to 68 mitochondria. Error bars, SEM. **(C)** Example of Drp1 puncta localization to mitochondria (arrowheads). **(D)** Effect of INF2-A149D expression (green) on Drp1 puncta. Mitochondria (red), Drp1 (blue). (Right) Close-ups of regions in INF2-A149D (1) and control cells (2). Scale bar, 20 μm. **(E** and **F)** Inhibition of Drp1 reduces the effect of INF2-A149D and makes mitochondria longer. (E) Quantification of mitochondrial length upon INF2-A149D expression and either Drp1 suppression or Drp1 K38E coexpression. $n = 199$ to 531 mitochondria. Error bars, SEM. (F) Confocal micrographs of U2OS cells coexpressing Mito Red (red), INF2-A149D (green), and Drp1 K38E (blue). Scale bar, 20 μm.

INF2 interacts with both actin and microtubules (*22*), and its effects on mitochondria could be mediated through either cytoskeletal element. We used the actin monomer–sequestering drug latrunculin B (LatB) to test a role for actin in mitochondrial fission. LatB significantly increased mitochondrial length in U2OS cells (Fig. 4, A and B), similar to its effect on other cell types (*11*). Furthermore, LatB antagonized INF2-A149D–induced mitochondrial shortening (Fig. 4, A and B). To test further the relevance of actin filaments to INF2's mitochondrial effects, we mutated a key actin polymerization residue, Ile^{643} (fig. S1) (*23*). The I643A mutation antagonized the effects of INF2-A149D on both mitochondrial length and mitochondrial mobility (Fig. 2 and movie S6). This mutation did not alter INF2-microtubule interactions (fig. S8), which indicated that its effects were specific to actin regulation. Thus, INF2 affects mitochondrial length and ER-mitochondrial interaction in an actin-dependent manner.

We sought direct evidence for actin filament accumulation at ER-mitochondrial contact sites, using laser scanning confocal microscopy to construct three-dimensional (3D) images. This analysis was difficult because of the abundance of stress fibers and other cytoplasmic actin filaments, which obscured potential mitochondrially associated actin. Analysis of U2OS cells transfected with INF2-WT revealed filament accumulation at 16% of ER-mitochondrial contact sites (fig. S9, B and C). Cells transfected with INF2-A149D displayed a higher percentage (65%) of actin-enriched ER-mitochondrial contacts (Fig. 4, C to E, and fig. S9, A and C), with peak filament staining occurring between the mitochondrial and INF2 staining (Fig. 4E). Thus, actin can polymerize at the ER-mitochondrial interface during constriction and/or fission. We postu-

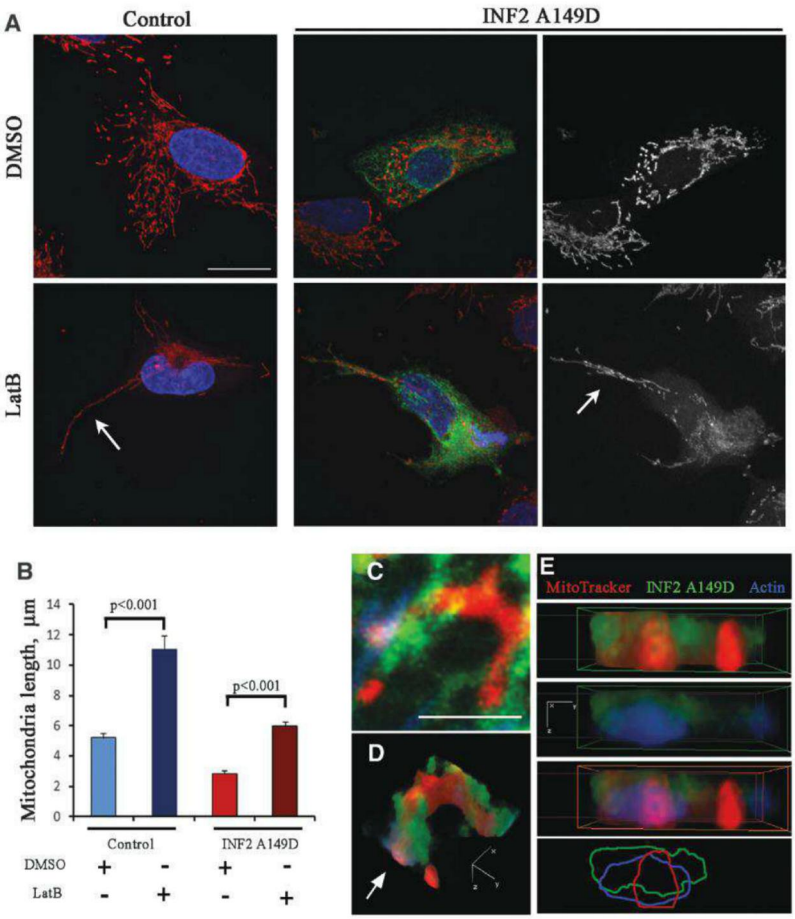

Fig. 4. Actin filaments are required for INF2-mediated mitochondrial fission. (**A**) Control or INF2-A149D U2OS cells treated with dimethyl sulfoxide (DMSO) or 0.5 μM LatB for 60 min. Maximum intensity projections of six to nine z steps. Scale bar, 20 μm. Arrows indicate long mitochondria. (**B**) Quantification of mitochondrial lengths after DMSO or LatB. n = 53 to 110 mitochondria. Error bars, SD. (**C** to **E**) 3D reconstruction of mitochondrion (red) in INF2-A149D cell (green) labeled with Alexa660-phalloidin (blue). (C) Maximum intensity projection of nine z steps (D) Volume rendering of (C). (E) Same mitochondrion viewed along x axis [arrow in (D)], presented as 3D combinations. (Bottom) Outlines of stains to illustrate relative positions. Scale bar, 2 μm.

late that actin is not observable at every ER-mitochondrial contact because these filaments are transient, as they may be both polymerized and depolymerized by INF2. It is also possible that actin polymerization is required for only a subset of fission events. Such heterogeneity is consistent with the variety of Drp1 isoforms, adaptors, and posttranslational modifications associated with mammalian mitochondrial fission (*24*).

We suggest a potential mechanism explaining the finding that ER association stimulates mitochondrial fission (*8*) (fig. S10). At the mitochondria-ER interaction site, INF2 is activated to polymerize actin. Actin polymerization between ER and mitochondrion could possibly enable force generation to drive initial mitochondrial constriction and to enhance Drp1 ring assembly at the constriction site. Drp1 activity further constricts the mitochondrion, which results in fission. INF2's severing and/or depolymerization activity could rapidly remove actin filaments after fission. Force could be generated directly through actin polymerization or through myosin motor activity (*25*). This model supports previous findings suggesting that Drp1 oligomeric rings are narrower than unconstricted mitochondria (*7*) and that mitochondria can constrict in a Drp1-independent manner (*8–10*).

References and Notes

1. J. Nunnari, A. Suomalainen, *Cell* **148**, 1145 (2012).
2. J. C. Martinou, R. J. Youle, *Dev. Cell* **21**, 92 (2011).
3. S. Hoppins, J. Nunnari, *Science* **337**, 1052 (2012).
4. R. J. Youle, A. M. van der Bliek, *Science* **337**, 1062 (2012).
5. H. Chen, D. C. Chan, *Hum. Mol. Genet.* **18** (R2), R169 (2009).
6. S. C. Correia *et al.*, *Adv. Exp. Med. Biol.* **724**, 205 (2012).
7. J. A. Mears *et al.*, *Nat. Struct. Mol. Biol.* **18**, 20 (2011).
8. J. R. Friedman *et al.*, *Science* **334**, 358 (2011).
9. A. M. Labrousse, M. D. Zappaterra, D. A. Rube, A. M. van der Bliek, *Mol. Cell* **4**, 815 (1999).
10. A. Legesse-Miller, R. H. Massol, T. Kirchhausen, *Mol. Biol. Cell* **14**, 1953 (2003).
11. K. J. De Vos, V. J. Allan, A. J. Grierson, M. P. Sheetz, *Curr. Biol.* **15**, 678 (2005).
12. E. S. Chhabra, H. N. Higgs, *J. Biol. Chem.* **281**, 26754 (2006).
13. E. S. Chhabra, V. Ramabhadran, S. A. Gerber, H. N. Higgs, *J. Cell Sci.* **122**, 1430 (2009).
14. V. Ramabhadran, F. Korobova, G. J. Rahme, H. N. Higgs, *Mol. Biol. Cell* **22**, 4822 (2011).
15. E. J. Brown *et al.*, *Nat. Genet.* **42**, 72 (2010).
16. O. Boyer *et al.*, *N. Engl. J. Med.* **365**, 2377 (2011).
17. R. Cartoni, J. C. Martinou, *Exp. Neurol.* **218**, 268 (2009).
18. A. Niemann, M. Ruegg, V. La Padula, A. Schenone, U. Suter, *J. Cell Biol.* **170**, 1067 (2005).
19. A. Vital *et al.*, *Neuromuscul. Disord.* **22**, 735 (2012).
20. T. Otomo, C. Otomo, D. R. Tomchick, M. Machius, M. K. Rosen, *Mol. Cell* **18**, 273 (2005).
21. M. J. Woźniak *et al.*, *J. Cell Sci.* **122**, 1979 (2009).
22. J. Gaillard *et al.*, *Mol. Biol. Cell* **22**, 4575 (2011).
23. V. Ramabhadran, P. S. Gurel, H. N. Higgs, *J. Biol. Chem.* **287**, 34234 (2012).
24. K. Elgass, J. Pakay, M. T. Ryan, C. S. Palmer, *Biochim. Biophys. Acta* **1833**, 150 (2013).
25. B. DuBoff, J. Götz, M. B. Feany, *Neuron* **75**, 618 (2012).

Acknowledgments: We thank M. Zick, J. Moseley, B. Wickner, and C. Barlowe for useful discussions; A. Lavanway for help with the microscopes; and M. Richio-Dalton for her tireless energy. Portions of this publication are covered in a pending patent application. "Methods for modulating mitochondrial function via INF2," H. Higgs author, Patent DC512US.L. Supported by NIH grants GM069818 and DK88826 to H.N.H. Funds to purchase the Nikon A1RSi confocal workstation were provided by NSF award DBI1039423.

Supplementary Materials

www.sciencemag.org/cgi/content/full/339/6118/464/DC1
Materials and Methods
Figs. S1 to S10
References
Movies S1 to S6

3 August 2012; accepted 29 November 2012
10.1126/science.1228360

TRANSILLUMINATOR

The advanced Bi-O-Vision Series transilluminators feature two workstations, producing both 312 nm ultraviolet (UV) and white light. The TD-1000R model offers fixed-intensity while the TVD-1000R model offers variable-intensity control of either UV or white light. These units are continuously adjustable from 100% down to 50%. This enables life science researchers to select the exact ultraviolet or white light illumination needed to photodocument samples with a single piece of equipment. The UV-B (312 nm) intensity of the TVD-1000R can be varied. This flexibility in irradiance control helps ensure the longest sample preparation time, while minimizing actual UV damage to the sample. The Bi-O-Vision has two adjacent workstations, each with a filter area of 8 x 8" (20 x 20 cm). The UV side is lit by five 8-watt UV-B tubes and delivers nanogram sensitivity for detecting ethidium bromide-stained DNA or RNA. The white light side has three 8-watt fluorescent tubes that ensure excellent illumination for viewing Coomassie blue-stained protein gels, methylene blue-stained DNA gels, and autoradiograms.

SPECTROLINE

For info: 800-274-8888 | www.spectroline.com

FFPET SAMPLE PREP

The new High Pure FFPET RNA Isolation Kit and the RealTime ready cDNA Pre-Amp Master & Primer Pools have been designed for gene expression analysis of formalin-fixed, paraffin-embedded tissue (FFPET) samples. FFPET samples from biopsies or microdissections are frequently used for retrospective studies. They also represent an increasingly important resource for biomarker research and investigating disease progression or drug responsiveness. The new High Pure FFPET RNA Isolation Kit delivers RNA of excellent integrity and yield—two key factors in ensuring high-quality results in the diversity of downstream applications such as qRT polymerase chain reaction, microarray analysis, and sequencing. For comprehensive gene expression studies, the isolated RNA can be transcribed into cDNA and subsequently preamplified with the new RealTime ready cDNA Pre-Amp Master. This kit makes it possible to preamplify minute amounts of cDNA with customized primer pools that correspond perfectly to the primers which can be applied in subsequent qPCR analysis.

ROCHE

For info: +49-8856-60-10210 | www.roche.com

SAMPLE PREPARATION

The Genevac Flip-Flop system is an innovative tool designed to facilitate post-accelerated sample extraction (ASE) concentration and preparation of samples. Samples are collected in the special Flip-Flop tube, the funnel and vial are fitted, the tube flipped over and second cap removed. Your ASE sample can now be concentrated directly into a GC autosampler vial using a Genevac Rocket Evaporator. The Genevac Rocket Evaporator enables rapid concentration or evaporation of up to 18 Dionex ASE vials simultaneously. Using this simple procedure eliminates manual transfer steps and helps automate the ASE sample concentration/preparation process resulting in improved laboratory workflow, increased reproducibility of results, and enhanced sample recovery.

GENEVAC

For info: +44-(0)-1473-240000 | www.genevac.com

EXTRACELLULAR MATRIX COMBINATORIAL LIBRARY

Containing nearly 300 biomimetics of fibronectin, vitronectin, laminin, and collagen for coating plates or creating 3-D culture scaffolds, the new Extracellular Matrix (ECM) Mimetic Library provides a powerful tool for identifying the cellular adhesion profile of cell lines or tumors against the widest commercially available collection of cell surface receptor binding peptide motifs. The extracellular microenvironment, defined by biochemical and physical cues, is a deciding factor in a wide range of cellular processes, including cell adhesion, proliferation, differentiation, and expression of phenotype-specific functions. Being able to engineer the ECM microenvironment provides clear benefits in studies of cell and tissue engineering and related applications. Currently existing technology offers simple (and merely adequate) environments that facilitate basic cell processes such as adhesion. The simple presentation of motifs involved in cell adhesion is not optimal for controlling more integrated processes. Crosstalk among signaling pathways acts synergistically to enhance cellular responses such as cell adhesion and/or proliferation.

AMS BIOTECHNOLOGY

For info: +44-(0)-1235-828200 | www.amsbio.com

WNT REPORTER ASSAY

The Leading Light Wnt Reporter Assay is a high-sensitivity system that accelerates screening analysis of Wnt pathway modulators. The Leading Light Wnt Reporter Assay guarantees confidence in the assay results by providing a system that is capable of detecting low concentration of effectors across a dynamic range of signal intensity. The assay uses a 3T3 mouse fibroblast cell line modified with a luciferase reporter gene under the control of Wnt-responsive promoters (TCF/LEF). It provides a true endpoint detection system for screening compounds without the need for overexpression or alteration of pathway signaling molecules. With a chemiluminescent readout amenable to both 96-well and 384-well plate formats, the kit allows for high throughput analysis of Wnt pathway activators and inhibitors. The Leading Light Wnt Reporter Assay Starter Kit is supplied with an easy-to-follow protocol, a validated cell line and all necessary media, reagents, and controls.

ENZO LIFE SCIENCES

For info: 800-942-0430 | www.enzolifesciences.com

Electronically submit your new product description or product literature information! Go to **www.sciencemag.org/products/newproducts.dtl** for more information.

Newly offered instrumentation, apparatus, and laboratory materials of interest to researchers in all disciplines in academic, industrial, and governmental organizations are featured in this space. Emphasis is given to purpose, chief characteristics, and availability of products and materials. Endorsement by *Science* or AAAS of any products or materials mentioned is not implied. Additional information may be obtained from the manufacturer or supplier.

Science Careers Advertising

For full advertising details, go to ScienceCareers.org and click For Employers, or call one of our representatives.

Tracy Holmes
Worldwide Associate Director
Science Careers
Phone: +44 (0) 1223 326525

THE AMERICAS

E-mail: advertise@sciencecareers.org
Fax: 202-289-6742

Tina Burks
East Coast/West Coast/South America
Phone: 202-326-6577

Allyson Rosen
Midwest/Canada/Corporate
Phone: 202-326-6578

Marci Gallun
Sales Administrator
Phone: 202-326-6582

Online Job Posting Questions
Phone: 202-312-6375

EUROPE / INDIA / AUSTRALIA / NEW ZEALAND / REST OF WORLD

E-mail: ads@science-int.co.uk
Fax: +44 (0) 1223 326532

Lucy Nelson
Phone: +44 (0)1223 326527

Kelly Grace
Phone: +44 (0) 1223 326528

JAPAN

Yuri Kobayashi
Phone: +81-(0)90-9110-1719
E-mail: ykobayas@aaas.org

CHINA / KOREA / SINGAPORE / TAIWAN / THAILAND

Ruolei Wu
Phone: +86-1367-1015-294
E-mail: rwu@aaas.org

All ads submitted for publication must comply with applicable U.S. and non-U.S. laws. *Science* reserves the right to refuse any advertisement at its sole discretion for any reason, including without limitation for offensive language or inappropriate content, and all advertising is subject to publisher approval. *Science* encourages our readers to alert us to any ads that they feel may be discriminatory or offensive.

Science Careers
From the journal *Science* AAAS

ScienceCareers.org

EBERHARD KARLS UNIVERSITÄT TÜBINGEN

WERNER REICHARDT CENTRE FOR INTEGRATIVE NEUROSCIENCE

Werner Reichardt Centre for Integrative Neuroscience (CIN) in Tübingen offers a

Junior Research Group in Neurotechnology

The **Werner Reichardt Centre for Integrative Neuroscience (CIN)** is an interdisciplinary institution at the **Eberhard Karls University Tübingen** funded by the German Excellence Initiative program. The CIN strives to deepen our understanding of how the brain generates function and how brain diseases impair functions. It tries to make use of newly acquired insights to help people with brain disorders and to launch new mind- and brain-inspired applications in many areas of engineering and computer science. Its scientific program is guided by the conviction that progress in the understanding of brain function can only be achieved by an integrative approach spanning multiple levels of organization and pooling the knowledge of researchers from many different fields.

In order to strengthen research on technical applications the CIN offers a junior group leader (JRG) position with tenure track option for up-and-coming young scientists with a promising track record, working in different fields of **Neurotechnology.** This might include fields such as:

- Brain machine interfaces, brain computer interfaces and neurorobotics
- Technology for sensory or motor neuroprostheses
- Rehabilitation technology
- Brain-inspired user interfaces and computing technology

We welcome additional proposals in other fields of neurotechnology. The CIN strives to increase the number of female scientists. Therefore **qualified female candidates are explicitly encouraged to apply.**

Framework:
The intended duration of the position is for 5 years with evaluations by external experts at regular intervals. In the event of positive evaluations after 3 years, the JRG will obtain a tenure track option, which may ultimately lead to a professorship at the University of Tübingen. Start-up funds as well as substantial funding for personnel and running costs will be available, but will depend on the applicant´s qualifications and prior experience. Appointees will be full members of and active participants in the CIN, which will also provide laboratory and/or office space. The JRG leader will be provided with opportunities to contribute to research oriented training within the framework of the CIN Graduate Training Centre and the faculties involved in the CIN will provide opportunities for the German habilitation according to established rules, if desired. According to German law, severely disabled persons with equal occupational aptitude will be given preferential consideration.

Application:
Applicants should submit a curriculum vitae, pdf files of up to 5 key publications, a statement of research achievements and future directions (not to exceed 3 pages) as well as the names and addresses of at least three referees. All documents should be submitted electronically to the Chairman of the Werner Reichardt Centre for Integrative Neuroscience Tübingen, Prof. Dr. Peter Thier, at cin@uni-tuebingen.de. For further information on the CIN see: http://www.cin.uni-tuebingen.de/. **Submission deadline is 15.02.2013.**

CIN Werner Reichardt Centre for Integrative Neuroscience

EBERHARD KARLS UNIVERSITÄT TÜBINGEN

WERNER REICHARDT CENTRE FOR INTEGRATIVE NEUROSCIENCE

The Werner Reichardt Centre for Integrative Neuroscience (CIN) in Tübingen offers a

Junior Research Group for Neuroscientists

The **Werner Reichardt Centre for Integrative Neuroscience (CIN)** is an interdisciplinary institution at the **Eberhard Karls University Tübingen** funded by the German Excellence Initiative program. The CIN strives to deepen our understanding of how the brain generates function and how brain diseases impair functions. It tries to make use of newly acquired insights to help people with brain disorders and to launch new mind- and brain-inspired applications in many areas of engineering and computer science. Its scientific program is guided by the conviction that progress in the understanding of brain function can only be achieved by an integrative approach spanning multiple levels of organization and pooling the knowledge of researchers from many different fields.

The CIN is offering a junior group leader (JRG) position with tenure track option for up-and-coming young scientists with a promising track record in any area of the neurosciences. Since the CIN strives to increase the number of women scientists, topics well represented by qualified female candidates will be preferred. Hence we explicitly encourage female candidates to apply. **Submission deadline is February 15th, 2013.**

Framework:
The intended duration of the position is for 5 years with evaluations by external experts at regular intervals. In the event of positive evaluations after 3 years, the JRG will obtain a tenure track option, which may ultimately lead to a professorship at the University of Tübingen. Start-up funds as well as substantial funding for personnel and running costs will be available, but will depend on the applicant´s qualifications and prior experience. Appointees will be full members of and active participants in the CIN, which will also provide laboratory and/or office space. The JRG leader will be provided with opportunities to contribute to research oriented training within the framework of the CIN Graduate Training Centre and the faculties involved in the CIN will provide opportunities for the German Habilitation according to established rules, if desired. According to German law, severely disabled persons with equal occupational aptitude will be given preferential consideration.

Application:
Applicants should submit a curriculum vitae, pdf files of up to 5 key publications, a statement of research achievements and future directions (not to exceed 3 pages) as well as the names and addresses of at least three referees. All documents should be submitted electronically to the Chairman of the Werner Reichardt Centre for Integrative Neuroscience Tübingen, Prof. Dr. Peter Thier, at cin@uni-tuebingen.de. For further information on the CIN see: http://www.cin.uni-tuebingen.de/.

CIN Werner Reichardt Centre for Integrative Neuroscience

EBERHARD KARLS
UNIVERSITÄT TÜBINGEN

WERNER REICHARDT CENTRE
FOR INTEGRATIVE NEUROSCIENCE

The **Werner Reichardt Centre for Integrative Neuroscience (CIN)** is an interdisciplinary institution at the **Eberhard Karls University Tübingen** funded by the German Excellence Initiative program. The CIN strives to deepen our understanding of how the brain generates function and how brain diseases impair functions. It tries to make use of newly acquired insights to help people with brain disorders and to launch new mind- and brain-inspired applications in many areas of engineering and computer science.

W3-Professorship 'Systems Neurobiology' at the Werner Reichardt Centre for Integrative Neuroscience (CIN) in Tübingen

The new professor is expected to direct innovative research on subcortical systems and cortico-subcortical interactions. Possible, but not exclusive, research areas are the functional role of the basal ganglia, the spinal cord, the vestibular system or the cortical-subcortical underpinnings of motor control. Candidates for professorships should have a long-standing experience in interdisciplinary research in the respective area. The candidate should have a proven track record of international excellence and external grant funding and be willing to contribute to research oriented training in the neurosciences at University of Tübingen. The new CIN professor will be a member of the Faculty of Science (Department of Biology). The position is tenured.

According to German law, disabled persons with equal occupational aptitude will be given preferred consideration. The University of Tübingen and CIN strive to promote equal opportunities in science and is committed to increasing the percentage of female scientists in teaching and research. Qualified female candidates are strongly encouraged to apply.

Applicants should submit a curriculum vitae, pdf files of up to 5 key publications, statements of research achievements and future directions together by **February 26th, 2013** to the **Dean of the Faculty of Science, Prof. Dr. Wolfgang Rosenstiel, at dekanat@mnf.uni-tuebingen.de/.**
For further information on the CIN see: http://www.cin.uni-tuebingen.de/

CIN Werner Reichardt Centre for Integrative Neuroscience

Chair, Department of Neurobiology Yale University School of Medicine

Yale University School of Medicine announces a search for Chair of the Department of Neurobiology. This department, which was founded by Pasko Rakic in 1978, plays a key role in Yale's broader neuroscience community. The successful candidate will be expected to possess an outstanding academic record in research and education, together with demonstrated leadership ability. He/she must meet the requirements for appointment as a Full Professor at Yale. Interested candidates should send a curriculum vitae and bibliography, a brief statement of programmatic interests and goals, and a list of professional references prior to **March 15, 2013** either electronically (to **charlene.bloch@yale.edu**) or by mail to:

Pietro DeCamilli
Chair, Neurobiology Search Committee
c/o Charlene Bloch
Yale University School of Medicine,
CNNR Program
295 Congress Ave, BCMM 436D
PO Box 9812
New Haven, CT 06536-0812

Yale University is an Equal Opportunity, Affirmative Action Employer. Minorities and women are encouraged to apply.

THE UNIVERSITY OF HONG KONG
香港大學

Founded in 1911, The University of Hong Kong is committed to the highest international standards of excellence in teaching and research, and has been at the international forefront of academic scholarship for many years. The University has a comprehensive range of study programmes and research disciplines spread across 10 faculties and about 100 sub-divisions of studies and learning. There are over 23,400 undergraduate and postgraduate students coming from 50 countries, and more than 1,200 members of academic and academic-related staff.

Teaching Consultant in Common Core Curriculum (Ref.: 201300007)

Applications are invited for appointment as Teaching Consultant in the Common Core Curriculum in the Faculty of Science, from as soon as possible, on a two-year fixed-term basis, with the possibility of renewal.

The University has established a Common Core Curriculum for all undergraduates since September 2012. The Faculty of Science offers courses in the area of Scientific and Technology Literacy to students from all ten Faculties. A senior Professor in the Faculty of Science will lead the teaching of these courses and work with the Teaching Consultants in the relevant area who will serve primarily as a tutor for small groups of students from multiple disciplines. The medium of instruction is English. Information about the Common Core Curriculum can be viewed at http://tl.hku.hk/common-core-curriculum.

Applicants should have a Master's degree, preferably in Physical Sciences and have substantial teaching experience in subjects related to general education at the university level. Those with a Ph.D. degree would have an advantage. The appointee's duties include conducting small-group tutorials for two courses per semester, marking assignments/examination scripts, preparing teaching materials, supervising student work, developing new courses, and undertaking other tasks related to science education. He/She will meet regularly with the Centre for the Enhancement of Teaching and Learning to reflect on and refine the teaching activities in Common Core courses.

A globally competitive remuneration package commensurate with the appointee's qualifications and experience will be offered. At current rates, salaries tax does not exceed 15% of gross income. The appointment will attract a contract-end gratuity and University contribution to a retirement benefits scheme, totalling up to 15% of basic salary, as well as leave, and medical benefits. Housing benefits will be provided as applicable. Please note that the University is not able to offer a relocation assistance package (including temporary University housing accommodation and a passage and baggage allowance) to a successful candidate recruited from overseas.

For enquiries about the specific job requirements, please write to Professor Sun Kwok, Dean of Science (e-mail: deansci@hku.hk). Applicants should send a completed application form, together with an up-to-date C.V. and a statement on teaching philosophy, which includes a portfolio of syllabi and descriptions of courses they have taught or co-taught by e-mail to sciappt@hku.hk. They should also arrange for submission of three references from senior academics who are familiar with their teaching approaches, skills and experience. Please indicate clearly "Ref.: 201300007 (Teaching Consultant in Common Core Curriculum)" in the subject of the email. Application forms (341/1111) can be obtained at http://www.hku.hk/apptunit/form-ext.doc. Further particulars can be obtained at http://jobs.hku.hk/. **Closes March 31, 2013.**

The University thanks applicants for their interest, but advises that only shortlisted applicants will be notified of the application result.

The University is an equal opportunity employer and is committed to a No-Smoking Policy

UCDAVIS

The **Department of Animal Science** at the **University of California, Davis** seeks applicants for an **Assistant Professor** in ruminant nutrition preferably with emphasis in anaerobic microbiology. The preferred appointee will be expected to establish a competitively-funded research program focused in the area of nutrient use for production and utilizing, and where appropriate the importance of rumen microbiology in this process. The emphasis will be on enhancing efficiency of food production, nutrient retention, and qualities of human food products and the effect of the gut microbiome population and/or function in this system. A component of the research conducted by the successful candidate should be readily applicable so that research endeavors are directly relevant to food producing animal systems. The successful candidate will also be expected to develop effective collaborative partnerships with other scientists working in ruminant systems where ruminant nutrition and/or microbiology are integral to the outcome response.

Understanding and creative research in the area of nutrient use is a necessary precursor to understanding how to reduce undesirable emissions from livestock production facilities. Research projects in nutrient utilization and rumen microbiology as related to feed and byproduct utilization are critical. Such knowledge enables the creation of management approaches to reduce the environmental impact of animal production systems and improve food safety while maximizing animal based food production.

The appointee will be expected to develop a national and international research program that contributes to maintaining the competitive edge of the dairy industry, California's number one agricultural commodity while reducing the environmental impact. The appointee will contribute to the Animal Science curriculum including teaching undergraduate courses in nutrition and/or biochemistry, as assigned by the department chair. Mentoring of graduate students, undergraduate student advising, and contributing to Departmental and University service is expected. This is an academic year (9-month) tenure track assistant professor position that includes an expectation to conduct mission-oriented research and outreach relevant to the California Agricultural Experiment Station and in support of the economic viability of California's animal industries.

For more information and to apply please visit **https://recruit.ucdavis.edu/apply/JPF00045**

深圳大学

Opening positions for full-time distinguished professors and lecturers

Shenzhen University (SZU) invites applications for full-time Distinguished Professor and lecturer positions for highly qualified candidates with special expertise in one of the following academic areas.

The University

The university is located in Shenzhen; a big city of over 8 million people in Southern China's Guangdong Province and directly adjacent to Hong Kong. Shenzhen is China's first Special Economic Zone, is well known for its economic, scientific and technological innovation, and is one of China's most advanced and prosperous cities. Shenzhen University was founded in 1983 and has been at the forefront and a central participant in the city's rapid development.

Shenzhen University consists of twenty-six colleges with a total enrollment over thirty-thousand undergraduate and graduate students. The university is highly committed to quality education and applied research across a number of fields important to the future development. We are aggressively seeking highly qualified international scholars to join us as we continue towards our mission of becoming a top-class research institution in China.

Areas of Interest for distinguished professors and lecturers

Economics, Law , Literature, Science, Engineering, Medicine, Management, Art

A. Distinguished professor

Qualifications

1. Candidates must have an earned doctorate in a closely related discipline with a track record of extraordinary accomplishment in teaching, research/scholarship, and professional service, judged by peers to be outstanding;
2. They should have at least associate-professor or above academic experience in world-renowned universities;
3. They should have been recognized nationally or internationally for the importance of their achievements and are expected to bring distinction to SZU and serve as a key contributor to achieving its strategic goal of becoming a World-Class university.
4. They should have strong research capability and great potential to become academic leader whose vision anticipates the development tendency of their field.
5. They should have a strong organizing and communicating ability to lead their research team to reach world-class level.

Salary/Benefits

Salary and benefits are very competitive; yearly salary starting from 100,000 to 200,000 US dollars and will be commensurate with qualifications and experience.

B. Lecturers (equivalent to the rank of Assistant Professor)

Qualifications

1. Candidates must have an earned doctorate in a closely related discipline;
2. Strong ability to conduct independent research and publish on peer-reviewed professional journals;
3. Fluent in communication with working language (Chinese and/or English) for teaching and research;
4. Satisfy the basic requirement on legal residence and work authorization (by the Chinese government) .

Salary/Benefits for Lecturer

Salary and benefits are competitive; and commensurate with qualifications and experience.

To Apply

Interested candidates should submit all application documents to the contacts below or submit all information to **http://szuhr.szu.edu.cn.** For more information please visit **http://www.szu.edu.cn/szu2007/indexe.asp**

Contact: Mr. Renqiang (szursc@sina.cn , 0086-755-26535295)
Ms. Yun LI (liyun@szu.edu.cn, 0086-755-26536111)

ETH

Eidgenössische Technische Hochschule Zürich
Swiss Federal Institute of Technology Zurich

Conducting research and teaching in an inspiring environment at one of the world's leading universities

ETH Zurich invites applications for new professorships.

www.facultyaffairs.ethz.ch

ETH Zurich has come to symbolise excellent education, groundbreaking basic research and applied results that are beneficial for society as a whole. Founded in 1855, ETH Zurich has more than 17,000 students from approximately 80 countries, 3,700 of whom are doctoral candidates. Today, it offers researchers an inspiring environment and students a comprehensive education as one of the world's leading universities for technology and the natural sciences.

ETH Zurich is an equal opportunity and affirmative action employer. In order to increase the number of women in leading academic positions, **we specifically encourage women to apply.** ETH Zurich is further responsive to the needs of dual career couples and qualifies as a family friendly employer.

Science Careers online @sciencecareers.org

Staff Scientist in Molecular Genetics

National Institute of Environmental Health Sciences
Research Triangle Park, North Carolina

The Laboratory of Molecular Carcinogenesis of the Division of Intramural Research is seeking a Staff Scientist in the Mammalian Genome Group to join a state-of-the-art molecular genetics research laboratory focused on studying the genetics and epigenetics associated with environmental exposures. The group utilizes next-gen whole-genome experimental approaches, including massively parallel genome/exon sequencing, RNA-seq, and ChIP-seq approaches, to better understand the molecular basis of complex traits.

Qualifications of the ideal candidate will include a PhD, MD, MD/PhD or equivalent with at least 5 years of experience (post doctorate) successfully conducting basic research in a cutting-edge molecular genetics laboratory with a demonstrated track record of productivity through publication in the peer-reviewed literature. Promising candidates with less experience will also be considered. The successful candidate will have good personnel management skills and be supportive of collaborative research. Expertise with a broad range of techniques in molecular and stem cell biology would be highly desirable, including massively parallel DNA sequencing, transcriptome analysis, genomic and cDNA molecular cloning and characterization, and culturing/characterization of ES/iPS cells. Specific knowledge and experience with the Collaborative Cross/Diversity Outcross or similar resources would be beneficial.

To apply, submit a Curriculum Vitae, brief statement of research experience and interests, and the names and addresses (including e-mail addresses and phone numbers) of three references to dir-appls@niehs.nih.gov or the below mailing address **by March 15, 2013**. Review of applications will begin immediately and continue until the position is filled. Salary is commensurate with level of experience. For additional information about this position, contact Dr. Rick Woychik, Deputy Director, NIEHS (rick.woychik@nih.gov).

Ms. Emily Starnes (Vacancy Number DIR 13-02)
Intramural Program Specialist
National Institutes of Health
National Institute of Environmental Health Sciences
P.O. Box 12233, Maildrop A2-06
Research Triangle Park, NC 27709
Email: dir-appls@niehs.nih.gov

DHHS and NIH are Equal Opportunity Employers
We are dedicated to building a diverse community in our training and employment programs.

Prototyping Staff Scientist / Engineer

As a Staff Scientist in the newly opened Joint Center for Artificial Photosynthesis (JCAP), this position will assume major responsibility for the activities of the Prototyping and Scale-Up Project (Prototyping). JCAP is a Solar Fuels Innovation Hub recently funded by the Department of Energy ($122M, 5 years) with physical locations at Caltech (JCAP-South) and LBNL (JCAP-North). Members of the Prototyping team design, develop, build and test fully integrated macroscale system prototypes that capture all of the critical-length scales and phenomena of importance for device operation, such as fluid flows, feedstock input and output streams, optical input paths, mechanical system properties, and physical form factors. This team also plays a central role in designing and developing highly efficient and durable components. The position offers a unique opportunity for an experienced engineer/researcher to assume a key role in the development and demonstration of a scalably manufacturable solar-fuels generator.

Position Qualifications:

- Ph.D. in engineering, physical science or similar experimental field.
- Post-Ph.D. experience in electrochemically or photochemically driven processes; industrial experience a plus.
- Demonstrated record of accomplishment in product development and/or production practice.
- Publications in appropriate scientific/technical journals.
- General knowledge of prototyping methods for electrochemical devices and systems.
- Excellent written and verbal communication skills.
- Demonstrated ability to guide and train technical support staff and work with students and postdoctoral fellows of multiple scientific backgrounds.
- Excellent interpersonal skills.
- Experience in developing strong working relationships and collaborating across an organization.

For a detailed position description and instructions regarding how to apply, please visit **www.lbl.gov**, access the careers page and reference **job number 75472.**

BERKELEY LAB
Lawrence Berkeley National Laboratory

Berkeley Lab is an affirmative action/equal opportunity employer committed to the development of a diverse workforce.

CENTER FOR MACROECOLOGY, EVOLUTION AND CLIMATE
UNIVERSITY OF COPENHAGEN

UNIVERSITY OF COPENHAGEN

Center of Macroecology, Evolution and Climate
Natural History Museum of Denmark and Department of Biology
University of Copenhagen

Faculty Professor and Associate Professor positions
&
Fixed-term postdoc and Assistant Professor positions

in

Biogeography, Phylogeography, Macroecology, Macroevolution and Community Ecology

We seek international competitive candidates with a strong publication record at the level of position interested in. We expect strong analytical and data handling skills and the ability to communicate within a cross-disciplinary research center. Competitive salaries are offered.

For full description of the individual positions see **www.bio.ku.dk** or **www.employment.ku.dk**.

Inquiries can be made to Professor Carsten Rahbek, e-mail: **crahbek@bio.ku.dk**.

The center (**http://macroecology.ku.dk/**) is a long-term funded *center of excellence* with a cross-disciplinary research program addressing fundamental questions on the origin, maintenance, conservation and future of life and biological diversity on Earth. Researchers at the center currently represent 14 nationalities and the working language is English.

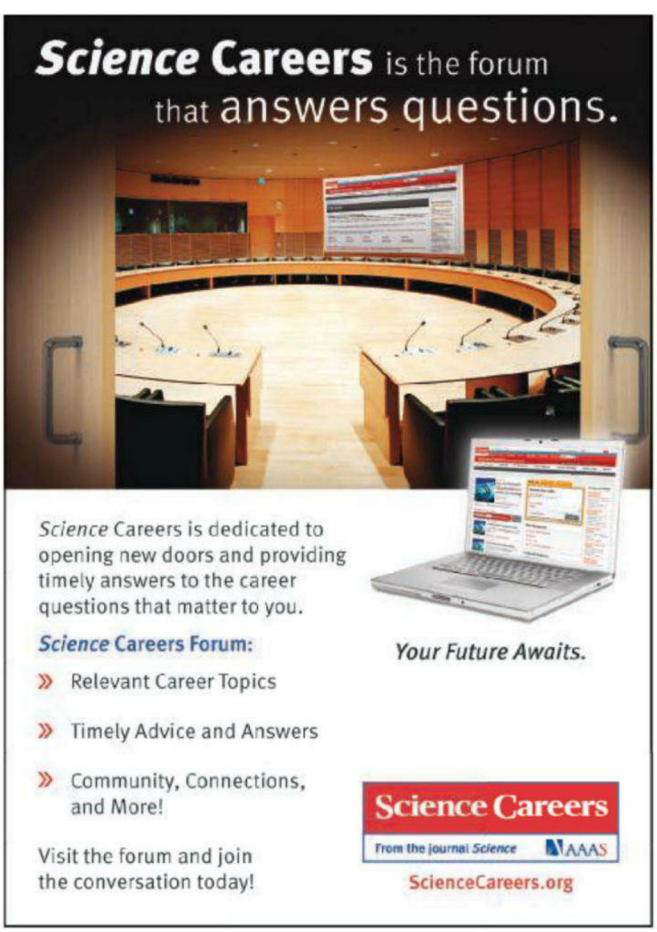

jobs.ornl.gov

The Neutron Sciences Directorate (NScD) at Oak Ridge National Laboratory (ORNL) invites applications for the position of Deputy Associate Laboratory Director. The NScD at ORNL operates the High Flux Isotope Reactor (HFIR), the United States' highest flux reactor-based neutron source, and the Spallation Neutron Source (SNS), the world's most intense pulsed accelerator-based neutron source. Together these facilities operate 24 instruments for neutron scattering research, each year carrying out in excess of 1,000 experiments in the physical, chemical, materials, biological, and medical sciences for more than 3,000 visiting scientists. HFIR also provides unique facilities for isotope production and neutron irradiation. To learn more about Neutron Sciences at ORNL go to: neutrons.ornl.gov.

The Deputy Associate Laboratory Director (ALD) supports the Associate Laboratory Director to develop and direct the scientific user and instrument and neutron source development programs at SNS and HFIR and help set the strategic scientific direction to meet the community needs of the future. The Deputy ALD serves as the acting ALD in the ALD's absence.

For a complete description and to apply online see jobs.ornl.gov.
Applications must be received by March 31st, 2013.

U.S. DEPARTMENT OF ENERGY
Office of Science
NEUTRON SCIENCES

13-G00011/gim

HARVARD
School of Engineering and Applied Sciences

The Disease Biophysics Group at Harvard University invites applications for a number of Postdoctoral Fellow positions open for projects pertaining to building microscale models of diseased organs. The project requires the assembly of engineered, human microtissues in microfluidic devices that can be interrogated for the genetic, morphological and functional indicators of health, disease, and injury.

The Disease Biophysics Group is a multidisciplinary research group based in the Harvard School of Engineering and Applied Sciences, the Wyss Institute for Biologically-Inspired Engineering, and the Harvard Stem Cell Institute.

Candidates with experience in neuronal cell biology, striated and smooth muscle tissue engineering, the cardiac valves, and experimental models of diabetes are encouraged to apply. Applicants are expected to hold a doctoral degree in engineering, physiology, or cell biology and have a proven record of high quality publications. For further information about The Disease Biophysics Group and its activities, see **http://diseasebiophysics.seas.harvard.edu/**.

Application Procedure: The application will be assembled as single pdf file: cover letter describing research interests and goals, CV, research statement, a full list of publications and up to three examples of first author papers, and a list of no less than three references with contact information. Please note that all requirements for the doctoral degree must be completed prior to the start date. The application should be sent to: **dbg-postdoc@seas.harvard.edu**. Full consideration will be given to all applications received by **February 15, 2013**; applications received thereafter will be considered until the positions are filled.

Harvard University is an Equal Opportunity Employer. Women and underrepresented minorities are particularly encouraged to apply.

It's not because we all wear white coats that we all do the same job

INRA IS RECRUITING
41 SCIENTISTS

First agricultural institute in Europe and second in the world, the French National Institute for Agricultural Research is recruiting in the following domains: • agronomy and ecology of landscapes • community ecology • economics • animal health economics • quantitative genetics and genomics • process engineering, physics and soils chemistry • mathematics and modeling • modeling in cell biology and biology of organisms • nutrition and physiology • veterinary sciences and immunology • sociology and organizational sciences.

orc.fr - Crédit photo : Corbis

Applications until 28 February 2013
on **jobs.inra.fr**

INRA
SCIENCE & IMPACT

Science | Careers

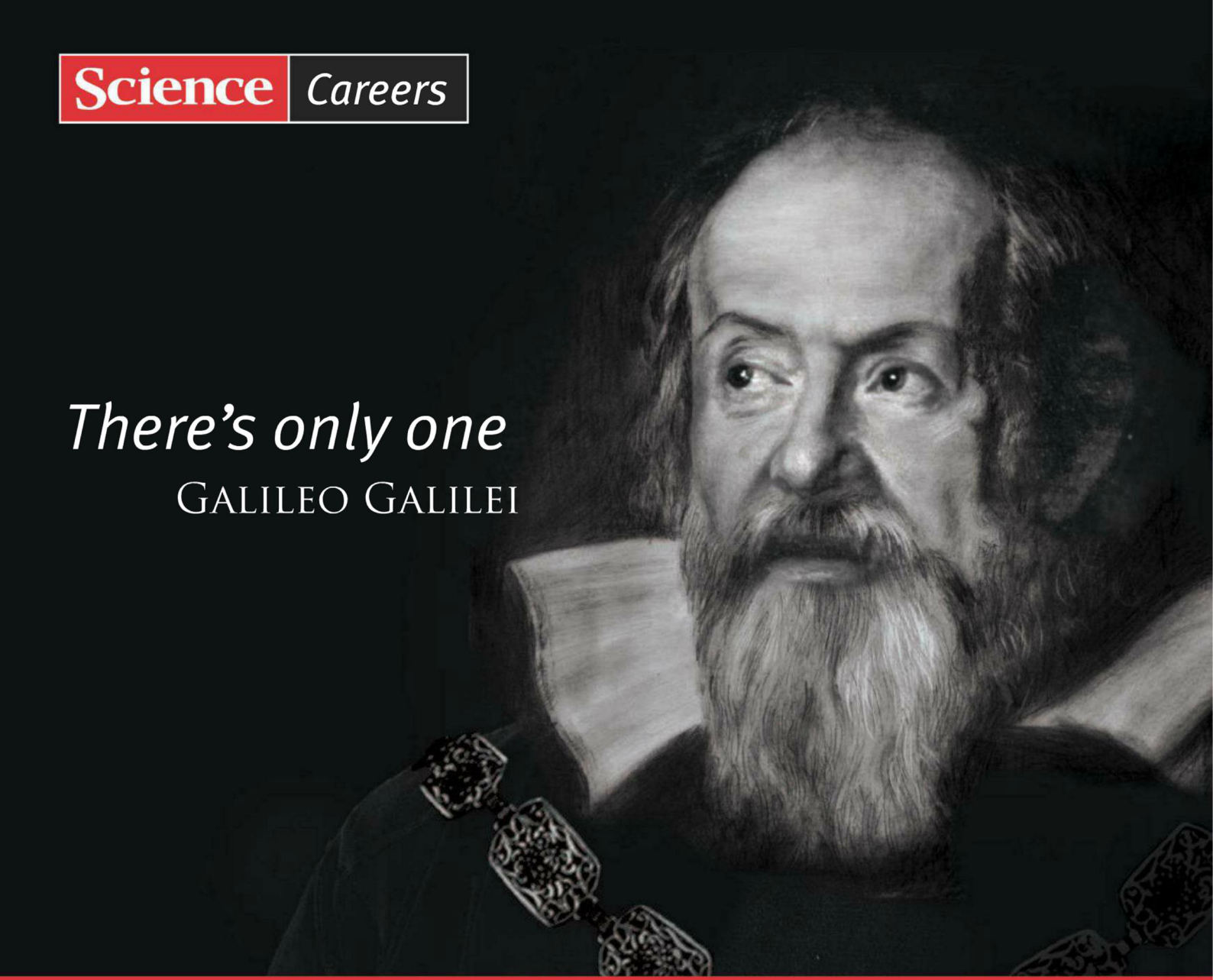

There's only one
Galileo Galilei

Born in 1564, Galileo Galilei once contemplated a career in the priesthood. It's perhaps fortunate for science that upon the urging of his father, he instead decided to enroll at the University of Pisa. His career in science began with medicine and from there he subsequently went on to become a philosopher, physicist, mathematician, and astronomer, for which he is perhaps best known. His astronomical observations and subsequent improvements to telescopes built his reputation as a leading scientist of his time, but also led him to probe subject matter counter to prevailing dogma. His expressed views on the Earth's movement around the sun caused him to be declared suspect of heresy, which for some time led to a ban on the reprinting of his works.

Galileo's career changed science for all of us and he was without doubt a leading light in the scientific revolution, which is perhaps why Albert Einstein called him the father of modern science.

Want to challenge the status quo and make the Earth move? At *Science* we are here to help you in your own scientific career with expert career advice, forums, job postings, and more — all for free. For your career in science, there's only one *Science*. Visit *Science* today at **ScienceCareers.org**.

For your career in science, there's only one **Science**

ScienceCareers.org

Career advice | Job postings | Job Alerts | Career Forum | Crafting resumes/CVs | Preparing for interviews

CONFERENCE

5th International Conference on Phospholipase A2 Mediated Signaling in Translational Medicine

LSUHSC Neuroscience Center of Excellence, New Orleans, LA, USA

May 20-21, 2013

Organizer: Nicolas G. Bazan

Selected abstracts for posters will be chosen for oral presentation.

Register early limited spaces available
www.PLA2-LSU.org

Award Lectures:

LSUHSC Chancellor's Award Lecture
Edward Dennis,
San Diego, CA

Journal of Lipid Research Lectureship
Charles N. Serhan,
Boston, MA

Lifetime Achievement Award Lecture
Takao Shimizu,
Tokyo, Japan

LSUHSC Dean's Award Lecture
Jesper Z. Haeggstrom,
Stockholm, Sweden

Innovator Award Lecture
Robert Murphy,
Denver, CO

Neuroscience Center of Excellence Award Lecture
Gérard Lambeau,
Nice-Sophia Antopolis, France

FACULTY POSITIONS

Neuroscience
NYU SHANGHAI

New York University Shanghai invites applications for several assistant (tenure-track), associate (tenured), and full professor (tenured) positions from candidates with research programs in systems, computational and cognitive neuroscience. The search is part of a major effort to establish a new Institute of Brain and Behavior at NYU Shanghai, with research areas that include computational modeling of neural circuits, investigations of neural circuit function, and human cognition.

Candidates must have completed a Ph.D. or equivalent by the time of application. The successful candidates will be expected to develop an independent, extramurally-funded research program, and to teach and otherwise contribute to the educational mission of NYU Shanghai. The search will remain open until the positions are filled, but review of applications is currently underway. The appointment could begin as soon as August 1, 2013, pending administrative and budgetary approval, or could be delayed until August 1, 2014.

NYU Shanghai is the first Sino-US higher education joint venture to grant a degree that is accredited in the US as well as in China. A research university with liberal arts and sciences at its core, it resides in one of the world's great cities, which is also a vibrant intellectual community (http://shanghai.nyu.edu/). NYU Shanghai will recruit scholars who are committed to our global vision of transformative teaching and innovative research.

New York University has established itself as a Global Network University, with three degree granting campuses - New York, Shanghai, and Abu Dhabi - complemented by 12 additional academic centers across five continents. Faculty and students circulate within the network in pursuit of common research interests and cross-cultural, interdisciplinary endeavors, both local and global.

The terms of employment in NYU Shanghai are comparable to U.S. institutions. Faculty may also spend time at NYU New York and other sites of the global network, engaging in both research and teaching opportunities. Tenure/tenure-track faculty will also be affiliated with the New York University Center for Neural Science, the Neuroscience Institute of the NYU School of Medicine, and/or with other suitable academic units at NYU New York.

Applicants should submit a curriculum vitae, a statement of research and teaching interests, electronic copies of up to five recent relevant publications, and the names and addresses of three or more individuals willing to provide letters of reference. Please visit our website at **http://shanghai.nyu.edu/about/open-positions** for instructions and other information on how to apply. If you have any questions, please e-mail **shanghai.faculty.recruitment@nyu.edu**.

NYU Shanghai is an Equal Opportunity/Affirmative Action Employer.

上海纽约大学
NYU SHANGHAI

CAREER TRENDS Running Your Lab

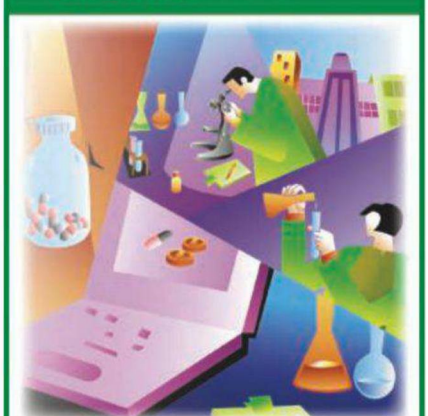

Download your free copy today at ScienceCareers.org/booklets

Science Careers
From the journal *Science* AAAS

Brought to you by the AAAS/*Science* Business Office

MEHARRY MEDICAL COLLEGE

Nashville, TN

EXECUTIVE DIRECTOR, Center for AIDS Health Disparities Research

Located in Nashville, Tennessee, Meharry Medical College is the largest private, historically black institution exclusively dedicated to educating biomedical scientists and health care professionals in the United States. The institution is composed of the Schools of Dentistry, Graduate Studies and Research, and Medicine. The screening of applications is ongoing and **the position will be filled by March 2013**. Salary is negotiable and the academic appointment will be commensurate with the individual's credentials and experience. Meharry Medical College and Vanderbilt University have a long-established affiliation, the Meharry-Vanderbilt Alliance (**http://www.meharry-vanderbilt.org/**), and Meharry faculty members can hold a secondary appointment at Vanderbilt.

Meharry Medical College is seeking a skilled, experienced research scientist to serve as Endowed Professor and Executive Director of the Center for AIDS Health Disparities Research (CAHDR). The CAHDR is reducing the burden of AIDS in local minority communities through basic, clinical, and translational research with community partnerships. The CAHDR has three major areas of focus including biology, behavioral, and community outreach. Center faculty members are extramurally funded to study new mechanisms of HIV infection, pathogenesis, immunity, and development of novels means for intervention. The CAHDR occupies ample space in a renovated area with outstanding laboratories, research equipment, a BSL-3 lab, and other core facilities.

The CAHDR faculty members are also integral members of the Vanderbilt-Meharry Center for AIDS Research (CFAR). They collaborate and work closely together with researchers in multiple disciplines on both campuses. The CFAR offers core services such as pilot project funding, biostatistical support, a clinical data and specimen repository, and BSL-3 cell sorting. The successful applicants will have a record of substantial and continuous extramural funding and scholarly productivity. Administrative and budget management experience in an academic setting is desirable. Applicants should hold an M.D., Ph.D., or M.D./Ph.D. degree. Interested individuals should submit a letter of interest summarizing their qualifications, along with CV and contact information for three references to:

Charles P. Mouton, MD, MS
Senior Vice President for Health Affairs
Dean, School of Medicine
Meharry Medical College
1005 Dr. D.B. Todd, Jr. Boulevard
Nashville, Tennessee 37208
Email: cmouton@mmc.edu
(615) 327-6204

AAAS is here – promoting universal science literacy.

In 1985, AAAS founded Project 2061 with the goal of helping all Americans become literate in science, mathematics, and technology. With its landmark publications *Science for All Americans* and *Benchmarks for Science Literacy*, Project 2061 set out recommendations for what all students should know and be able to do in science, mathematics, and technology by the time they graduate from high school. Today, many of the state standards in the United States have drawn their content from Project 2061.

Every day Project 2061 staff use their expertise as teachers, researchers, and scientists to evaluate textbooks and assessments, create conceptual strand maps for educators, produce groundbreaking research and innovative books, CD-ROMs, and professional development workshops for educators, all in the service of achieving our goal of universal science literacy.

As a AAAS member, your dues help support Project 2061 as it works to improve science education. If you are not yet a AAAS member, join us. Together we can make a difference.

To learn more, visit **aaas.org/plusyou/project2061**

AAAS + U = Δ

AAAS is here – helping scientists achieve career success.

Every month, over 400,000 students and scientists visit ScienceCareers.org in search of the information, advice, and opportunities they need to take the next step in their careers.

A complete career resource, free to the public, *Science* Careers offers a suite of tools and services developed specifically for scientists. With hundreds of career development articles, webinars and downloadable booklets filled with practical advice, a community forum providing answers to career questions, and thousands of job listings in academia, government, and industry, *Science* Careers has helped countless individuals prepare themselves for successful careers.

As a AAAS member, your dues help AAAS make this service freely available to the scientific community. If you're not a member, join us. Together we can make a difference.

To learn more, visit **aaas.org/plusyou/sciencecareers**

AAAS + U = Δ

POSITIONS OPEN

ASSISTANT/ASSOCIATE PROFESSORS
College of Medicine
Department of Biomedical Sciences

The Department of Biomedical Sciences at the James H. Quillen College of Medicine at East Tennessee State University invites applications for two tenure-track faculty positions. The department is seeking a candidate with a nationally competitive research program in Neuroscience, and a similarly qualified candidate in Microbiology and/or Immunology. Successful applicants will join established research groups focused on pathology of neurological and psychiatric disorders, neural remodeling in cardiovascular disease, demonstrated ability to teach neuroanatomy (neuroscience position) or microbiology/immunology is desired because responsibilities will include teaching medical and graduate students. Applicants must have a Ph.D., M.D., and/or D.V.M. and postdoctoral research training, a strong record of research productivity and preferably a nationally funded research program. Appointments will be commensurate with qualifications and experience. Successful applicants will be provided competitive salaries and startup packages. East Tennessee State University (**website: http://www.etsu.edu**) is located in one of the nation's most beautiful regions, just north of the Great Smoky Mountain National Park. Johnson City has a moderate cost of living and highly ranked public schools. Applicants should submit an ETSU application through eJobs (**website: https://jobs.etsu.edu**) including curriculum vitae, brief statement of current and future research goals, and names and addresses of three references. Review of applications will begin on January 1, 2013 and will continue until positions are filled. *Equal Opportunity/Affirmative Action Employer.*

The Illinois Natural History Survey (INHS) is soliciting applications for a two-year postdoctoral **RESEARCH ASSOCIATE**. Scientists whose research interests fit within those of the INHS are encouraged to apply. A salary of $42,000 per year with benefits is provided, as well as a $5,000/year research stipend. Applicants should submit a curriculum vitae and Research Proposal (RP). The RP is limited to three pages, not including references, and should address the research plan proposed for the two-year postdoctoral position. Applicants should identify and contact a research sponsor at the INHS (**website: http://wwx.inhs.illinois.edu/opportunities/postdocsponsors/list/**) in advance of the application deadline, who is willing to host the postdoctoral Associate and provide a letter of support. Preference will be given to applicants who can develop a strong research plan that merits additional and continued external funding. Research plans that build on existing INHS research strengths by adding new directions or new analytical techniques are encouraged.

Applicants should have completed a Ph.D. by the start date of the position (expected before December 31, 2013) and within the last five years. In addition to the RP, host support letter, and curriculum vitae, applicants should arrange for two letters of recommendation to be sent. Applications must be sent electronically to **e-mail: hroffice@inhs.illinois.edu** by March 15, 2013. *Illinois is an Affirmative Action/Equal Opportunity Employer.* **Website: http://www.inclusiveillinois.illinois.edu.**

SYSTEMS BIOMEDICINE
SHANGHAI JIAO TONG UNIVERSITY

FACULTY POSITIONS are available at Shanghai Center of Systems Biomedicine (SCSB) at Shanghai Jiao Tong University at all ranks (**website: http://scsb.sjtu.edu.cn/news/showDetail.aspx?id=225**). Candidates should have a Ph.D. or M.D. and an excellent research record in the following areas (nonexclusive): cancer, metabolic diseases, immunology, bioinformatics, molecular cell biology, metabolomics, synthetic biology, animal models, biomarkers and drug discovery and regenerative medicine. Those qualified for the "QianRen Plan" or "Chang Jiang Scholarship" are particularly welcome. Salary and startup are competitive. Up to 15 are expected to be filled as soon as possible. Applicants should send a full curriculum vitae, research plan, and a list of three to five references to **Professor Bingya Liu,** associate dean (**e-mail: liubyrj@yahoo.com.cn**), preferably before January 31, 2013.

POSITIONS OPEN

ASSISTANT/ASSOCIATE PROFESSOR
Department of Pharmaceutical Sciences

The College of Pharmacy, Washington State University (WSU) on Riverpoint campus in Spokane, invites applications for a full-time, tenure-track faculty position at the rank of Assistant or Associate Professor (commensurate with experience) in the Department of Pharmaceutical Sciences. Applicants must have an advanced degree (M.D., PharmD., or Ph.D. in Pharmacology, Pharmaceutical Sciences, or a related discipline) before date of hire. The Assistant Professor candidate must possess a track record of accomplishment to demonstrate the potential to become an outstanding scholar and educator. Associate Professor candidates must possess the a track record of accomplishment demonstrating he/she as an outstanding scholar and educator with an active, nationally recognized, extramurally funded, research program. Preference will be given to applicants who have a demonstrated ability to teach pharmacogenetics and genomics at the graduate level. The successful candidate will be expected to maintain an active, extramurally funded research program in the general area of pharmacogenetics and genomics, to mentor graduate students and fellows, and to teach in the professional and graduate curricula.

Screening of applications will begin January 16, 2013 and will continue until a suitable candidate is identified. To apply and see complete position description visit **website: http://www.wsujobs.com.**

WSU is an Equal Opportunity/Affirmative Action/ADA Educator and Employer.

ACADEMIC NEUROINTENSIVIST

The Department of Neurology at Columbia University Medical Center seeks a neurologist with specialty training in neurointensive care for a tenure-track faculty position at the **ASSISTANT PROFESSOR** level. The candidate will join three neurointensivists in the Neurocritical Program, headed by **Dr. Stephan Mayer**, and share attending responsibilities in a state-of-the-art 18-bed neuro-ICU equipped with dedicated CT and 3.0 Tesla MR scanners and EEG and multimodality neuromonitoring capability in every room. Teaching responsibilities include the instruction of nurses and physician assistants; neurology, neurosurgery, and emergency medicine residents; and seven neurocritical care fellows. Applicants with credible potential for or a track record of success in obtaining peer-reviewed funding will be given preference. Substantial protected time for research, teaching, and administrative responsibilities will be provided. Send curriculum vitae, the names of three references, and a brief letter describing your career goals to **Laura Lennihan**, M.D., Chair, Neurocritical Care Search Committee; **e-mail: ll18@columbia.edu**. Please apply at **website: https://academicjobs.columbia.edu/applicants/Central?quickFind=57277**. *Columbia University is an Affirmative Action/Equal Opportunity Employer.*

RESEARCH GRANTS MANAGER

Applications are invited for the position of Research Grants Manager. Ph.D. in any Biomedical Sciences or related discipline required. The candidate will be responsible for grant and manuscript writing, progress report preparation, and obtaining approvals from regulatory boards. Submit application to: **Department of Pathology, Microbiology and Immunology, University of South Carolina, School of Medicine, Columbia, SC 29208 (e-mail: grantsmgrapps@uscmed.sc.edu).**

Affirmative Action/Equal Opportunity Employer.

Help employers find you.
Post your resume/cv.
www.ScienceCareers.org

POSITIONS OPEN

FACULTY POSITION in
Ecology and Evolutionary Biology

Ecology and Evolutionary Biology: The University of California, Irvine (UCI), Department of Ecology and Evolutionary Biology and the Center for Environmental Biology seek to fill a tenure-track **ASSISTANT PROFESSOR** position. We seek candidates who bring ecological or evolutionary perspectives to issues of global change, conservation, and sustainability and will complement our existing strengths. Possible areas of specialization for the position include (but are not limited to) physiological ecology, population ecology/genomics, conservation genetics, community ecology, restoration ecology, ecosystem ecology, ecohydrology, biogeography, macroecology and global change biology of terrestrial, aquatic, or marine systems. We are interested in candidates who may utilize either experimental, synthetic, or computational techniques. Successful candidates will be expected to contribute to the undergraduate and graduate curriculum in ecology and evolutionary biology.

Review of applications will begin on March 15, 2013 and continue until the position is filled. Applicants should submit curriculum vitae, a research description, and a statement of teaching philosophy. In addition, applicants should arrange for three letters from references to be submitted. Applicants should use the following online recruitment **website: https://recruit.ap.uci.edu/apply/JPF01885.**

UCI is an Equal Opportunity Employer committed to excellence through diversity and strongly encourages applications from all qualified applicants, including women and minorities. UCI is responsive to the needs of dual career couples, is dedicated to work-life balance through an array of family-friendly policies, and is the recipient of an NSF ADVANCE Award for gender equity.

Your career is our cause.
Get help from the experts.
www.sciencecareers.org
- Job Postings
- Job Alerts
- Resume/CV Database
- Career Advice
- Career Forum

Science Careers
From the journal Science AAAS

Support the sciences. **Get rewarded.**

Show your AAAS pride and reward yourself with the new AAAS Platinum Advantage Rewards Card from NASA Federal Credit Union.

Apply now and get
10,000 bonus points!

Go to nasafcu.com/AAASpromo

Get **10,000 bonus points** if you sign up for a card and spend $3,000 within 90 days of account opening.

Learn more at
nasafcu.com/AAASpromo.

Subject to credit approval.
Membership in AAAS and NASA FCU is required.
NASA FCU is federally insured by NCUA.

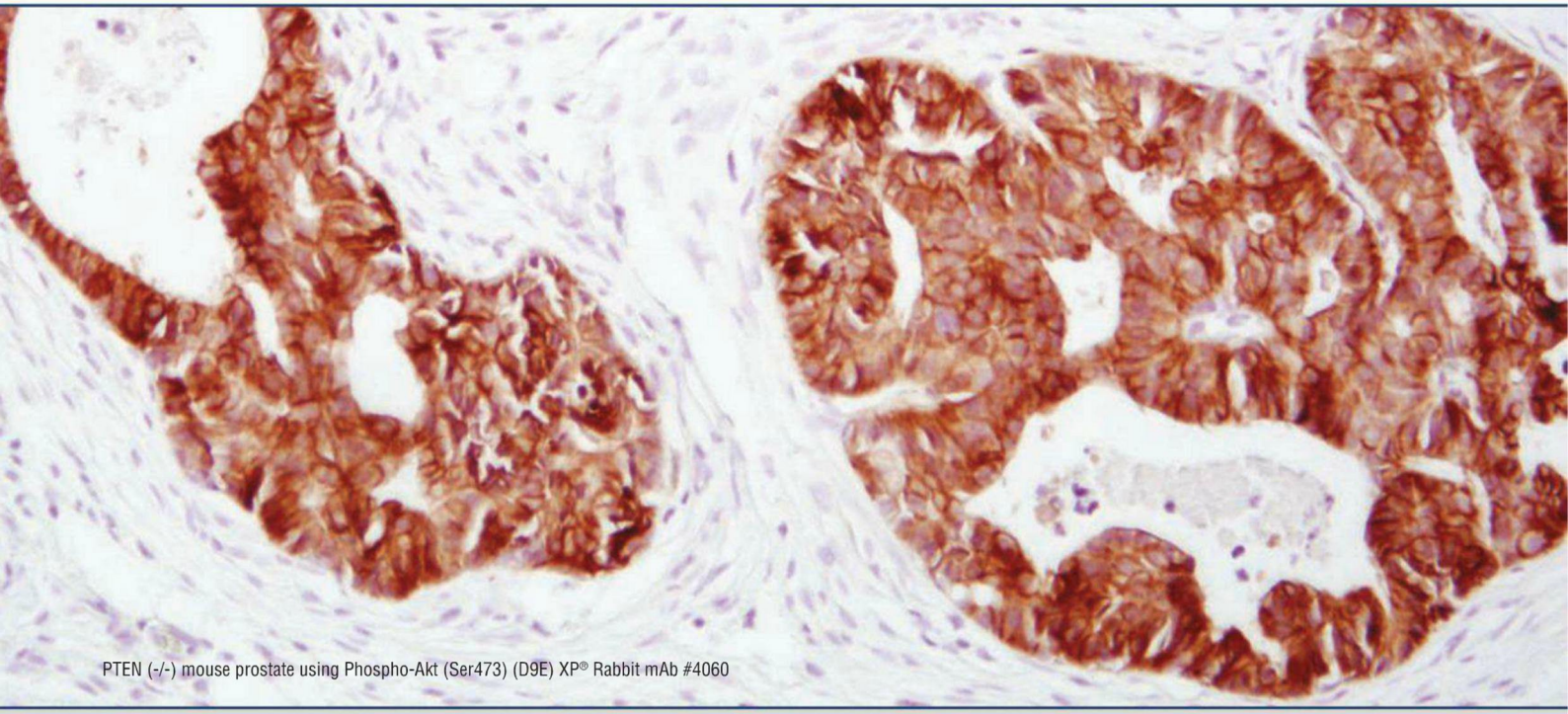

PTEN (-/-) mouse prostate using Phospho-Akt (Ser473) (D9E) XP® Rabbit mAb #4060

XP® Monoclonal Antibodies,
one antibody, multiple applications

Unparalleled product quality, validation, and technical support.

XP® monoclonal antibodies are a line of high quality rabbit monoclonal antibodies exclusively available from Cell Signaling Technology. Any product labeled with XP has been carefully selected based on superior performance in the most relevant research applications.

Exceptional specificity
As with all of our antibodies, the antibody is specific to your target of interest, saving you valuable time and resources.

+ Exceptional sensitivity
The antibody will provide a stronger signal for your target protein in cells and tissues, allowing you to monitor expression of low levels of endogenous proteins, saving you valuable materials.

+ Exceptional stability and reproducibility
XMT technology combined with our stringent quality control ensures maximum lot-to-lot consistency and the most reproducible results.

= Exceptional performance™
XMT technology coupled with our extensive antibody validation and stringent quality control delivers XP monoclonal antibodies with exceptional performance in the widest range of applications.

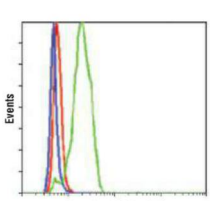

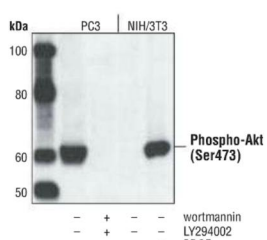

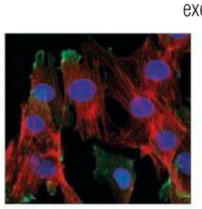
Insulin-treated C2C12 cells

◀ ***Phospho-Akt (Ser473) (D9E) XP® Rabbit mAb #4060 demonstrates exceptional performance in a wide range of applications.***

For experimental details, additional information, and a complete list of available XP® monoclonal antibodies visit…
www.cellsignal.com/sci

Cell Signaling TECHNOLOGY®

Orders (toll-free) 1-877-616-2355 | **Technical support** (toll-free) 1-877-678-8324 support@cellsignal.com | **Inquiries** info@cellsignal.com | **Environmental Commitment** eco.cellsignal.com

© 2012 Cell Signaling Technology, Inc. XP®, Exceptional performance™, and Cell Signaling Technology® are trademarks of Cell Signaling Technology, Inc.